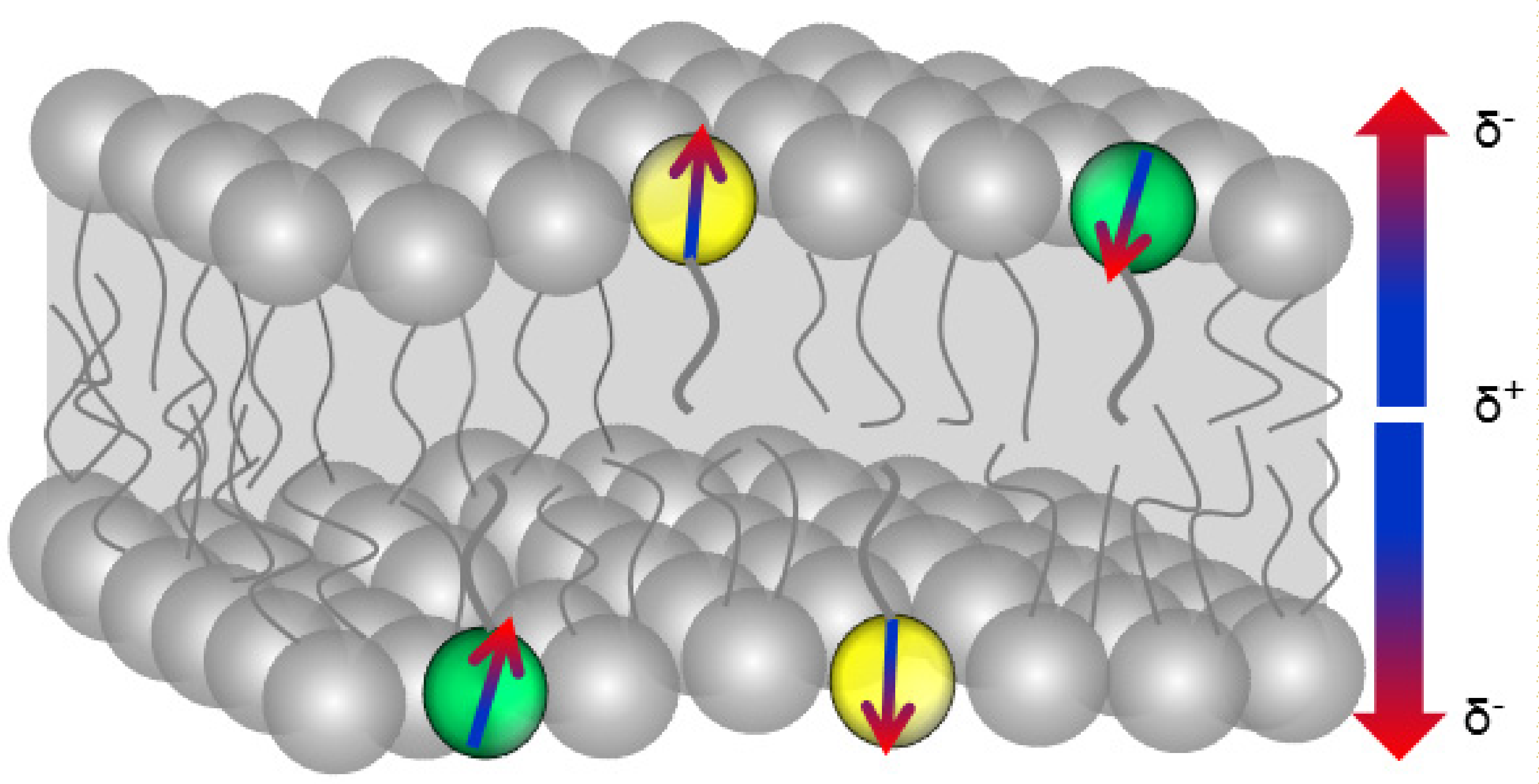

Renato Manuel Soares Cardoso

Kinetics and Thermodynamics of Interaction between Amphiphiles and Membranes: Interplay of Amphiphile Dipole Moment and Membrane Dipole Potential

Tese de Doutoramento em Química, especialidade Química Biológica,
orientada pela Professora Doutora Maria João Pedrosa Ferreira Moreno
Silvestre e pelo Professor Doutor Winchil Luís Cláudio Vaz e apresentada
à Faculdade de Ciências e Tecnologia da Universidade de Coimbra

Coimbra/2013

Universidade de Coimbra

Faculdade de Ciências e Tecnologia da Universidade de Coimbra

Departamento de Química

Renato Manuel Soares Cardoso

Kinetics and Thermodynamics of Interaction between Amphiphiles and Membranes: Interplay of Amphiphile Dipole Moment and Membrane Dipole Potential

Tese de Doutoramento em Química, especialidade Química Biológica, apresentada à Faculdade de Ciências e Tecnologia da Universidade de Coimbra, sob a orientação da Professora Doutora Maria João Pedrosa Ferreira Moreno Silvestre e do Professor Doutor Winchil Luís Cláudio Vaz.

2013

Coimbra

“… For I observe, that of late Chymistry begins, as indeed it deserves, to be cultivated by Learned Men who before despis'd it; and to be pretended to by many who never cultivated it, that they may be thought not to ignore it: Whence it is come to passe, that divers Chymical Notions about Matters Philosophical are taken for granted and employ'd, and so adopted by very eminent Writers both Naturalists and Physitians. Now this I fear may prove somewhat prejudicial to the Advancement of solid Philosophy: For though I am a great Lover of Chymical Experiments, and though I have no mean esteem of divers Chymical Remedies, yet I distinguish these from their Notions about the causes of things, and their manner of Generation. And for ought I can hitherto discern, there are a thousand Phænomena in Nature, besides a Multitude of Accidents relating to the humane Body, which will scarcely be clearly & satisfactorily made out by them that confine themselves to deduce things from Salt, Sulphur and Mercury, and the other Notions peculiar to the Chymists, without taking much more Notice than they are wont to do, of the Motions and Figures, of the small Parts of Matter, and the other more Catholick and Fruitful affections of Bodies. Wherefore it will not perhaps be now unseasonable to let our Carneadeswarne Men, not to subscribe to the grand Doctrine of the Chymists touching their three Hypostatical Principles, till they have a little examin'd it, and consider'd, how they can clear it from his Objections, divers of which 'tis like they may never have thought on;”

In the Sceptical Chymist, 1661, by Robert Boyle

Agradecimentos

«Aqueles que passam por nós, não vão sós, não nos deixam sós.
Deixam um pouco de si, levam um pouco de nós.» - *Antoine de Saint-Exupéry*

Um doutoramento é um desafio da vida que me levou a crescer como químico e principalmente como pessoa. Este percurso, que não pode resumir apenas à dedicação e ao esforço do doutorando, foi partilhado com muitas pessoas que com o seu contributo para o meu trajecto de estudante de doutoramento tornaram este caminho mais fácil, mais compartilhado e mais enriquecedor e às quais não posso deixar de agradecer. Sei, no entanto, que estas curtas palavras não serão suficientemente reconhecedoras e lisonjeias.

À Professora Doutora Maria João Moreno não me ocorrem palavras mais adequadas do que as do Sir Isaac Newton: "Se vi mais longe foi por estar de pé sobre ombros de gigantes". Se consegui chegar até aqui muito se deve a si, ao seu encorajamento, rigor, exigência, espírito crítico e amizade. O meu percurso sob sua orientação iniciou-se durante o ano de 2006 e desde aí temos trabalhado em conjunto. A sua disponibilidade e o seu apoio constante (até mesmo no laboratório) foram sem qualquer dúvida essenciais para o meu crescimento como homem e como cientista. Foi sob a sua alçada que conheci um grupo extraordinário, que muitas recordações me trouxe. Muito Obrigado por tudo…

Ao Professor Doutor Winchil Vaz, co-orientador e grande Homem da Ciência. O mundo das membranas biológicas surgiu na minha vida pelas suas mãos era ainda estudante de licenciatura. Na verdade, toda a paixão que depositava nas aulas que leccionava e o que exigiu de mim enquanto aluno conduziu-me até ao grupo de Processos Biológicos. Agradeço-lhe, ainda, por todas as conversas sábias com que sempre me deliciou e toda a disponibilidade e entusiasmo com que respondeu a qualquer desafio que lhe propus.

Ao Professor Doutor Anibal Disalvo por me acolher no seu laboratório durante os três meses que passei na Argentina e à Professora Doutora Fabiana Lairion por me ter ajudado na obtenção dos potenciais dipolares em monocamadas.

Uma palavra de reconhecimento ao Professor Doutor João Sérgio Seixas de Melo e ao Doutor João Pina pela prontidão e acessibilidade demonstrada nas medições e análise dos tempos de vida de fluorescência.

Ao Professor Doutor Eurico Melo por me ter acolhido no seu laboratório e por toda ajuda e empenho na determinação o momento dipolar das anfifílas utilizadas no meu trabalho experimental

Aos meus amigos e companheiros de laboratório Hugo, Filipe, Patrícia com quem tive o prazer de partilhar não só o laboratório mas também discussões científicas, alegrias e tristezas. O ambiente que todos nós conseguimos criar no grupo foi extraordinário e difícil de equiparar, o meu obrigado a todos.

Aos meus colegas dos Processos Biológicos, Rui, Pedro, Inês e David um muito obrigado pelo ambiente de amizade que sempre senti.

A todos os meus amigos, que se torna impossível de discriminar (mas vocês sabem), por toda a vossa ajuda, pelo carinho, pela partilha… enfim, pela amizade.

Ao meu grande amigo Gonçalo de Sá com quem partilhei, desde os tempos da Faculdade, todo o meu percurso académico e que de forma decisiva contribuiu para o meu crescimento e que neste caminho me prestou uma inigualável ajuda e encorajamento na escrita desta tese. Obrigado Amigo.

Uma palavra de agradecimento aos meus Tios, Primos e Avós obrigado por todo o apoio que sempre me deram.

À Ângela, que ao longo deste percurso foi companheira de muitas batalhas e com quem aprendi a partilhar a minha vida. Pelo amor, pela perseverança, por todo o incentivo que foi determinante e tornou possível chegar até aqui. Por me conseguires compreender, por vezes de forma quase incompreensível, sobretudo durante estes últimos tempos onde a ansiedade por vezes falou mais alto, por fazeres parte da minha vida, o meu obrigado.

Aos meus sobrinhos, Francisca e Henrique, por terem sem dúvida marcado a minha vida com as vossas pinceladas de alegria, ternura, sinceridade e alguma doce inoportunidade.

À minha irmã, Sofia, e ao meu “irmão”, Alexandre, como sei que vocês são apenas um os meus agradecimentos serão para os dois. Obrigado por todo amor com que sempre olharam por mim e pelos conselhos que me deram ao longo da minha vida. Por tudo o que vocês me ensinaram, pelos erros que me deixaram cometer, pelas lutas que travámos juntos, por me darem o que preciso quando mais preciso, por serem pessoas extraordinárias e porque sei que estarão sempre a meu lado. O meu Obrigado.

Aos meus pais tenho de agradecer por me terem transmitido os valores e as bases morais com que pautei toda a minha vida, por aquela pessoa que sou hoje. Por todo o vosso Amor, por sempre acreditarem em mim e pela família que somos, obrigado Pai e Mãe.

Table of Contents

Resumo i

Abstract iii

Abbreviations v

List of Figures ix

List of Tables xv

I OBJECTIVES AND OUTLINE **1**

I.1 Objectives **3**

I.2 Outline **3**

II LITERATURE REVIEW **5**

II.1 The cell membrane **7**

II.1.1 Biological Membranes: Historical Perspective and Function 7

II.2 The Lipid Bilayer and Membrane Lipids **9**

II.2.1 Membrane Lipids: From Diversity to Function 9

II.2.2 Lipid Assemblies: Liposomes 13

II.2.3 The Asymmetric Lipid Distribution in the Plasma Membrane 15

II.3 Membrane Thermotropic Behaviour **19**

II.3.1 Lipid Phases 19

II.3.2 Cholesterol and the Liquid Ordered Phase in Membranes 21

II.4 Membrane Hydration **24**

II.4.1 Properties of Water as Solvent 24

II.4.2 Interfacial Water in Biological Supramolecular Assemblies 25

II.5 Electrostatic Potential of a Membrane **26**

II.5.1 The Membrane Electric Profile 26

II.5.2 Methods to Measure the Membranes Dipole Potential: A Long Way to Go… 29

II.5.3 Contributions to Membrane Dipole Potential and Models in Monolayers 31

II.5.4 Biological Role of the Membrane Dipole Potential 35

II.6 Membrane Dynamics and Permeability 38

II.6.1 Lipid Dynamics 38

II.6.2 Membrane Permeation 39

III MATERIAL AND METHODS 47

III.1 Material 49

III.2 Equipment 49

III.3 Aqueous Buffer 50

III.4 Preparation of Large Unilamelar Vesicles (LUVs) 50

III.5 Liposomes Chemical Composition and Quantification 52

III.5.1 The Bartlett Phosphate Assay: 53

III.5.2 The Lieberman-Burchard Cholesterol Assay: 53

III.6 Synthesis and Purification of the RG-C_{14} and CBF-C_{14} Amphiphiles 54

III.7 Determination of the Amphiphile Critical Aggregation concentration (CAC) 57

III.8 Amphiphile Aggregation Studies in Membranes 57

III.9 Determination of the CBF-C_{14} Ionization Constant in LUVs 59

III.10 Methodology for the Partition of RG-C_{14} and CBF-C_{14} between Donor POPC LUVS and Acceptor LUVs 59

III.11 Methodology for the Kinetics of Interaction of RG-C_{14} and CBF-C_{14} between Donor POPC LUVS and Acceptor LUVs 60

III.12 Fluorescence Anisotropy and Lifetimes 61

III.13 Monolayers Experiments 62

III.13.1 Measurement of the Potential Difference across Lipid Monolayers 62

III.13.2 Monolayer Surface Pressure Experiments 63

IV DIPOLE POTENTIAL OF MONOLAYERS WITH BIOLOGICALLY RELEVANT LIPID COMPOSITIONS 65

IV.1 Introduction 67

IV.2 Dipole Potential in Lipid Monolayers 70

IV.3 Area per Lipid in Monolayers 72

IV.4 Effect of Lipid Composition in the Dipole Potential of Membranes 75

IV.5 Chapter Highlights 81

V EFFECT OF AMPHIPHILE DIPOLE MOMENT IN SOLUBILITY AND PARTITION TO LIPID BILAYERS IN LIQUID ORDERED AND LIQUID DISORDERED PHASES 83

V.1 Introduction 85

V.2 Aqueous Solubility of RG-C_{14} and CBF-C_{14} 88

V.3 Partition of RG-C_{14} and CBF-C_{14} between Donor POPC LUVs and Acceptor LUVs with Various Lipid Compositions 90

V.4 Aggregation of RG-C_{14} and CBF-C_{14} in Lipid Bilayers 98

V.5 Spectral Properties of the RG-C_{14} and CBF-C_{14} in Liquid Ordered and Liquid Disordered Phases 104

V.6 Fluorescence Anisotropy and Lifetimes 107

V.7 Rationalization of the Experimental Results with Membrane Dipole Potential 110

V.8 Chapter Highlights 115

VI EFFECT OF THE AMPHIPHILE DIPOLE MOMENT IN THE KINETICS OF INTERACTION WITH LIPID BILAYERS IN LIQUID ORDERED AND LIQUID DISORDERED PHASES _____ 117

VI.1 Introduction _____ 119

VI.2 Kinetics of RG-C_{14} and CBF-C_{14} Exchange between LUVs _____ 121

VI.3 Kinetics of Translocation of the RG-C_{14} and CBF-C_{14} in LUVs _____ 130

VI.4 Thermodynamics of the Interaction of RG-C_{14} and CBF-C_{14} with LUVs _____ 136

VI.4.1 Transition State for Insertion/Desorption of RG-C_{14} and CBF-C_{14} _____ 136

VI.4.2 Thermodynamics of CBF-C_{14} and RG-C_{14} Desorption from LUVs _____ 140

VI.4.3 Thermodynamics of CBF-C_{14} and RG-C_{14} Translocation in LUVs _____ 142

VI.5 Effect of the pH in Kinetics and Thermodynamics of Interaction of CBF-C_{14} with LUVs _____ 146

VI.5.1 Effect of the pH in Desorption of CBF-C_{14} from LUVs _____ 147

VI.5.2 Effect of the pH in Translocation of CBF-C_{14} in LUVs _____ 152

VI.6 Role of Membrane Dipole Potential and Amphiphile dipole Moment in Kinetics and Thermodynamics of interaction with lipid bilayers, in *l*l_d and l_o phase. _____ 157

CONCLUSIONS _____ 161

APPENDIX _____ 167

REFERENCES _____ 177

Resumo

A principal via para determinar a biodisponibilidade de um fármaco é a permeação passiva através de membranas biológicas. No entanto, para se prever a permeação de um fármaco através de uma membrana é necessário o conhecimento quantitativo das velocidades de interacção com as diferentes barreiras biológicas (inserção, desorção e translocação). Para a grande maioria dos fármacos este perfil cinético é desconhecido e a velocidade de permeação é estimada através da sua hidrofobicidade, que é determinada pela constante de partição entre o octanol e a água. Considerando que as membranas são sistemas altamente anisotrópicos, é demasiado redutora a simples comparação com as fases homogéneas (octanol). A orientação dos lípidos membranares com o seu grupo polar, em contacto com a fase aquosa e as cadeias hidrocarbonadas orientadas para o centro da bicamada, origina gradientes de polaridade, densidade e carga. Dessa assimetria surge uma propriedade importante que é o potencial dipolar. Além disso, a maioria dos fármacos e ligandos biológicos têm uma distribuição assimétrica de carga, sendo expectável que a inter-relação entre o momento dipolar de uma anfifíla e o potencial membranar desempenhe um papel importante nos seus parâmetros de interacção. No entanto, esta questão não tem merecido a devida importância por parte da comunidade científica.

Neste trabalho apresenta-se um estudo detalhado da cinética e termodinâmica de interacção entre duas anfifílas fluorescentes, RG-C_{14} e CBF-C_{14}, e membranas com diferentes composições lipídicas, características das membranas de células eucarióticas. Adicionalmente, determinou-se o seu coeficiente de partição relativo (água/membrana) e solubilidade em diferentes membranas, bem como se atendeu à sua localização na interface membranar. As anfifílas fluorescentes foram escolhidas tendo em conta a orientação oposta do seu momento dipolar, quando inseridas na membrana, e contendo uma cadeia hidrofóbica de 14 carbonos. Os resultados experimentais foram racionalizados em termos do potencial membranar, cujo valor para as composições lipídicas de interesse, foi determinado usando monocamadas. Observou-se um aumento do potencial dipolar, em membranas contendo colesterol, devido ao o efeito de condensação do colesterol, bem estabelecido, promovendo um maior empacotamento dos lipídos. O grupo carbonilo na cadeia acilo *sn*-2 dos fosfolípidos demonstrou ter um

papel preponderante no potencial dipolar final, e a sua ausência no caso da SpM leva a uma diminuição do potencial dipolar. Os resultados obtidos permitem uma previsão do perfil do potencial dipolar da membrana plasmática que é assimétrica, enriquecida em SpM e colesterol na monocamada externa e com quantidades significativas de PE e PS na monocamada interna. Surpreendentemente observou-se que o potencial dipolar reforça o potencial transmenbranar. A RG-C_{14} demonstrou uma solubilidade em água menor do que a CBF-C_{14}, revelando o seu carácter mais hidrofóbico. Adicionalmente, a RG-C_{14} demonstrou uma tendência para agregar, quando inserida na membrana, em particular para bicamadas na fase líquido-ordenado (POPC:CHOL(5:5) e SpM:CHOL(6:4)). O coeficiente de partição relativo, para ambas as sondas, entre POPC e membranas aceitantes distintas demonstrou um decréscimo linear com o potencial dipolar para membranas de POPC:CHOL. No entanto, o declive encontrado foi maior para a RG-C_{14} (mesma orientação do dipolo que a potencial membranar) do que para CBF-C_{14} indicando uma maior estabilidade para esta última nas fases do líquido ordenado. A caracterização da cinética e termodinâmica de interacção entre a CBF-C_{14} e a RG-C_{14} com diferentes bicamadas lipídicas, obtidas neste trabalho, representa um avanço determinante na actual literatura sobre este assunto. Os resultados permitem estabelecer regras de inter-relação entre o momento dipolar de anfifílas e o potencial membranar. Observou-se que a desorção da RG-C_{14} é mais lenta do que a da CBF-C_{14}, de acordo com uma maior estabilização da RG-C_{14} quando inserida na membrana. Para o movimento transmembranar das amostras, verificou-se que a velocidade de translocação é maior para a RG-C_{14} do que para a CBF-C_{14}, em concordância com o grupo mais polar da CBF-C_{14} (carregada negativamente). A interacção entre o momento dipolar das anfifilas, em diferentes localizações, e o potencial membranar (estado inserido equilíbrio e estado de transição para desorção/inserção e translocação) contribui significativamente para a energia global dos diferentes estados, sendo particularmente evidente no termo entálpico. A variação de entalpia para a formação do estado de transição, tanto para a desorção como para translocação, é menos favorável para a RG-C_{14} do que para CBF-C_{14}, de acordo com uma maior estabilização do estado da RG-C_{14} quando inserido na membrana. Este facto será atribuido à força atractiva entre o momento dipolar da RG-C_{14}, quando inserida na membrana, e o potencial dipolar da membrana, enquanto que para a CBF-C_{14} esta força é repulsiva.

Abstract

The passive permeation across biological membranes is a main route determining a drug bioavailability. However, the prediction of its permeability requires the quantitative knowledge of the kinetic parameters for interaction with the distinct membrane barriers (insertion, desorption and translocation). For most drugs this kinetic profile is unknown and their permeability rate is estimated based on their general hydrophobicity, assessed through partition between octanol and water. Considering that membranes are highly anisotropic systems, the comparison with homogenous phases is simpleminded. The orientation of the lipids in membranes, with their polar groups oriented to the aqueous phase and the non-polar hydrocarbon chains oriented towards the bilayer mid-plane, generates transversal gradients of polarity, density and charge. One important property that arises from this asymmetry is the dipole potential. Moreover, most drugs and biological ligands have an asymmetrical charge distribution, and the interplay between the amphiphile dipole moment and membrane potential is expected to play an important role in their interaction parameters. This question has however been overlooked by the scientific community.

In this work we presented a detailed study of the kinetics and thermodynamics of the interaction between two fluorescent amphiphilic molecules, RG-C_{14} and CBF-C_{14}, and membranes with distinct lipid compositions characteristic of eukaryotic cell membranes. Furthermore, their relative water/bilayer partition coefficient and solubility in distinct membranes, as well as the location at the membrane interface, were recovered. The probes were chosen to have an opposite dipole moment orientation, once inserted in the bilayer, and a hydrophobic chain of 14 carbons length. The experimental results were rationalized in terms of the membrane dipole potential, whose value was determined for the lipid compositions of interest using monolayers. The well-established condensation effect of cholesterol promotes lipid packing and, consequently, the dipole potential is increased. The carbonyl group in the *sn*-2 acyl chains of phospholipids showed a preponderant role in the final dipole potential, and its absence in SpM leads to a decrease in the dipole potential. The results obtained allow the prediction of the dipole potential profile of the asymmetric plasma membrane, enriched in SpM and cholesterol in the outer and with significant amounts of PE and PS in the

inner monolayer. Interestingly, it is found that the dipole potential reinforces the observed transmembrane potential. The RG-C_{14} showed a smaller aqueous solubility than CBF-C_{14}, revealing its more hydrophobic character. Moreover, RG-C_{14} showed a tendency to aggregate when inserted in the membranes, especially for bilayers in the liquid ordered phase (POPC:CHOL(5:5) and SpM:CHOL(6:4)). The relative partition coefficient, of both probes, between POPC and the different acceptor membranes, showed a linear decrease with the membrane dipole potential for POPC:CHOL membranes. Moreover, the slope was higher for the RG-C_{14} (same dipole orientation has the membrane) than for CBF-C_{14} indicating a higher stability for the latter in the liquid ordered phases.

The characterization of the kinetics and thermodynamics for the interaction of both CBF-C_{14} and RG-C_{14} with the different lipid bilayers performed in this work represents a major step forward in the currently available literature on this subject. The results obtained lead to the establishment of rules for the interplay between the amphiphiles dipole moment and the membrane dipole potential. We observe that desorption of RG-C_{14} is slower than that of CBF-C_{14}, in agreement with a stabilization of the inserted state for RG-C_{14}. For the transbilayer movement of the probes, it was observed that the rate of translocation was faster for RG-C_{14} than for CBF-C_{14}, in agreement with the more polar headgroup for the CBF-C_{14} (negative charge). The interaction between the amphiphile dipole moment and the membrane dipole potential at the different location of the amphiphiles (inserted state at equilibrium and transition states for desorption/insertion and translocation) contributes significantly to the overall energy of the distinct states, and is particularly evident in the enthalpy term. The enthalpy variations upon formation of the transition state in both desorption and translocation was more unfavourable for RG-C_{14} than for CBF-C_{14}, in agreement with a more stabilized state of RG-C_{14} when inserted in the membrane. This was attributed to the attractive force between the dipole moment of RG-C_{14}, when inserted in the bilayer, and the dipole potential of the membrane while it is repulsive for the case of CBF-C_{14}.

Abbreviations

Latin Alphabet

A – Amphiphile

BBB – Blood Brain Barrier

BSA – Bovine Serum Albumin

CAC – Critical Aggregation Concentration

CBF-C_{14} – Carboxyfluorescein fluorescent headgroup attached to a 14 carbons length alkyl chain

CHOL – Cholesterol

CNS – Central Nervous System

CPP – Critical Packing Parameter

e_0 – Elemental electrostatic charge

DMPC – 1,2 dimyristoyl-sn-glycero-3-phosphocholine

DPPC – 1,2dipalmitoyl-sn-glycero-3-phosphocholine

DMPE – 1,2 dimyristoyl-sn-glycero-3-phosphoethanolamine

DHE – Ergosta-5,7,9(11),22-tetraen-3β-ol (dehydroergosterol)

DHPC – 1,2-diheptanoyl-sn-glycero-3-phosphocholine

EDTA – Ethylenediamine tetra-acetic acid

EggPC – L-α-phosphatidylcholine

e. g. – from latin: *exempli gratia*, for example

F – Faraday constant

GPI – Glycosylphosphatidylinositol

HEPES – 4-(2-hydroxyethyl)-1-piperazineethanesulfonic acid

K_d – Equilibrium Aggregation Constant

$K\mathrm{p}$ –Equilibrium Partition Coefficient

$K\mathrm{p}_{\mathrm{rel}}$ – Relative Equilibrium Partition Coefficient

k_+ – Bimolecular insertion rate constant

$k_{-,}$ k_{out} – Desorption rate constant

k_f– Translocation rate constant

k_1 – First order disaggregation constant

k_2 – Second order aggregation constant

k_{diff}– Rate constant for diffusion controlled process

L – Lipid

l_{d} – Liquid disordered phase

l_o – Liquid ordered phase

LUV or LV – Lipid Unilamellar Vesicle (LUVs or LVs for plural)

MLV – Multilamellar Vesicle (MLVs for plural)

MeOH – Methanol

NBD – 7-nitrobenz-2-oxa-1,3-diazol-4-yl

NBD-C_{14} – 7-nitrobenz-2-oxa-1,3-diazol-4-yl with an alkyl chain of 14 carbons

NBD-C_{n} – Homologous series of NBD with an alkyl chain of different lengths

NDB-DMPE – NBD- 1,2 dimyristoyl-*sn*-glycero-3-phosphoethanolamine

NBD-LysoMPE – NBD-lyso-1-myristoylphosphatidylethanolamine

NMR – Nuclear Magnetic Resonance

NaCl – Sodium Chloride

$\mathrm{NaN_3}$ – Sodium Azide

PC – Phosphatidylcholine

PE – Phosphatidylethanolmamine

PS – Phosphatidylserine

PA – Phosphatidic Acid

POPC – 1-palmitoyl-2-oleoyl phosphatidylcholine

POPE – 1-palmitoyl-2-oleoyl phosphatidylethanolamine

POPS – 1-palmitoyl-2-oleoyl phosphatidylserine

p*K*a –Logarithm of the acid dissociation constant

R – Ideal gas constant

RG – Rhodamine Green ™

RG-C_{14} – Rhodamine Green fluorescence headgroup attached to a 14 carbons length alkyl chain

RhB-DPPE – 1,2 Dipalmitoyl-sn-Glycero-3-Phosphoethanolamine-N-(Lissamine Rhodamine B Sulfonyl)

SpM or SM – Egg yolk Sphingomyelin

SUV – Small Unilamellar Vesicle (SUVs for plural)

TPP^+ - Tetraphenylphosphonium

UV-Vis – Ultraviolet-visible spectroscopy

$\overline{V}$ - Molar volume

z_i – Charge of specie *i*

Greek Alphabet

β – Exchange rate constant

ε – Molar extinction coefficient

π – Surface pressure

λ – Wavelength

τ – Fluorescence Lifetime

φ_i – Proportionality constant relating the fluorescence or absorption with the concentration of specie *i*

η – Viscosity

Ψ_0 – Surface Charge Potential

List of Figures

Figure II.1. The fluid mosaic model of Singer and Nicolson (1972). Adapted from [8] **8**

Figure II.2. Geometrical shapes of amphiphilic molecules and their correspondent macromolecular assemblies. The balance between the volume under projection of the effective headgroup area, and the alkyl chain volume is one of the main determinants in geometrical packing. Adapted from [28]. **14**

Figure II.3. Schematic drawing of the spontaneous formation of lipid vesicles, in aqueous solution, with multi layers of lipids (MLVs). Separating each lipid layer there is the aqueous solution (dark blue). By extrusion or sonication of the MLVs one can obtain vesicles composed by a single lipid bilayer (LUVs and SUVs) with aqueous solution in its interior and outside.... **15**

Figure II.4. Phospholipid asymmetry and ATP dependent lipid-translocating enzymes in the plasma membrane of normal eukaryotic cells. Phosphatidylcholine (PC) and sphingomyelin (SM) are primary located in the external leaflet, while phosphatidylethanolamine (PE), phosphatidylinositol (PI) and phosphatidylserine (PS) are mostly in the internal leaflet. Adapted from [52] and [53]. **18**

Figure II.5. Representative structures of L_β, L_β’, Lα, and ripple (P_β’) membrane phases. Adapted from [67]. **20**

Figure II.6. Structural formula of cholesterol. **21**

Figure II.7. Phase diagrams of mixtures of DPPC/Cholesterol and POPC/Cholesterol obtained from ^{2}H-NMR [72] and from *trans*-Parinaric Acid Fluorescence [74] respectively. **23**

Figure II.8. Electrostatic potential profile across a symmetrical membrane with different ion concentration in each side of the bilayer. The figure shows the transmembrane potential ($\Delta\Psi$), the surface potential (Ψs) and the dipole potential of both monolayers (ΨD_1, ΨD_2). Electrical fields of these potentials are represented by arrows in the upper part of the figure. Adapted from [100]. **28**

Figure II.9. Structures of styryl probes used in dipole potential measurements. The probe location is illustrated by showing two phosphatidylcholine (PC). From reference [103]. **31**

Figure II.10. Schematic representation of the Voglius Mobius 2-layer (left panel) and Demchak and Fort three-layer (right panel) capacitor model of monolayer and at the air-water interface. While in the 2-layer model the μ1 represents the lipid headgroup moment as well as the effects in the subphase the tree-layer capacitor separates the headgroup momentum from the moment arising from effects occurring in the subphase, additionally it adds the different permittivity constant in each region. Adapted from [125]. **34**

Figure II.11. Dipole arrangement in proteins. Panel A: Dipolar charges on a peptide bond. Panel B: Multiple peptide dipoles aligned along the axis of theα-helix summate to produce a macrodipole. From reference [127]. **36**

Figure II.12. Schematic representation of membrane lipid motions and their characteristic time scale for a bilayer in the fluid state. Adapted from [133]. **38**

Figure II.13. Two distinct mechanisms for solute permeation across membrane. Panel A: The solubility-diffusion mechanism. The solute in one side of the bilayer enters in hydrophobic core diffuse across the bilayer and leaves in the other side of the membrane. Panel B: Permeation through transient hydrophilic pore formation due to thermal fluctuations................................ **41**

Figure III.1. Typical results, obtained by dynamic light scattering (DLS), for the size distribution of a POPC sample prepared by extrusion through two staked polycarbonate filters 0.1 μm. The average diameter considered for this sample was that given by the volume distribution ≈ 113 nm. **52**

Figure III.2. Determination of the phosphate (A) and cholesterol (B) concentration in LUVs. The circles represent the standard and the squares the sample solutions. **54**

Figure III.3. HPLC chromatogram for the final reaction product RG-C_{14} (A) and CBF-C_{14} (B). Conditions: reverse phase column (see above for details); room temperature; mobile phase, MeOH:H_2O (98:2) for RG-C_{14} and MeOH:H_2O (80:20) for CBF-C_{14}; the detection was performed through λ_{exc}= 502 nm and λ_{exc}= 490 nm with the retention time (tR) of ≈ 8 min; ≈20 min for RG-C_{14} and CBF-C_{14} respectively. **56**

Figure III.4. Schematic representation of the nucleophilic attack of the tetradecylamine to the partially positive carbon attached to the C-5 of the fluorophore (Rhodamine green). A similar chemical reaction leads to formation of CBF-C_{14}. **56**

Figure III.5. Panel A: Dispersion free absorption spectra of RG-C_{14} (Blue) obtained by subtracting to the raw spectra (Black) a polynomial curve that describe the LUVs dispersion (Red). Panel B: Absorption spectra of RG-C_{14} at t= 0 h (Red) and t~ 2 h (Blue). The green line represents the deconvoluted monomer absorption spectra at t~ 2 h, obtained through the overlap of the absorption spectra at t= 0 h (red) to the t~ 2 h (blue). **58**

Figure III.6. Chemical structure of the fluorescence quencher RhB-DPPE used in this work.. **60**

Figure III.7. Typical results for π-total lipid (nmol) isotherm where the two lines represent the plateau at high pressures and the region with steepest slop, respectively. The saturation point is represented by interception of both regimes. **63**

Figure IV.1. Dipole potential in pure POPC, POPE, POPS and SpM monolayers at pH 7.4 with hepes buffer at 25 ºC. The dipole potential of POPS was determined from equation IV-1 with a Ψ_0≈-135mV. **71**

Figure IV.2. Dipole Potential, at 25 ºC, in monolayers composed by a mixture of lipids, where PC, PS, PE, C and SpM abbreviations entitle POPC, POPS, POPE, Cholesterol and SpM, respectively. The numbers between commas correspond to the lipid molar fraction in the mixture. **72**

Figure IV.3. Formation of monolayers of phospholipids measured by the changes in surface pressure as a function of nmol of lipid added at 25 ºC. Panel A: Pure POPC (□); POPC: POPS(9:1, molar ratio) (O); POPC:POPE(8:2) (Δ); Panel B: POPC:CHOL:POPE(5:3:2) (◊); POPC:CHOL:POPE:POPS (4:3:2:1)(◁); at 25 ± 1 ºC. The line is a guide to the eye. **73**

Figure IV.4. Mean Area per lipid isotherm for POPC (□), POPC:POPS(90:10), ○, and POPC:POPE(80:20) Δ at 25 ºC. The line is the best fit of a polynomial equation for areas smaller than 100 Å^2 in the liquid expanded state. **74**

Figure V.1. Panel A: The saturated palmitoyl fatty acid chains allow the protein to pack within the liquid-ordered domains of a membrane lipid raft. Panel B: Schematic structure of common palmitoylated and miristoylated membrane proteins. **86**

Figure V.2. Chemical structures for the fluorescent amphiphiles used in this work at pH 7.4.. **88**

Figure V.3. Typical experimental results obtained for the dependence of the fluorescence intensity at the maxima of RG-C_{10} (panel A, □) and CBF-C14 (Panel B;○; Δ) as a function of its total concentration in the aqueous solution at 25 ºC. In plot A the linear best fit of the fluorescence intensity *vs* amphiphile concentration for values below the CAC is also shown. The inset represents the linear region of the fluorescence with amphipile concentration. In Plot B the lines represent the linear best fit for the fluorescence *vs* CBF-C14 concentration and the interception between the two regimes was considered to be the amphiphile CAC (2.6 nM). **89**

Figure V.4. Partition of RG-C_{14} (A) and CBF-C_{14} (B), at pH 7.4, between donor POPC LUVs and different acceptor Luvs at 25 °C. Plot A: Typical results obtained for the titration of RG-C_{14} from POPC LUVs 0.1 mM (final concentration) at 0.2 μM with acceptor POPC LUVs (□), POPC:CHOL(7:3) (○), POPC:CHOL(5:5) (∇), and SpM:CHOL(6:4) (◊). The line is the best fit of equations V-1 to V-3 with $Kp_{Acceptor}/Kp_{POPC}$ ~ 1, 0.39, 0.20 and 0.03 for, POPC, POPC:CHOL(7:3), POPC:CHOL(5:5) and SpM:CHOL(6:4) acceptor vesicles. Plot B: Typical results obtained for the titration of CBF-C_{14} from POPC LUVs (0. 1 mM, final concentration) at 0.2 μM with acceptor POPC:CHOL(7:3) LUVs between 0 M and 1.2x10^{-8} M (□), POPC:CHOL:POPE(5:3:2) (∇), POPC:CHOL(5:5) (○), and SpM:CHOL(6:4) (◊). The line is the best fit of equations *V-1* to*V-3* with $Kp_{POPC}/Kp_{Acceptor}$ = 0.6, 0.3, 0.4 and 0.07 for, POPC:CHOL(7:3), POPC:CHOL:POPE(5:3:2), POPC:CHOL(5:5) and SpM:CHOL(6:4) acceptor vesicles.. **94**

Figure V.5. Variation of the characteristic rate constant for POPC (left, □) and PC:CH(5:5) (right, 0) as a function of [LUV] at 25 ºC. The line is the best fit of equation V-7 to all experimental results with a K_L=2.6x10^{10} M^{-1} for POPC and K_L=7.5x10^{9} M^{-1} for POPC:CHOL(5:5). The inset shows the rate of association between CBF-C_{14} at 15 nM with POPC (left) and 5 nM with PC:CHOL(5:5) (right) being the experimental results represented by a grey line and the best fit to a monoexponential by a black line. **96**

Figure V.6. Time evolution of the RG-C_{14} absorption spectra in LUVs inserted into LUVs prepare from pure POPC (A), POPC:CHOL:POPE (5:3:2) (B), POPC:CHOL (5:5, molar ratio) (C) and SpM:CHOL(6:4) (D). The molar ratio of the fluorescent lipid amphiphile to the host lipid was 1:50 for all cases except POPC:CHOL (5:5) and SpM:CHOL (6:4) where it was 1:200... **99**

Figure V.7. Time dependence at 25 ºC of the local concentration of RG-C_{14} in SpM:CHOL(6:4) (A) and POPC:CHOL(7:3) (B) LUVs at a lipid: probe molar ratio of 1:200 and 1:50 respectively. The open squares are the experimental data and the line is the best fit of the experimental results with equations V-8 and k_2=4.4x10^{-3} M^{-1}s^{-1} and a k_1= 3.7x10-6 s^{-1} for SpM:CHOL(6:4) and k_2=1.6x10^{-4} M^{-1}s^{-1} and a k_1= 4.9x10^{-6} s^{-1} for POPC:CHOL(7:3)........... **101**

Figure V.8. Panel A: Time dependence absorption spectra of the CBF-C_{14} in SpM:CHOL(6:4) LUVs at 25 ºC at a lipid: probe molar ratio of 1:50. The straight line is at time = 0 h, dash at t= 24 h and dot t= 6th day. Panel B: Reversibility test in the absorption of CBF-C_{14} in SpM:CHOL (6:4, molar ratio) LUVs at 60 ºC at a lipid: probe molar ratio of 1:50. The straight line is at 60 ºC and t = 0 h, dashed line is after incubation at 60 ºC during 8 h and dot is the spectrum of the aggregated solution after the 6th day at 25 ºC... **104**

Figure V.9. Normalized Absorption spectra of CBF-C_{14} (A) and RG-C_{14} (B) in, methanol (straight line), POPC (dash line), POPC:CHOL(5:5) (grey line) and SpM:CHOL(6:4) (dotted dashed line), at 25 ºC and LUVs concentration of 1mM and lipid to probe ratio of 1:500 mole ratio. **106**

Figure V.10. Typical titration curve obtained for CBF-C_{14} (2 μM) inserted in POPC bilayers (1 mM) at 25 ºC. The red line is best fit of equations A-21 (see appendix) with pKa_2= 6.4 and pKa_3= 8.8. .... **107**

Figure V.11. Anisotropy results for the RG-C_{14} (A) and CBF-C_{14} (B) in 1 mM LUVs of POPC (○), POPC:CHOL(5:5) (□) and SPM:CHOL(6:4) (Δ) between 530 and 570 nm at 25 ºC. The amphiphile concentration was 2 μM for CBF-C_{14} while for RG-C_{14} was 3.3 μM. **109**

Figure V.12. Fluorescence emission decay for RG-C_{14} in 0.5 mM POPC (A) and CBF-C_{14} in SpM:CHOL (6:4) (B) LUVs obtained with λexc = 460 nm at 25 ºC. The thinner lines in the decays are the instrumental response function (IRF). For a better judgment of the quality of the fits, weighted residuals (W.R. scale, $-3 \leq \sigma \leq +3$), autocorrelation functions (Autocorr.), and chi-square values (χ^2) are also presented. **109**

Figure V.13. Structures of RG-C_{14} and CBF-C_{14} (dianion) and the correspondent orientation and magnitude of the dipole moment obtained from semi-empirical quantum mechanical calculations (AM1) using the Hyperchem® version 8 package. Two views are presented showing the orientation of the fluorophore relative to the alkyl chain. Black, blue and red filled balls represent carbon, nitrogen and oxygen balls, respectively. **111**

Figure V.14. Dependence of the RG-C_{14} (filled symbols) and CBF-C_{14} (non-filled symbols) Kp_{rel} (A) and $\Delta G_{relative}$ (B) with experimental dipole potential for POPC (square), POPC:CHOL (7:3) (circle), POPC:CHOL:POPE(5:3:2) (triangle), POPC:CHOL(5:5) (diamond), POPC:CHOL:POPE:POPS(4:3:2:1) (inverted triangle) and SPM:CHOL(6:4) (pentagon) membranes. The line is the linear fit to the experimental results for POPC, POPCHOL(7:3), POPC:CHOL(5:5) and POPC:CHOL:POPE(5:3:2) lipid compositions. **113**

Figure VI.1. Typical curve at 25 ºC for the time dependence of the fluorescence intensity of RG-C_{14} (A and B) and CBF-C_{14} (C and D) upon transfer between 0.1mM (final concentration) donor vesicles and 1.2 mM (final) acceptor vesicles with the same lipid composition, POPC (□), POPC:CHOL(5:5) (Δ). At negative times the experimental points represent the fluorescence of each probe exclusively in the donor vesicles while at t= 0 s the acceptor LUVs were manually added. The red lines are the best fit of equations VI-1 .... **124**

Figure VI.2. Panel A: Time dependence at 25 ºC of the RG-C_{14} fluorescence intensity variation upon its transfer between donor (0.1 mM) and acceptor (0.2 mM) POPC LUVs, using the stopped-flow equipment (short time experiment) and the steady-state fluorimeter results (long times, inset). The red line is the global fit of differential equations VI-1 to the experimental results with a k_- and k_f equal to 1.5×10^{-2} and 2.6×10^{-3} s^{-1}, respectively. Panel B: Dependence of desorption rate constant obtained with the acceptor concentration, leading to k_- equal to $(1.6 \pm 0.04)\times10^{-2}$ s^{-1}. **126**

Figure VI.3. Panel A: Time dependence, at 25 ºC, of the CBF-C_{14} fluorescence intensity variation upon its transfer from donor POPC (0.1 mM) to acceptor POPC:CHOL(5:5) vesicles at 0.1, 0.2, 0.4, 2 and 4 mM. The arrow indicates the increase in acceptor concentrations. Panel B: Dependence of the exchange rate constant,*β*, with the POPC:CHOL(5:5) concentration. The best fit to the experimental data using equation VI-2 is also shown, with k_-^A= 1.0 s^{-1} and k_-^D= 4.7×10^{-1} s^{-1} **127**

Figure VI.4. Simulation, at 25 ºC, of the percentage of quencher (RhB-DPPE) associated with donor (black line) and acceptor (red line) vesicles, for the worst case scenario considered in this work (higher concentration of acceptor vesicles), with the lipid composition POPC:CHOL(5:5) or SpM:CHOL(6:4), panel A or B respectively. The data was generated using the kinetic parameters of NBD-DMPE [136, 252]. **131**

Figure VI.5. Time dependence ,at 25 ºC, of the fluorescence intensity of RG-C_{14} (A) and CBF-C_{14} (B) upon transfer between similar vesicles of SpM:CHOL(6:4) (A) and POPC:CHOL(5:5) (B), with a final lipid concentration of 0.1 mM for donor and 1.2 mM for the acceptor vesicles. The parameters for RG-C_{14} were obtained from the global best fit to the results obtained in two different times scales, the inset shows the best fit of the same parameters to the results obtained at small times, more sensitive to the desorption step. The red line is the best fit of the differential equations in VI-1 with k_{-}= 2.7×10^{-1} s^{-1} and k_f=1.6×10^{-4} s^{-1} for RG-C_{14} and k_f = 1.4×10^{-4} s^{-1} for CBF-C_{14} (B). **132**

Figure VI.6. Dependence of RG-C_{14} translocation rate constant with the SpM:CHOL(6:4) (Panel A, 25 ºC) and POPC:CHOL(5:5) (Panel B, 55 ºC) acceptor concentration with an average $k_f \approx$ 2.7±0.4(×10^{-4}) $s^{-1}$and 1.4±0.1(×10^{-1}) s^{-1}, respectively. **133**

Figure VI.7. Schematic representation of the insertion into and desorption from lipid bilayers with the correspondent high energy transition state. **137**

Figure VI.8. Arrhenius type plot for the desorption of RG-C_{14} (Panel A) and CBF-C_{14} (Panel B) from POPC (□), POPC:CHOL(5:5) (Δ) and SpM:CHOL(6:4) (◊), at pH 7.4. The average experimental value ± standard deviation of, at least, three independent experiments is shown. The line is the best fit of equation VI-6, the grey dashed line is the extrapolation of the desorption rate constant to temperatures not measured experimentally. **140**

Figure VI.9. Schematic representation of the translocation of an amphiphile with the correspondent high energy transition state. **142**

Figure VI.10. Arrhenius type plot for the translocation of RG-C_{14} (Panel A) and CBF-C_{14} (Panel B) in POPC (□), POPC:CHOL(5:5) (Δ) and SpM:CHOL(6:4) (◊) bilayers. The results show the average experimental value ± standard deviation of, at least, three independent experiments. The line is the best fit of equation VI-6 and the grey dashed line are the extrapolation of experimental results for POPC. **143**

Figure VI.11. Typical curves, at 25 ºC for the time dependence of the fluorescence intensity of CBF-C_{14} upon transfer between 0.1 mM (final concentration) donor vesicles and 1.2 mM (final) acceptor vesicles with the same lipid composition, at pH= 6 (A and C) and pH= 7 (C, D), POPC (□), POPC:CHOL(5:5) (Δ). In inset there are the independent experimental curves for desorption step in a smaller timescale. The red line represents the best fit of equations VI-1. **148**

Figure VI.12. Arrhenius type plots for the desorption of CBF-C_{14} from POPC (Panel A) and POPC:CHOL(5:5) (Panel B) at pH= 6 (□); pH= 6.5 (○); pH= 7.0 (Δ) and pH= 7.4 (◊).The results show the average experimental value ± standard deviation of, at least, three independent experiments. The line is the best fit of equation VI-6. .... **149**

Figure VI.13. Desorption rate constants obtained, at 25 ºC, for CBF-C_{14} in POPC (□) and POPC:CHOL(5:5) (Δ) lipid bilayers at different pH buffer solutions. The line is the best fit of equations VI-7 and VI-8 to the experimental results, with pKa_2= 6.9, pKa_3= 8.9 and k_{-} for the neutral, monoanionic and dianionic equal to 0, 2.4×10^{-1} and 14 s^{-1}, for POPC. For POPC:CHOL(5:5) bilayers the best fit was performed with pKa_2= 5.3 and pKa_3= 7.6 with the k_{-} for the neutral monoanionic and dianionic forms equal to 0, 2.5×10^{-1} s^{-1} and 2.3 s^{-1}, respectively. **152**

Figure VI.14. Arrhenius type plots for the translocation of CBF-C_{14} in bilayers of POPC (Panel A) and POPC:CHOL(5:5) (Panel B) at pH= 6 (□); pH= 6.5 (○); pH= 7.0 (Δ) and pH= 7.4 (◊).The results show the average experimental value ± standard deviation of, at least, three independent experiments. The line is the best fit of equation VI-6... **153**

Figure VI.15. Translocation rate constants, at 25 ºC, obtained for CBF-C_{14} in POPC (□) and POPC:CHOL(5:5) (Δ) lipid bilayers at different values of pH. The line is the best fit of equations VI-7 and VI-8 to the experimental results, with p*K*a_2= 6.9, p*K*a_3= 8.9 and k_- for the neutral equal to 1.2×10^{-2} $s^{-1}$and 0 s^{-1} for the monoanionic and dianionic, in POPC. For POPC:CHOL(5:5) bilayers the best fit was performed with p*K*a_2= 5.3 and p*K*a_3= 7.6 with the k_- for the neutral, monoanionic and dianionic forms equal to 1.4×10^{-2} , 5.6×10^{-4} and 0 s^{-1}, respectively. **155**

Figure VI.16. Schematic representation of CBF-C_{14} (yellow) and RG-C_{14} (green) and respective dipole moment orientation when inserted in a monolayer of lipids (grey). The large arrow represents the membrane dipole potential orientation with a gradient fill from blue (positive pole) to red (negative pole). Once inserted in the bilayer CBF-C_{14} and RG-C_{14} have distinct dipole orientations. The amphiphiles are exaggerated for a best understanding from the reader. **157**

Figure VI.17. Schematic representation of the effect of RG-C_{14} (green amphiphile) and CBF-C_{14} (yellow amphiphile) interfacial headgroup localization in the enthalpy variation for the formation of the transition state in POPC (1), POPC:CHOL (5:5) (2) and SpM:CHOL (6:4) (3) membranes. The arrow in the amphiphile headgroup represents its dipole moment orientation and the thicker arrow represents the membrane dipole potential orientation, being the red and the blue ends the negative and the positive pole, respectively. For simplicity the energy was normalized for the transition state and the blue arrows represent the enthalpy variation from the inserted state to the transition sate.. 158

List of Tables

Table II.1. Most common structural Glycerolipids and Sphingolipids in eukaryotic cells R,R_1,R_2 and R_3 represent the fatty acid acyl chain, and highlighted in red is the glycerol backbone. **11**

Table II.2. Fatty acid composition of most representative phospholipids in the Major Lipid classes of Rat Liver Plasma Membranes. The highlights correspond to the more demonstrative saturated and unsaturated fatty acid acyl chain. Adapted from [24]. **12**

Table II.3. Lipid composition (%mol) of the plasma membrane in several organisms. Adapted from [39]. **16**

Table IV.1. Summary of the mean area per lipid and the dipole potential obtained for different lipid compositions monolayers formed at the air/water interface, at 25 ºC. **75**

Table IV.2. Monolayer properties in pure lipids according to DF model. **78**

Table V.1. Equilibrium Parameters for the transfer of the RG-C_{14} and CBF-C_{14} from POPC donor bilayers to acceptor bilayers at distinct lipid compositions and phase states at 25 ºC. **98**

Table V.2. Kinetic parameters for aggregation of RG-C_{14} in bilayers at 25 ºC **102**

Table V.3. Spectroscopic characteristics of the probes used in this work in distinct solvents at 25 ºC. **107**

Table V.4. Fluorescence Anisotropy (r) and Lifetimes (τ) of RG-C_{14} and CBF-C_{14} in membranes in the l_o and l_d phase, at 25 ºC. The results were obtained for three independent experiments being the fluorescence anisotropy the average calculated value for the wavelength range from 530 to 570 nm. **110**

Table VI.1. Kinetic rate constants and equilibrium for the association of RG-C_{14} and CBF-C_{14} to lipid bilayer membranes at pH 7.4 and 25 ºC **128**

Table VI.2. Summary of the desorption and insertion rate constants, at 25 ºC, for different amphiphiles including this and other works from our research group. **129**

Table VI.3. Values of the translocation rate constants in distinct lipid composition LUVs, at 25 ºC. **134**

Table VI.4. Literature reported data for the translocation of different amphiphiles in membranes **135**

Table VI.5. Thermodynamic parameters, for desorption of RG-C_{14} and CBF-C_{14} from lipid bilayers. **140**

Table VI.6. Thermodynamic parameters for translocation of RG-C_{14} and CBF-C_{14} in lipid bilayers. **143**

Table VI.7. Thermodynamic parameters for translocation of NBD-DMPE and NBD-LysoMPE in lipid bilayers, recovered from literature. **145**

Table VI.8. Thermodynamic parameters for the formation of the transition state and rate constant for desorption of CBF-C_{14} from lipid bilayers of POPC and POPC:Chol (5:5), at different values of pH.. **149**

Table VI.9. Thermodynamic parameters, for the transition state, and rate constant for translocation of CBF-C_{14} in lipid bilayers at different pH. **154**

I

Objectives and Outline

I.1 Objectives

The dipole potential of membranes has been implicated in several biological phenomena such as modulating the activity of membrane proteins [1] or affecting the interaction of drugs with membranes [2]. Additionally, our group proposed that the magnitude and orientation of the dipole moment of amphiphiles could influence the partition of amphiphiles into lipid bilayers with distinct dipole potentials [3]. However, quantitative data regarding the interaction of amphiphiles (with different dipole moment) with different membranes has not been the preferential target of the scientific community. This is important given that most drugs have a dipole moment which may differently affect the interaction with membranes and, therefore, their bioavailability. Moreover, this subject is particularly important in design and development of xenobiotics which have to cross biological membranes to be pharmacologically available.

The subject of this work is to study the interaction of two fluorescence amphiphiles, a Rhodamine (RG-C_{14}) and Carboxyfluorescein (CBF-C_{14}) derivative with membranes. Both probes have a 14 carbon alkyl chain but a distinct dipole moment either in magnitude and orientation. The rationalization of the experimental data in terms of the amphiphile dipole moment and membrane dipole potential is the main focus of this work. Does this interplay affect the positioning, partition, and kinetics of interaction of amphiphiles with membranes?

I.2 Outline

The Chapter II consists on a literature review of biological membranes that is crucial for the comprehension and critical analysis of the experimental results. Starting with a brief historical overview we address, during this review, important physical-chemical properties of membranes with a main focus in the electrostatic characteristics.

Chapter III consists in a compilation of most material and equipment used in the experimental work along with detailed description of the methodologies followed throughout the experiments.

In Chapter IV the dipole potential of pure and biologically relevant lipid mixtures was obtained using lipid monolayers formed at the air-water interface. Studies of mean area per lipid, in lipid mixtures, were also performed. The results were rationalized first in single component monolayers and afterwards in mixtures, according to the lipids physical-chemical properties.

The Chapter V describes the relative partition coefficient (Kp_{rel}) of the fluorescence amphiphiles between bilayers with distinct lipid composition. Moreover, fluorescence anisotropy and lifetimes measurements were obtained to address the localization of the amphiphilic probes in the membrane-water interfacial region. The aggregation of amphiphiles in membranes was attained for different membranes. The results were rationalized considering both the amphiphiles dipole moment and membrane dipole potential previously determined.

The Chapter VI addresses the kinetics and thermodynamics of interaction of RG-C_{14} and CBF-C_{14} with membranes in the liquid disordered and liquid ordered phase. A detailed study at different pH for the carboxyfluorescein derivative was performed and, once again, a rationalization with the membrane dipole potential was obtained.

In the conclusions we summarize the relevant results from the previous chapters.

II

Literature Review

II.1 The cell membrane

“It can truly be said of living cells, that by their membranes ye shall know them”

In Battaglia, 1997 as reference to Davson and Danielli

II.1.1 Biological Membranes: Historical Perspective and Function

In 1855, the botanists Naegeli and Cramer proposed the existence of an osmotic barrier surrounding plant cells, which explained the plasmolysis phenomena. They observed that cells can modify its volume upon osmotic changes induced in the surrounding environment [4]. Later, 1877, Pfeffer published his major work "Osmotische Untersuchungen” formulating the concept that a Plasma-membrane surrounds the protoplasm of cells, which separates the aqueous environments with different composition [5]. He further postulated that this plasma skin was a barrier to the free passage of water and solutes from surrounding media to the cell interior making the analogy with the observed properties of copper ferrocyanide artificial membrane [5]. The observations presented by Pfeffer and later by de Vries 1884 were fundamental to the acceptance of membrane as a semi-permeable barrier and settled the pillars for the development of membrane theory [6].

In 1895 Ernest Overton examined different solutes and recognized a relationship between the chemical characteristics of solutes and their osmotic properties. He declared that substances that dissolved in lipid permeate the cell faster than the ones dissolved in water [4]. Furthermore, Overton made the first observation regarding the chemical nature of the plasma membrane asserting that this must be a lipid-impregnated boundary layer with properties similar to those of cholesterol esters and lecithin [7].

Since Overton, the picture of the correct model describing cell membrane has been exchanging. However, in 1972 Singer and Nicolson proposed the fluid mosaic model of biomembranes which became widely accepted [8]. They considered the lipid membrane as a two dimensional fluid where proteins are embed and free for laterally diffuse (Figure II.1). Although nowadays increasing evidence sustain a highly heterogeneous and dynamic biological membrane, such as existence of more ordered domains in the bilayer (lipid rafts), the fluid mosaic model remains as the central membrane model structure. This model proposed the establishment of strong interactions between proteins and close lipids promoting a short-range order, which do not influences the remaining lipids. It is interesting to recognize that these interactions may, in fact, require different kinds of lipids supporting one plausible argument for the critical vast diversity of lipids controlled by cells.

Biological membranes are very important cell structures they provide a boundary, physically separating the interior of all cells from the outside environment. Being selectively-permeable, biological membranes regulate solute permeation rigorously controlling the fluid content within a cell, crucial to keep cells under physiological activity [9]. Their low permeability to charged solutes allows establishing a non-equilibrium state within a cell, essential to maintain its correct function and avoid death by apoptosis [10]. Cell membranes are involved in several other processes such as the transfer of signals, between cells, through complex systems of communication (cell signalling). They comprise associated proteins that are vital to cell function *e.g.* cell adhesion, transport proteins and cell receptors. In addition, cell membrane serves as support surface for the extracellular glycocalyx and intracellular cytoskeleton [9, 11, 12].

By now, it is explicit that membranes are complex dynamic heterogeneous lipid structures that perform various vital roles in the accurate function of cells. In the next section, we will exploit with more detail the lipid organization within membranes taking into account the structural constraints and chemical variety of lipid molecules.

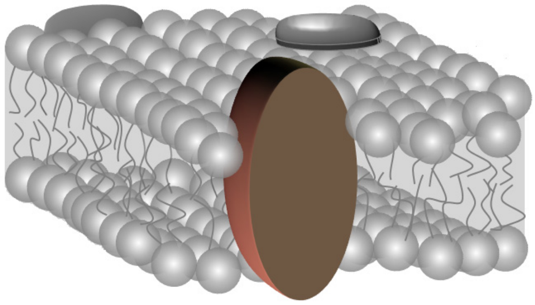

Figure II.1. The fluid mosaic model of Singer and Nicolson (1972). Adapted from [8]

II.2 The Lipid Bilayer and Membrane Lipids

"It is clear that all our results fit in well with the supposition that the chromocytes are covered by a layer of fatty substances that is two molecules thick."

Gorter and Grendel 1924

II.2.1 Membrane Lipids: From Diversity to Function

The vast lipid repertoire and complexity which confers a countless number of functions to lipids is intrinsically related to their particular chemical features as bimodal molecules. Lipids comprehend two chemically different domains; one that is hydrophobic and, therefore, repelled from the water and other that is hydrophilic and readily interacts with the water environment. This amphiphilic nature of lipids is the structural characteristic that allows cells to segregate its inner constituents from the external media.

A eukaryotic cell in order to synthesize its lipids diversity spends a substantial amount of genome [13-15]. Hence, the biological role of lipid molecules as macro-assemblies cannot be resumed to structurally support membrane proteins, which mediate fundamental cell functions such as protein-trafficking and signaling. Lipids accomplish diverse functions such as energy storage in the form of triacylglycerols and steryl esters, in some cellular processes they change the membrane features of associated proteins, and they work as secondary messengers and signalling molecules in recognition processes [13, 15-17]. Depending on the residence time on the proteins, different surrounding lipids can be identified and named either restricted or annular (interfacial), this connection between lipids and membrane proteins may, in fact, affect their biological activity. Cholesterol and phosphatidylinositol are necessary lipids for activity of the membrane associated proteins Na^+/K^+-ATPase and Glycophorin, respectively [18-20].

There are a vast number of diseases commonly called lipid-related disorders that along with cardiovascular diseases, cancer and Alzheimer's have a lipid component. This has increase the interest of researchers in the lipids quantification [21]. Moreover, there are a number of drugs such as statins that target lipid metabolism and signalling pathways.

One of the main biological functions of lipids is serving as structural components of cell membranes. The structural lipids present in eukaryotic membranes are predominantly glycerol and sphingosine backbone lipids, and the other widely existing class has a chemical composition based in sterol. Within glycerol lipids membranes contain glycerophospholipids, which result from the phosphodiester connection between the glycerol backbone and the polar headgroup, remaining the hydrophobic tail (one) or tails (two) attached by an ester or ether linkages.

The Sphingolipids are based in a sphingosine backbone, which associated to a fatty acid forms a ceramide. The hydroxyl groups present at the ceramide backbone provide the capability of additional linkages and, by attaching a phosphocholine headgroup to a hydroxyl group sphingomyelin may be achieved (Table II.1).

The complexity and variety of these biological molecules increases by changing both the hydrophilic (headgroup) and the hydrophobic components (alkyl chain length and unsaturation). The headgroup may be modified through a phosphodiester linkage in the *sn*-3 position of the glycerol backbone leading to phosphatidylcholine (PC) phosphatidylethanolamine (PE), phosphatidylserine (PS), phosphatidylglycerate (PG), phosphatidylinositol (PI) and the unmodified phosphatidic acid (PA). The alkyl chains, at positions *sn*-1 or *sn*-2, may be changed in three different ways: by its total length (number of carbons); by the number of double bonds; and by changing the nature of the linkage between the backbone and the alkyl chains (ether, ester, alkenyl ether). The possible combination of headgroup and lipid tails allows the existence of more than 1000 different lipid species in an eukaryotic cell [22].

The most common phospholipids in the cells are PC, PE, PS, PA and PI. The PC is commonly used in biophysical membrane studies and is one of the most biologically prevailing lipid headgroup. It accounts for about 50% of the total lipid in most eukaryotic cells, is a zwitterionic lipid with a negative charge on the phosphate and a positive charge on the amino group and, due to its cylindrical shape, it self-organizes into planar bilayers. PA, PG and PS are the most general negatively charged lipid headgroups. The PE, due to their small and less hydrated headgroup, displays a distinct conical shape that inflicts curvature stress on the bilayer surface exposing the hydrocarbon chains. The primary sphingophospholipid present in mammalian cells is sphingomyelin (SpM), which has narrower cylindrical shape length than PC lipids with same alkyl chain length. Moreover, this straightening in the geometrical form allows promoting a greater packing within bilayers.

Table II.1. Most common structural Glycerolipids and Sphingolipids in eukaryotic cells R,R_1,R_2 and R_3 represent the fatty acid acyl chain, and highlighted in red is the glycerol backbone.

Glycerolipids	Triacylcerol	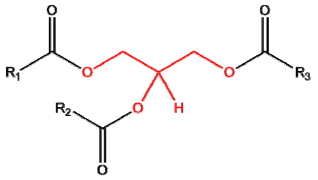	
	Phospholipids 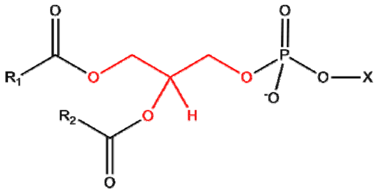	**Formula of *x*:**	**Name of the phospholipid:**
		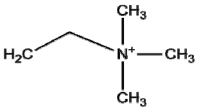	*Phosphatidylcholine*
		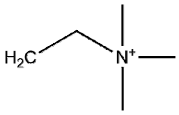	*Phosphatidylethanolamine*
		-H	*Phosphatidic acid*
		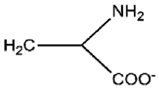	*Phosphatidylserine*
		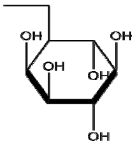	*Phosphatidylinositol*
Sphingolipids	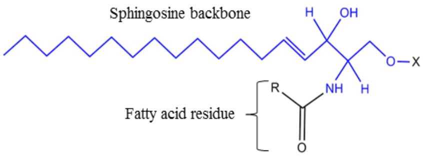 	**Formula of *x*:**	**Name of the Sphingolipid:**
		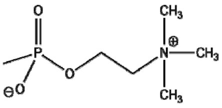	*Sphingomyelin*
		-H	*Ceramide*

The fatty acids are the fundamental building blocks of lipids, and most biological abundant fatty acids have an even number of carbons [23]. The alkyl chains of lipids (either saturated or unsaturated) may have lengths between 12 and 26 carbon atoms. While saturated chains, have a more common numbers of carbons of 16 or 18, the unsaturated composition is mostly 18 with one or two double bonds (C18:1 or C18:2) and 20 with four double bonds (C20:4) (Table II.2) [12]. The alkyl chains of lipids always tend to be straight due to Van Der Walls forces, but the rotation of the carbon-carbon bonds allows different bond conformations and consequently to either separating (gauche) or maintaining (trans) both chains in proximity. The nature of the C-C bonds in lipids alkyl chains establishes some important biophysical properties of membranes such as dynamics, permeability and fluidity. The double bonds in lipids acyl chains are *cis* and introduce a kink in the acyl chain orientation, which affects the lipid packing.

Table II.2. Fatty acid composition of most representative phospholipids in the Major Lipid classes of Rat Liver Plasma Membranes. The highlights correspond to the more demonstrative saturated and unsaturated fatty acid acyl chain. Adapted from [24].

Carbons Number	LysoPC	SPM	PC	PS+PI	PE	FFA
<14:0	t.a.	t.a.	0.1	t.a.	t.a.	t.a.
14:0	0.2	0.2	0.5	t.a.	0.2	2.93
15:0	1	0.2	0.5	t.a.	0.6	-
16:0	33.4	18.7	30.2	12.1	26	31.6
16:1	0.1	0.1	0.8	0.5	0.3	3.07
17:0	3.4	0.1	t.a.	t.a.	1.5	-
18:0	45	39.2	29.8	49.2	31.9	21.9
18:1	4.0	3.7	9.6	4.6	6.5	19
18:2	3.7	4.2	15.3	5.2	12.4	13.2
20:4	5.9	12.8	11.6	26.4	15.4	6.26

Values expressed as percentage of total fatty acids; FFA- free fatty acid; t.a.- trace amounts

II.2.2 Lipid Assemblies: Liposomes

In 1924, Gorter and Grendel examined the surface area of the plasma membrane of mammalian erythrocytes. They initially predicted that if it is a bilayer the surface area should be half of that occupied by the lipids in a monolayer. The comparison between the measurements in a monolayer and red blood cells provided, within error, a ratio cell:monolayer of 1:2 reinforcing a plasma membrane model formed by a bilayer [25]. This simple yet significant experimental finding in the coming years supported the development of membrane models where a lipid bilayer structure was the central feature.

The amphipathic structural identity of a lipid molecule concedes that, at physiological concentrations, (well above its aggregation concentration) they may associate in distinct macromolecular structures, which are inherently dependent on the geometrical shape of the molecule (Figure II.2). The formation of these aggregated lipid structures is favoured due to the increase in system entropy, once the water molecules do not need to self-organize surrounding the non-polar part of the solute. The relationship between molecular shape, aggregated structure and the way how they could be controlled was examined by Tanford [26] and later by Israelachevily *et* a*l* (1976). The latter author proposed a mathematical theory that describes how the molecular shape affected the size and arrangement of the aggregate, commonly named critical packing parameter [27]. Accordingly, the aggregate geometry depends on three packing constraints, the optimal cross sectional area occupied by the polar interface (S_0), the maximum length of the alkyl chain (l_c) and the molecular volume of the hydrocarbon portion of the amphiphile (v). Those parameters, together, determine the critical packing parameter (CPP).

$$CPP = \frac{v}{l_c . S_0} \qquad (II\text{-}1)$$

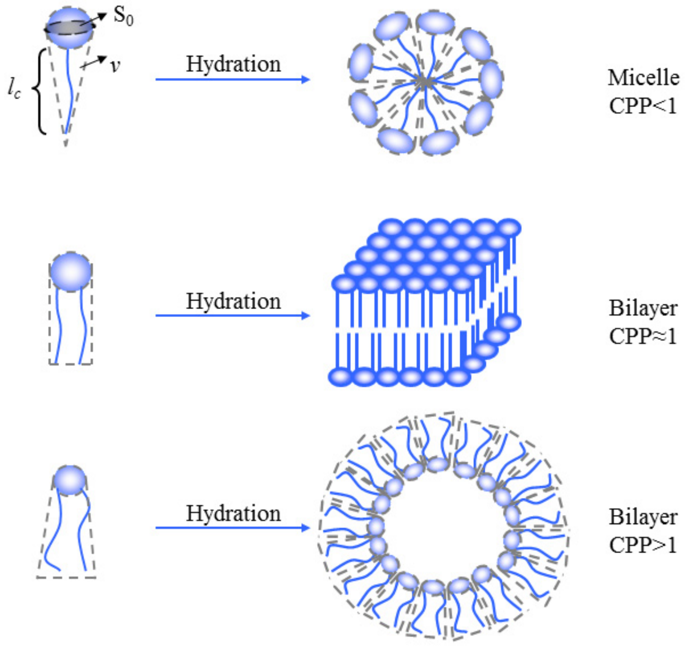

Figure II.2. Geometrical shapes of amphiphilic molecules and their correspondent macromolecular assemblies. The balance between the volume under projection of the effective headgroup area, and the alkyl chain volume is one of the main determinants in geometrical packing. Adapted from [28].

Bilayers are the key structural basis for cell membranes, and they can be prepared to produce close vesicles with a radius that goes from some angstroms to millimetres [12] (Figure II.3). This arrangement of lipids into bilayers permits the hydrocarbon core to be tightly packed apart from water and, moreover by imposing curvature in the bilayer sheet so that it will form a vesicle, the hydrophobic edge can be removed avoiding the exposure of hydrophobic groups to water molecules [29]. The liposomes are spherical lipid vesicles made either by a single (unilamellar) or multiple bilayers enclosing small volumes of aqueous solution in the inner compartment of the vesicle. These vesicles are widely used in in-vitro studies to mimic cell membranes [30] or cell organelles [31]. They are also utilized to reconstitute membrane proteins in their natural lipid environment examining the effects either in lipid structure or protein conformation [32]. In in-vitro studies, the curvature of the vesicles is a fundamental property, and below a given value it strongly influences membrane properties [33-35]. The phase behaviour of pure dipalmitoyl-phosphatidylcholine (DPPC) vesicles is dependent on the vesicles diameter for values below 70 nm [36, 37]. Since the topology of the vesicle changes, via increasing curvature, there is some difficulty for lipids with cylindrical geometry to fit and this DPPC miss packing in highly curved bilayers leads to a decrease in the phase transition temperature. Structures with high curvature are found normally in biological systems and this has a vital role, allowing them to have a higher bending energy facilitating membrane fusion processes [34]. In this work unilamellar vesicles (LUV) with a diameter of 100 nm are used, consequently, under those experimental conditions the effects of curvature stress can be neglected.

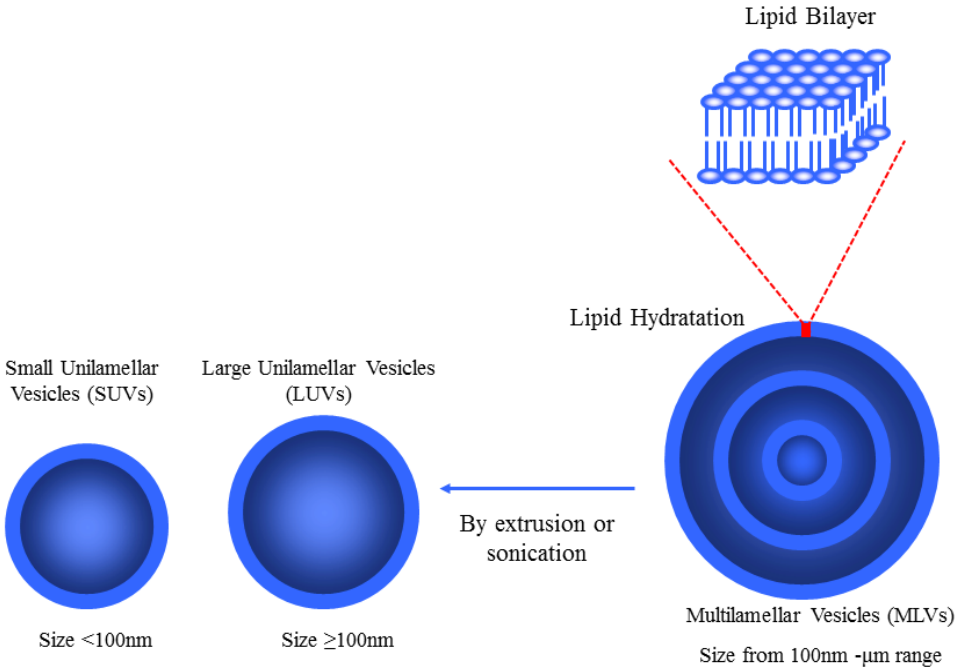
Lipid Bilayer
Lipid Hydratation
Small Unilamellar Vesicles (SUVs)
Large Unilamellar Vesicles (LUVs)
By extrusion or sonication
Size <100nm
Size ≥100nm
Multilamellar Vesicles (MLVs)
Size from 100nm -µm range

Figure II.3. Schematic drawing of the spontaneous formation of lipid vesicles, in aqueous solution, with multi layers of lipids (MLVs). Separating each lipid layer there is the aqueous solution (dark blue). By extrusion or sonication of the MLVs one can obtain vesicles composed by a single lipid bilayer (LUVs and SUVs) with aqueous solution in its interior and outside.

II.2.3 The Asymmetric Lipid Distribution in the Plasma Membrane

Biological membranes contain a broad variety of lipids in each membrane fraction which is different for the distinct cell types and organelles. Glycerophospholipids account for nearly 70% of the total lipid content in mammalian cells while the remaining 30% comprise cholesterol, sphingomyelin and glycosphingolipids. (Table II.3). As mentioned earlier in the text (II.2.1 above) phosphatidylcholine is the most prevailing phospholipid (40-50%), phosphatidylethanolamine is the second most abundant phospholipid and its quantity ranges from 20% up to 45% depending on the organism. Phosphatidylserine, Phosphatidylinositol and Phosphatidic acid are present in smaller amounts (10%) [38].

Table II.3. Lipid composition (%mol) of the plasma membrane in several organisms. Adapted from [39].

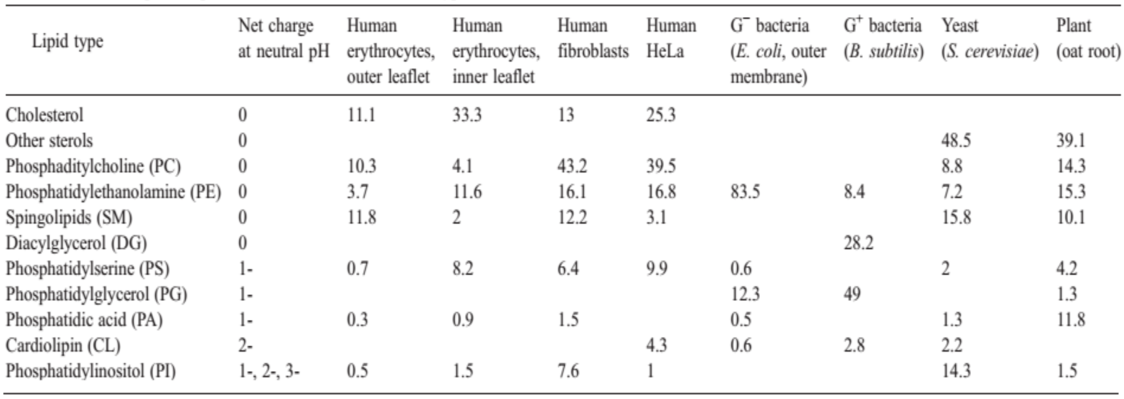

Lipid type	Net charge at neutral pH	Human erythrocytes, outer leaflet	Human erythrocytes, inner leaflet	Human fibroblasts	Human HeLa	G^- bacteria (*E. coli*, outer membrane)	G^+ bacteria (*B. subtilis*)	Yeast (*S. cerevisiae*)	Plant (oat root)
Cholesterol	0	11.1	33.3	13	25.3				
Other sterols	0							48.5	39.1
Phosphaditylcholine (PC)	0	10.3	4.1	43.2	39.5			8.8	14.3
Phosphatidylethanolamine (PE)	0	3.7	11.6	16.1	16.8	83.5	8.4	7.2	15.3
Spingolipids (SM)	0	11.8	2	12.2	3.1			15.8	10.1
Diacylglycerol (DG)	0						28.2		
Phosphatidylserine (PS)	1-	0.7	8.2	6.4	9.9	0.6		2	4.2
Phosphatidylglycerol (PG)	1-					12.3	49		1.3
Phosphatidic acid (PA)	1-	0.3	0.9	1.5		0.5		1.3	11.8
Cardiolipin (CL)	2-				4.3	0.6	2.8	2.2	
Phosphatidylinositol (PI)	1-, 2-, 3-	0.5	1.5	7.6	1			14.3	1.5

The asymmetric distribution of proteins in cell membranes is well established and vital for cells. The observation that some proteins require specific surrounding lipids to acquire their native structure points towards an asymmetric distribution of lipids as well. [18]. The lipids structural diversity, the cytoskeleton and the different chemical nature of the internal and external environments, in contact with membranes, promoted the additional arguments to foretell a different lipid distribution within a cell membrane [12, 40]. A membrane whose asymmetric distribution of lipids is well characterized is the plasma-membrane. The outer leaflet lipid composition of this membrane is PC, SpM and cholesterol and the inner cytoplasmic leaflet includes considerable amounts of PE and negatively charged phospholipids [39-41] (Figure II.4).

The indicated transmembrane asymmetry of membrane cells can be related to relevant biological phenomena such as: maintenance of membranes proteins activity [42] or mechanical stability [43, 44]. A further enlightening example of the importance of this asymmetric distribution arises from the, almost exclusive, inner leaflet localization of PS in erythrocytes plasma membranes. This PS lipid is well known as a signaling molecule for clearance by the reticuloendothelial system [45] and, by restraining its localization to the inner leaflet, the removal of healthy functional erythrocytes is avoided [38].

The transversal movement (translocation) of phospholipids in membranes is slow due to the polar headgroup, generally with charges, whose solubility in the hydrophobic core of a membrane is very low. Therefore, to maintain lipids asymmetric distribution membranes have specific carriers (proteins) that translocate lipids against the concentration gradient (Figure II.4). The ATP-dependent aminophospholipid translocase and floppase enzymes move particular lipids and are the foremost responsible for their uneven distribution in the plasma membrane [46]. The aminophospholipid translocase, transfers PS and PE from the outer to the inner leaflet of the plasma membrane, in a selective manner (PS transfer is faster than PE) [47, 48], while PC is not transferred by the enzyme [49]. The floppase is less specific because transfers several phospholipids (PS, PE and PC), and unlike translocase, catalyses lipids movement from the inner to the outer leaflet being the transfer rate by floppase much smaller than the translocase [47, 48]. The work promoted by both ATP dependent floppase and aminotranslocase maintaining the transversal lipid asymmetry may be disrupted by the activity of scramblase other enzyme that is much less lipid specific and promotes a bidirectional transfer of phospholipids between leaflets. Scramblase, as the others, is also ATP-dependent, but in order to be effective it demands the presence of Ca^{2+}, that under physiological conditions is in the micromolar range [46-48]. Therefore, the indicated enzyme is essentially inactive in normal conditions being the asymmetry ensured by both floppase and aminotranslocase [44]. Nevertheless the role of the scramblase protein is essential, once active it facilitates the transbilayer movement exposing PS lipids to the surface of apoptotic cells [46].

The phosphatidylserine transversal asymmetry rigorously secured with the help of the aforementioned protein macro-assemblies is necessary since, it provides some electrostatic interactions with proteins present in the inner leaflet like the membrane skeletal protein, spectrin, [50] and structural protein kinase C [51] confined to the membrane cytoplasmic side. Additionally it is striking to mention that the inclusion of charged molecules exclusively in the inner leaflet of eukaryotic cells promotes itself a transmembrane potential.

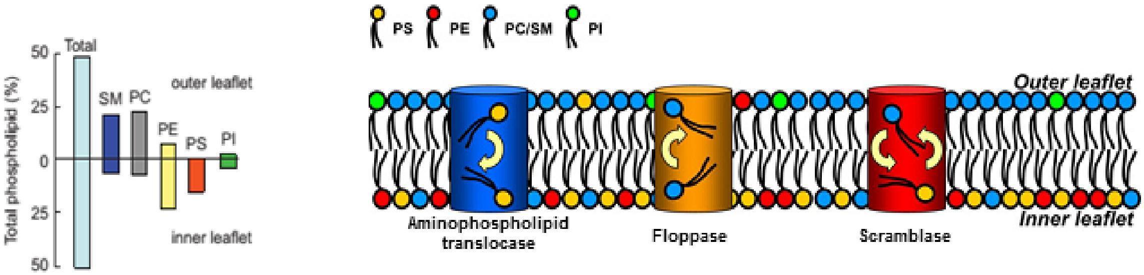
Total phospholipid (%)
50
25
0
25
50
Total
SM
PC
PE
PS
PI
outer leaflet
inner leaflet
PS
PE
PC/SM
PI
Outer leaflet
Inner leaflet
Aminophospholipid translocase
Floppase
Scramblase

Figure II.4. Phospholipid asymmetry and ATP dependent lipid-translocating enzymes in the plasma membrane of normal eukaryotic cells. Phosphatidylcholine (PC) and sphingomyelin (SM) are primary located in the external leaflet, while phosphatidylethanolamine (PE), phosphatidylinositol (PI) and phosphatidylserine (PS) are mostly in the internal leaflet. Adapted from [52] and [53].

II.3 Membrane Thermotropic Behaviour

"One of the most remarkable characteristics of lipids is their ability to combine in one phase a periodically ordered long-range organization (in one, two or three dimensions) and a highly disordered short-range conformation; many properties of lipids, and probably their function in biological membranes, are closely related to this peculiar mingling of order and disorder."

In Tardieu 1973

II.3.1 Lipid Phases

In the last 5 decades the scientific community spent a significant effort trying to understand the phase behaviour of biological membranes, nonetheless, the extended lipid variety found in biomembranes and their complex chemical structure makes this task challenging [22, 54-59].

Membranes arrange in oriented layers exhibiting, on one hand, a partial and long range order and, on the other hand, they contain some level of fluidity and disorder; therefore they can be classified as liquid crystals [60]. Within liquid crystals, membranes have characteristics that resemble a thermotropic and lyotropic liquid crystal, forming lipid phases with different properties by variations in either temperature or water content. A lipid bilayer may exist in different physical phases depending on lipid mobility, lateral organization or the molecular order, moreover changing a certain feature of the system (*e.g.* temperature) may result a discrete transition from one state towards the other.

The interaction between hydrocarbon chains of lipids is essentially ruled by Van der Walls forces which are also responsible for packing and lateral order of a bilayer [12, 61]. The phase transformation that occurs in lipids results from their motional freedom relative to nearby lipids, and during these alterations bilayers change their packing density and organization (disorder). For phospholipids whose geometrical shape favours a bilayer macro-structure, *e.g* phosphocholine, there is a sequence of phases with increasing temperature. The thermotropic phase transformation may occur at a particular well defined temperature (T_m), for instance the transition from gel phase (L_β) to liquid crystalline phase (L_α) in DPPC, classified as a first order transition [62].

In the gel (L_β), also called solid (S_o), phase, lipid alkyl chains exhibit a stiff and fully extend all-trans conformation corresponding to a two-dimensional hexagonal lattice [55, 63]. This high lipid packing existing in L_β phase bilayers, dramatically diminishes the lipid lateral diffusion which is 10^{-11} cm^2s^{-1} compared to ~ 10^{-8}–10^{-7} cm^2s^{-1} [64] in fluid phases. Depending on the water content of the bilayer the L_β phase may be converted into $L_\beta{}'$, which, is very similar to the L_β with the exception of the alkyl chains that present a tilt with respect to the normal plane of the bilayer [12, 65]. The tilting occurs when the area packing requirements of the lipid headgroup exceed that of the chains, and the tilt permits to accommodate this packing mismatch. The acyl chain tilt angle increases with the membrane water content and, hence, the phase L_β’ have a larger incorporation of water molecules than L_β [55]. Moreover, the tilted alkyl chains lead to a decrease in the membrane thickness which is more obvious in the presence of water.

The membrane fluid phase (L_α) can be distinguished due to a substantial fraction of trans-gauche isomerization of the hydrocarbon alkyl chains and lateral diffusion significantly higher than gel phase. Additionally, the phospholipids headgroup hold an orientation parallel while the hydrocarbon chains have an average perpendicular orientation relative to the membrane surface normal (Figure II.5).

At very-low temperatures, there is the formation of a crystal phases (L_C/L_C’’) where the alkyl chains of the phospholipids are in the all-trans conformation and the headgroups form an ordered 3D lattice [66]).

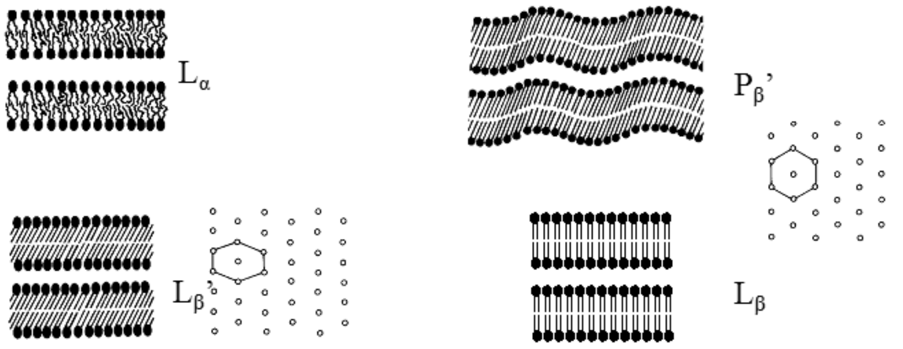

Figure II.5. Representative structures of L_β, L_β’, Lα, and ripple (P_β’) membrane phases. Adapted from [67].

II.3.2 Cholesterol and the Liquid Ordered Phase in Membranes

Regardless of the fact that phospholipid molecules are the building blocks of biological bilayers, sterols are other fundamental part of membranes. The phospholipid diversity (previously addressed) contrasts with the major sterol component present in eukaryotic cells membranes, the cholesterol. It is the primary component in plasma membranes controlling its fluidity and intervening in some signalling processes [68].

Cholesterol molecular structure derives from the tetracyclic hydrocarbon *perhydrocycloentanophenantrene* with a single hydroxyl group attached to carbon 3, an *iso*-octyl hycrocarbon side chain at carbon 17 and a double bond between carbon 5 and 6 (Figure II.6). The *trans* arrangement of the four fused rings makes cholesterol a planar and rigid molecule whereas the hydroxyl group confers its amphiphilic character. The presence of the hydrophilic OH group orients the cholesterol molecule in the membrane so that this functional group will face interfacial water, with localization near the polar headgroups of phospholipids, maximizing the hydrogen-bonding interactions. Cholesterol ring structure is embedded in the hydrophobic core of the membrane and, notably, this hydrophobic part may be distinguished in two separate "faces". A rough (β) one that contain the methyl groups, the iso-Octyl side chain and the OH group, which are attached to the same planar face of the ring structure, and a smoother (α) side of the cholesterol that contains hydrogen atoms [69].

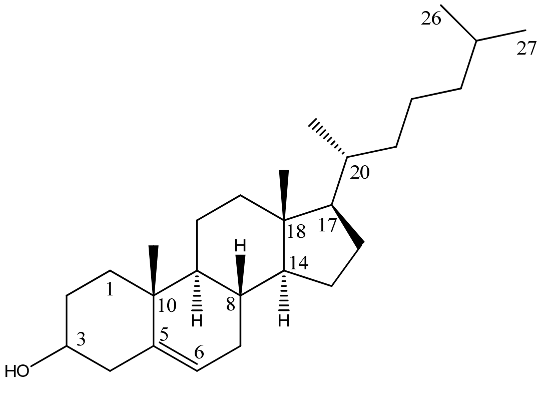

Figure II.6. Structural formula of cholesterol.

The asymmetric distribution, recognized for phospholipids in the plasma membrane of eukaryotic cells, is less apparent with regard to cholesterol due to its fast translocation rate between leaflets [70]. Therefore, there is the assumption that cholesterol equally distributes between both leaflets or, it may be partially enriched in the outer monolayer due to its greater affinity for phosphatidylcholine and sphingomyelin [40]. Cholesterol is present in the plasma membrane at high proportions, so it is necessary to study the structure and organization of membranes both in the absence and the presence of cholesterol.

Being a flat and rigid molecule, cholesterol packing with all-*trans* alkyl chains (gel phase) is better than with chains containing a large fraction of gauche conformations. However, the geometrical shape of cholesterol is distinct from the lipid ordered alkyl chains and therefore, cholesterol tends to disturb their lateral packing. The addition of cholesterol leads to a different membrane physical state whose properties are in between the L_β and L_α state, named a liquid ordered phase (L_o or l_o) [71]. This liquid ordered phase, promoted by the presence of high cholesterol contents can be distinguished by a high acyl chain order and a high translational mobility, supported through NMR measurements and micromechanical studies [72, 73].

Several studies were performed using different phospholipid membranes containing cholesterol to observe the thermotropic behaviour of these mixtures. In a DPPC:Cholesterol mixture for cholesterol mole concentrations above 7 % there is an abolishment of the pre-transition, and above 50 %, the main phase transition also disappears [72]. Vist et al, 1990, further revealed that within a broad cholesterol % mole range and below the main phase transition temperature there is coexistence of Gel and liquid phase while, above Tm, the Lo phase coexists with Lα (Figure II.7). From the Figure II.7, as aforementioned, changes in the phospholipid acyl chain nature lead to a bilayer with different thermotropic properties and, the final phase diagram may vary drastically. In the POPC:Cholesterol mixture for cholesterol percentages above 50% the membrane is exclusively in the liquid ordered state. Moreover, coexistence between L_α and L_β occurred, at 25 ºC, for Cholesterol percentages from less than 10 % up to 40 %.

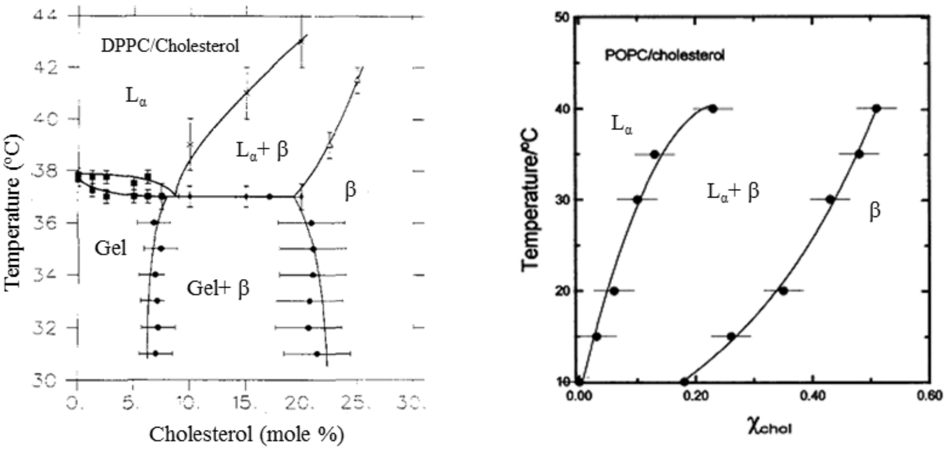

Figure II.7. Phase diagrams of mixtures of DPPC/Cholesterol and POPC/Cholesterol obtained from ^{2}H-NMR [72] and from *trans*-Parinaric Acid Fluorescence [74] respectively.

II.4 Membrane Hydration

"Biomembranes are composed of lipids, proteins and carbohydrates (glycolipids and glycoproteins). The basic structure is generally a lipid bimolecular sheet in which the integral proteins are embedded. The relationship between water structure and these various components is most important for determining the final biomembrane structural arrangement."

From D. Chapman 1994

II.4.1 Properties of Water as Solvent

Water is the most universal solvent since nearly all the chemical substances partially dissolve in water. Furthermore, the aqueous environment provides the midst for molecular interactions in living organisms since it constitutes half of the weight of a living cell [75]. Despite its abundance water is a relatively small molecule which possesses unique physicochemical properties (vaporization heat, melting and boiling points) that dramatically differ from other liquids with comparable size [75, 76].

The Hydrogen bonding between molecules is the main feature allowing water to form a three-dimensional tetrahedral network like structure. An important physical aspect of hydrogen bonds is their polarizability, which confers to water a high dielectric constant and a different dipole moment in gas (1.86 D) and bulk phase (2.4-2.6 D) [77]. The water high dielectric constant permits an effective decrease in the electrostatic interactions (charge screening) allowing high solubility of salts.

The chemical nature of the interactions between the first shell of water molecules and the groups present at the surface is of extreme importance to the properties of the hydration water. For instance, in the presence of nonpolar solutes water forms polygonal cages around the solute with the first shell of water molecules forming the maximum number of possible hydrogen bonds between them [75]. Additionally, to reduce the number of first shell water molecules and associated decrease in entropy, the nonpolar solutes, above a certain concentration, associate in water. The aqueous solvent provides the driving force (entropic) for the self-assembly of nonpolar solutes.

II.4.2 Interfacial Water in Biological Supramolecular Assemblies

The biological stability of a supramolecular assembly strongly depends on the water present at the interface of the biological structures and, at such constrained environment the water-macromolecule and water-water interactions have a primary role in physiological processes [78]. For instance, the water that is solvating DNA does not have the same interactions and, therefore, an equal pattern behaviour than the one confined to lipid bilayers [79].

In solution, the intermolecular forces that promote or repel the interaction between macromolecules are the attractive Van der Waals and repulsive double layer forces [80, 81]. While the presence of the former is irrevocably, the double layer force is dependent on the existence of a surface charge. Moreover, studies with neutral bilayers, in water, revealed a strong exponentially repulsive force when they were separated by nanometres [82]. This disjoining force is due to the oriented boundary layers of water adjacent to the surfaces restricting the approximation of macromolecules and colloids [83].

Molecular dynamics revealed that water presents a tetrahedral ordering from the membrane surface that exponentially decreases with the distance from the bilayer surface [84, 85]. Furthermore, the dynamics of membrane bound water is significantly reduced compared to bulk water [86], showing a dependence with lipid headgroup [87-90] and apolar part [88]. The presence of cholesterol, influences bilayers hydration increasing the number of bound water per phospholipid, due to a larger distance between adjacent phospholipid headgroups [88, 91]. Accordingly, in DPPC and DMPC bilayer, a high cholesterol content promotes an inefficient packing of the acyl chains, increasing water penetration (see II.3.2 above) [92].

The effect of macromolecules promoting order in water like structures generates the so-called hydration force [93]. This hydration force was confirmed as a dominant short range interaction (1-3 nm) accounting for a repulsive pressure between bilayers [82]. The ordered water layer may modify properties at the membrane interface, like the electrostatic dipole potential, or its physical features such as the main transition temperature [94]. Those bilayer properties will affect the activity of membrane associated proteins as is the case for voltage gated pumps [95].

II.5 Electrostatic Potential of a Membrane

"The positive potential presumably arises at the level of the dipoles of the ester linkage, with the oxygens oriented towards the aqueous phase. The general implications of such a potential for membrane transport have only just begun to be considered."

By Haydon , D A and Hladky, S B (1972)

II.5.1 The Membrane Electric Profile

There are numerous membrane-mediated physiological processes such as, adsorption/desorption of peripheral and insertion/desorption of acylated membrane proteins, ionic channels and solutes transport which affect or involve movement of charge within or through the membrane. The hydrophobic core of the membrane constitutes an energetic barrier to the transfer of polar solutes and ions between both sides of a cell. Therefore, the discovery of particular ion-transporting proteins elucidated the mechanisms behind their transport. One of the stimuli that regulate the opening of these channel proteins is the voltage across a bilayer, e.g. Na^+, K^+ Ca^{2+} ion pumps. The electric field, generated by the movement of ions, varies the membrane potential, which changes the proteins conformation and allows the unidirectional transportation of ions. Hence, this transmembrane potential ($\Delta\Psi$) is responsible for regulation of ion-pump proteins [9]. It is accepted that the main origin for this transmembrane potential relies in the dissimilar charge balance between the inside and outside of the cell.

The distribution of specific ions inside and outside cells is not at equilibrium. This asymmetry, together with the distinct permeability of each ion, generates a charge unbalance which leads to the development of a transmembrane potential of about 10-100mV being the cytoplasmic side negative relative to the outside [96]. This potential can be readily measured by placing a microelectrode on both sides of the membrane, using fluorescent probes, hydrophobic ions or Spin-labeled EPR probes [12]. At the steady state the transmembrane potential can be determined from the relative ions concentrations ([X]) and their relative permeability (P_x), applying the Goldman-Hodgkin-Katz equation.

$$\Delta\Psi = -\frac{RT}{F}\ln\left(\frac{P_{K^+}\left[K^+\right]_{in} + P_{Na^+}\left[Na^+\right]_{in} + P_{Cl^-}\left[Cl^-\right]_{out}}{P_{K^+}\left[K^+\right]_{out} + P_{Na^+}\left[Na^+\right]_{out} + P_{Cl^-}\left[Cl^-\right]_{in}}\right) \tag{II-2}$$

where R is the gas constant, T is the temperature and F is the faraday constant. This equation is for a case where the K^+ Na^+ and Cl^- are the dominant permeable ions.

Typically most biological membranes have negatively charged phospholipids (see II.2.3 above for details), resulting in a negative surface charge. This superficial charge is electrically neutralized by the counterions, which create a diffuse double layer. Therefore, in the presence of charged lipids a surface potential component must be considered, in addition to the transmembrane potential, when the electrostatic potential of the membranes are considered. This reports the potential difference between the membrane surface and the aqueous bulk.

The surface potential exponentially decays over a certain distance from the membrane surface, and its measurement is not a simple task. The common method to experimentally evaluate the surface potential is through the measurement of the zeta-potential (ξ). This is the potential at the hydrodynamic plane of shear, usually considered to be about 2 Å beyond the charged vesicle surface [97]. The ξ potential can be calculated from the electrophoretic mobility (μ) of lipid vesicles, which in an electric field will migrate towards an electrode of opposite sign, using the Henry equation [98].

$$\xi = \frac{3\eta\mu}{2\varepsilon_0\varepsilon_r f(ka)} \tag{II-3}$$

where η is the aqueous solution viscosity, ε_0 is the permittivity of free space, ε_r is the relative permittivity of the medium and $f(ka)$ is the Henry function. The zeta potential of biological membranes is usually only tens of millivolts in magnitude.

In a bilayer, lipids are subject to a restricted orientation with the hydrocarbon chains facing each other forming a nonpolar region and the headgroups in contact with the aqueous solution. This orientation of the lipids leads to preferential orientation of their dipoles as well as to an orientation of the water molecules interacting with the interface. The alignment of dipoles leads to a new potential called the dipole potential, which magnitude is ≈ 400 mV in PC monolayers [99].

According to the aforementioned, it is clear that the electric profile of a biological membrane does not change linearly across the bilayer. Instead it depends on the sum of several internal potentials from different origins such as the transmembrane potential, the surface potential and the dipole potential (Figure II.8). From the three electrostatic potential components of lipid bilayers, the dipole is the less well characterized due essentially to the experimentally drawbacks of its measurement. Furthermore, this potential decays over a small distance within the membrane, of approximately 1nm (lipid headgroup region), generating an electric field, in monolayers, in the range of 10^8-10^9 V/m. This magnitude is much larger than the transmembrane potential (≈90 V/m) [9]. During the last decades, several approaches have been followed to obtain information on the magnitude of the dipole potential (either using lipid monolayers or vesicles). In the next section the different methodologies available to measure this potential will be presented and the advantages and drawbacks of each one will be discussed.

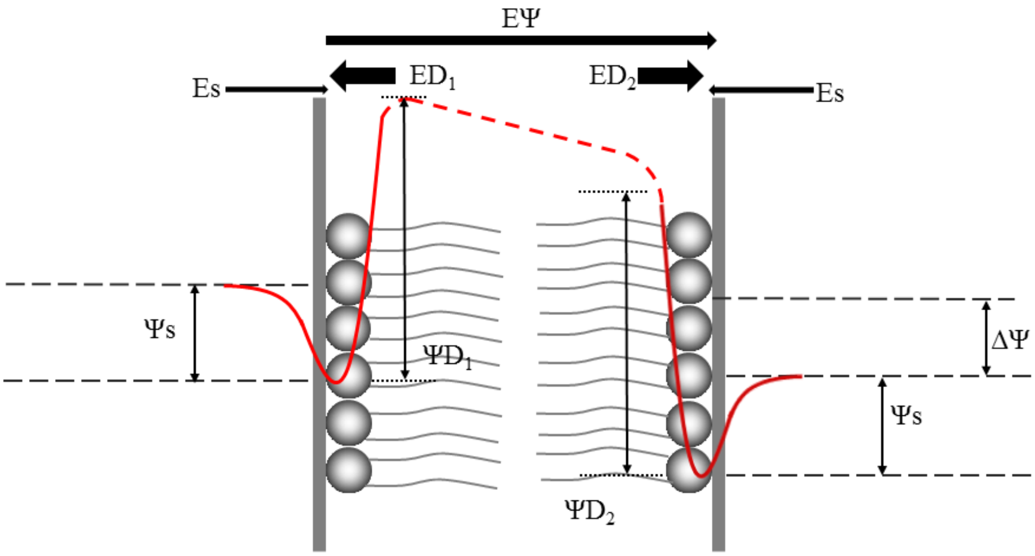

Figure II.8. Electrostatic potential profile across a symmetrical membrane with different ion concentration in each side of the bilayer. The figure shows the transmembrane potential (ΔΨ), the surface potential (Ψs) and the dipole potential of both monolayers (ΨD$_1$, ΨD$_2$). Electrical fields of these potentials are represented by arrows in the upper part of the figure. Adapted from [100].

II.5.2 Methods to Measure the Membranes Dipole Potential: A Long Way to Go…

The dipole potential of lipid membranes can be obtained through two distinct approaches. One uses monolayers of lipids, formed at an interface between water and air, and in the other the potential is obtained using bilayers but is an indirect measurement that relies on molecular probes (from the study of permeability of different ions or ratiometric behaviour of external probes). The dipole potential determined using monolayers is direct, yet, the properties of the monolayers may differ from those of half a bilayer.

The most common method to obtain the dipole potential in monolayers is the Kelvin or Vibrating plate method, in which an applied voltage suppress the potential difference when the dipoles are at the air-water interface [99]. Typically, the difference in potential that arise due to the dipoles present at the interface is approximately 400 mV for PC monolayers [99]. The potential in monolayers is, usually, recovered at a pressure of 30 mN/m accepted to be the lateral pressure in bilayers. Nevertheless, the results obtained in monolayers are higher, 100-200 mV, then in bilayers. Brockman *et al* put a lot of effort trying to understand and analyse this difference, which had to do with the methodology and its limitations [99]. One of the major contributions attributed to the different dipole potential obtained in monolayers and bilayers is related with the water rearrangement that occurs at air/water interfaces in the presence of a lipid monolayer. The potential measured is the difference between the one observed for the lipid monolayer at 30 mN and that of the water/air interface, and changes observed in the water orientation due to the presence of the lipid affect the dipole potential measured. Further addressing this limitation of the monolayers experiments, Brockman include some alterations to the classical Helmholtz equation. It assumed a dielectric constant of 1 and added a potential component due to water rearrangement (Ψ_0).

$$\Psi = \Psi_0 + 12\pi \frac{\mu_\perp}{A} \tag{II-4}$$

The Ψ_0 parameter was extensively studied for several types of lipids and lipid mixtures. They observed that it was dependent on the lipid being approximately

100-150 mV for phosphatidylcholines and close to zero for the negatively charged lipids. With this component, the agreement between the values obtained for monolayers and bilayers improved. However, this interesting and thorough work done by Brockman did not have continuity and this area independent potential did not get out of the speculative field.

In bilayers, two approaches were used to measure the dipole potential. In the first approach Liberman and Topaly,1969, estimated the dipole moment comparing the activation energies for permeation of two hydrophobic ions, which was smaller for the anion than for cation due to a positive membrane potential in the interior [101]. However, they neglected the distinct hydration energies of the ions considered, which proved to be significant leading to a large inaccuracy in the final dipole potential obtained. The second methodology, introduced by Gross *et al* [100], measured the fluorescence shifts in voltage sensitive dyes, such as RH421 and di-8-ANEPPS (Figure II.9). However, to apply this methodology some requirements must be attained. First the concentration of probes must be low enough so that the membrane dipole potential is not affected by the presence of the probe. Second, the probe must report exclusively the dipole potential and no other changing membrane features such as fluidity. However, this is not always attained and both RH421 and di-8-ANEPPS showed a strong dependence with membrane viscosity being the choice of the emission wavelength crucial to avoid this effect. Another limitation of this method is due to the fact that these probes report changes in the local electrical field, being the fluorescence strongly dependent on the positioning of the chromophore. This subject is particularly important given that the membrane electric profile is a sum of several potentials, therefore, depending on the interfacial localization the probe may be sensing other potential change rather than membrane dipole potential. Moreover, to correlate the fluorescence shifts and the membrane dipole potential, for RH421 and di-8-ANEPPS, a calibration curve was performed using the membrane dipole potential observed in monolayers and a final correlation value of 0.8 was obtained [102]. Therefore, the experiments using ratiometric probes require a careful design to relate the observed changes with the membrane dipole potential and for each probe used a detailed study with different membranes must be done in order to confirm that the probe is actually reporting the membrane dipole potential.

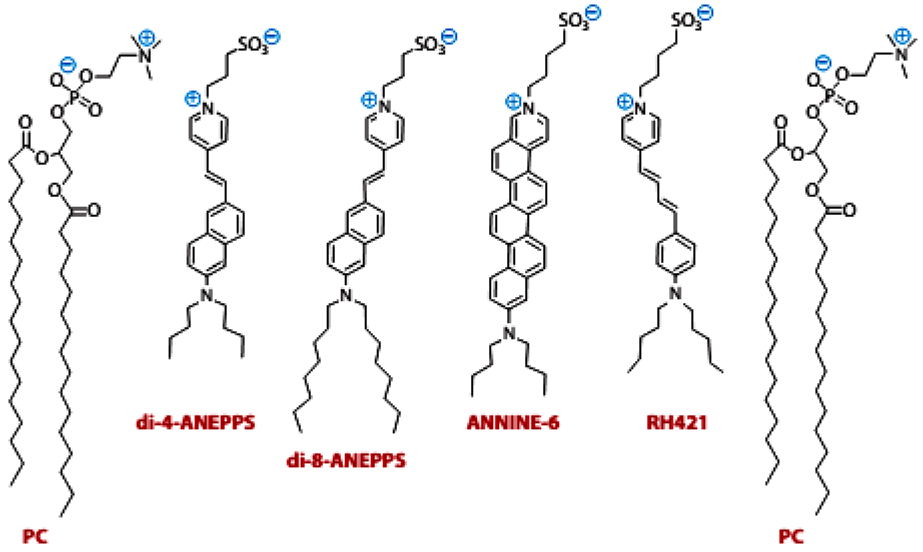

Figure II.9. Structures of styryl probes used in dipole potential measurements. The probe location is illustrated by showing two phosphatidylcholine (PC). From reference [103].

During this topic, we established that none of the conventional techniques, due to their limitations, gives a solid and reliable value for the dipole potential of biological membranes. Although the dipole measurements using monolayers may be not comparable to the real one in bilayers the drawbacks found using other methodologies lead us to measure the dipole potential using monolayers. Moreover, the monolayers technique is one of the main methodologies to obtain the dipole potential, and there is a considerable amount of data available

II.5.3 Contributions to Membrane Dipole Potential and Models in Monolayers

The potential in the water lipid interface may be subdivided in two distinct kinds of potential, the surface potential and the dipole potential. While the former is well described using the Guoy-Chapman theory the latter is very difficult to estimate and measure.

The breakthrough experiment of Liberman and Topally, 1969, revealed that two structurally related hydrophobic ions (TPB^- $TPBB^+$) were able to permeate lipid bilayer at surprisingly different rates. From electric conductivity measurements they observed that the negative hydrophobic ion had a 10^5 times higher conductivity than the positive ion. Assuming the same diffusion coefficient they speculated that a different partition coefficient towards the bilayer centre would originate their distinct conductivity. According to these results they hypothesized that the membrane had a positive potential inside [101]. The term dipole potential, however, emerged a few years later, also, from conductivity experiments [104].

During the years, the research community has spent a meaningful amount of time, investigating the contributions to the membrane overall dipole potential. It is now accepted that the phospholipids headgroups, the carbonyl groups, the terminal methyl groups and the interfacial water molecules promote the major contribution to the global membrane dipole [99, 105]. In phospholipid headgroup region there are the $P^{\delta+}–O^{\delta-}$, the $C^{\delta+}= O^{\delta-}$ and $P^{\delta-}–N^{\delta+}$ dipoles, which account a total dipole moment of ≈20 D. In PC the $P^{\delta-}–N^{\delta+}$ dipole does not contribute significantly to the total membrane dipole potential due to its preferential parallel orientation relative to the membrane surface [106, 107]. However, in ethanolamines the $P^{\delta-}–N^{\delta+}$ is oriented towards the aqueous phase and a contribution to the final dipole moment is expected [108, 109]. Moreover, the binding of charged molecules may also change the magnitude and orientation of this dipole [110, 111]. In the case of the phosphatidic acid (PA), which does not have any $P^{\delta-}–N^{\delta+}$, it is interesting to note that an increase in the dipole moment is observed, suggesting a minor role for this dipole in the global dipolar potential.

The orientation of the carbonyl group of the lipids, pointing towards the aqueous phase, was confirmed through x-ray diffraction [112] and infrared-spectroscopy [113]. Moreover, it has strong dipole magnitude which is positioned near the hydrocarbon region, with low dielectric constant. Those considerations support a significant contribution of this group to the total membrane dipole potential [114]. Furthermore, the replacement of ester-bonded fatty acids chains (DPPC) for ether-bonded alkyl chains, 2-dihexadecyl-sn-glycero-3-phosphocholine (DHPC) showed a 118 ± 15 mV decrease in the overall bilayer potential [115]. However, the contribution from a distinct orientation of the hydration layer can not be ignored.

The role of the $P^{\delta+}=O^{\delta-}$ and $P^{\delta+}–O^{\delta-}$ dipoles in the membrane electrostatic dipole potential has not been studied in detail. Nevertheless a preferential orientation of the oxygen atoms towards the aqueous media, observed through infrared spectroscopy, reinforces the membrane potential [116].

In contrast to the aforementioned dipoles, the contribution of the acyl chains has been controversial [117, 118]. In 1955 Davies and Rideal [119] proposed a role of CH_2 groups in the membrane dipole potential. However, in late 80's Vogel and Mobius [120] assumed that only the terminal methyl groups contribute to the final dipole potential. In 2002, a study using black lipid membranes showed a reduction in the final dipole potential due to the substitution, in one hydrocarbon chain, of carbons by sulphur atoms. They conclude that the methyl groups contribute for the increase/decrease in lipid packing, therefore, changing the dipole potential [121].

The contribution of water molecules to the membrane dipole potential arises from many evidences. First the lipid dipole potential in monolayers shows a strong dependence with the composition of the subphase (despite their related area per lipid). Secondly, structurally distinct lipids revealed a similar dipole potential, highlighting the role of the solvent [122]. Third, in DHPC membranes the dipole potential was positive inside, although the absence of the carbonyl group, and the authors proposed a compensation by the water molecules [115]. Moreover, the ions nature, present in the subphase, significantly influenced the water organization, changing the dipole potential [123].

The discovery of new molecular contributions to the membrane dipole potential was, closely, supported the mathematical models using monolayers (Figure II.10). Considering that most lipids are zwitterionic at physiological pH the dipole potential can be assumed as resulting from the sum of dipoles present in the lipid and water. Therefore, the presence of lipid molecules in the interface may be interpreted as a capacitor between air and water. Based in this capacitor model and assuming a dielectric constant for the interfacial region of 1 Helmholtz generated an equation that relates the dipole potential with the area per lipid in monolayers:

$$\Delta\Psi = 12\pi \frac{\mu_{\perp}}{\mathrm{A}} \tag{II-5}$$

where $\Delta\Psi$ is the dipole potential, $\mu_{\perp}$ is the effective molecular dipole moment oriented according to the normal of the interface and A is the molecular area occupied by each lipid (see [99] for details). However, this model does not distinguish between the contributions of the several dipoles situated at different localizations within the monolayer. Therefore, Vogel and Mobius described the two layer capacitor, and then Davies and Rideal introduced the three layer capacitor equation. This is the recent theoretical model, which was improved by Demchak and Fort to include the effective dielectric constants in each layer (II-6) [124].

$$\Delta\Psi = \frac{1}{A\varepsilon_0}\left[\frac{\mu_1}{\varepsilon_1}+\frac{\mu_2}{\varepsilon_2}+\frac{\mu_3}{\varepsilon_3}\right] \tag{II-6}$$

where, μ_n and ε_n are the dipole moment and the dielectric constant at different regions of the monolayer (for more details [125]).

The sources of the dipole potential, briefly addressed in this section, not only reveal the contribution of the aligned dipoles present in the lipid molecules but also the ones that are present in the solvent. The contribution of each one to the final membrane dipole potential is experimentally impossible to obtain because of the inherent limitations presented, nevertheless, the ever growing literature concerning the dipole potential importance in membrane-mediated physiological processes makes the answering of the origins of the dipole potential a crucial concern.

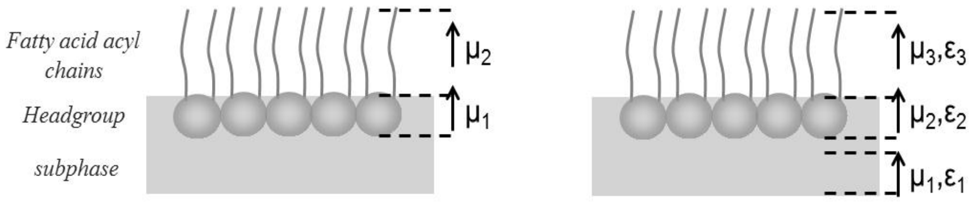

Figure II.10. Schematic representation of the Voglius Mobius 2-layer (left panel) and Demchak and Fort three-layer (right panel) capacitor model of monolayer and at the air-water interface. While in the 2-layer model the μ1 represents the lipid headgroup moment as well as the effects in the subphase the tree-layer capacitor separates the headgroup momentum from the moment arising from effects occurring in the subphase, additionally it adds the different permittivity constant in each region. Adapted from [125].

II.5.4 Biological Role of the Membrane Dipole Potential

The magnitude of the dipole potential, significantly larger than the other membrane electrostatic potentials, highlights its important biological function. Moreover, the cell developed several pathways through which the membrane dipole potential may be affected, such as changes in the lipid headgroup, lipid compositions or cholesterol content. Hence, the developments of these pathways, that may modify/regulate the membrane potential, may constitute an indirect proof of the important biological role of membrane dipole potential.

In their structure proteins have several polar groups, being polarizable macromolecules. Therefore, when subjected to an electrical field they have different responses such as topology changes. These conformational changes are particularly important in membrane attached proteins, where the protein orientation is constrained by the anisotropic nature of the membrane. Typically the transmembrane portions of proteins are organized in an alpha-helix secondary structure with all the peptide residues oriented in the same direction along the helical axis (Figure II.11). A single peptide unit has a characteristic dipole moment of 3.5 Debye. Considering that 20-25 amino acid residues are necessary for an alpha helix to cross the hydrophobic core of biological membranes. This would account for a total dipole moment of 70-88 Debye with the partial positive net charge at the amino terminal and a negative charge at C-terminal. Roughly this electrostatic dipole moment corresponds to the appearance of approximately two opposite sign 0.5 elementary charges in each side of a 4 nm bilayer [126]. Membrane proteins need to be oriented to develop their function as channels or transporters. We speculate that the interaction between membrane dipole potential and protein dipole moment is a major determinant in the orientation and function of membrane proteins.

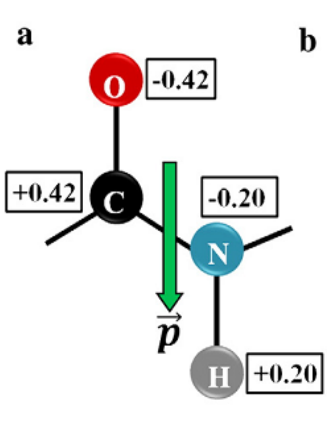

Figure II.11. Dipole arrangement in proteins. Panel A: Dipolar charges on a peptide bond. Panel B: Multiple peptide dipoles aligned along the axis of theα-helix summate to produce a macrodipole. From reference [127].

The effect of the dipole potential has been essentially overlooked by the scientific community and is addressed in very few studies. One of those works showed that the mechanisms for the formation and dissociation of the gramicidin channel involve dipole movements, which are controlled by the membrane dipole potential [128, 129]. In another work, the activation of Phospholipase C, due to the mediated bradykinin receptor leads to an increase in the intramembranous potential. Given that the surface and transmembrane potentials were minor contributors, the authors hypothesized that the dipole potential increase was due to a higher dipole moment of the reaction product (Dyacylglicerol) compared to substrate (phosphatidylinositol) [1].

In order to unravel the biological role of the membrane dipole potential, most of the scientific literature uses molecules that once inserted in the membranes change its dipole potential (*e.g.* phloretin and 6-Ketocholestanol). The addition of phloretin leads to an increase in the translocation of cations while for anions it decreases. This was attributed to the phloretin mediated decrease in the membrane dipole potential. Moreover, changes in the membrane dipole potential lead to opposite effects in conductance and lifetime of the voltage-gated syringomycin E channel [130, 131]. The association of β-amyloid peptide (Aβ) with negatively charged lipid membranes was inhibited by the presence of phloretin [132]. This methodology may seem very indirect or even controversial due to the addition of molecules, which biological function may be far beyond the change in the membrane dipole. However, evidences for the membrane dipole potential physiological role start to grow.

The cholesterol and sphingolipids in biological membranes form a liquid ordered phase which is segregates from a fluid phase composed of PC, called rafts. This ordered phase has a higher dipole potential than the rest of the membrane. As aforementioned membrane proteins have a well oriented and considerable dipole moment, can their segregation into, or out off, lipid rafts be modulated by the membrane dipole potential?

II.6 Membrane Dynamics and Permeability

"It occurred to me early on that all those compounds that are readily soluble in ether, fatty oils, and similar solvents, or better are more readily soluble in these than they are in water, for that is what really matters, penetrate faster into the Protoplast; whereas those compounds that are readily soluble in water but very sparingly soluble in fatty oils do not penetrate or only penetrate the Protoplast extremely slowly."

By E. Overton (1899) (translated by W. Vaz)

II.6.1 Lipid Dynamics

The biological membranes are highly flexible and dynamic self-assembled structures that can undergo conformational transitions vital to several biological processes. This membrane dynamic state is related to the phospholipids motions that can go from individual motions; such as trans-gauche isomerization and bond oscillation; phospholipid rotation about a long axis; lateral diffusion; phospholipid transbilayer movement (Flip-Flop); to combined motions like undulations of large patches of the membrane (Figure II.12).

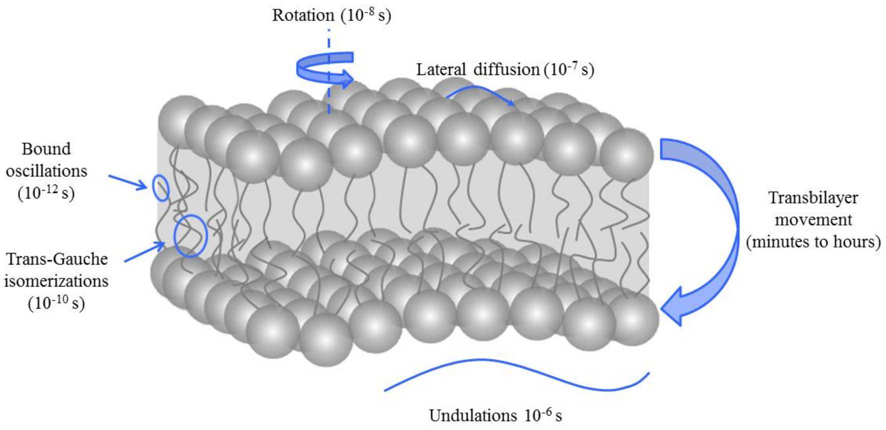
Rotation (10^{-8} s)
Lateral diffusion (10^{-7} s)
Bound oscillations (10^{-12} s)
Trans-Gauche isomerizations (10^{-10} s)
Transbilayer movement (minutes to hours)
Undulations 10^{-6} s

Figure II.12. Schematic representation of membrane lipid motions and their characteristic time scale for a bilayer in the fluid state. Adapted from [133].

Membranes conformational and dynamic transitions at different time scales are biologically relevant. Macroscopically, the lateral diffusion of lipids affects signal transduction processes and microscopically, the membrane fluidity and order has a considerable impact in solute permeation and uptake/release processes. The membrane fluidity implies that all its components, even the proteins, are able to have different types of motions with different time scales. Additionally, changes in membrane fluidity may strongly affect the electrical profile of a membrane. It is known that sterols modulate the properties of a bilayer not only in its fluidity but also in the membrane dipole potential. Therefore, by changing its fluidity/dipole potential the membrane may modulate the interaction and permeability of dipolar molecules. Accordingly, our research group showed that amphiphilic molecules partitioning and kinetics of interaction is different for membranes containing cholesterol [134-136].

II.6.2 Membrane Permeation

The permeability restrictions in membranes allow the establishment of solute concentrations gradients which are very important in biological systems. Transport across biomembranes is however crucial in many cellular processes and its importance is being increasingly acknowledged in medical and pharmaceutical industry [137].

There are different pathways for a molecule to pass through a lipid membrane. While in passive transport mechanisms, the permeation of particles through the bilayer occurs in the direction of a concentration gradient. In active transport, particles may go through the bilayer in the direction opposing the concentration gradient, requiring the consumption of energy. If the permeation of most solutes, across membranes, were done through carriers the cell would spend a considerable amount of energy synthesizing these highly distinct protein assemblies. Moreover, several xenobiotic would not be able to permeate these biological barriers, given their structural diversity. Since most of the pharmaceutical active drugs are not substrates of the carriers available in biomembranes, the passive diffusion is a major process for their absorption.

The membrane permeability was first addressed by Overton who, together with Meyer, formulated the well-known rule for passive permeation. Briefly, it states that the permeability coefficient of a molecule correlates linearly with its partition coefficient between oil and water [4]. In other words, a more hydrophobic substance would permeate the membrane faster than a more hydrophilic. This correlation, accurately predicts the permeability trends for a large number of solutes and, most of the currently used permeability models account for this relation between permeability and partition coefficient.

II.6.2.1 Solubility-Diffusion Model

Based on the Overton's laws for the permeation the solubility-diffusion mechanism emerged. It treats the membrane as a thin static slab of hydrophobic matter surrounded by an aqueous environment [138]. This model makes some simplifications and assumptions which may challenge its reliability such as; the rate-limiting step for a solute to cross a membrane is its diffusion through the bilayer hydrophobic region. Nevertheless, this model has been extensively and successfully applied to predict the permeation of small nonpolar solutes across the lipid bilayers. Accordingly, for the permeating solute to cross the membrane it has to follow three important steps:

1) Partition of the permeant into the hydrophobic region of the membrane

2) Diffusion across the apolar region of the membrane

3) Partition into the aqueous phase on the other side of the membrane

This model, in essence, combines the Overton's rules for permeability across a bilayer with Fick's first law of diffusion which describes the movement of the solute down a concentration gradient, allowing the calculation of a solute permeability coefficient (P) across a membrane.

$$P = K_p \frac{D}{d} \tag{II-7}$$

Where, K_p is the partition coefficient, D is the diffusion coefficient (m^2/s) across the hydrocarbon region and d (m) is the bilayer thickness. However, some inconsistencies using this model and the experimental results are described below.

For more ordered membranes (high cholesterol content) there is a divergence of the experimentally obtained permeability coefficient with the one obtained through the model [139]. Furthermore, depending on the hydrophobic nature of the solute the main barrier for permeation may not be the bilayer hydrophobic core [140]. Accordingly, our group showed that in a homologous series of fluorescent fatty amines the translocation step is not always the rate-limiting step [141].

A major discrepancy between the predicted and the experimentally obtained permeability was observed for ions. The main source for this inconsistency is their relative insolubility in the membrane (low partition coefficient), which is described by the Born energy electrostatic term. This term reports the energy involved in the transfer of an ion or dipole from a medium with a high dielectric constant (water) to a medium with a low dielectric constant (membrane interior). To account for the failure of the solubility-diffusion model in the description of ion permeability, an alternative solute permeation mechanism emerged. In this model, the permeant is assumed to cross the bilayer through transient water-filled pores, produced by thermal fluctuations in the bilayer (Figure II.13, Panel B). These membrane thermal fluctuations create some voids that are filled by water molecules, forming with each other hydrogen bonds and creating a hydrophilic pore. This pore allows the charged particles to overcome the Born energy required to permeate and explain the high permeability rates encountered by Nichols and Deamer for protons and hydroxyl ions.

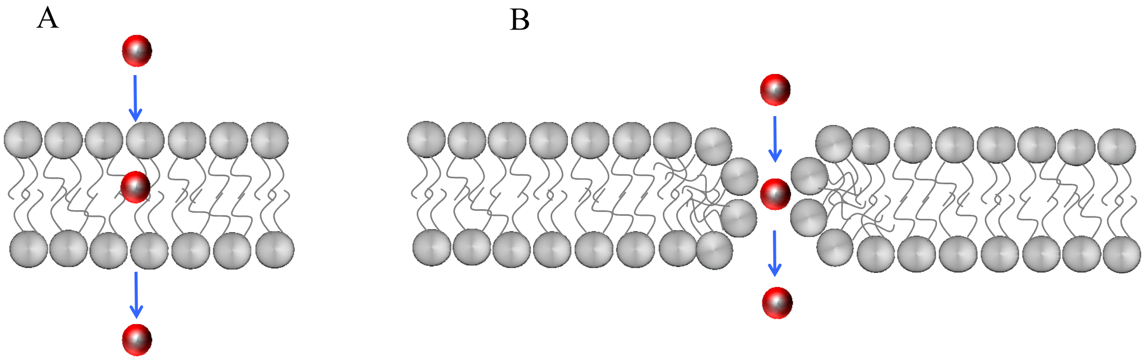

Figure II.13. Two distinct mechanisms for solute permeation across membrane. Panel A: The solubility-diffusion mechanism. The solute in one side of the bilayer enters in hydrophobic core diffuse across the bilayer and leaves in the other side of the membrane. Panel B: Permeation through transient hydrophilic pore formation due to thermal fluctuations.

From the two models presented above it is clear that while the solubility-diffusion model correctly predicts the permeability of small and neutral solutes with a large affinity for membranes, for small polar solutes (ions) the results are best explained by the pore mechanism. Consequently the applicability of the solubility-diffusion model is much broader than the pore mechanisms. Despite its vast applicability the solubility-diffusion model simplifies a complex system such has a bilayer and exceptions (besides proton permeability already mentioned) have been found that may question the model. If we consider the case of amphiphilic molecules, which have a preferential orientation in the membrane exceptions to this model may occur, even within structurally related solutes [141]. This oversimplified vision that the solubility-diffusion model imposes to the biological membranes, lead to the appearance of more complex models. An example is the 4 regions model by Marrink and Berendesen, which divide the membrane in 4 regions with different properties [142, 143]. Another example is the 3 layers of Nagle that calculates the permeability across a bilayer by combining the permeation across each layer [144].

The alignment of the lipids in membranes, with their polar groups oriented to the aqueous phase and the non-polar hydrocarbon chains oriented towards the bilayer mid-plane, generates transversal gradients of polarity, density and charge. This asymmetry is described by the membrane large internal dipole potential that arises from preferred alignment of lipid and water dipoles, at the membrane-solution interface. Moreover, most membrane permeating drugs are amphiphilic and have a considerable dipole moment which provides a preferential alignment of the drug in the membrane. Therefore, the electrostatic interplay of drug dipole moment and membrane dipole potential should be an important factor affecting the permeability of amphihilic drugs. However, the lack of knowledge of the correct partition coefficient and diffusion rate constant across the bilayer for a large number of molecules makes this task challenging.

II.6.2.2 Factors Influencing the Membrane Permeability

Molecules permeability across membranes depends on several factors, which correlate with the membrane and solute chemical properties such has dipole moment [145, 146]. The relationship between solute properties and bilayer structure may contribute to a deeper understanding of rules that govern drug permeation, and new improved predictive models for unique groups of molecules could arise. Moreover, the ability to forecast drug permeability across biological barriers such as membranes is a valuable tool in drug design and modulation.

In this topic, we will briefly, address some molecular factors that are significant in drug modulation and design to predict their permeability across biological membranes.

II.6.2.2.1 Partition Coefficient

In drug development and design, the oil/water partition coefficient (K_p) is a central parameter because the biological fate of a drug (absorption, distribution, etc) until it reaches the final target involves the passage through several lipid membranes. Therefore, the drug effectiveness is associated to their tendency to permeate these membranes. As described above, Overton made the correspondence between the solute permeation and its ability to solubilize in the hydrophobic interior of the lipid bilayer [4]. This propensity for molecules to be more/less soluble in the membrane may be estimated by their partition coefficient, which describes the solute concentration ratio in the hydrophobic and the aqueous phase at equilibrium. Hence, a larger partition coefficient point out a greater affinity of the solute for the lipid phases (higher lipophilicity).

The Kp estimates drug lipophilicity and, frequently, it is obtained utilizing octanol as solvent to mimetize the membrane.

$$Kp_{o,w} = \frac{[X]_o}{[X]_w} \qquad (II\text{-}8)$$

Where, $Kp_{o,w}$ is the partition coefficient between octanol (o) and water (w) and [X] represents the molar concentrations of species X. This partition coefficient is widely used essentially due to its relative simple experimental determination and the success in determining the permeability of several related solutes. However, there are several limitations which make the *K*p octanol/water a questionable approximation. i) the octanol homogeneous phase does not account for the complexity of biological membranes, and the interactions between drugs and membranes may not be well described by a simple homogeneous fluid; ii) biological membranes have several lipid compositions which can not be mimicked by octanol; iii) the apolar environment of octanol do not support the introduction of membrane proteins.

The anisotropic nature of biological membranes makes the use of the partition coefficient octanol/water, commonly considered to represent K_p, a very shallow approximation. This may in fact, explain some deviations of the solubility diffusion model to the experimental results. It is therefore extremely important to determine the correct partition coefficient of the amphiphiles to membranes. This will enable the accurate assessment of the permeability rate.

Moreover, by studying the partition coefficient of amphiphiles with distinct structural properties, *e.g.* headgroups, allows the establishment of rules, which govern their permeation. Some rules are already well established and will be presented below.

II.6.2.2.2 Hydrogen Bonding

The hydrogen bond capacity of a solute has a crucial role and can significantly affect its permeation across biological membranes. Depending on the ability of the solute to establish hydrogen bonds with water (water solubility) or lipid headgroups the partition and the translocation energy barrier may be affected. Upon transfer from water to the apolar membrane interior, the polar groups of the solute will suffer desolvation. Additionally, lipid bilayers have several groups located in the phospholipid headgroup region that are able to establish hydrogen bonds. In order to translocate, a solute must be hydrophobic enough to break all the hydrogen bonds and overcome the energy penalty.

Partridge *et al*, 1979, showed that the blood brain barrier (BBB) penetration increased with the lowering of the solute overall ability to hydrogen-bond [147]. Moreover, permeation studies of several compounds across the BBB indicated that the parameter Δ log P, which is related to the overall hydrogen-bonding ability of a compound, has a strong correlation with experimentally determined brain permeation [148]. The compound hydrogen bond ability is a fundamental chemical property (descriptor) to predict the permeability of new drugs across membranes, and its most simple estimation relies on the calculus of H-bond donor and H-bond acceptor of the drug. Nevertheless, depending on the software, more complex models related to the compound hydrogen bond ability may be applied [149, 150].

II.6.2.2.3 Molecular Size

Lieb and Stein (1969) compared the size dependence for solutes permeability and their diffusion across the apolar interior of the membrane. They established that solutes with higher molecular weight would diffuse more slowly in the membrane hydrophobic core [146]. Accordingly, other study [151] using small solutes with partition coefficients ranging over 4 orders of magnitude, observed that the dependence of the partition coefficient with the solute size could not explain the high permeability found. Therefore, the size dependence diffusion through the hydrocarbon core was the main reason. These studies, however, showed that the comparison between the membrane interior and an isotropic hydrocarbon solution was simpleminded, being the membrane close related to a soft polymer [146, 151, 152].

In the 90´s simulations revealed that there is a molecular size dependence for solute partition, and the permeation is a combination of both partitioning as well as diffusion in the ordered-chain region of the lipid bilayer, although their relative roles in determining the overall size selectivity are still unknown [143, 145].

In 2001, Lipinski analysed the permeability of several compounds formulating the well-known rules for drugs absorption, which point out among other factors that drugs with a molecular weight smaller than 500 Da have a favourable absorption [153]. In agreement with the Lipinski rules for permeation, in 1995 Pardridge showed a good correlation between permeation through the blood-brain barrier and logP up to a molecular size threshold of 400-600 Da.

III

Material and Methods

III.1 Material

1-Palmitoyl-2-oleoyl-*sn*-glycero-3-phosphocholine (POPC), 1-palmitoyl-2-oleoyl-*sn*-glycero-3-phosphoethanolamine (POPE), 1-palmitoyl-2-oleoyl-*sn*-glycero-3-phospho-L-serine (POPS), cholesterol (CHOL) and egg-sphingomyelin (SpM) were from Avanti Polar Lipids, Inc. (Alabaster, Alabama, USA) and bovine serum albumin (BSA) was from Applichem (Darmstadt, Germany). The 5-carboxyfluorescein, succinimidyl ester (single isomer) (CBF) and rhodamine green carboxylic acid n-hydroxysuccinimidyl ester hydrochloride 5(6)-mixed isomers (RG) were from Molecular Probes and 1,2 dipalmitoyl-*sn*-glycero-3-phosphoethanolamine-n-(lissamine rhodamine B sulfonyl) (Avanti) (RhB-DPPE) was from Avanti. The tetradecylamine was from Fluka. All other reagents and solvents were of high purity grade, from Sigma-Aldrich Química S.A. (Sintra, Portugal).

The aqueous solutions used throughout this work were prepared using distilled water (Aquatron A4000), further purified in a system containing particles and charcoal filters and UV irradiation. The final purity of water was evaluated through conductivity analysis and kept below 0.5 μS.

III.2 Equipment

- Steady state fluorescence spectra, fluorescence anisotropy and fluorescence kinetics measurements were performed on a Cary Eclipse fluorescence spectrophotometer (Varian) equipped with a thermostatted multicell holder accessory and automatic polarizers.
- Fluorescence lifetime measurements were done on a home-built TCSPC apparatus with a Horiba-JI-IBH NanoLED at excitation wavelength (λ_{exc}) of 460 nm, a Jobin-Ivon monochromator, a Philips XP2020Q photomultiplier, and a Canberra instruments TAC and MCA as described elsewhere [154].

- UV-Vis absorption was performed on a Unicam UV530 spectrophotometer (Cambridge, U.K.).
- Fluorescence fast step kinetics (up to 1000 s) were performed on a thermostated stopped-flow fluorimeter (Hi-Tech model SF-61) by mixing equal volumes of two solutions, as required for each particular case studied. The λ_{exc} was defined by a monochromator and an appropriate band-pass (Thermo Corion) 520 nm emission wavelength filter.
- The probes purification was performed by High Performance Liquid Chromatography (HPLC) with a Diode Array (model G1315D from Agilent, USA) and Fluorescence detector (model G1321A from Agilent, USA)
- The surface pressure in different monolayers was measured in a Kibron µtrough S instrument

III.3 Aqueous Buffer

The aqueous buffer solution used throughout this experimental work was composed of 150 mM NaCl, 10 mM hepes, 1 mM EDTA and 0.02 % (m:v) NaN_3 and adjusted to physiological pH (7.4) using sodium hydroxide (NaOH).

III.4 Preparation of Large Unilamelar Vesicles (LUVs)

First, 40×10^{-3} M stock solutions of POPC, POPE, POPS, SpM, and CHOL were, independently, prepared in an azeotropic mixture composed of chloroform and methanol ($CHCl_3$:MeOH, (87%:13%, v:v)). To obtain the final desired lipid mixture compositions, appropriate amounts of the pure component solutions were mixed and stirred in a vortex. The solvent was rapidly evaporated to dryness under a gentle stream of nitrogen while the solution was simultaneously heated by blowing hot air over the external surface of the tube. The dry lipid residue was maintained, at room temperature and reduced pressure, in a vacuum desiccator for 6-8 h to remove trace amounts of solvent.

The lipid film was hydrated with a pH 7.4 aqueous buffer (III.3 above) pre-heated in a water bath at 60 ºC, for cholesterol containing mixtures, or at room temperature ~25 ºC, for pure POPC and lipid mixtures without cholesterol. The hydration volume added was previously determined to obtain the final desired total lipid concentrations. The samples were submitted to vortex/incubation cycles, at the described temperatures, until the entire residue was fully hydrated, generally 30-60 min.

In order to obtain 100 nm LUVs the resulting multilamellar vesicle (MLV) suspensions were extruded, using a minimum of 15 passes, through two stacked polycarbonate filters (Nucleopore) with a pore diameter of 0.1 µm (Figure III.1) [155]. During the procedure, the water-jacketed extruder (Lipex Biomembranes, Inc., Vancouver, Canada) was maintained at desired temperature depending on the lipid mixture. The final LUVs samples containing mixtures of lipids were subject to at least two slow cycles of heating, to 60 ºC, and cooling to the lowest temperature used in the experimental work. This heat treatment is called annealing and is widely used in metallurgy refining the structure properties and making it more homogeneous. All the LUVs samples were left to equilibrate for ~1 h at the final experimental temperature.

Considering that the prepared LUVs were used within 1-2 weeks the storage of the samples was different taking into account their lipid composition. While the final cholesterol containing mixtures were stored at the room temperature the other solutions were kept at 7 ºC, all protected from light exposure.

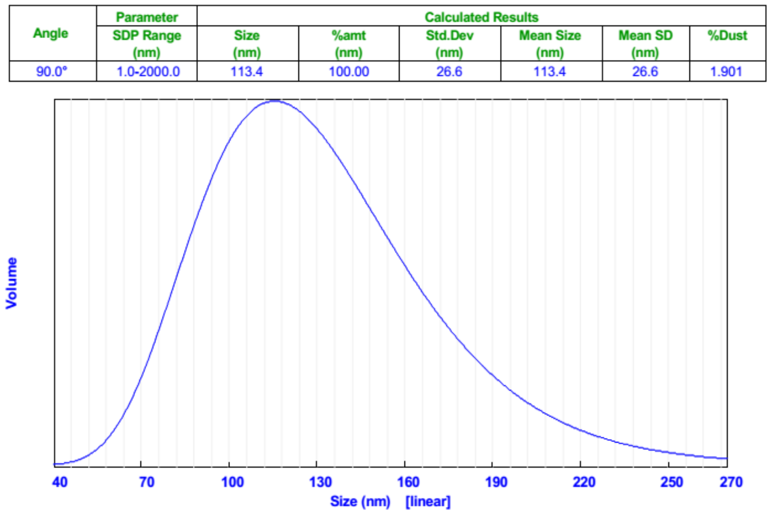

Angle	Parameter	Calculated Results					
	SDP Range (nm)	Size (nm)	%amt (nm)	Std.Dev (nm)	Mean Size (nm)	Mean SD (nm)	%Dust
90.0°	1.0-2000.0	113.4	100.00	26.6	113.4	26.6	1.901

Figure III.1. Typical results, obtained by dynamic light scattering (DLS), for the size distribution of a POPC sample prepared by extrusion through two staked polycarbonate filters 0.1 µm. The average diameter considered for this sample was that given by the volume distribution ≈ 113 nm.

III.5 Liposomes Chemical Composition and Quantification

The methodology, described above, to obtain LUVs is complex having several small steps that end with a turbulent mechanic extrusion procedure therefore, it is reasonable to expect that the total lipid concentration may suffer some small variations. This is more critical when we use complex lipid mixtures where a drastic loss of one or more components may actually induce completely different membrane properties (different phase state). Hence, is fundamental to quantify and analyse the lipid composition of each sample used in the experiments.

The total phospholipid concentration of LUVs was analysed using a phosphate quantification method which was modified from its original version of Bartlett phosphate assay [156]. The cholesterol content was analysed through the Lieberman-Burchard method described by Taylor et al [157]. Both methods are briefly described below.

III.5.1 The Bartlett Phosphate Assay:

- A calibration curve was generated using a stock 1 mM potassium hydrogen phosphate (K_2HPO_4) solution and pipetting appropriated volumes (in duplicate) in a final range of 0-1 μmol.
- The samples, whose phospholipid concentrations remained to be determined, were diluted to a final expected concentration of 0.5 μM (in duplicate) and the final volume of all samples was set to 300 μL using deionized water.
- 700 μL of perchloric acid was added to the solutions which were vortexed, covered with marbles and placed in a block heater at 190 ºC for 1-2 h, until complete colourless.
- After the samples cooling, 2 ml of a solution containing 1% (m:v) of ammonium molybdate and 2 ml of a 4% (m:v) solution of ascorbic acid were added to each tube, and all the samples were kept at 37 ºC for 1-2 h.
- The absorbance of the solutions was read at 700 nm and a calibration curve was obtained as well as the final phosphate concentration of the LUVs samples of interest (Figure III.2, Panel A).

III.5.2 The Lieberman-Burchard Cholesterol Assay:

- A calibration curve was prepared pipetting the appropriated volumes, from a 2.4 mM stock solution of cholesterol in isopropanol to give a final range of concentrations from 0 to 0.5 μmol
- The LUVs samples containing cholesterol were diluted to give a final concentration of 0.25 μM and all the tubes were filled to same volume with isopropanol (100 μl).
- 3 ml of a solution composed of glacial acetic acid, acetic anhydride and sulphuric acid (35:55:10, v:v:v), previously prepared and kept on ice, were added to each tube.

- After 20 min of incubation at 37 ºC the absorbance of the samples was read at 625 nm (Figure III.2, Panel B).

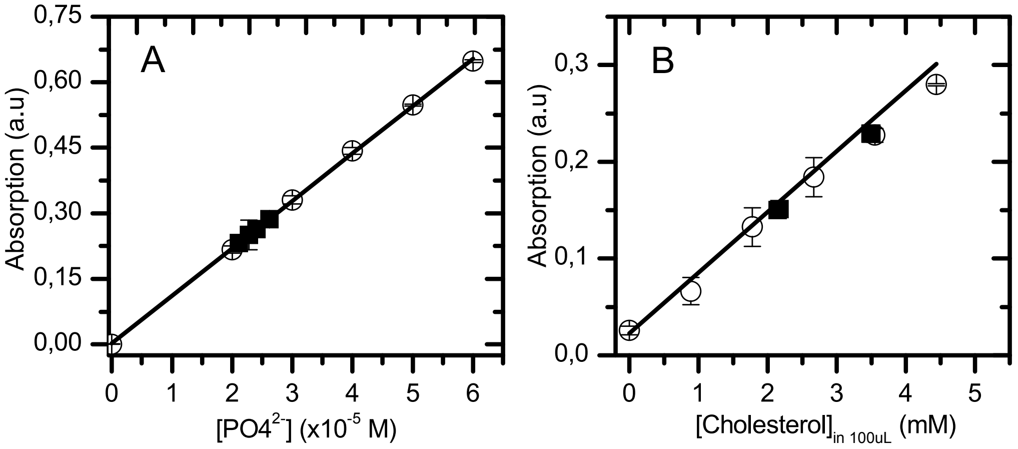

Figure III.2. Determination of the phosphate (A) and cholesterol (B) concentration in LUVs. The circles represent the standard and the squares the sample solutions.

III.6 Synthesis and Purification of the RG-C_{14} and CBF-C_{14} Amphiphiles

The RG-C_{14} and CBF-C_{14} fluorescence amphiphiles were synthesized by the addition of a chloroform/methanol (1:1,v:v) solution containing the tetradecylalkylamine (10-fold molar excess over dye reagent) to a dimethylformamide (DMF) solution of the dye reagent (Rhodamine green carboxylic acid N-hydroxysuccinimidyl ester hydrochloride ‘‘mixed isomers’’ or 5-carboxyfluorescein succinimidyl ester (single isomer)), with a few grains of anhydrous sodium carbonate. Ever since the formation of a precipitate or turbulence was detected in the solution a small amount of DMF was added. The reaction mixture was stirred using vortex and allowed to stand for 24 h at room temperature under constant agitation (exposure to direct light was avoided). The solvent was evaporated at a reduced pressure and using small amounts of methanol, facilitating the evaporation procedure.

The solvent free residue was dissolved in a chlorophorm:methanol (1:1, v:v) solution after which the desired product along with other compounds present in the solution were separated in a preparative thin layer chromatography plate using a chlorophorm:methanol (1:1, v:v) eluent. The final bands with different retention factors were separately removed from the silica with chlorophorm and methanol solution. Considering that methanol also dissolves the silica we performed an additional reverse phase chromatography step using the C_{18}-RP as a stationary phase and methanol as eluent.

The final fractions, with different retention factors, for both RG-C_{14} and CBF-C_{14} were further purified by HPLC through a reverse phase column from Agilent Technologies (Zorbax ODS 4.6×250 mm) with methanol/water (98:2, v:v) for RG-C_{14} and methanol/water (80:20, v:v) for CBF-C_{14}, as eluent. The fraction, suspected to be the one with a higher concentration of the desired probe, was firstly injected and a highest peak appeared in the chromatogram for both probes with a retention time of 8 and 20 min for RG-C_{14} and CBF-C_{14}, respectively (Figure III.3). Given the separations obtained for the peak of interest and other smaller peaks we were able to further purify and isolate fractions containing RG-C_{14} and CBF-C_{14} from the other components, so that only one major peak appeared in the chromatogram. The final purity of RG-C_{14} and CBF-C_{14} was verified being >85% (Figure III.3).

The fluorescent amphiphiles concentrations in methanol solution were determined by absorption spectrophotometry using a molar extinction coefficient of 7.8×10^{4} M^{-1} cm^{-1} for RG-C_{14} and 6.5×10^{4} M^{-1} cm^{-1} for CBF-C_{14} at 502 nm and 490 nm, respectively.

The reaction scheme for the formation of the RG-C_{14} fluorescent probe is represented in Figure III.4.

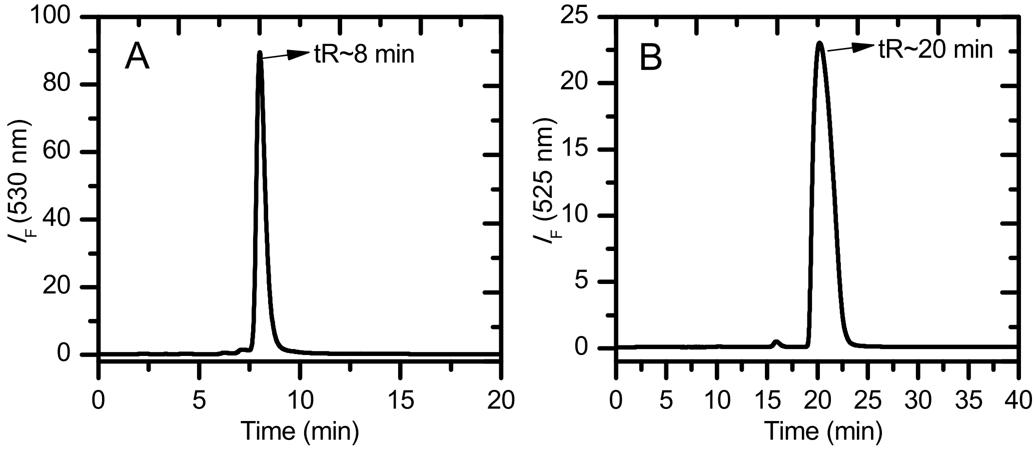

Figure III.3. HPLC chromatogram for the final reaction product RG-C_{14} (A) and CBF-C_{14} (B). Conditions: reverse phase column (see above for details); room temperature; mobile phase, MeOH:H_2O (98:2) for RG-C_{14} and MeOH:H_2O (80:20) for CBF-C_{14}; the detection was performed through λ_{exc}= 502 nm and λ_{exc}= 490 nm with the retention time (tR) of ≈ 8 min; ≈20 min for RG-C_{14} and CBF-C_{14} respectively.

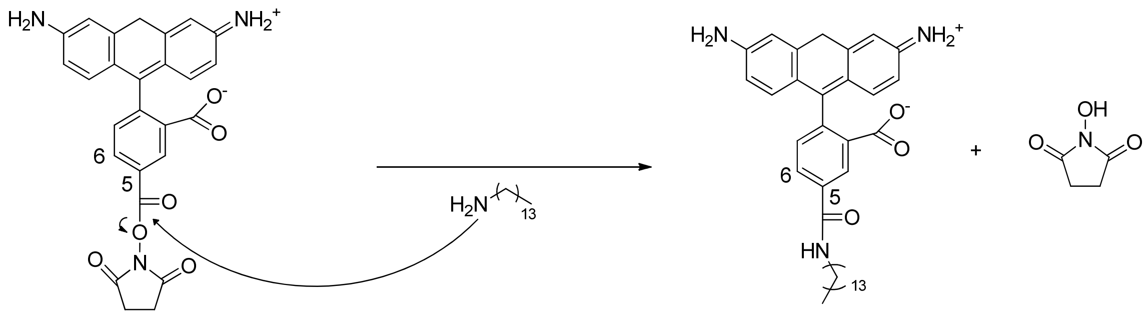

Figure III.4. Schematic representation of the nucleophilic attack of the tetradecylamine to the partially positive carbon attached to the C-5 of the fluorophore (Rhodamine green). A similar chemical reaction leads to formation of CBF-C_{14}.

III.7 Determination of the Amphiphile Critical Aggregation concentration (CAC)

The amphiphile aggregation experiments were performed for a Rhodamine derivative with a shorter (10 carbons) alkyl chain length, RG-C_{10}, due to a predicted very low water solubility of the RG-C_{14} making it impossible to experimentally determine. For CBF-C_{14} and considering it is negatively charged we expected a higher CAC therefore it was directly measured using steady state fluorescence.

A set of 3 concentrated stock solutions of RG-C_{10} or CBF-C_{14} in methanol were prepared so that a minimum volume (20-100 μL) was collected to prepare the different dilutions of interest. Several solutions containing different volumes of each probe, covering the relevant experimental range of concentrations (0-100 nM for RG-C_{10} and 0-25 nM for CBF-C_{14}), was prepared from the methanol stock solutions. Methanol was rapidly evaporated under a gentle nitrogen stream while the solution was simultaneously heated by blowing hot air over the external surface of the tube. The dry residue of each probe was hydrated with 2 ml of buffer solution and gently stirred using vortex (with a very low speed), and the solutions were left to equilibrate at 25 ºC for 1 h. The emission fluorescence intensity of the RG-C_{10} and CBF-C_{14} was observed at 530 nm and 525 nm with an excitation wavelength of 502 nm and 490 nm respectively.

The fluorescence intensity was measured with a cuvette path length of 1cm and a slow integration step so that the spectra had a significant signal:noise ratio.

III.8 Amphiphile Aggregation Studies in Membranes

The LUVs containing the amphiphile of interest were prepared, according to the previously described procedure (III.4 above), using a RG-C_{14} probe: lipid molar ratio 1:200, at 60 ºC and a lipid concentration of 1 mM. Such high temperature permitted the amphiphile aggregation to be avoided during the extrusion procedure. A higher probe to lipid ratio (1:50) was used for membranes with a very slow aggregation process at 1:200.

An absorption spectrum of the amphiphile (t= 0 h) was obtained, with the solution at 60 ºC, after which the temperature was rapidly decreased to 25 ºC being followed in time. Considering that the LUVs samples significantly disperse light, giving high absorptions, the final dispersion-free absorption spectrum was attained by subtracting to the raw experimental absorption spectrum a simulated dispersion curve that served as baseline. To do this, the solver utility from excel® program was used generating a line described by a polynomial expression of the degree *n* that best fitted the values of absorbance between 300 nm and 400 nm and between 650 nm and 700 nm for RG-C_{14} and CBF-C_{14}, respectively. This line serves as a dispersion baseline for the experimentally obtained absorption spectrum (Figure III.5, Panel A).

The absorption maximum of the samples was recovered and the time evolution of the calculated local monomer concentration fitted with a dimerization process. The probe local concentration at each time frame was calculated based on absorption maximum and taking into account the experimental concentration and the molar volume of the lipids of interest (Figure III.5, Panel B).

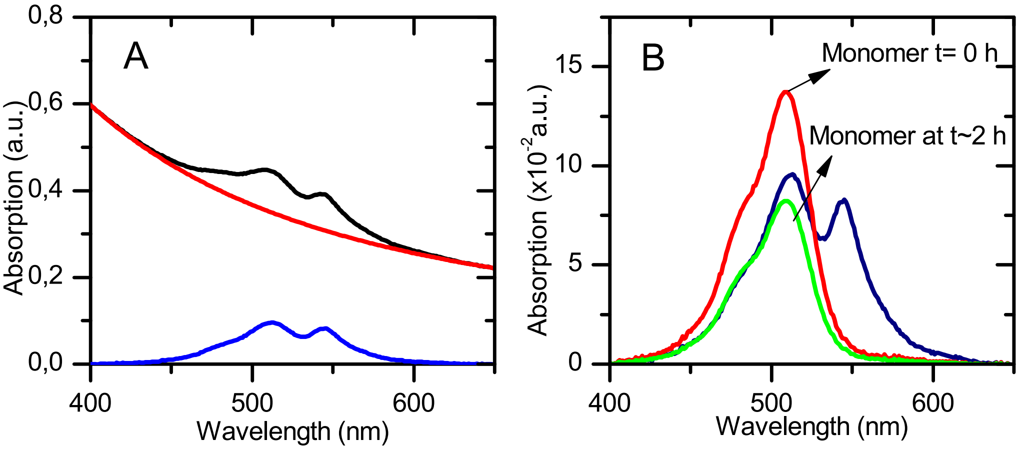

Figure III.5. Panel A: Dispersion free absorption spectra of RG-C_{14} (Blue) obtained by subtracting to the raw spectra (Black) a polynomial curve that describe the LUVs dispersion (Red). Panel B: Absorption spectra of RG-C_{14} at t= 0 h (Red) and t~ 2 h (Blue). The green line represents the deconvoluted monomer absorption spectra at t~ 2 h, obtained through the overlap of the absorption spectra at t= 0 h (red) to the t~ 2 h (blue).

III.9 Determination of the CBF-C_{14} Ionization Constant in LUVs

LUVs with different lipid compositions containing the CBF-C_{14}, in a probe: lipid molar ratio 1:100 and a final concentration of 1 mM, were prepared according to III.4 above) and hydrated with a solution containing NaCl 150 mM, NaN_3 0.02%, EDTA 1 mM in a controlled pH range between 11-12. Three stock solutions of hydrochloric acid (HCl) with 0.01 M, 0.1 M and 1 M were previously prepared. Through the addition of small aliquots (1-5 μL) of the HCl correspondent stock solution, directly to the cuvette, going from the more diluted towards the more concentrated while stirring the solution to homogenize, we were able to decrease, by a small value, the pH of the solution. The stirring was maintained during approximately 3-5 min after which the pH, with the help of an electrode, was directly measured in the cuvette. The absorption spectrum was obtained after the pH stabilization. Finally, a second reading of the solution pH was measured in order to have a more accurate value.

III.10 Methodology for the Partition of RG-C_{14} and CBF-C_{14} between Donor POPC LUVS and Acceptor LUVs

The low water solubility of RG-C_{14} precluded the direct measurement of the partition coefficient between water and membranes, restraining the method to the transfer between different vesicles. From this methodology one may obtain the relative partition coefficient between the distinct membranes, given that the partition to the donor membrane is known or that the fraction of amphiphile in the aqueous media is negligible. The donor vesicles were composed of a final 0.1 mM (after addition of acceptor vesicles) POPC, loaded with RG-C_{14} or CBF-C_{14}, at a probe: lipid molar ratio of 1:500 for RG-C_{14} and CBF-C_{14}, and the fluorescence lipid, RhB-DPPE (Figure III.6) at 1:100, molar ratio. The acceptor vesicles were composed of single POPC or a mixture of phospholipids, POPC:CHOL(5:5), POPC:CHOL(7:3) SPM:CHOL(6:4), POPC:CHOL:POPE(5:3:2) and POPC:CHOL:POPE:POPS(4:3:2:1), at different l_o, l_d

phases or with phase coexistence. The transfer of the amphiphiles was followed by an increase in RG-C_{14} (at 530nm) or CBF-C_{14} (at 525 nm) fluorescent intensity upon the addition of growing concentrations of an acceptor vesicle in a final range of concentrations of 0.05 mM to 2 mM, depending on the acceptor lipid composition. The solutions were allowed to equilibrate at a constant temperature 25 ºC for 2 h before the fluorescence readings. The cuvette path length used was such that the maximum optical density (absorption *plus* scattering) was smaller than 0.12 at the excitation wavelength.

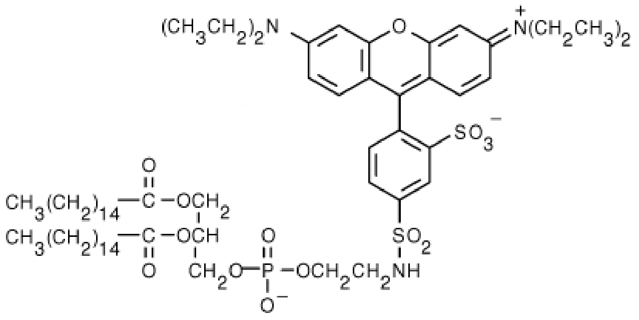

Figure III.6. Chemical structure of the fluorescence quencher RhB-DPPE used in this work.

III.11 Methodology for the Kinetics of Interaction of RG-C_{14} and CBF-C_{14} between Donor POPC LUVS and Acceptor LUVs

The aqueous solubility of the amphiphiles, namely RG-C_{14}, was very low and the kinetics of their interaction with membranes was obtained using the transfer between donor and acceptor vesicles. The donor vesicles were composed of 0.1 mM of pure POPC or a mixture of lipids loaded with RG-C_{14} or CBF-C_{14}, at a probe: lipid molar ratio of 1:500, and the fluorescence lipid quencher RhB-DPPE at 1:100. Considering that the observed experimental time for transfer (less than 1 min) was considerably fast the possibility of occurring cholesterol exchange between vesicles was negligible.

Therefore, we have exploited the transfer rate for distinct, or the same lipid compositions for donor and acceptor vesicles.

The donor and acceptor vesicles solutions were mixed, using stopped-flow equipment, at an equal volume, and an increase in the fluorescence, due to binding of the amphiphiles to the acceptor LUVS was followed in time. The excitation was set as 530 and 490 nm for RG-C_{14} and CBF-C_{14}, respectively and the emission was recorded through a band pass filter of 520 nm.

The data collected proved to be bi-exponential, with a slower step for longer times, due to the translocation of the amphiphiles between lipid monolayers. For the correct quantitative assessment of the slower rate process we have opted to perform the experiment in the kinetic mode of the spectrofluorimeter. Experimentally, we added a solution containing the donor vesicles (0.4 mM, initial concentration) loaded with the amphiphile of interest and the quencher RhB-DPPE, at the aforementioned molar ratios, to acceptor vesicles (at different concentrations) previously in the cuvette and followed the final solution fluorescence intensity while stirring. In this case and taking into account that this slow step could take several hours the vesicles had the same lipid composition avoiding any cholesterol exchange during the experiment.

III.12 Fluorescence Anisotropy and Lifetimes

The fluorescence anisotropy, lifetime and quantum yield was obtained for both RG-C_{14} and CBF-C_{14} in different lipid composition bilayers and in methanol, at a final concentration of 2 μM for CBF-C_{14} and for RG-C_{14} and a lipid concentration of 0.5 mM. For the anisotropy a determination of the geometrical factor (G factor) was attained using a fluorescence non-dispersive methanol solution with 2 μM of the fluorescent probe of interest.

Fluorescence lifetime measurements were done on a home-built TCSPC apparatus with a Horiba-JI-IBH NanoLED at λexc =460 nm.

III.13 Monolayers Experiments

The main focus of this work is the interplay of both the membrane dipole potential and amphiphile dipole moment. Therefore, experimental measurements of the membrane potential have to be attained. For this we used the well-known monolayers methodology (see II.5.2), which experimental details are described below.

III.13.1 Measurement of the Potential Difference across Lipid Monolayers

The potential was measured in lipid monolayers formed at the air-aqueous interface. The system utilized is based on a high impedance circuit which connects an ionizing electrode of polonium in the air and a reference (Ag/AgCl) electrode immersed in the aqueous solution. The monolayers are formed, at the air-aqueous solution interface (NaCl 150 mM, Sodium azide 0.02% (m:v), EDTA 1 mM and Hepes 10 mM at pH 7.4), by gently adding crescent aliquots of lipids (dissolved in chlorophorm) with a microseringe until we reach a point, where further addition of lipid does not induce any change in the measured dipole potential(V_{lipid}). The difference between the potential without any lipid (V_{solution}) and the potential V_{lipid} allow us to recover the dipole potential of the formed monolayer [158].

For zwitterionic lipids the measured potential is exclusively of dipolar origin while for POPS containing monolayers it includes the contribution of the surface charge potential (Ψ_0). An approximate value for the Ψ_0 was obtained from the electrical density charge at the experimentally determined area per lipid at the saturation pressure (π_{sat}), using the Guoy-Chapman theory.

$$\sigma^2 = 2000\varepsilon_0\varepsilon_r RT\sum_i C_i\left(e^{\frac{-z_i F\Psi_0}{RT}} - 1\right) \qquad \textit{(III-1)}$$

where, σ is the electric charge density, ε_0 is the vacuum permittivity, ε_r the relative permittivity, R is the ideal gas constant, T is the temperature, F is the Faraday constant, C_i and z_i are the concentration and formal charge of the *i* species, respectively.

III.13.2 Monolayer Surface Pressure Experiments

The formation of monolayers at an aqueous surface was monitored through changes in the surface pressure, using Kibron µTrough S equipment, with the addition of lipid at a constant area and temperature (25 ºC). Small aliquots of a chlorophorm solution containing the lipids of interest (0.5 mM) were carefully spread on a clean surface of an aqueous buffer and left to equilibrate until the surface pressure reaches a constant value. When the addition of further lipid results in no visible changes in surface pressure (saturation) the excess lipid form aggregates in the subphase and the thermodynamic and interfacial properties are comparable to those of a bilayer. This procedure allows for a spontaneously lipid stabilization in the aqueous-air interface without applying any lateral pressure [158, 159]. The areas per lipid at the saturation pressure (π_{sat}) were obtained from the variation of the surface pressure *versus* the amount of lipid through the interception of two lines, one describing the high pressures region (small slope) and other describing the region with the steepest slope (Figure III.7).

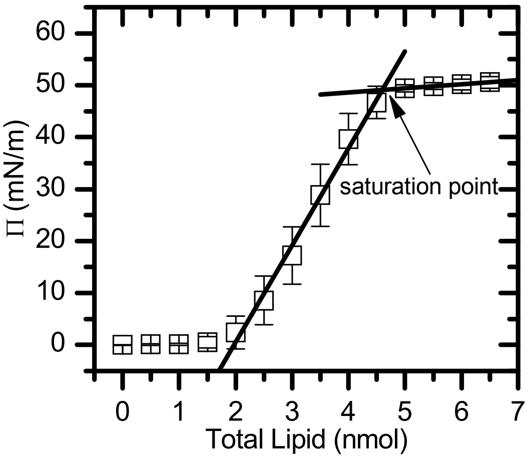

Figure III.7. Typical results for π-total lipid (nmol) isotherm where the two lines represent the plateau at high pressures and the region with steepest slop, respectively. The saturation point is represented by interception of both regimes.

IV

Dipole Potential of Monolayers with Biologically Relevant Lipid Compositions

IV.1 Introduction

The total electric profile of a membrane may be defined by three distinct kinds of potential: the transmembrane potential, the surface charge potential and the dipole potential. The first is a consequence of the charge displacement from one side to the other of a membrane, due to a difference in ion concentrations between both compartments. The surface charge potential, which is described by Guoy-Chapman theory, results from the presence of charged groups and ion distribution in the electrical double layer on the membrane surface. The latter, but not less important, is the membrane dipole potential, which is originated from the preferred alignment of water molecules and certain constitutive dipoles of lipid groups.

The dipole potential was first discovered by Liberman and Topaly, 1969, through membrane conductivity changes upon addition of large hydrophobic anion and cation ($TPPB^-$, $TPPB^+$). They observed that the membrane conductivity was much larger for the hydrophobic anions than for the cations. This difference was attributed to their distinct partition into the centre of the membrane and they supposed that the presence of a more positive potential within the membrane was the main reason for the permeability differences [101].

The main sources contributing to this membrane internal dipole potential are considered to be the lipid carbonyl groups, the dipole resulting from the phospholipid headgroup (choline-phosphate dipole in the case of phosphatidylcholines), the alkyl chain terminal methyl group and the interfacial water hydrating the phospholipid headgroups [96, 160]. These sources account for a larger value of the dipole potential than the surface charge or the transmembrane potentials (see II.5.3 for details).

Studies in monolayers with phosphatidylcholines revealed a dipole potential of approximately 400 mV and, such high value suggests an important biological role for the dipole potential. The binding affinity or the orientation of a membrane peptide can be affected by the dipole potential [161, 162], moreover the permeability of charged molecules is further affected by the dipole potential [163, 164] and alterations in the activity of a membrane embedded peptide was attributed to changes in the internal dipole potential [165].

The dipole potential can be changed through the addition of certain dipolar molecules such as phloretin [166], cholesterol and an analogue 6-ketocholestanol [167, 168], that consequently modify the membrane permeability properties. The cholesterol molecule is one of the main lipids of many biological membranes and its effect in the dipole moment was first addressed by Szabo et al in 1974 using the hydrophobic ions. They observed that upon the addition of cholesterol to a neutral membrane there was a 30-fold increase in anion permeability relative to a 100-fold decrease in cation permeability. This distinct behaviour for anion and cation was compatible with an increase in dipole potential of cholesterol containing membranes. Later this observation was confirmed through measurements of the dipole potential of Egg Phosphatidylcholine (EggPC) with cholesterol monolayers [169]. The main reason why cholesterol increases a membrane potential is by promoting an enhancement of the membrane lipid packing, the so-called condensation effect [170].

Biological membranes are asymmetric structures composed not only by cholesterol but also by several kinds of phospholipids, which abundance depends on the chemical environment that is in direct contact with each monolayer [40].

While sphingomyelin (SpM) phosphatidylcholines (PC) and cholesterol (CHOL) are the major components of the outer exoplasmic leaflet of the plasma membranes in eukaryotic cells, the composition of the inner leaflet composition is mainly PC, phosphatidylethanolamines (PE) and phosphatidylserines (PS) phospholipids [171]. The dipole potential of phosphatidylcholines, sphingomyelin and mixtures with cholesterol has been a subject widely discussed in literature, to get insights on the sources contributing to the dipole potential change [108]. However the dipole potential of biologically relevant lipid mixtures has not been addressed in literature, gap that we pretend to fulfil with this work.

Typically, the erythrocyte membrane contains between 10-20% of serine phospholipids and 10-25% of phosphatidylethanolamines [172] so, the dipole potential study of mixtures of POPC and cholesterol with 10% of POPS and 20% of POPE is biologically relevant.

The dipole potential for pure lipid and lipid mixtures has been studied mainly through experiments using monolayers. Briefly it consists in measuring the potential difference across an air/water interface first in the absence and then in the presence of a formed monolayer [99, 173]. The difference between both measured potentials will give the contribution of the dipole of lipids therefore, the dipole potential (in zwitterionic lipids). For charged lipid molecules the measured potential comprehends a contribution of the lipids dipole potential and the surface charged potential (Ψ_0) (IV-1). Therefore, in order to obtain the dipole potential in monolayers containing charged lipids we must determine the Ψ_0 using the Guoy-Chapman theory.

$$\Psi_{measured} = \Psi_{Dipole} + \Psi_0 \qquad \textit{(IV-1)}$$

While the surface potential is more relevant for charged molecules near the membrane interface affecting their partition coefficient, the dipole potential is particularly important for amphiphilic molecules and membrane proteins which are inserted in membranes being in close interaction with this strong electrical field.

The quantification of the membrane dipole potential with different lipid compositions is important to understand its role in permeation of certain amphiphilic molecules, especially the ones which contain a preferential dipole moment orientation. Moreover, in the latest years, our group has characterized the interaction of different amphiphiphiles and drugs with distinct zwitterionic lipid bilayers [134, 174, 175] and the magnitude of the membrane dipole potential seems to have a crucial role [3].

In this work the membrane dipole potential results were complemented by mean area per lipid data, either obtained from literature or through experimental measurements. The obtained results showed that cholesterol increases the dipole potential of a monolayer formed at the air-water interface due to a decrease in the average area per lipid. The effect of POPE strongly depends on the constituting lipids of the monolayer, while in the presence of POPC it increases the dipole potential of the membrane in mixtures with cholesterol a decrease is observed. The presence of negatively charged POPS increases the dipole potential of monolayers even though an enhancement in the monolayer packing is not evident. This increase in the dipole potential due to POPS and the smaller dipole of monolayers containing large amounts of SpM generates a non-zero transmembrane potential in the asymmetric plasma membrane. The lipid composition mimicking the inner leaflet of plasma membrane of eukaryotic cells showed a large dipole potential and an unexpected, given the presence of cholesterol, high area per lipid.

IV.2 Dipole Potential in Lipid Monolayers

The quantification of the dipole potential through lipid monolayers gives an important contribution to understand their organization in bilayers [159]. The comprehension of dipole potential variation in biologically relevant lipid mixtures requires a primary analysis of less complex mixtures and pure lipid behaviour. Consequently, pure POPC, POPE, SpM and POPS dipole potentials were obtained in monolayers formed at the air-water interface (

Figure IV.**1**). In agreement with other studies [99, 176], our results show that ethanolamine and serine headgroups pack densely leading to an increase in monolayer dipole potential compared to pure POPC.

A much smaller dipole potential for SpM compared to POPC was obtained although a higher packing (smaller area at the same pressure) was observed by other authors [177]. SpM alkyl chain motional constraints and its ability to establish a network of hydrogen bonds between headgroups increases the lipid packing in these membranes [178-180]. Despite this increase in packing there are structural differences compared to POPC (an OH instead of a carbonyl) that influence the dipole potential, and account for the observe decrease in dipole potential.

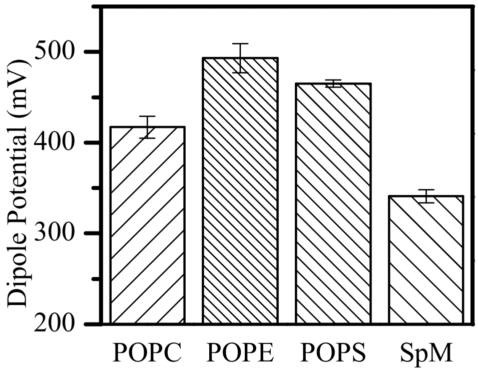

Figure IV.1. Dipole potential in pure POPC, POPE, POPS and SpM monolayers at pH 7.4 with hepes buffer at 25 ºC. The dipole potential of POPS was determined from equation IV-1 with a $\Psi_0 \approx$-135mV.

The addition of increasing percentages of cholesterol to POPC enhances the dipole potential from 417 mV to ~ 490 mV, at 50% cholesterol, due to the increase in membrane lipid packing in those membranes (Figure IV.2) [177, 181]. This dipole potential variation (15%) is in agreement with the observed difference for EggPC:Cholesterol monolayer at equimolar concentrations [176] and smaller than the observed using bilayers containing 40% of cholesterol [182]. The addition of biologically relevant percentages of POPS (10%) and POPE (20%) to POPC lead to a small increase in the final dipole potential obtained. The lipid packing of both monolayers is affected in opposing ways and while the mean area per lipid at saturation pressure is the same for the pure POPC and POPC:POPS (90:10) in the presence of 20% POPE there is a substantial decrease in the mean area per lipid.

Upon the addition of POPE (20%) and in the presence of cholesterol there is a dipole potential increase of approximately 4% from 463 mV in POPC:CHOL(7:3) to 482 mV in POPC:CHOL:POPE(5:3:2), though compared with the more packed POPC:CHOL(5:5) monolayer the dipole potential is slightly smaller. The quaternary mixture representing the inner leaflet of plasma membrane showed that the presence of POPS does not, significantly, change the dipole potential comparing the 482 mV obtained for POPC:CHOL:POPE(5:3:2) monolayer with 474 mV. This is in agreement with the results obtained for POPC:POPS(9:1) which almost no variation occurred when compared to pure major component. Although both SpM:CHOL(6:4) and

POPC:CHOL(5:5) monolayers have a similar lipid packing at 30 mN/m the dipole potential obtained at π_{sat} is much smaller for the former than for the latter.

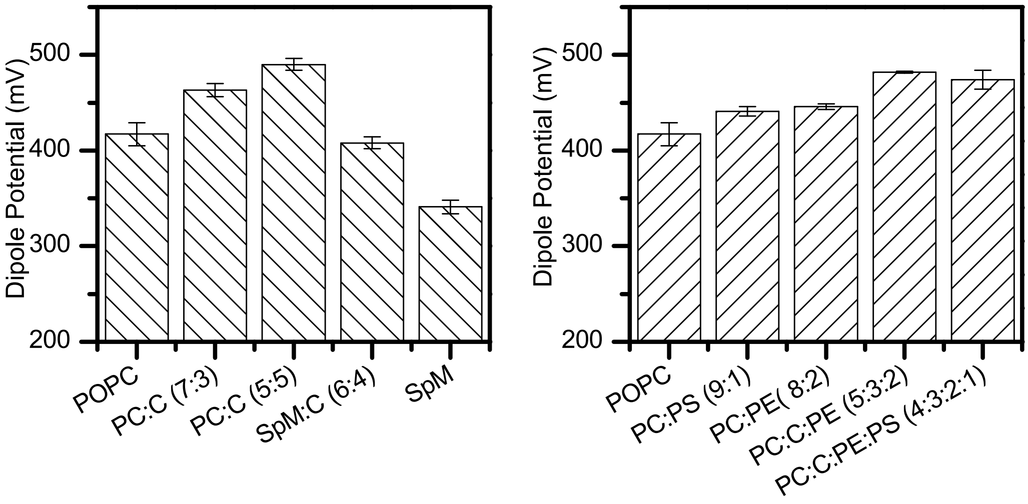

Figure IV.2. Dipole Potential, at 25 ºC, in monolayers composed by a mixture of lipids, where PC, PS, PE, C and SpM abbreviations entitle POPC, POPS, POPE, Cholesterol and SpM, respectively. The numbers between commas correspond to the lipid molar fraction in the mixture.

IV.3 Area per Lipid in Monolayers

The area per lipid parameter describes quantitatively the differences in lipid packing within a monolayer and, studies the effect on the membrane dipole potential promoted by mixing different zwitterionic lipids. Moreover, this study together with the results of dipole potential allows rationalizing the effect (condensation/expansion) of different lipids in more complex lipid mixtures. In this work we calculated the area per lipid from the changes in the surface pressure as a function of the amount (nmol) of lipid added (Figure IV.3).

The lipid compositions were chosen considering the previously obtained dipole potential as well as the literature data. We measured the area per lipid in a well characterized monolayer such as POPC and taking into account the mixtures reported in the literature we selected most biologically relevant mixtures, POPC:POPS(9:1), POPC:CHOL:POPE(5:3:2) and POPC:CHOL:POPE:POPS(4:3:2:1).

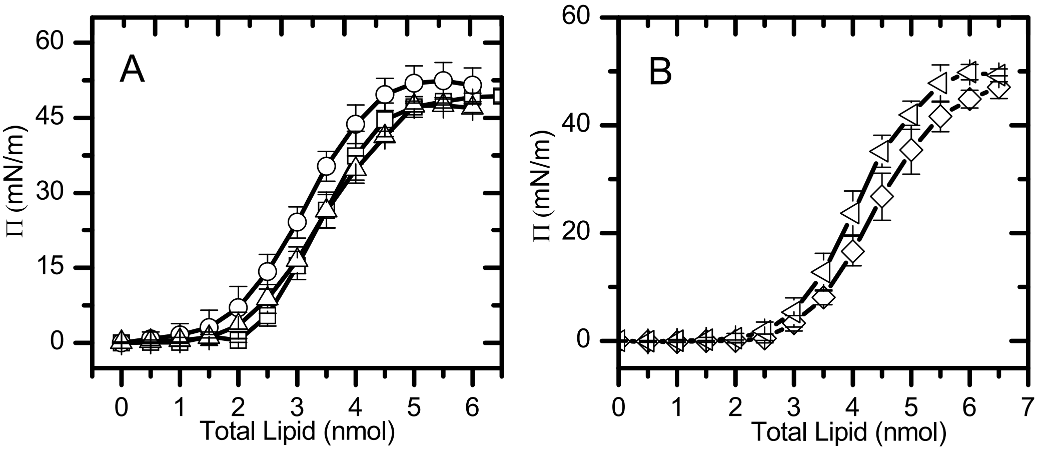

Figure IV.3. Formation of monolayers of phospholipids measured by the changes in surface pressure as a function of nmol of lipid added at 25 ºC. Panel A: Pure POPC (□); POPC: POPS(9:1, molar ratio) (O); POPC:POPE(8:2) (Δ); Panel B: POPC:CHOL:POPE(5:3:2) (◊); POPC:CHOL:POPE:POPS (4:3:2:1)(◁); at 25 ± 1 ºC. The line is a guide to the eye.

For either pure or mixtures of lipids the mean area per lipid found in literature is, generally, presented at a surface pressure of 30 mN/m which is assumed to be the lateral pressure in a bilayer [183] and in order to compare our results with previously reported data we fitted a polynomial equation, for areas smaller than 100 $Å^2$ (liquid expanded/condensed state), to the experimental results of π-Area isotherm and the area per lipid at a surface pressure of 30 mN/m may be recovered (Figure IV.4).

The π- Area isotherm profile and the area per lipid obtained for the pure POPC molecule at π_{sat} and 30 mN/m is similar, within error, to the values obtained either experimentally [184, 185] and by molecular dynamics studies [186]. For the POPC:POPE(8:2) mixture the area per lipid decreases, both at 30 mN/m and at saturation pressure, compared to the major lipid component and the π-area profile is similar in either a more expanded or condensed state of the monolayers. In the presence of 10% of POPS an increase in the mean area per lipid of pure POPC was observed at 30mN/m, and the curve is shifted to higher surface pressures indicating a more expanded monolayer than POPC and POPC:POPE(8:2), yet in a more condensed state it present a surface and area per lipid similar to pure POPC. At pressures below ~50 mN/m it seems that there is some electrostatic repulsion between the negatively charged serine groups (higher areas) that with further compression of the monolayer weakened. Considering that in literature there is considerable amounts of work regarding the effect of cholesterol in POPC we have focus our interest in other biologically relevant mixtures containing lipids such has POPE and POPS.

The ternary mixture containing POPC:CHOL:POPE(5:3:2) showed an area per lipid at π_{sat} and 30mN/m slightly smaller than POPC:POPE(8:2) but significantly higher than POPC:CHOL(5:5) which indicates that the condensation of cholesterol is somehow less efficient in the presence of POPE. The lipid composition mimicking the inner leaflet of plasma membrane showed an area per lipid close to the pure POPC monolayer. Although the presence of POPE and cholesterol may in fact contribute to a more condensed monolayer as observed by the decrease in area per lipid of POPC:POPE(8:2) and POPC:CHOL(5:5) leading to a consequent increase the dipole potential, this condensation effect is lost by inclusion of POPS. Moreover, the area per lipid isotherm for the quaternary mixture is deviated towards higher areas per lipid when compared with the ternary mixture. A summary of data obtained in this work or reported in literature, for monolayers, is presented in Table IV.1.

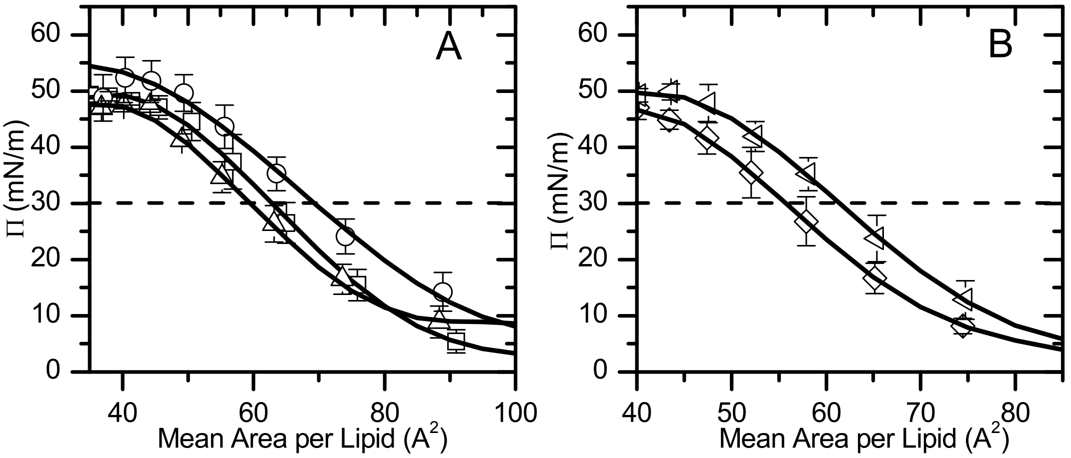

Figure IV.4. Mean Area per lipid isotherm for POPC (□), POPC:POPS(90:10), ○, and POPC:POPE(80:20) Δ at 25 ºC. The line is the best fit of a polynomial equation for areas smaller than 100 Å^2 in the liquid expanded state.

Table IV.1. Summary of the mean area per lipid and the dipole potential obtained for different lipid compositions monolayers formed at the air/water interface, at 25 ºC.

Lipid composition	Area per lipid at π=30mN/m ($Å^2$)	Area per lipid at π_{sat} ($Å^2$)	Total lipid at π_{sat} (nmol)	Saturation Pressure (mN)	Dipole Potential at π_{sat} (mV)
POPC	64.5	49.4±3.4	4.6	50	417±12
POPS	55.0(a)	-	-	-	465±4.2(e)
POPE	56.0(b)	-	-	-	494±16
SPM	48.0(c)	-	-	-	341±7.1
POPC:POPS(9:1)	69.8	51.0±4.0	4.3	51	441±2.5(e)
POPC:POPE(8:2)	59.6	45.4±3.0	4.8	47	424±15
POPC:CHOL(7:3)	48.0(d)	-	-	-	463±6.9
POPC:CHOL(5:5)	44.0(d)	-	-	-	490±5.7
POPC:CHOL:POPE(5:3:2)	56.0	46.4±2.7	5.6	46	481±1.4
POPC:CHOL:POPE:POPS (4:3:2:1)$^{\text{Inner}}$	61.5	49.7±2.6	5.3	49	474±11(e)
SPM:CHOL(6:4)$^{\text{outer}}$	39.0(c)	-	-	-	408±6.3

(a) [186]; (b) [187]; (c) [188]; (d) [181]; (e) Final dipole potential obtained from equation IV-1.

IV.4 Effect of Lipid Composition in the Dipole Potential of Membranes

The mean area per lipid obtained for pure POPC both at saturation and 30 mN/m agrees with the published experimental and molecular dynamics results. At the saturation pressure the POPC monolayer is in a more condensed state given that the observed small area per lipid and surface pressure are close related to other results in which the POPC is in a transition from a liquid expanded to a more condensed state [189].

The dipole moment normal to the aqueous subphase ($\mu_{\perp}$) of unionized monolayers may be calculated using the Helmholtz equation and assuming 1 has dielectric constant of the medium [99].

$$\Delta V = 12\pi\mu_{\perp} / A \qquad (IV\text{-}2)$$

Where, the ΔV is the dipole potential variation between aqueous phase and the monolayer (mV) and A is the mean area per molecule (Å^2). According to other results the dipole moment normal to the aqueous phase ($\mu_{\perp}$) of POPC monolayers is very similar to POPE [189], therefore considering the experimentally obtained dipole potential we may determine the area per lipid of POPE monolayer at the saturation point (43 Å^2). The small area per lipid determined, at saturation pressure, agrees with the observed higher dipole potential compared to pure POPC, this thigh packing of POPE is due to the ability of the ethanolamine headgroup to form an hydrogen bond network significantly decreasing its area per lipid [187] [190]. For POPS monolayer, although its smaller area per lipid at 30 mN/m [186] at the saturation pressure it has a similar area to POPC [189, 191]. This negatively charged phospholipid showed a lower measured potential (Ψ_{dipole}+Ψ_0) compared to other phospholipids in accordance with other reported results containing negatively charged lipids [189, 191].

The contribution of the surface potential (Ψ_0) to the experimentally observed dipole potential of POPS was obtained (-135 mV) through the Gouy-Chapman theory (see equation III-1) considering a formal charge of -1 per lipid [192] originating a surface charge density (σ) of -3.1 C/m^2 at an area equal to POPC (49.4 Å^2). The dipole potential of POPS is smaller (465 mV) than POPE revealing a lower packing of the monolayer, in the saturation pressure, and give, according to the Helmholtz equation, a dipole moment normal to the aqueous phase of ≈ 610 mD. The dipole potential of POPS monolayer considerably higher than POPC at both 30 mN/m and π_{sat} due to the presence of a primary amine in the POPS which is able to form hydrogen bonds that significantly increase its lipid packing [193], therefore we would expect an area per lipid for POPS at the π_{sat} smaller than POPC and close related to the area per lipid of POPE.

The $\mu_{\perp}$ of pure lipid monolayers calculated using the Helmholtz equation may be separated in different dipolar contributions according to the three layer capacitor model of Demchak and Fort (DF) [124]. They considered three main contributions to the monolayer normal dipole moment with different relative permittivity (see II.5.3 for details). The aqueous subphase as a dipole moment contribution, μ_1, due to the water molecules polarization with the monolayer formed, the headgroup, μ_2, and the acyl chain, μ_3, dipole moments are the other contributors to the $\mu_\perp$ which should be written as:

$$\mu_\perp = (\mu_1 / \varepsilon_1) + (\mu_2 / \varepsilon_2) + (\mu_3 / \varepsilon_3) \qquad \textit{(IV-3)}$$

where, ε_1, ε_2 and ε_3 represent the relative permittivity in each region of the monolayer. The acyl chain group was assumed to contribute with a dipole moment ($\mu_3/\ \varepsilon_3$) twice the one obtained for a stearic acid monolayer (236 mD) [191] and using the interfacial parameters suggested from Oliveira *et al* [194] (ε_2=6.4 mD and $\mu_1/\ \varepsilon_1$=-65 mD) we are able to obtain the contribution from the different headgroups using the DF model (Table IV.2).

The values obtained for the headgroup dipole moment contribution agree well with other published results using the same model [191] and are smaller than the calculated dipole moment of the P-N vector dipole (20 D), nevertheless this dipole moment contribution is negligible because is lying flat to membrane surface [195], hence the main input to the total dipole potential comes from the carbonyl group which is aligned vertically to membrane surface [115]. The observation that the contribution of the carbonyl group is prominent is further supported by the results obtained for SpM whose μ_2 is considerably smaller given the absence of a carbonyl in its *sn*-2 acyl chain. Accordingly, McIntosh *et al*, 1992, observed that the dipole potential difference between brain sphingmyelin and dipalmitoylphosphatidylcholine (DPPC) membranes was, essentially, due to the presence of the hydroxyl group in the sphingomyelin [176]. Although the mean area per lipid for SpM at the saturation was assumed, by excess, to be 43 Å^2 it should be notice that an even smaller area would decrease the calculated μ_2 accentuating the difference between SpM and the other studied lipids. It is observed a higher $\mu_\perp$ for the POPS monolayer probably due to a distinct orientation of the carbonyl group reinforcing the dipole moment in these monolayers.

Table IV.2. Monolayer properties in pure lipids according to DF model.

	POPC	POPE	POPS	SpM
Area$_{sat}$ (Å^2)	49	43	49	43
$\Delta V_{measured}$ (mV)	417	494	331	341
Ψ_{Dipole} (mV)	417	494	465	341
Ψ_0 (mV)	0	0	-135	0
$\mu_\perp$ (mD)	546	564	612	390
$\mu_1/\ \varepsilon_1+\mu_2/\ \varepsilon_2$ (mD)	328	328	306	154
μ_2 (D)	2.52	2.52	2.94	1.4

Considering that most mammalian cell membranes in their composition have some amount (~10%) of negatively charged lipids the study of mixtures containing negative lipids have a preponderant role (see II.2.3 above for details). The mixture of POPC with 10% of POPS showed an increase in the dipole potential compared to pure POPC. Considering that for this mixture and for pure POPC a similar packing was observed at the saturation point, where the dipole potential is obtained, the differences are due to the interfacial dipoles either from polarizable in the membrane interface water or from lipid headgroup in the presence of the POPS. The subphase used in the experiments contain Na^+ counter ions which are known to induce a considerable dehydration of POPC/POPS bilayer and promote a P-N dipole reorientation of the POPC headgroup, that in pure water is lying flat on the membrane surface and in the presence of the salt and POPS has narrower and smaller angle distribution [196].

In the mixture POPC:POPE(8:2) there is a decrease in the area per lipid at both 30 mN/m and at π_{sat} leading to a higher dipole potential in this mixture, at $\pi_{sat,}$ compared to POPC, however the increase in membrane packing should suppose an even higher dipole potential. Therefore, the difference must rely on the dipole moment normal to the membrane surface that decreases from 564 mD in pure POPC to 510 mD with the presence of 20% of POPE. The magnitude of the dipole moment of both headgroups is similar then the observed decrease can be attributed to changes in the interfacial water in POPC in the presence of POPE. The ternary mixture showed a distinct behaviour and the area at 30 mN/m increases compared to both POPC:CHOL mixtures, nevertheless the dipole potential is very similar to the POPC:CHOL(5:5) monolayer which is in a liquid ordered phase [74] [197]. Since that the hydrogen and electrostatic interactions between POPE headgroups is stronger than the interactions between POPE and Cholesterol [198, 199] it could be that in this mixture there is a coexistence between two liquid phases being one more enriched with cholesterol than the other. In this ternary mixture the formation of cholesterol rich domains was observed by Atomic Force Microscopy using monolayers [199]. These more ordered domains and oriented water dipoles present at interface may explain the reinforcement of the dipole potential in POPC:CHOL:POPE(4:3:2) relative to POPC:CHOL(7:3) monolayer although its higher area per lipid at 30mN/m.

The quaternary mixture, which mimics the inner leaflet of the erythrocyte membranes, at π_{sat}, has a dipole potential slightly smaller than the ternary mixture due to a smaller packing of the monolayer (larger mean area per lipid) in the presence of the POPS phospholipid.

Although SPM:CHOL(6:4) and POPC:CHOL(5:5) similar area per lipid at 30mN/m the latter has a smaller dipole potential in accordance with the fact that SpM hydroxyl group in the *sn*-2 acyl chain rather than a carbonyl of POPC contributes to a lower dipole potential.

The dipole orientation and magnitude, is the main responsible force for the total potential observed in the zwitterionic membranes, we can predict the total transmembrane potential of a bilayer arising from different zwiterrionic monolayers that exclusively result from the transmembrane asymmetry in phospholipids distribution. A POPC and POPE asymmetric bilayer, according to our experimental results, give a non-zero transmembrane potential (~77 mV) in good agreement with experimental results in bacterial PE and 1,3 Diollein [200] and further observed by molecular dynamics simulations [201].

Even though cholesterol, according to our results, is one of the main contributors to the membrane dipole potential, in the plasma membrane is essentially equally distributed in both leaflets while SpM is almost exclusively in the outer leaflet. Interestingly if we consider a lipid composition POPC:POPE:CHOL:POPS(4:3:2:1) mimicking the inner leaflet of eukaryotic cell membranes and SpM:CHOL(6:4) as the outer leaflet this would give a total non-zero transmembrane potential (~30 mV) being negative in the interior of the cell relative to its exterior, reinforcing the measured transmembrane potential in eukaryotic cells [9]. From the mixtures studied we observe that POPS has also an important role and in its absence the inner leaflet composition would have a smaller dipole potential, fact that could have important biological implications. POPS molecule it is known as a recognition molecule in apoptotic cells and when exposed to the outer leaflet it serves as a signal for phagocytosis [45]. According to our results the disruption in transmembrane lipid asymmetry by exposing POPS to the outer leaflet leads to an increase in the intrinsic dipole potential of this monolayer and a consequent decrease in the magnitude of the transmembrane potential which may influence the normal function of membrane proteins accelerating the programed cell death.

IV.5 Chapter Highlights

In this chapter we have characterized the dipole potential and the area per lipid for monolayers, at the water-air interface, with relevant lipid compositions. The dipole potential for the pure lipids was in accordance with the literature reported values. With POPE and POPS presenting a higher dipole potential due to the headgroup ability to form hydrogen bonds and, therefore, decrease the mean area per lipid. Moreover, the pure SpM showed a smaller dipole potential due to the presence of a hydroxyl group in the sphingosine alkyl chain. Consequently the mixture SpM:CHOL(5:5) also had a smaller dipole potential than POPC:CHOL(5:5), despite their reported similar areas per lipid.

An increase in the dipole moment with cholesterol content was observed for POPC:CHOL mixtures due to a decrease in the mean area per lipid. For the ternary mixture, POPC:CHOL:POPE(5:3:2), although it presented a similar area to POPC:CHOL(7:3) a significant increase in the dipole potential was observed for the former mixture, due to the an reorientation of the interfacial dipoles (water+ lipids). The quaternary mixture showed a lower packing than the ternary mixture and therefore a smaller dipole potential. Considering the composition of the inner and outer leaflet we predict a non-zero dipole potential variation being negative in interior of the cell, reinforcing the transmembrane potential observed in cells.

V

Effect of Amphiphile Dipole Moment in Solubility and Partition to Lipid Bilayers in Liquid Ordered and Liquid Disordered Phases

V.1 Introduction

Lipid anchored proteins that include the Glycosylphosphatidylinositol (GPI) anchors, sterols and saturated or unsaturated fatty acid modifications are functionally important for cells. The lipid modification not only provides a stable membrane anchor for a water soluble protein, through changes in its hydrophobicity and conformation, as it also promote some protein sorting within the membrane either by preferential protein-protein or protein-lipid interactions contributing to biological membrane heterogeneity [202-204]. The correct functioning of acylated proteins requires their binding to the membrane being the lipid modification imperative in protein activity control and targeting.

The most common protein fatty acylation are N-myristoylation and *S*-acylation. In the latter the protein is covalently attached, by a cysteine residue via *thiol*, to a long fatty acid acyl chain, and in the former the protein is linked via the N-terminal of the glycine residue to myristate acyl chains (14 carbons) Figure V.1. Previous studies showed that palmitoylation and myristoylation was a pre-requisite to find transmembrane proteins associated with detergent resistant membranes, being the fatty acid anchor hydrophobicity the main factor for protein targeting in lipid rafts [203, 205]. The preferential packing of the saturated acyl chains for more ordered lipid domains leads to a predicted association with these microenvironments while proteins with unsaturated long acyl chains are preferentially located in disordered membrane domains [206]. More recently, results obtained using giant plasma membranes vesicles proved that although palmitoylation may be necessary for the partition of transmembranes proteins into rafts it is not the unique requirement since that some palmitoylated transmembrane proteins may be found segregated from rafts [207, 208]. Moreover, although the mysristoylation is required for some membrane associated proteins a single acyl chain lipid modification is barely sufficient to attach the protein to the membrane and additional acylations (palmitoylation) or some hydrophobic transmembrane fragments of the proteins are required [209]. Therefore, the presence of increasing hydrophobicity is not the only driven force responsible for the association of acylated proteins to lipid rafts [210].

The presence of oriented water molecules and lipid dipoles at the interface of a lipid bilayer originates a membrane potential with a positive pole near the centre of the bilayer hydrocarbon region. This dipole potential, 400 mV for phosphatidylcholine monolayers [99], is located in a small region of each lipid monolayer (~1 nm) generating a very strong local electrical field (10^9 V m^{-1}). It is several orders of magnitude larger than the one generated by transmembrane potential (10^7 V.m^{-1}), which modulates and controls the activity and function of membrane proteins such as the voltage gate proteins ion transporters [211]. It is therefore expected a strong influence of the dipole potential on the association of proteins with membranes and on the function of transmembrane or lipid anchored proteins. Additionally, the liquid ordered microdomains present in lipid bilayers have a dipole potential different from the continuous lipid phase, due to the higher lipid packing, and this may have a fundamental role in the sorting and function of membrane proteins.

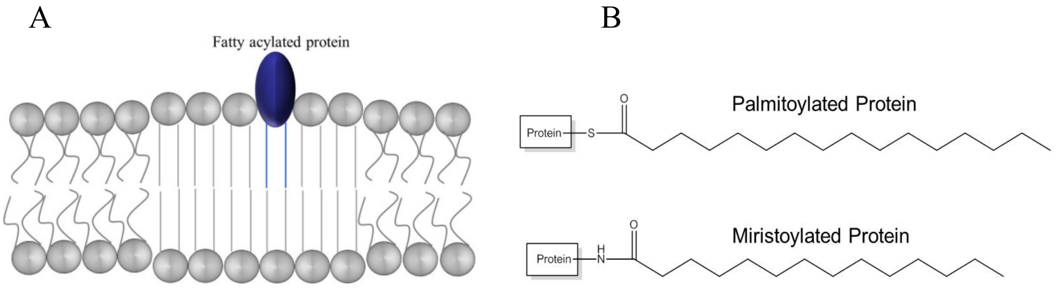

Figure V.1. Panel A: The saturated palmitoyl fatty acid chains allow the protein to pack within the liquid-ordered domains of a membrane lipid raft. Panel B: Schematic structure of common palmitoylated and miristoylated membrane proteins.

The interaction of small molecules with lipid bilayers (association, location and permeation) may also be significantly affected by the magnitude and the orientation of the membrane dipole potential and the ligand dipole moment. The binding interaction of human immunodeficiency virus protease inhibitor saquinavir was shown to be affected by the bilayer dipole potential having a crucial role in the interaction of this molecule with lipid bilayers [212]. Furthermore the presence of amphiphilic molecules such as 6-ketocholestanol and phloretin, that induce alterations in the global membrane potential, where shown to affect the conformation and insertion of a mitochondrial peptide [162]. The adsorption of peptides to membranes is strongly affected by electrostatic and hydrophobic forces and also by the free area and dielectric properties at the membrane interface [213]. These factors are intrinsically related with the global membrane dipole potential, that arises from the alignment of several small dipoles from the lipids and solvating water which are constrained in the interfacial region.

It is well established that the function of several membrane anchored proteins is dependent on their degree of self-association and clustering with additional membrane proteins. The formation of clusters of GPI-anchored proteins in the cell surface is the initial trigger in signal transduction cascades [214, 215]. Although the interactions between the protein and the membrane have been appointed as the main reason behind protein clustering the mechanism is not well known. Computer simulations studies indicate that one fundamental property affecting the rate and extent of protein clustering in the membrane is the length of the hydrophobic anchor (hydrophobic mismatch) [216, 217]. Given the high dipole potential of the membranes, and the usually significant dipole moment of the proteins, it is expected that the electrostatic properties of proteins and membranes plays a significant role in protein-protein interactions but this has been only elusively addressed.

Previous work done by our group addressed the role of the amphiphiles dipole moment in their interaction and solubility in membranes [3]. Following the same line of work we now present a detailed study of the relative partition between POPC vesicles and several acceptor vesicles with different lipid compositions, for two distinct fluorescent amphiphiles. The lipid composition of the acceptor vesicles was chosen to be either in the liquid ordered phase (l_o), liquid disordered phase (l_d) or with l_o and l_d phase coexistence. Both amphiphiles have the same hydrophobic myristic acyl chain and different hydrophilic headgroups, one being a Rhodamine derivative (RG-C_{14}) and the other a Carboxyfluorescein (CBF-C_{14}) (Figure V.2). The polar headgroups were chosen to have opposite orientations of the dipole moment and similar magnitudes (Figure V.2). The effect of those electrostatic properties on the relative association of amphiphiles and vesicles with lipid composition representative of cell membranes was characterized through their transfer between POPC LUVs and lipid vesicles with distinct dipole potentials. The kinetics and equilibrium parameters for their aggregation in the different membranes were also characterized, to gain insight on the effect of amphiphile dipole moment and membrane dipole potential on the aggregation of membrane associated amphiphiles. While Carboxyfluorescein did not aggregate in any of the membranes studied (even at high local concentrations, 2 mol %), RG-C_{14} showed a time and concentration dependent aggregation which was more extensive for membranes in the liquid ordered state. Additionally, results for the fluorescence anisotropy and lifetimes showed that in liquid ordered membranes CBF-C_{14} has a more shallow localization, at the lipid-water interface, while RG-C_{14} was buried deeper in the membrane. A notable exception was obtained for POPC membranes were both probes were essentially in the same region.

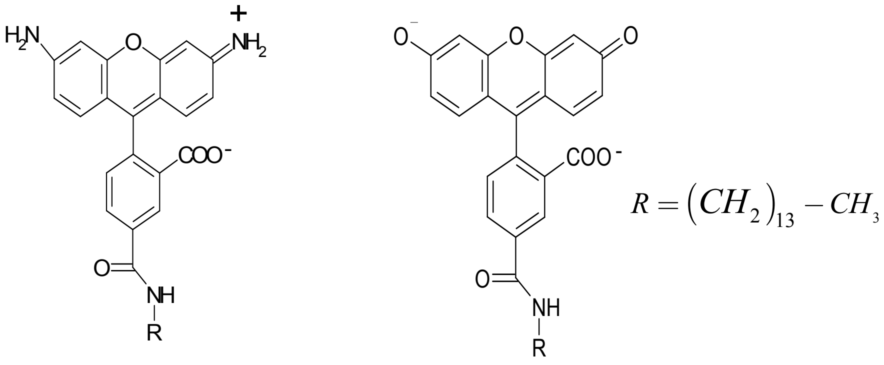

Rhodamine green ™ *5-Carboxyfluorescein™*

Figure V.2. Chemical structures for the fluorescent amphiphiles used in this work at pH 7.4.

V.2 Aqueous Solubility of RG-C_{14} and CBF-C_{14}

The solubility of RG-C_{14} in aqueous solution was too small to be experimentally characterized. Therefore, we measured the solubility, as monomer, for a smaller chain derivative (RG-C_{10}) and extrapolated to the 14 carbons length amphiphile based on the dependence with the alkyl chain length obtained previously for other homologous series of amphiphiles [175].

Solutions of the amphiphiles in the aqueous buffer (III.3 above) were set through hydration of a recently formed film of the amphiphile, prepared from evaporation of the required amount of solution in methanol, and were allowed to equilibrate for 1 h at 25 ^{o}C with occasional vortex (see III.7 above). The aqueous solubility of the amphiphile in the monomeric form (critical aggregation concentration, CAC) was obtained through deviations from the, predicted, linearity dependence of the fluorescence intensity with the amphiphile concentration (Figure V.3, A). The amphiphile with the shorter alkyl chain, RG-C_{10}, showed a linear behaviour up to 10 nM, while at higher amphiphile concentrations there were clear deviations, with the aggregated form presenting smaller fluorescence quantum yield. Additionally, the standard deviation associated with the fluorescence results at concentrations above 10 nM are much higher due to stochastic events involved in the formation of aggregates in very dilute solutions. Based on the CAC dependence with the length of the alkyl chain obtained previously for a homologous series of fatty amines [175], $\Delta\Delta G^0$= -3.4 kJ/mol per CH_2, the CAC predicted for RG-C_{14} is 42 pM. The other fluorescence amphiphile in study, CBF-C_{14}, was found to be soluble in aqueous solution up to 2.5 ± 1 nM (Figure V.3, Panel B).

The results obtained for the solubility of the monomeric form of the amphiphiles are in accordance with the fact that CBF-C_{14} is negatively charged presenting a higher CAC while RG-C_{14} is zwitterionic at pH 7.4. The value obtained for the CAC of RG-C_{10} is 5 times smaller than the one recently obtained by our group for the neutral amphiphile NBD-C_{10} (50 nM) [175] highlighting the smaller aqueous solubility of the Rhodamine polar group.

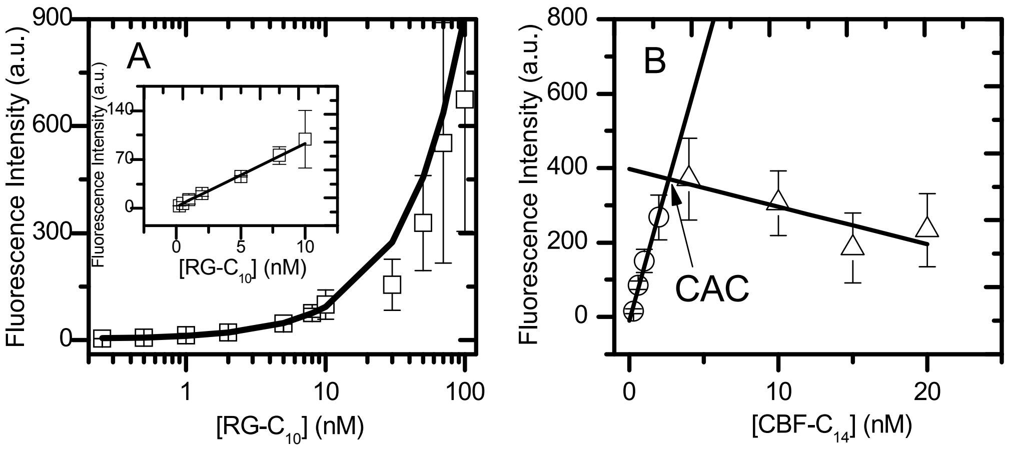

Figure V.3. Typical experimental results obtained for the dependence of the fluorescence intensity at the maxima of RG-C_{10} (panel A, □) and CBF-C14 (Panel B;○; Δ) as a function of its total concentration in the aqueous solution at 25 ºC. In plot A the linear best fit of the fluorescence intensity *vs* amphiphile concentration for values below the CAC is also shown. The inset represents the linear region of the fluorescence with amphipile concentration. In Plot B the lines represent the linear best fit for the fluorescence *vs* CBF-C14 concentration and the interception between the two regimes was considered to be the amphiphile CAC (2.6 nM).

V.3 Partition of RG-C_{14} and CBF-C_{14} between Donor POPC LUVs and Acceptor LUVs with Various Lipid Compositions

Partition between aqueous and lipid phases cannot be directly assessed for the case of amphiphiles with solubility in the aqueous phase below the sensitivity of the method used. This difficulty has been overcome by us through the prior binding of the amphiphile to Bovine Serum Albumin (BSA), which is faster and requires smaller concentrations due to little scattering in the UV-Visible region. The amphiphile is then transferred from BSA and the relevant lipid bilayer allowing the characterization of the partition coefficient to the membrane [135, 175]. This methodology was initially attempted with RG-C_{10}, but the binding efficiency was extremely high requiring the use of BSA concentrations in the nM range to accurately characterize the equilibrium binding constant, K_B, (data not shown). We have therefore characterized the association of the amphiphiles with the various lipid bilayers from their transfer between liposomes. This methodology was commonly used in the eighties [218, 219] and permits the characterization of the relative partition coefficient between donor and acceptor vesicles, $K_{P(Acceptor)}/K_{P(Donor)}$. The transfer was followed by fluorescence intensity that increased upon partition of the amphiphile into the acceptor vesicles due to quenching by energy transfer to RhB-DPPE in the POPC donor vesicles. Typical titration curves for both amphiphiles are shown in Figure V.4. The association is assumed to occur according to the following kinetic scheme.

$$ALV_D^{in} \underset{k_{-f}^D}{\overset{k_f^D}{\rightleftharpoons}} ALV_D^{out} \underset{k_+^D LV_D}{\overset{k_-^D}{\rightleftharpoons}} A_w$$

$$A_w \underset{k_-^A}{\overset{k_+^A LV_A}{\rightleftharpoons}} ALV_A^{out} \underset{k_f^A}{\overset{k_{-f}^A}{\rightleftharpoons}} ALV_A^{in}$$

$$\boxed{\begin{aligned} KL_D &= \frac{k_+^D}{k_-^D} = \frac{ALV_D}{A_w\ LV_D} \\ KL_A &= \frac{k_+^A}{k_-^A} = \frac{ALV_A}{A_w\ LV_A} \\ ALV_D &= ALV_D^{out} + ALV_D^{in} \\ ALV_A &= ALV_A^{out} + ALV_A^{in} \end{aligned}}$$

Where, A_w is the amphiphile (RG-C14 or CBF-C14) as a monomer in the aqueous phase, ALV_D^{in} , ALV_D^{out} , ALV_A^{out} ALV_A^{in} represent the amphiphile associated with the inner (in) or the outer (out) leaflets in the donor (LV_D) and acceptor (LV_A) LUVs respectively, KL_D and KL_A are the equilibrium associations constants for donor and acceptor vesicles. The k_f, k_- and k_+ represent the translocation, desorption and insertion rate constants respectively, in either donor (D) or Acceptor (A) vesicles. After the equilibration for 2 h the amphiphile concentration associated with the acceptor, $\left[ALV_A\right]_t$, and donor, $\left[ALV_D\right]_t$ vesicles are given by V-1;

$$\left[\mathrm{ALV_A}\right]_t = \left[A\right]_T^* \frac{2\delta_A KL_A\left[\mathrm{LV_A}\right]}{1+2\delta_D KL_D\left[\mathrm{LV_D}\right]+2\delta_A KL_A\left[\mathrm{LV_A}\right]},$$

$$\left[ALV_D\right]_t = \left[A\right]_T \frac{2\delta_D KL_D\left[\mathrm{LV_D}\right]}{1+2\delta_D KL_D\left[\mathrm{LV_D}\right]}\left(1-\delta_D\right)+\left[A\right]_T^* \frac{2\delta_D KL_D\left[\mathrm{LV_D}\right]}{1+2\delta_D KL_D\left[\mathrm{LV_D}\right]+2\delta_A KL_A\left[\mathrm{LV_A}\right]},$$

$$\left[A\right]_T^* = \left[A\right]_T - \left[ALV_D\right]_{(t=0)}\left(1-\delta_D\right), \tag{V-1}$$

where, $[A]_T$, is the total concentration of amphiphile in the system and $[A]_T^*$ is the total concentration of amphiphile that is free to equilibrate between the donor and the acceptor vesicles. Depending on translocation, insertion and desorption rate constants of the amphiphiles in donor and acceptor vesicles two additional parameters are required, δ_D and δ_A, related with the amphiphile equilibration in both vesicles. The equilibration factors, δ_D and δ_A, represents the ratio between the variation in amphiphile concentration in the inner monolayer of the donor or the acceptor vesicles and in the outer monolayer during the experimental time (2 h in this work, equation V-2). When translocation is fast, the amphiphile is equilibrated between both monolayers and the variation is equal for both resulting in $\delta_{D(A)}=1$. If the rate of translocation is very small, no variation is observed in the concentration of amphiphile in the inner monolayer and $\delta_{D(A)}=0.5$. Partial equilibrium between the inner and the outer monolayer leads to an equilibration factor range from 0.5 to 1. For donor POPC vesicles the δ_D=1 for both amphiphiles. In the acceptor vesicles for RG-C$_{14}$ the parameters considered were $\delta_{PC:CH(5:5)}=1$, $\delta_{PC:CH(7:3)}=1$, $\delta_{SM:CH(6:4)}=0.7$, $\delta_{PC:CH:PE(5:3:2)}=1$ and $\delta_{PC:CH:PE:PS(4:3:2:1)}=1$ while for CBF-C$_{14}$ were $\delta_{PC:CH(5:5)}=0.8$, $\delta_{PC:CH(7:3)}=1$, $\delta_{SM:CH(6:4)}=0.5$, $\delta_{PC:CH:PE(5:3:2)}=0.8$, and $\delta_{PC:CH:PE:PS(4:3:2:1)}=1$. The parameters were determined from the rate constants observed for pure POPC, POPC:CHOL(5:5) and SpM:CHOL(6:4) for the 2 h experimental time. For all other lipid compositions a rational value was assumed based on the experimental data obtained.

$$\delta_{A(D)} = 0.5\left(1+\frac{\left[ALV_{A(D)}^{in}\right]_t-\left[ALV_{A(D)}^{in}\right]_{(t=0)}}{\left[ALV_{A(D)}^{out}\right]_t-\left[ALV_{A(D)}^{out}\right]_{(t=0)}}\right) \tag{V-2}$$

The fluorescence increase that occurs upon partition of the amphiphile from donor to acceptor vesicles was used to determine the apparent partition coefficient between POPC LUVs and distinct membrane acceptors in l_d and l_o phases. The experimental total fluorescence at equilibrium is given by the quantum yields and the amphiphile concentration in each compartment;

$$I_F \;\alpha\; \Phi_A\left[A\right]_t+\Phi_{ALV_A}\left[ALV_A\right]_t+\Phi_{ALV_D}\left[ALV_D\right]_t \tag{V-3}$$

where, the relative quantum yields of the amphiphile in water (Φ_A), in acceptor vesicles (Φ_{ALV_A}) and POPC donor vesicles (Φ_{ALV_D}) as well as binding constants of the amphiphile to the donor (KL$_D$) and acceptor vesicles (KL$_A$) can be obtained from the best fit to the experimental results of equations *V-1* and *V-2* simultaneously. From the best fit to the experimental results the value of the relative partition coefficient, $K_{P_{rel}}$, may be obtained;

$$Kp_{rel} = \frac{\left(\dfrac{KL_A}{\overline{V}_{LUV^0_{Acceptor}}}\right)}{\left(\dfrac{KL_D}{\overline{V}_{LUV^0_{Donor}}}\right)} = \frac{K_{P_{Acceptor}}}{K_{P_{Donor}}} \qquad (V\text{-}4)$$

where, $\overline{V}_{LUV^0_{Donor}}$ and $\overline{V}_{LUV^0_{Acceptor}}$ represent the molar volume of the outer monolayer of donor and acceptor vesicles. Being the donor LUVs composed of pure POPC it was considered a vesicle formed by 9×10^4 lipid molecules with 0.757 dm^3 per mole of lipid [220]. For the lipid mixtures used as acceptor vesicles the number of lipid molecules per LUV was obtained based on the experimental area per lipid of 40 $Å^2$ for the SpM:CHOL(6:4) [188], and POPC:CHOL(5:5) [181], 48 $Å^2$ for POPC:CHOL(7:3) [181], 48 $Å^2$ for POPC:CHOL:POPE(4:3:2) and 52 $Å^2$ for PC:CHOL:PE:PS(4:3:2:1), obtained using monolayers (see chapter IV). Additionally, we assumed, in the determination of $\overline{V}_{LUV^0_{Acceptor}}$, a volume for POPC, POPE, POPS of 0.757 dm^3/mol independently on the cholesterol composition, 0.702 dm^3/mol for SpM [220] and 0.325 dm^3 for cholesterol [221]. With the considered volumes of phospholipids and cholesterol a thickness of 4.5 nm for POPC:CHOL(5:5), 4.6 nm SpM:CHOL(6:4) and 4 nm, for all other lipid compositions was obtained in accordance with experimental [222] and simulation data [223].

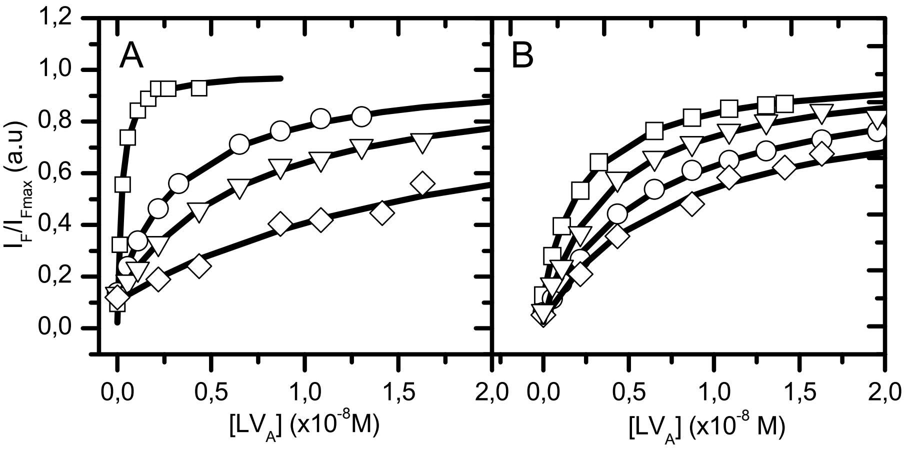

Figure V.4. Partition of RG-C_{14} (A) and CBF-C_{14} (B), at pH 7.4, between donor POPC LUVs and different acceptor Luvs at 25 °C. Plot A: Typical results obtained for the titration of RG-C_{14} from POPC LUVs 0.1 mM (final concentration) at 0.2 μM with acceptor POPC LUVs (□), POPC:CHOL(7:3) (○), POPC:CHOL(5:5) (∇), and SpM:CHOL(6:4) (◊). The line is the best fit of equations V-1 to V-3 with $Kp_{Acceptor}/Kp_{POPC}$ ~ 1, 0.39, 0.20 and 0.03 for, POPC, POPC:CHOL(7:3), POPC:CHOL(5:5) and SpM:CHOL(6:4) acceptor vesicles. Plot B: Typical results obtained for the titration of CBF-C_{14} from POPC LUVs (0. 1 mM, final concentration) at 0.2 μM with acceptor POPC:CHOL(7:3) LUVs between 0 M and $1.2x10^{-8}$ M (□), POPC:CHOL:POPE(5:3:2) (∇), POPC:CHOL(5:5) (○), and SpM:CHOL(6:4) (◊). The line is the best fit of equations *V-1* to*V-3* with $Kp_{POPC}/Kp_{Acceptor}$ = 0.6, 0.3, 0.4 and 0.07 for, POPC:CHOL(7:3), POPC:CHOL:POPE(5:3:2), POPC:CHOL(5:5) and SpM:CHOL(6:4) acceptor vesicles.

The value obtained for the $Kp_{Acceptor}$ is somewhat dependent on Kp_{Donor} when the fraction of the amphiphile in the aqueous phase is significant. This is not the case for the RG-C_{14} that is expected to partition efficiently to the donor liposomes, we predict that Kp_{Donor} ~10^7 based on its low solubility in water and on the equilibrium constants obtained for the homologous series of fluorescent fatty amines NBD-C_n [175]. The affinity of the CBF-C_{14} for donor POPC vesicles may however be lower and the Kp_{Donor} was experimentally obtained at 25 ºC, Figure V.5. The low CAC of CBF-C_{14} (≈3 nM) associated to the observed decrease in quantum yield upon partitioning to membranes difficult the attainment of CBF-C_{14} binding constant by traditional fluorescence titration methodology (low signal:noise). Therefore, we used a different approach and measured the kinetic of interaction (transfer rate constant) between CBF-C_{14}, at probe concentrations slightly higher than CAC (to improve the signal:noise ratio), and POPC at increasing concentrations. The aqueous solutions containing the CBF-C_{14} were always freshly prepared and different concentrations were tested from 1 nM to 15 nM with no noteworthy changes in the final binding constant indicating that the probe aggregation is not significant. The recovered binding constant from the insertion and desorption rate constants lead to a Kp_{Donor}= (7.4 ± 0.5) ×10^5 in POPC. The comparison between $K\mathrm{p}_{\mathrm{rel}}$ obtained for the transfer of CBF-C_{14} between POPC and POPC:CHOL (5:5), 0.37, vesicles and its direct transfer from water to both membranes (0.33) shows a very good agreement, giving a considerable confidence to the recovered results using the vesicles transfer experiments.

The amphiphile as a monomer in water interacts with the lipid vesicles (LV) according to the following scheme:

$$A_w \underset{k_-}{\overset{k_+ LV}{\rightleftharpoons}} ALV^{out} \underset{k_f}{\overset{k_{-f}}{\rightleftharpoons}} ALV^{in}$$

$$\begin{aligned}
\frac{d[ALV^{out}]}{dt} &= k_+[A_w][LV] + k_f[ALV^{in}] - [ALV^{out}]\left(k_- + k_{-f}\right)\\
\frac{d[ALV^{in}]}{dt} &= k_{-f}[ALV^{out}] - k_f[ALV^{in}]\\
\frac{d[A_w]}{dt} &= k_-[ALV^{out}] - k_+[A_w][LV]\\
\frac{d[ALV]}{dt} &= \frac{d[ALV^{out}]}{dt} + \frac{d[ALV^{in}]}{dt}
\end{aligned} \qquad (V\text{-}5)$$

The system can be analytically solved if we consider either fast or slow amphiphile translocation rate, resulting in equations V-6 or V-7 respectively (see appendix for details).

Fast translocation step:

$$[ALV]_{(t)} = \frac{2K_L LV}{1+2K_L LV}[A]_T\left(1-e^{-\beta t}\right); \qquad (V\text{-}6)$$

$$\beta = k_+ LV + \frac{k_-}{2}; \qquad KL = \frac{k_+}{k_-}$$

Slow translocation step:

$$[ALV]_{(t)} = \frac{K_L LV}{1+K_L LV}[A]_T\left(1-e^{-\beta t}\right) \qquad (V\text{-}7)$$

$$\beta = k_+ LV + k_-; \qquad KL = \frac{k_+}{k_-}$$

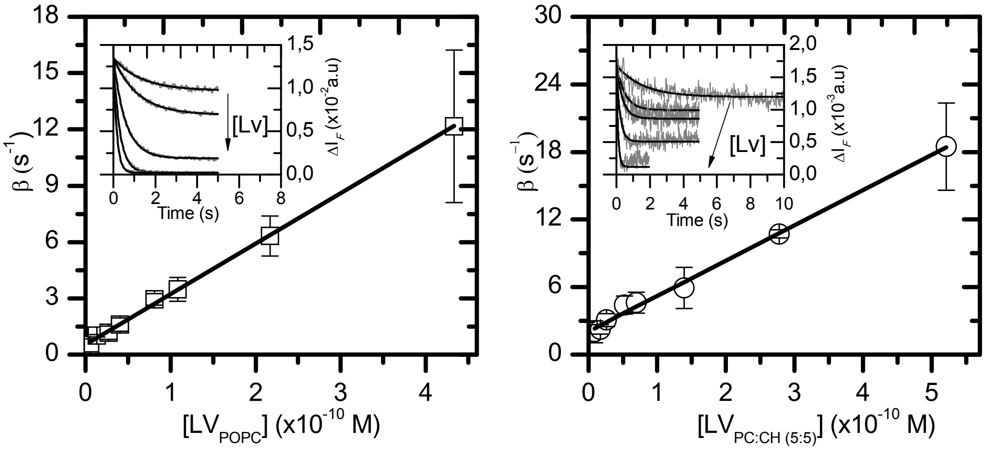

Figure V.5. Variation of the characteristic rate constant for POPC (left, □) and PC:CH(5:5) (right, 0) as a function of [LUV] at 25 ºC. The line is the best fit of equation V-7 to all experimental results with a K_L=2.6x10^{10} M^{-1} for POPC and K_L=7.5x10^{9} M^{-1} for POPC:CHOL(5:5). The inset shows the rate of association between CBF-C$_{14}$ at 15 nM with POPC (left) and 5 nM with PC:CHOL(5:5) (right) being the experimental results represented by a grey line and the best fit to a monoexponential by a black line.

With the predicted (RG-C$_{14}$) and experimentally obtained (CBF-C$_{14}$) partition coefficients to POPC LUVs one could calculate the aqueous concentration of each amphiphile under the experimental conditions used in the transfer experiments. In the most unfavourable conditions, no acceptor vesicles present, the RG-C$_{14}$ water concentration is equal to its predicted CAC value, while for the CBF-C$_{14}$ is 3 nM, slightly above the determined CAC. Therefore, the experiments were done under no striking amphiphile aggregation conditions. Another experimental concern was the eventual transfer of cholesterol from the acceptor to the donor LUVs during the 2 h equilibration time. This was evaluated from the known rates of interaction of the fluorescent cholesterol analogue Ergosta-5,7,9(11),22-tetraen-3β-ol (dehydroergosterol, DHE) with relevant lipid bilayers at 25 °C [224]. During the experimental time (2 h) we predict that less than 5% of cholesterol leaves the

SpM:CHOL(6:4) acceptor vesicles while for other acceptor lipid compositions the variation is smaller than 1%. For the incorporation of cholesterol in the donor vesicles and considering other worst case scenario, high concentrations of POPC:CHOL(5:5), there is an absorption of 1% of cholesterol in the POPC donor vesicles, being the number much smaller for other acceptor lipid compositions.

In the partition of an amphiphile into lipid bilayers in distinct phases, is accepted that it depends mainly on its apolar portion, but this and previous work done by our group [3] show that the polar region of an amphiphile also have an important role regarding the global amphiphile solubility in membranes with distinct phase properties. From the obtained results it is clear that the relative partition coefficient of the RG-C_{14} derivative from POPC to different acceptor membranes is smaller than its homologous CBF-C_{14} (Table V.1). Furthermore, for both fluorescent probes there is a decrease in the Kp_{rel} with the bilayer ordering. The presence of 20 % POPE in POPC:CHOL:POPE(5:3:2) bilayers as well as 10 % of POPS in POPC:CHOL:POPE:POPS(4:3:2:1) decrease the Kp_{rel} (neglecting the charge repulsion for CBF-C_{14}) for RG-C_{14} and CBF-C_{14} relative to the POPC:CHOL(7:3). For membranes in the same liquid ordered state, SpM:CHOL(6:4) and POPC:CHOL(5:5) there is a highest difference in Kp_{rel} for the RG-C_{14} (≈ 7 times) relative to CBF-C_{14} (≈6 times) being the Kp_{rel} always smaller in SpM:CHOL(6:4) than in POPC:CHOL(5:5). Previous work done by our group using NBD fluorescent phospholipids (NBD-DMPE) and lysophospholipids (Lyso-MPE) also corroborate the fact that SpM:CHOL(6:4) membranes are a more unfavorable solvent than POPC:CHOL(5:5) for amphiphilic molecules [134, 136].

Table V.1. Equilibrium Parameters for the transfer of the RG-C_{14} and CBF-C_{14} from POPC donor bilayers to acceptor bilayers at distinct lipid compositions and phase states at 25 °C.

	RG-C_{14}		CBF-C_{14}	
Acceptor Bilayer	$KP_{rel}=\frac{KP_{Acceptor}}{KP_{POPC}}$	$\Delta G_P{}^{0\,(a)}$ (kJ/mol)	$KP_{rel}=\frac{KP_{Acceptor}}{KP_{POPC}}$	$\Delta G_P{}^{0\,(a)}$ (kJ/mol)
POPC:CHOL (7:3)	0.4±0.05	2.3±0.3	0.6±0.07	1.7±0.3
POPC:CHOL (5:5)	0.2±0.008	4.1±0.1	0.4±0.03	2.5±0.2
SpM:CHOL (6:4)	0.03±0.004	8.9±0.4	0.06±0.01	6.9±0.6
POPC:CHOL:PE (5:3:2)	0.30±0.02	3.0±0.2	0.5±0.09	1.9±0.5
POPC:CHOL:PE:PS (4:3:2:1)	0.30±0.05	3.2±0.5	0.2±0.04 0.6 ± 0.1^{b}	4.0±0.5

(a) $\Delta G_p{}^0 = \Delta G_{Acceptor} - \Delta G_{POPC}$

(b) Relative partition coefficient excluding the charge repulsion effect between POPS and CBF-C_{14}, obtained using Guoy-Chappman theory. It was considered for mathematical purposes a $\Psi_0 = -17$ mV recovered from reference [174].

V.4 Aggregation of RG-C_{14} and CBF-C_{14} in Lipid Bilayers

The aggregation of RG-C_{14} and CBF-C_{14} in different membranes was studied to characterize the equilibrium and kinetics dependence with membrane composition (Figure V.6). This particular topic endorses an important biological issue, trying to understand the clustering of acylated membrane proteins. Moreover, it allows us to have some insights regarding the effect of the bilayer properties in the stabilization of the aggregated form of amphiphiles with different headgroups and electrostatic properties under high probe: lipid molar ratio. In LUVs prepared from pure POPC, mixtures of POPC:POPE(80:20) and POPC:POPS(90:10) the absorption spectra of the RG-C_{14} fluorescent amphiphile remains practically unchanged up to 230 h (larger experimental time measured) even at a probe: lipid molar ratio as high as 1:50. The obtained results and the fact that the fluorescence spectra has a similar shape to the one obtained in methanol, lead us to the conclusion that under these conditions the probe is monomeric in those lipid bilayers. In POPC:CHOL:POPE(5:3:2) and POPC:CHOL(7:3) LUVs the RG-C_{14} amphiphile showed a distinct behaviour with a time dependent decrease in the absorption intensity maxima at 502 nm and an associated appearance of a second band in the spectral region of approximately 545 nm, which was considered to correspond to an aggregated form of the fluorophore in the membrane. This behaviour was more extended in POPC:CHOL(5:5) and SpM:CHOL(6:4), even at a smaller lipid: probe ratio of 1:200, and the red shifted absorption band was deviated to higher wavelength (574 nm) in POPC:CHOL(5:5), (Figure V.6).

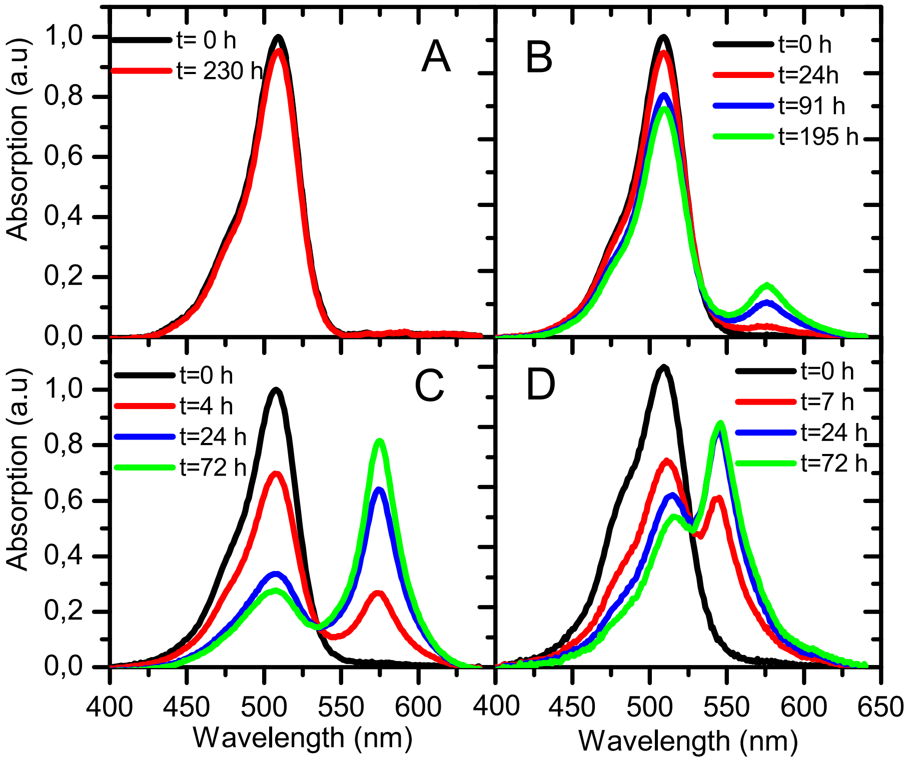

Figure V.6. Time evolution of the RG-C_{14} absorption spectra in LUVs inserted into LUVs prepare from pure POPC (A), POPC:CHOL:POPE (5:3:2) (B), POPC:CHOL (5:5, molar ratio) (C) and SpM:CHOL(6:4) (D). The molar ratio of the fluorescent lipid amphiphile to the host lipid was 1:50 for all cases except POPC:CHOL (5:5) and SpM:CHOL (6:4) where it was 1:200.

The fact that the absorption spectrum of the RG-C_{14} in SpM:CHOL(6:4) was completely reverted to its initial shape within 35 min at 60 ºC and the excitation at the red shift absorption band resulted in no fluorescence emission intensity, were indications that fluorescent probe is aggregating in the membrane. The decrease in the absorption maxima at 502 nm was followed in time and the kinetic curve was well fitted by a dimerization process (Figure V.7). This type of aggregation profile for this particular amphiphile has been observed by our group using MLVs instead of the LUVs [3]. Furthermore, dimerization of xanthene dyes has been widely studied and characterized both in water and in liposomes [225-227] and a similar behaviour was found. The aggregation process was defined by the following kinetic scheme:

$$M + M \underset{k_1}{\overset{k_2}{\rightleftharpoons}} D \quad ; \qquad K_d = \frac{k_2}{k_1} = \frac{[D]}{[M]^2},$$

where, M and D are the monomer and dimer species, and K_d is the dimerization equilibrium constant. From the best fit of the resulting equation for the dimer formation to the experimental results we obtain the second order aggregation constant, k_2, the first order disaggregation rate constant, k_1, and, K_d summarized in Table V.2. The time dependent variation in the concentration of the monomer is specified by V-8 and the correspondent derivation may be found in the appendix.

$$\begin{aligned}
&[M]_t = [M]_{t=\infty} - \frac{2 \times \Delta[D]_0 \times \exp(-kt)}{1 - \left(\frac{4k_2}{k}\right) \times \Delta[D]_0 \times \left(1 - \exp(-kt)\right)} \\
&\Delta[D]_0 = [D]_{t=0} - [D]_{t=\infty} \\
&k = k_2 \times \left(4 \times [M]_{t=\infty} + \frac{k_1}{k_2}\right)
\end{aligned} \qquad (V\text{-}8)$$

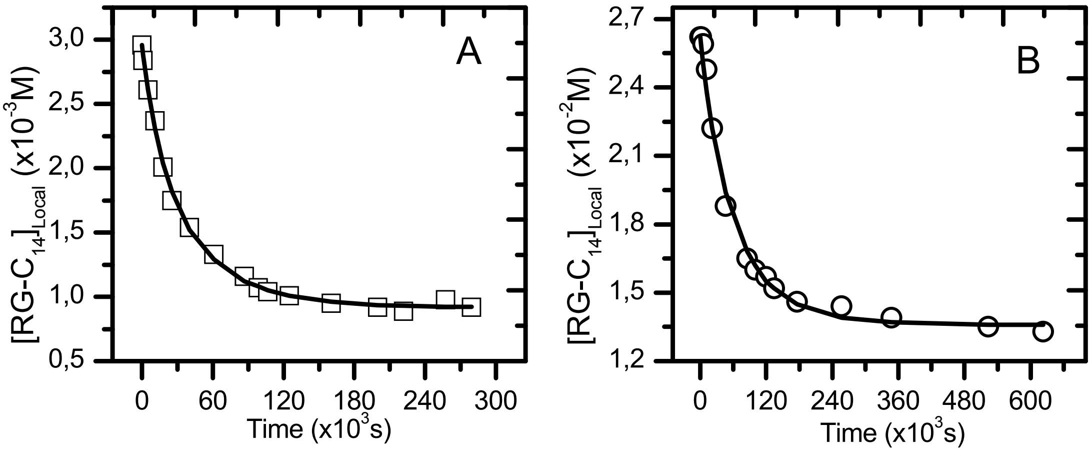

Figure V.7. Time dependence at 25 °C of the local concentration of RG-C_{14} in SpM:CHOL(6:4) (A) and POPC:CHOL(7:3) (B) LUVs at a lipid: probe molar ratio of 1:200 and 1:50 respectively. The open squares are the experimental data and the line is the best fit of the experimental results with equations V-8 and k_2=4.4x10^{-3} $M^{-1}s^{-1}$ and a k_1= 3.7x10-6 s^{-1} for SpM:CHOL(6:4) and k_2=1.6x10^{-4} $M^{-1}s^{-1}$ and a k_1= 4.9x10^{-6} s^{-1} for POPC:CHOL(7:3).

There is a substantial difference between the recovered aggregation constants for RG-C_{14} in the POPC:CHOL(7:3) and the results previously obtained by our group [3]. Unlike the previous work we selected LUVs instead of MLVs and permanently agitated the solution, this procedure avoids vesicle sedimentation at long times that may explain the divergence in the obtained results. From the experimental results we can observe that the second order aggregation constant is greater in membranes with higher cholesterol content. Furthermore, while the first order rate constant for the disaggregation has comparable values in both liquid ordered phases composed of POPC:CHOL (5:5) and SpM:CHOL(6:4), the dimerization is 1.6 times slower in the former than in the latter bilayer. The presence of 20% of POPE increases both the dimerization and the disaggregation rate constants of RG-C_{14}, resulting a ≈1.8 times favorable K_d relative to the POPC:CHOL(7:3) bilayer. So, the ethanolamine small headgroup promotes, even at a small 20% quantity, the aggregation of RG-C_{14} in the membrane.

Table V.2. Kinetic parameters for aggregation of RG-C_{14} in bilayers at 25 ºC.

	POPC:CHOL (5:5)	SpM:CHOL (6:4)	POPC:CHOL (7:3)	POPC:CHOL:PE (5:3:2)
k_2 ($\times 10^{-3}$ $M^{-1}s^{-1}$)	2.4±0.9	3.6±1.4	0.2±0.04	0,5±0,1
k_1 ($\times 10^{-6}$ s^{-1})	3.4±0.8	3.9±0.8	4.2±0.6	7.2±1.0
K_d ($\times 10^2$ M^{-1})	7.0±1.5	9.0±2.5	0.4±0.1	0.7±0.3
K_m ($\times 10^2$)[(a)]	12±0.3	16±0.4	0.6±0.1	1±0.4
ΔG (kJ mol^{-1}) [(b)]	-8.8±0.3	-9.1±0.4	-5±0.3	-6±0.6

[(a)] Mole fraction equilibrium constant: $K_m = \dfrac{(n_D / n_T)}{(n_m / n_T)^2}$; $n_T = n_D + n_L + n_m$, where n_D, n_m and n_L are the number of moles of dimer, monomer and lipid in the system, respectively.

[(b)] $\Delta G = -\dfrac{RT}{2}\ln K_m$, where 2 is the number of amphiphiles in the aggregate (for details see [228])

The aggregation of CBF-C_{14} amphiphile was studied in SpM:CHOL(6:4) bilayer, which gave the higher K_d for RG-C_{14}, at a probe: lipid molar ratio 1:50. The absorption was followed during 6 days and after an initial lag period of one day there was a decrease of approximately 15% of the band maxima at 490 nm and an increase in the other absorption band at 468 nm, contrasting with the RG-C_{14} where a new band appeared at longer wavelengths (Figure V.8, Panel B). Although the experiments were done at considerable higher concentrations a similar aggregation behaviour was observed for the 6-Carboxyfluorescein (6-CBF) in egg phosphatidylcholine liposomes [226]. According to the ionization equilibrium for carboxyfluorescein the CBF-C_{14} is negatively charged at pH 7.4, however there was an increase in absorption at 468 nm indicating the presence of aggregates, which may be occurring either within the bilayer or in the aqueous solution. It is known that fluorescein dimerization in water occurs at a range of concentrations 10^{-5}-10^{-4} M [229], moreover CBF-C_{14} has a CAC of approximately 3nM, so it is predicted under the experimental conditions ([SpM:CHOL,6:4]= 1 mM and lipid:CBF-C_{14}= 1:50, molar ratio) the formation of aggregates in water due to the high aqueous concentration of CBF-C_{14} (~0.9uM). Furthermore, when the CBF-C_{14} in SpM:CHOL(6:4) solution, stored at 25 ºC for 6 days, is heated to 60 ºC it takes a considerable longer time (8 h) than RG-C_{14} (35 min) for the final absorption spectra to have the same profile has the initial spectra recovered at no aggregation conditions

(Figure V.8, A). To further clarify whether the aggregates of the CBF-C_{14} where actually in the aqueous phase another procedure was followed. Both RG-C_{14} and CBF-C_{14} solutions containing the aggregates where independently extruded through a pore with a diameter of 100 nm. We expected that the membrane aggregates would not be affected by the extrusion methodology, with the absorption spectra maintaining its profile, while aggregates in water with sizes bigger than the 100nm would be trapped in the filter and the final absorptions spectra should be similar to the one at time zero. Although some probe was lost during the extrusion procedure, remarkably while the shape of the spectra for RG-C_{14} was maintained, with the aggregation characteristic red shifted band, for the CBF-C_{14} the spectra was very similar to the one obtained for the same solution at time= 0 h. This result, the long-time reversibility at 60 ^{o}C, the fact that no additional red shifted band was present and the low partition coefficient of the CBF-C_{14} (high water concentrations) lead us to speculate that its aggregated form is mainly in the aqueous solution rather than in the membrane. Since that in the more ordered SpM:CHOL(6:4) membrane the aggregation of the carboxyfluorescein amphiphile was not evident no further studies with the other lipid mixtures membranes were performed. So, both probes studied presented a completely different aggregation profiles and while RG-C_{14} aggregates in the membrane phase appearing a new band in the region of 675 nm, the CBF-C_{14} aggregates in aqueous solution without any band maxima appearance in the 550-700 nm spectral region. The aggregation of the RG-C_{14} occurred more drastically in membranes which contained cholesterol enhancing the fact that the increase in membrane packing, order and dipole potential stabilizes the aggregated form of RG-C_{14}.

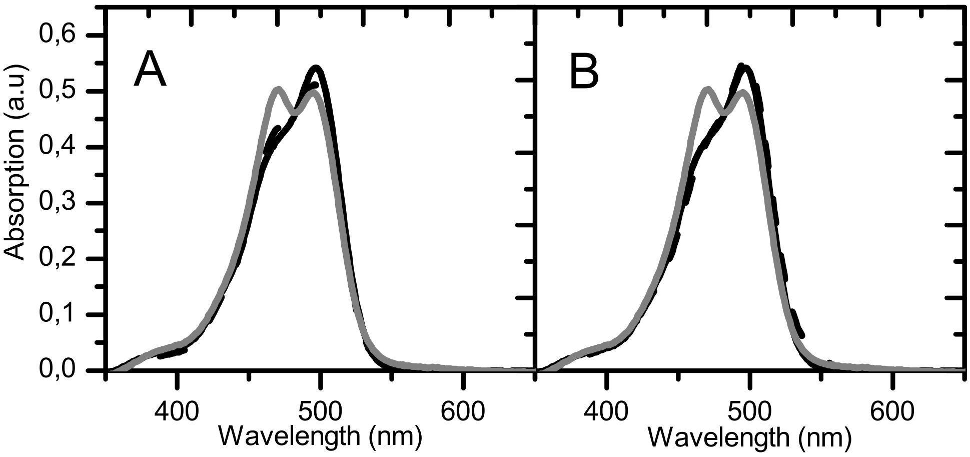

Figure V.8. Panel A: Time dependence absorption spectra of the CBF-C_{14} in SpM:CHOL(6:4) LUVs at 25 ºC at a lipid: probe molar ratio of 1:50. The straight line is at time = 0 h, dash at t= 24 h and dot t= 6th day. Panel B: Reversibility test in the absorption of CBF-C_{14} in SpM:CHOL (6:4, molar ratio) LUVs at 60 ºC at a lipid: probe molar ratio of 1:50. The straight line is at 60 ºC and t = 0 h, dashed line is after incubation at 60 ºC during 8 h and dot is the spectrum of the aggregated solution after the 6th day at 25 ºC.

V.5 Spectral Properties of the RG-C_{14} and CBF-C_{14} in Liquid Ordered and Liquid Disordered Phases

The absorption and fluorescence spectra of probes like Rhodamine and in particular Carboxyfluorescein are very sensible to the media where they are located and shifts may be observed depending on the probe local environment [230]. Considering the amphiphilic nature of the Rhodamine and Carboxyfluorescein derivatives, used in our work, the absorption and fluorescence emission spectra were obtained in methanol and lipid bilayers, either in the liquid ordered or the liquid disordered state, with a total lipid concentration of 1 mM and a final amphiphile concentration of 2 μM, decreasing the amphiphile aggregation probability (Figure V.9). To perform this study we selected the POPC membrane, used as donor in the partition experiments and in the liquid disordered state, POPC:CHOL(5:5) and SpM:CHOL(6:4) membranes both in the liquid ordered state but with distinct results either in amphiphiles K_{Prel} and membrane aggregation of RG-C_{14}. When the RG-C_{14} fluorescent probe was dissolved in methanol solution the differences were significant, with both the absorption and fluorescence emission spectra showing an evident red shift in membranes, indicating that the RG-C_{14} chromophore in methanol is sensing a different viscosity and polarity than in membrane. Considering that the probe is most probably localized in the interfacial region of the lipids headgroup where the dielectric constant changes from 80 in water to 2 in the hydrocarbon region, RG-C_{14} is in a more polar environment than in methanol. In the membranes no relevant changes in the absorption of RG-C_{14} was notice, but in the fluorescence emission spectra of CBF-C_{14} there were continuous small blue shift going from the POPC to POPC:CHOL(5:5) and then to SpM:CHOL(6:4) membranes. For the CBF-C_{14} amphiphile in the more disordered bilayer (POPC) the absorption spectra presented a completely different shape from the one obtained for both liquid ordered membranes, with two band maxima at 490 nm and 468 nm which are red shifted compared to the spectra in methanol. Within POPC:CHOL(5:5) and SPM:CHOL(6:4) liquid ordered membranes the absorption maintains the same profile with a single band maxima, nonetheless comparing to the amphiphile in POPC there is a evident red shift of 9 nm and 8 nm for POPC:CHOL(5:5) and SpM:CHOL(6:4), respectively. With regard to CBF-C_{14} fluorescence emission in SpM:CHOL(6:4) it presents a maximum at 524 nm while for POPC and POPC:CHOL(5:5) bilayers the spectra it is slightly red shifted by 3 and 4 nm respectively (Table V.3). The spectral changes of CBF-C_{14} are more evident when the probe is inserted in the liquid disordered POPC bilayers, showing that the amphiphile headgroup is in a distinct environment when compared to membranes in l_o phase. Song *et al* (2000) observed that depending on whether it was on a anionic or cationic surfactant vesicles the absorption spectra shape of a butyl derivative of fluorescein changed drastically, essentially due to the fact that the p*K*a in both micelles was very distinct, while in anionic micelles the predominant specie was the monoanion in cationic micelles was the dianion form. [231] The relative quantum yield obtained in membranes showed a distinct behaviour for both probes. While for RG-C_{14} inserted in POPC the quantum yield presented a higher value than the POPC:CHOL(5:5) and SpM:CHOL(6:4) bilayers, for the CBF-C_{14} probe the relative quantum yield was minimum in the more disordered pure POPC bilayer.

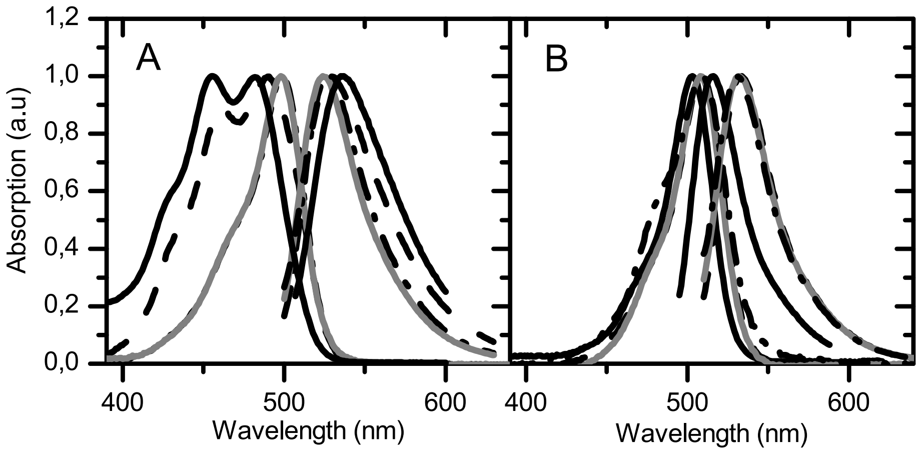

Figure V.9. Normalized Absorption spectra of CBF-C_{14} (A) and RG-C_{14} (B) in, methanol (straight line), POPC (dash line), POPC:CHOL(5:5) (grey line) and SpM:CHOL(6:4) (dotted dashed line), at 25 ºC and LUVs concentration of 1mM and lipid to probe ratio of 1:500 mole ratio.

Carboxyfluorescein is widely known as a pH sensible dye where both the ground and the excited state may be affected by the solvents [232] and, as a result of a distinct probe location within the membrane, its p*K*a may change depending on whether it is inserted in a more ordered or disordered liquid phase membrane. In water carboxyfluorescein present three distinct ionization equilibrium, a first one at 2.1, where the cation and the neutral species are prevalent, a second around 4.3, where both neutral and monoanion exist in equilibrium, and a third around 6.4, for the conversion of monoanion to the dominant fluorescent form, the dianion [232]. To determine the ionization constant we have followed the decrease in the absorption maxima band at 497 nm of CBF-C_{14} as a function of the pH decrease in POPC, POPC:CHOL(5:5) (Figure V.10). The titration curve showed that, inserted in the membranes, CBF-C_{14} has two near p*K*a. In POPC the $pKa_2 \approx 6.9 \pm 0.6$ and $pKa_3 \approx 8.9 \pm 0.5$ while in POPC:CHOL(5:5) the $pKa_2 \approx 5.2 \pm 0.4$ and $pKa_3 \approx 7.6 \pm 0.1$. This difference between membranes reflect the more external localization of the CBF-C_{14} headgroup in the POPC:CHOL(5:5) compared to POPC. The reported value for the ionization constant of fluorescein in water is 6.4, which is considerably lower than the values obtained for CBF-C_{14} in membranes, but an increase in the p*K*a due to a change in polarity sensed by the fluorescein or other fluorescent derivatives, upon their solubilization in liposomes, has been observed [233,175]. Furthermore in non-ionic surfactant micelles the value obtained for the fluorescein p*K*a was in total agreement with values found in pure POPC bilayers [234].

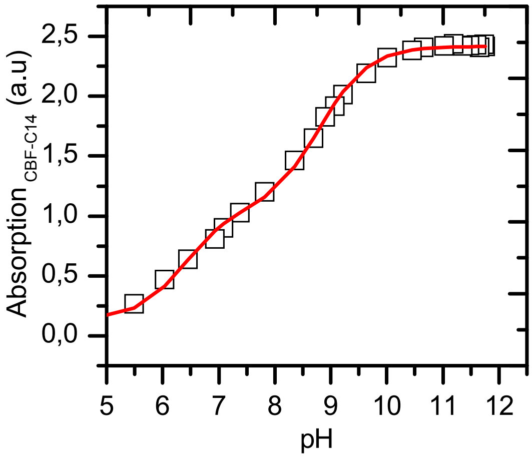

Figure V.10. Typical titration curve obtained for CBF-C_{14} (2 μM) inserted in POPC bilayers (1 mM) at 25 ºC. The red line is best fit of equations A-21 (see appendix) with pKa_2= 6.4 and pKa_3= 8.8.

Table V.3. Spectroscopic characteristics of the probes used in this work in distinct solvents at 25 ºC.

	λ_{Max} Absorption (nm)		λ_{Max} Fluorescence (nm)		Quantum Yield[(a)]	
	RG-C_{14}	CBF-C_{14}	RG-C_{14}	CBF-C_{14}	RG-C_{14}	CBF-C_{14}
Methanol	503	455	528	535	-	-
POPC	509	490	534	528	1	0.16±0.01
POPC:CHOL (5:5)	508	499	532	527	0.25±0.05	1
SpM:CHOL (6:4)	509	498	530	524	0.30±0.08	0.71±0.02

[(a)] The quantum yield are given with reference to quantum yield of RG-C_{14} in POPC and CBF-C_{14} in POPC:CHOL(5:5)

V.6 Fluorescence Anisotropy and Lifetimes

The apparent partition coefficient, the aggregation equilibrium and the spectral properties of the RG-C_{14} and CBF-C_{14} in lipid bilayers suggest that there is a strong dependence with the amphiphile headgroup or with the membrane phase and electrical properties. Nevertheless, these parameters do not allow predicting the position of the probe within the membrane, so it is interesting to relate all the determined parameters with the positioning of the amphiphile in distinct membranes. With the photophysical characterization, namely fluorescence anisotropy and lifetimes, of RG-C_{14} and CBF-C_{14} we pretend to elucidate about the effect of the membrane and compare, taking into account their polarity, the differences between both probes used. The steady state anisotropy and the fluorescence lifetime may in fact produce important information regarding the local environment sensed by the probe within the membrane. Moreover, we can observe whether the dipole moment of the probe together with the membrane dipole potential contributes towards a shallower or a deeper positioning of the probe. The experimental steady state fluorescence anisotropy and lifetime of the RG-C_{14} and CBF-C_{14} are reported in Figure V.11 and Figure V.12, respectively. For RG-C_{14} the fluorescence anisotropy increases with membrane order from pure POPC to equimolar POPC:CHOL bilayers, moreover there is also a further increase for the SpM:CHOL (6:4) bilayers. The fluorescent lifetimes of the CBF-C_{14} and RG-C_{14} were obtained for pure POPC, POPC:CHOL(5:5) and SpM:CHOL(6:4) membranes, and the data was well fitted to a single exponential decay formalism. Considering the membrane where they are inserted the lifetimes of the excited state seems to decrease slightly with the increasing order degree of the lipid bilayer, from POPC to POPC:CHOL(5:5) and finally SpM:CHOL(6:4). The lifetime in methanol was also studied and a similar 3.93 ns and 4.17 ns for CBF-C_{14} and RG-C_{14} were obtained, Table V.4. The lifetimes of the RG-C_{14} and CBF-C_{14} compare well with literature reported values for the fluorescein molecule and for Rhodamine 110 in water which present a single lifetime of approximately 4 ns [226, 235, 236]. In a fully saturated di-palmitoyl phosphatidylcholine (DPPC) liposomes a multiexponential decay (with up to 3 lifetimes) for some carboxyfluorescein compounds was obtained, but under such saturation conditions there is a large probability that the membrane physical chemical properties may change conditioning and restricting the probe localization, moreover in such conditions some energy transfer was observed.

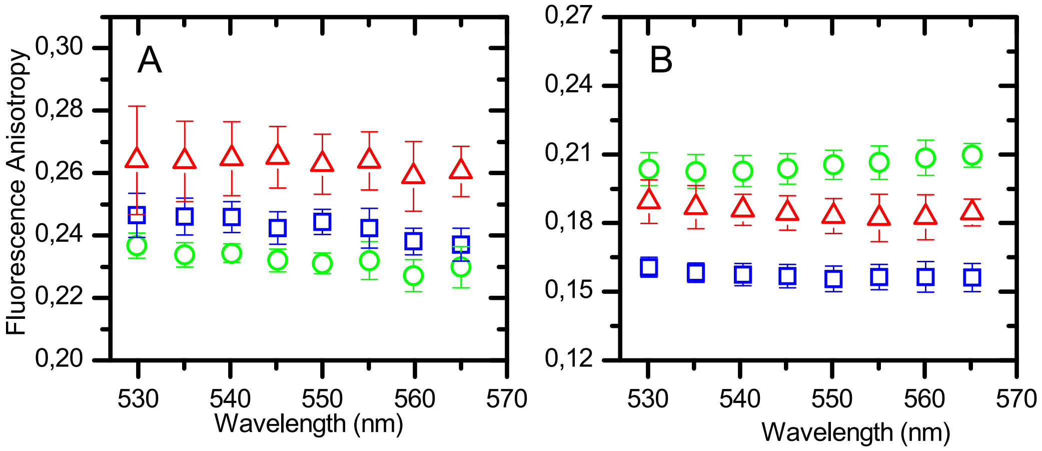

Figure V.11. Anisotropy results for the RG-C_{14} (A) and CBF-C_{14} (B) in 1 mM LUVs of POPC (○), POPC:CHOL(5:5) (□) and SPM:CHOL(6:4) (Δ) between 530 and 570 nm at 25 ºC. The amphiphile concentration was 2 µM for CBF-C_{14} while for RG-C_{14} was 3.3 µM.

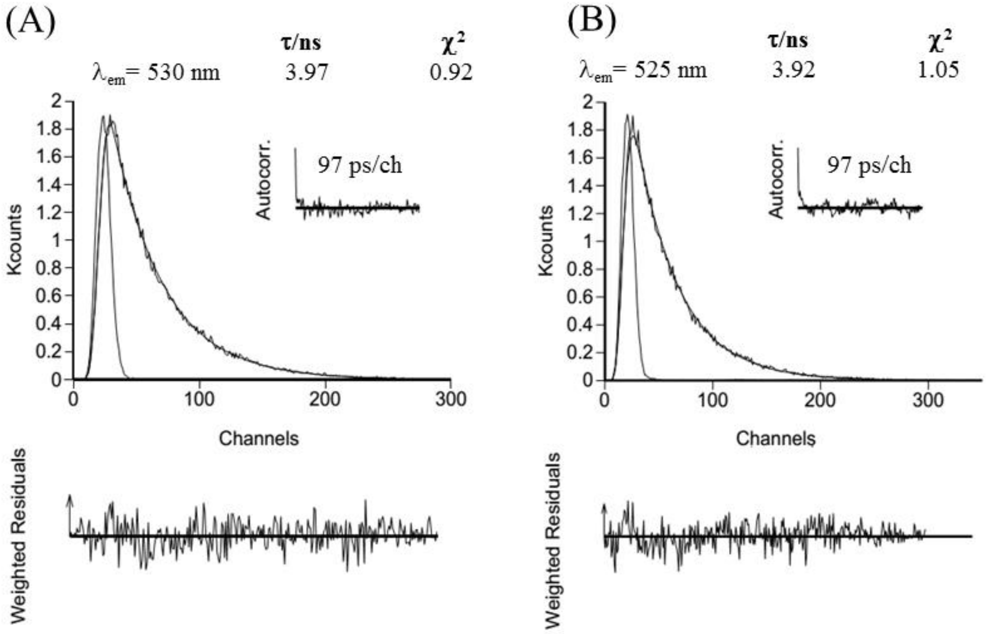

Figure V.12. Fluorescence emission decay for RG-C_{14} in 0.5 mM POPC (A) and CBF-C_{14} in SpM:CHOL (6:4) (B) LUVs obtained with λexc = 460 nm at 25 ºC. The thinner lines in the decays are the instrumental response function (IRF). For a better judgment of the quality of the fits, weighted residuals (W.R. scale, $-3 \leq \sigma \leq +3$), autocorrelation functions (Autocorr.), and chi-square values (χ^2) are also presented.

Table V.4. Fluorescence Anisotropy (r) and Lifetimes (τ) of RG-C_{14} and CBF-C_{14} in membranes in the l_o and l_d phase, at 25 ºC. The results were obtained for three independent experiments being the fluorescence anisotropy the average calculated value for the wavelength range from 530 to 570 nm.

	r ($\times 10^{-2}$ a.u)		τ (ns)	
	RG-C_{14}	CBF-C_{14}	RG-C_{14}	CBF-C_{14}
Methanol	-	-	4.2±0.03	3.9±0.04
POPC	23±0.5	21±0.7	3.9±0.04	4.2±0.04
POPC:CHOL (5:5)	24±0.3	16±0.6	3.9±0.02	4.2±0.1
SPM:CHOL (6:4)	27±1.0	18±0.8	3.8±0.09	4.0±0.04

V.7 Rationalization of the Experimental Results with Membrane Dipole Potential

The relative partition of probes between coexisting phases has been widely studied in different lipid compositions and longer saturated acyl chains fluorophores partition preferentially towards a more ordered phase while the ones with smaller (< C12) or unsaturated acyl chains prefer more disordered phases. The headgroup of a certain amphiphilic probe is somehow neglected to predict the relative partition between phases. De Almeida *et al* (2009) [237] showed that NBD- [1,2-dioleoyl-sn-glycero-3-phosphoethanolamine] (NBD-DOPE) prefers more ordered membrane phases while Rhodamine-DOPE has a 4 times higher partition favouring a more disordered phase. Forster resonance energy transfer experiments, using NBD and Rhodamine fluorescent derivatives with the same acyl chain length, showed that the headgroup itself seems to play an important role in partition between phases [238]. In our experimental work the acyl chain of the amphiphiles have the same 14 carbons length while the polarity of their headgroup is distinct. Therefore, the observed differences in partition, aggregation and photophysics for CBF-C_{14} and RG-C_{14} are essentially due to headgroup polar properties and positioning in the lipid-water interfacial region. In this region there is an ordering of the water molecules due to hydrogen bond interactions with the lipids headgroup [87], this more ordered water has a 100 times decrease in mobility compared to bulk water [86]. With the exception of POPC:CHOL:POPE:POPS(4:3:2:1) we studied membranes with a neutral charge, so the surface potential may be neglected and the only electrostatic potential present in those membranes is of dipolar origin. To compare the effect of dipole moment orientation and magnitude for RG-C_{14} and CBF-C_{14} with membrane dipole potential we performed the AM1 semi empirical theoretical calculations of the amphiphiles in the minimum energy conformations, method included in the Hyperchem® version 8 package [1]. They emphasize a higher hydrophilic character of CBF-C_{14} (23 D) relative to RG-C_{14} (15 D), corroborating our water solubility measurements, and opposite dipole orientations Figure V.13. If on one hand the dipole moment orientation of the CBF-C_{14} points in the same direction as the membrane dipole potential, on the other hand the RG-C_{14} have an opposite dipole moment orientation.

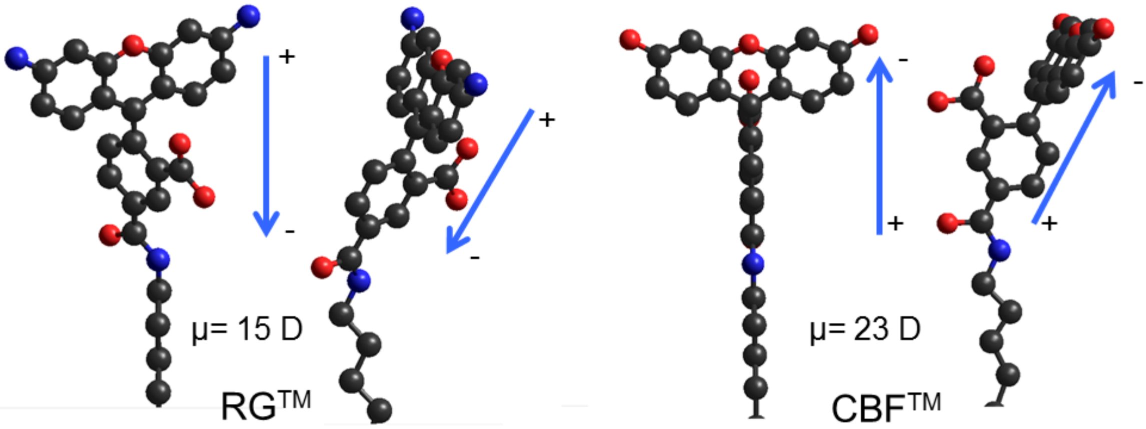

Figure V.13. Structures of RG-C_{14} and CBF-C_{14} (dianion) and the correspondent orientation and magnitude of the dipole moment obtained from semi-empirical quantum mechanical calculations (AM1) using the Hyperchem® version 8 package. Two views are presented showing the orientation of the fluorophore relative to the alkyl chain. Black, blue and red filled balls represent carbon, nitrogen and oxygen balls, respectively.

The addition of cholesterol to a POPC monolayer up to 50% leads to a concomitant increase in the dipole moment of the monolayer of some mV due essentially to the decrease in the area per lipid (increase in lipid packing) [163, 169] (see chapter IV). Comparing Kp_{rel} for distinct membrane compositions (with different dipole potential) with the polar nature of the amphiphile (dipole moment) we observe a linear dependence of Kp_{rel} with dipole potential increase in cholesterol containing membranes, ($\Psi_{\text{POPC}} < \Psi_{\text{POPC:CHOL (7:3)}} < \Psi_{\text{POPC:CHOL:POPE (5:3:2)}} < \Psi_{\text{POPC:CHOL(5:5)}}$). This dependence was observed for both probes being the slope slightly higher for RG-C_{14} than for CBF-C_{14} (Figure V.14).

---

[1] To validate the geometry optimization and the dipole moment determined for our molecules we previously tested the same methodology in small well-known molecules such as the acetic acid.

The higher dependence of Kp_{rel} and ΔG_{rel} with membrane dipole potential for RG-C_{14} results from a lower stability of its fluorescent headgroup in the interfacial region of the membrane phase compared to the CBF-C_{14}. These results are corroborated by the fact that an increase in cholesterol content further contributes to RG-C_{14} faster aggregation, with the K_d in POPC bilayers containing 30% and 50% of cholesterol of $7.2\text{x}10^2$ M^{-1} and $3.8\text{x}10^1$ M^{-1} respectively while for CBF-C_{14} no membrane aggregation was observed. When inserted in the membrane the distinct dipole moment orientation of RG-C_{14} compared to CBF-C_{14} induce a more unfavourable membrane solvation contributing to an energy minimum in its aggregated state. Moreover, the presence of crescent amounts of cholesterol in POPC containing membranes increasing the membrane dipole potential that further destabilizes the RG-C_{14} in the membrane decreasing the Kp_{rel} and increasing the K_d of RG-C_{14}. Although CBF-$C_{14,}$ at pH 7.4 is negatively charged we predict a higher dependence on the Kp_{rel} compared to RG-C_{14} due to the Born energy effect upon transfer of the charged amphiphile headgroup from water (higher dielectric constant) to membrane-water interface (lower dielectric constant). Our results show that a favourable amphiphile dipole orientation leads to a reduced perturbation of the CBF-C_{14} once in the membranes overcoming the unfavourable born-energy effect due to the presence of charges.

The POPE phospholipid has a NH_3 group which is capable of establish intramolecular and intermolecular hydrogen bonding with lipids, leading to a significant decrease in the area per lipid and higher order parameter (aligned tails relative to lipid bilayer normal) [239]. The lipid packing promoted by both the presence of cholesterol and the ability of POPE to hydrogen bond in the mixture of POPC:CHOL:POPE(5:3:2) endorses an higher dipole potential of this lipid mixture relative to the POPC:CHOL(7:3). This increase in the dipole potential due to the presence of the POPE phospholipid supports the observed decrease in RG-C_{14} membrane solubility and the decrease in partitioning of both amphiphiles relative to POPC:CHOL(7:3). Nevertheless the effect of POPE phospholipid in the Kp_{rel} of CBF-C_{14} is smaller than RG-$C_{14.}$ The addition of 10% of

POPS had no additional effect in the *K*p$_{rel}$ of both probes (neglecting the charge repulsion effect in the case of CBF-C$_{14}$) and in the RG-C$_{14}$ solubility, being the value similar to POPC:CHOL:POPE(5:3:2) membranes.

The partition coefficient reveals the difference in interactions of the amphiphile in the membrane and in bulk water. From the results it was observed that compared to CBF-C$_{14}$ the RG-C$_{14}$ is less stabilized in the membrane with the increase in dipole potential. However, the amphiphile partition coefficient to membranes may be defined by the insertion and desorption rate constants and in the next chapter we will address this topic for membranes with different dipole potential.

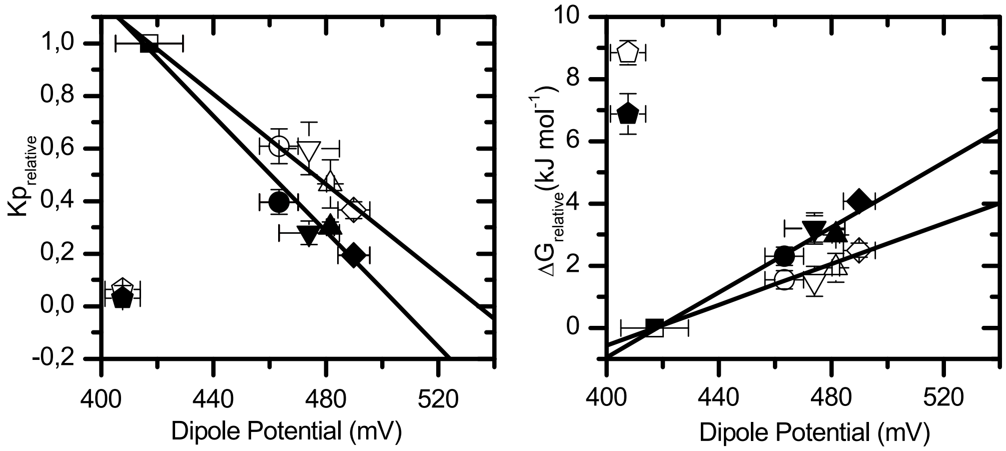

Figure V.14. Dependence of the RG-C$_{14}$ (filled symbols) and CBF-C$_{14}$ (non-filled symbols) Kp$_{rel}$ (A) and ΔG$_{relative}$ (B) with experimental dipole potential for POPC (square), POPC:CHOL (7:3) (circle), POPC:CHOL:POPE(5:3:2) (triangle), POPC:CHOL(5:5) (diamond), POPC:CHOL:POPE:POPS(4:3:2:1) (inverted triangle) and SPM:CHOL(6:4) (pentagon) membranes. The line is the linear fit to the experimental results for POPC, POPCHOL(7:3), POPC:CHOL(5:5) and POPC:CHOL:POPE(5:3:2) lipid compositions.

The fact that the increase in dipole potential of POPC containing membranes differently affects the probes either in partitioning or in aggregation studies prompted us to analyse the chromophore localization in membranes in the liquid ordered and liquid disordered phase. The fluorescence anisotropy and lifetimes experimental results showed that the negative charge of the CBF-C$_{14}$ has a determinant role in its shallower localization compared to RG-C$_{14}$. Kachel, K *et al* (1998), using the parallax method, showed that in liposomes the presence of a charge in the fluorescein derivative "pulled" the probe towards the aqueous media, while a zwitterionic probe (Rhodamine) would be buried deeper within a membrane [240]. An interesting exception was observed in this study for POPC membranes where the smaller fluorescence anisotropy of the CBF-C_{14} relative to RG-C_{14} is compensated by its higher fluorescence lifetime and both probes are sensing the same environment viscosity in these particular membranes. Additionally, its smaller relative quantum yield and the shape of the absorption spectra (similar to the carboxyfluorescein neutral form) support a CBF-C_{14} deeper location in POPC than in POPC:CHOL(5:5) and SpM:CHOL(6:4). An explanation for the similar localization of the CBF-C_{14} and RG-C_{14} in POPC is the presence of hydrogen bond between the CBF-C_{14} and lipid headgroups holding the chromophore in a deeper region. Hydrogen bonds between other fluorescent amphiphiles and the POPC headgroup was previously observed by our group by molecular dynamics simulations [241]. Additionally, the observed higher p*K*a of CBF-C_{14} in POPC membranes further support an increase in its neutral form leading to a deeper localization.

The photophysical studies together with the partition and aggregation demonstrate that both in the liquid ordered phase the SpM:CHOL(6:4) and POPC:CHOL(5:5) have distinct physical properties that makes them different solvents for the studied amphiphiles. The change of glicerophospholipid by a sphingolipid contributed to stabilization of the aggregated state of RG-C_{14} (higher K_d) and a higher decrease of the K_{Prel} for both probes. Based on the SpM:CHOL(6:4) dipole potential we expected that its smaller value compared to the POPC:CHOL(5:5) bilayers [176] would increase the RG-C_{14} solubility, instead of the observed decrease. Nevertheless sphingomyelin containing membranes have peculiar properties, they pack more densely than POPC at the same surface pressures in the presence or absence of equimolar cholesterol concentrations [177]. The water permeability in di-palmitoyl-phosphatiodylcholine (DPPC) and palmitoyl sphingomyelin (PSM) bilayers under cholesterol equimolar concentrations is much smaller for the latter than for the former PC containing bilayer [242], moreover the fact that cholesterol molecule has an preferential interaction for sphingolipids rather than with the glicerophospholipids [243], contribute to a more ordered and rigid SpM:CHOL (6:4) membrane relative to POPC:CHOL (5:5).

This structural properties of SpM:CHOL (6:4) bilayers overlap the effect of the decrease in their dipole potential, promoting a lowering of the relative partition coefficient of both probes compared to POPC:CHOL (5:5). Although the tendency of $K\mathrm{p}_{\mathrm{rel}}$ with membrane dipole potential showed for other membranes was not observed for SpM:CHOL (6:4) the $K\mathrm{p}_{\mathrm{rel}}$ continues to be lower for the RG-C_{14} than CBF-C_{14}

reinforcing the idea that the dipole orientation of amphiphiles has an important role in partitioning to membranes.

V.8 Chapter Highlights

In this chapter, we studied the effect of the amphiphile dipole moment in their partition into lipid bilayers with different dipole potential. We observed, through semi empirical calculations that RG-C_{14} and CBF-C_{14} have opposite dipole potentials when inserted in the membrane. While, the latter has a dipole moment orientation opposite to the membrane dipole potential, the former has the same orientation. The CAC predicted for RG-C_{14} is 42 pM while for CBF-C_{14} is 2.5 ± 1 nM, in accordance with the fact that the latter is negatively charged and the former is zwitterionic. Given their low solubility the partition coefficient was measured through transfer between donor and acceptor vesicles, assessing a $K\mathrm{p}_{\mathrm{rel}}$. For POPC:CHOL membranes we observed that as the dipole potential increases the $K\mathrm{p}_{\mathrm{rel}}$ for both probes decreases. In spite of the smaller dipole potential of SPM:CHOL(6:4) membranes, a lower $K\mathrm{p}_{\mathrm{rel}}$ was observed for both probes due to peculiar properties of these membranes (higher packing density).

The RG-C_{14} showed a time dependent decrease at 502 nm and an associated appearance of a second band at 545 nm, which was considered to be an aggregated form of the fluorophore in the membrane. In POPC:CHOL membranes as the dipole potential increases the aggregation of RG-C_{14} increases.

The negative charge of CBF-C_{14} has a determinant role in its shallow localization in POPC:CHOL(5:5) and SPM:CHOL(6:4) when compared to RG-C_{14}. However, in POPC membranes CBF-C_{14} and RG-C_{14} are sensing the same environment viscosity due to an increase in p*K*a of the CBF-C14.

In the next chapter we will address the effect of the membrane dipole potential in the kinetics parameters (insertion and desorption).

VI

Effect of the Amphiphile Dipole Moment in the Kinetics of Interaction with Lipid Bilayers in Liquid Ordered and Liquid Disordered Phases

VI.1 Introduction

The passive permeation of molecules across lipid bilayers is a fundamental process both in cell biology and drug design and development. The discussion of whether passive permeation is the major transport route for solutes and metabolites is increasing and, some researchers assume different opinions. A few authors support a negligible role for passive route in biological cells, being drugs mostly transported by carriers [244]. Other authors, nevertheless, support a dominant role for passive permeation based on: i) the structural diversity of membrane permeating molecules and metabolites ii) the fact that a lipid bilayer does not have specific binding site, so molecules are less subject to transport inhibition due to their structure and iii) it is a non-saturable route [245, 246]. Some other authors support the coexistence between carrier-mediated and passive transport across membranes [247]. However, evidence that several carriers are limited by substrate size, creates an additional argument for the importance of passive permeation [246]. Moreover, if the passive permeation of an amphiphilic drug is very fast so that it overcomes the effluxes of a carrier mediated protein it is the interaction with the membrane that dictates the bioavailability of the drug. A study employing central nervous systems drugs (CNS-drugs) revealed that passive transportation is a key point, with 94% of the reported drugs displaying a high passive permeability along with non CNS-drugs [248].

Passive transcellular permeation of amphiphilic molecules requires their insertion in the outer leaflet of the biological membrane followed by translocation through the hydrophobic core and finally desorption from the inner leaflet into the other aqueous compartment. The permeation through passive routes involves a critical balance between molecular hydrophobic and hydrophilic components. While a very hydrophobic compound will remain in the bilayer interior, a more hydrophilic, will persist in the aqueous solution. Therefore, the partition coefficient of molecules into membranes allows quantitatively assessing solute lipophilicity and, for simplicity, this parameter has been obtained from the relative distribution of amphiphilic molecules between octanol and water solvents. This over simplistic methodology does not detain the anisotropic nature of biological membranes and, it has been criticized by different authors [249-251].

The solubility-diffusion model predicts the passive permeability rate of molecules across biological membranes (see II.6.2.1 for details). The foundations of this model are the well-known Overton rule, which consider that the rate-limiting step, in permeation, is the translocation of the amphiphilic molecule in the hydrophobic core of the bilayer. The quantitative assessment of the permeability rate, using solubility-diffusion model, requires knowing both the partition coefficient and the translocation rate of the solute in membranes. However, the latter step is frequently unknown for most of the amphiphiles, being assumed to be slow and not strongly dependent on the structure of the solute. This premise it is not always valid and our group showed that, even within the same homologous series, exceptions to the Overton rule occur namely due to variations in the rate limiting step that may be the desorption from the bilayer [141]. Therefore, the quantitative description of the rates for each step (insertion, translocation and desorption) is extremely important to predict the permeability across membranes. Additionally, the asymmetric lipid distribution in membranes makes it crucial to study the kinetics of the interaction of amphiphiles with membranes containing distinct lipids. Our research group, in the latest years, has been committed to fulfil this scientific gap by independently studying the partition coefficient and kinetics of interaction between different homologous series of molecules and bilayers with distinct lipid compositions [134-136, 141, 174, 175, 224, 252-255].

Most amphiphilic molecules have an asymmetric charge distribution (defined has the dipole moment) and when inserted in a membrane they are subject to a considerable electric field resulting from the membrane dipole potential (see II.5 for details). This membrane dipole potential, generated from the contributions of small dipoles present in the lipid, may modulate the interaction with amphiphles. In the former chapter, the dipole potential was shown to affect the partition of two amphiphilic molecules towards bilayers in distinct physical states. In this chapter we will characterize the kinetics of interaction between RG-C_{14} and CBF-C_{14} amphiphiles and distinct lipid bilayers, in terms of the membrane dipole potential and the amphiphile dipole moment. This is the first work that correlates desorption and translocation rates with the electrical properties of both membranes and amphiphiles. Moreover, the contribution of this work is unquestionable once that, markedly, increases the available data where a full characterization of kinetics and thermodynamics of the interaction of amphiphiles with membranes was attained.

VI.2 Kinetics of RG-C_{14} and CBF-C_{14} Exchange between LUVs

The aqueous solubility of the amphiphiles, specifically RG-C_{14}, is very low (see V.2 above for details), and the kinetics of their interaction with membranes, of different composition, could not be obtained directly. This difficulty was overcome through the transfer between donor and acceptor vesicles. The donor vesicles composition was 0.1 mM (final) of pure POPC or a mixture of lipids, loaded with RG-C_{14} or CBF-C_{14} at a probe:lipid molar ratio of 1:500 and the fluorescence lipid quencher RhB-DPPE at 1:100, molar ratio (see III.11). The acceptor vesicles were composed of pure lipids with the composition in study.

In the experiments, fluorescence equipment's with different time resolution were used so that the transfer and translocation rates could be accurately obtained. In the stopped flow equipment the time limit is 1000 s and the slowest step, at lower temperatures, can not be well determined. Moreover, using a steady state fluorimeter the mixture has to be prepared manually, within the cuvette (see III.11), and if the fast step occurs within a few minutes (which is the case for RG-C_{14} and CBF-C_{14} at pH 7.4) its kinetics is poorly defined. Hence, for experimental times larger than 1000 s both methodologies had to be applied. The complete kinetic scheme and the set of differential equations for the transfer of the amphiphiles from donor to acceptor vesicles are given below.

$$\begin{gathered}
ALV_D^{in} \xrightleftharpoons[k_{-f}^D]{k_f^D} ALV_D^{out} \xrightleftharpoons[k_+^D LV_D]{k_-^D} A_w \\
A_w \xrightleftharpoons[k_-^A]{k_+^A LV_A} ALV_A^{out} \xrightleftharpoons[k_f^A]{k_{-f}^A} ALV_A^{in}
\end{gathered} \qquad (1)$$

Set of differential equations for amphiphile in different compartments:

$$\frac{d\left[ALV_D^{out}\right]}{dt}=-\left[ALV_D^{out}\right]\left(k_-^D+k_{-f}^D\right)+k_+^D\left[LV_D\right]\left[A_w\right]+k_f^D\left[ALV_D^{in}\right]$$

$$\frac{d\left[ALV_A^{out}\right]}{dt}=-\left[ALV_A^{out}\right]\left(k_-^A+k_{-f}^A\right)+k_f^A\left[ALV_A^{in}\right]+k_+^A\left[A_w\right]\left[LV_A\right]$$

$$\frac{d\left[ALV_A^{in}\right]}{dt}=k_f^A\left[ALV_A^{out}\right]-k_{-f}^A\left[ALV_A^{in}\right] \qquad (VI\text{-}1)$$

$$\frac{d\left[ALV_D^{in}\right]}{dt}=k_{-f}^D\left[ALV_D^{out}\right]-k_f^D\left[ALV_D^{in}\right]$$

In this scheme the subscript A and D, represent the acceptor and donor lipid vesicles respectively. Briefly, the amphiphile symmetrically loaded to the inner ALV^{in}_D and outer ALV^{out}_D leaflet of donor vesicles, is in equilibrium with its monomeric form in the aqueous medium (A_w). Upon addition of the acceptor vesicles (LV_A) the amphiphile in the aqueous phase equilibrates with the outer (ALV^{out}_A) leaflet of the acceptor vesicles and, from here, with the inner leaflet (ALV^{in}_A). The kinetic rate constants k_-, k_+ and k_f, represent desorption, insertion and translocation, while the correspondent superscript A and D denote the acceptor and donor vesicles, respectively.

The transfer of the amphiphiles between vesicles was observed *via* increase in fluorescence intensity upon partition of the probes from donor LUVs, where it is quenched by the RhB-DPPE, to an acceptor lipid bilayer. The increase in the fluorescence intensity of the RG-C_{14} or CBF-C_{14}, after mixing both donor and acceptor vesicles, is displayed on Figure VI.1. It is evident that for both probes the experimental data is biphasic, with a fast process accounting for 60-70% of the total fluorescence variation for all vesicles studied. This indicates that the equilibrium distribution of the amphiphiles is not symmetric, being enriched in the outer leaflet of donor and/or acceptor vesicles, or that the fluorescence quantum yield of the amphiphiles is smaller when inserted in the outer than in the inner leaflet of the donor vesicles (due to an enrichment of quencher in the outer leaflet). We have obtained information from independent experiments (irreversible quenching of RhB-DPPE by dithionite) that indicate a preferential location of the quencher in the external monolayer of the donor vesicles in agreement with its molecular shape with a larger cross-sectional area for the polar region. Based on the same arguments it is also expected a small enrichment of the amphiphiles in the outer leaflet of the LUVs (both donor and acceptor) and, consequently, the rate constant for translocation from the inner to the outer leaflet (k_f) will be slightly larger than that for the reverse direction (k_{-f}). We have however considered that both rate constants have the same value because they could not be both obtained accurately from the experimental data and also because the difference expected is small ($k_f / k_{-f} \approx 1.5$). It should also be stressed that the asymmetry should be very similar for both amphiphiles in the LUVs with all lipid compositions because of the similar molecular shapes and LUVs curvature.

The characteristic time of the fast process, at 25 ºC and pH 7.4, is smaller than 2 minutes, while the slower step may take several hours for both amphiphiles. This biphasic behaviour, observed in the experimental data, was due to two processes occurring at distinct time scales. An initial fast process owed to the transfer of the amphiphile from donor to the outer monolayer of the acceptor vesicles, which was responsible for the highest fluorescence intensity variation, and the slowest step was attributed to translocation of the probe in the acceptor vesicle. Additionally, as translocation of the probe from the inner to the outer monolayer of the donor vesicles occurs it allows more amphiphile to partition into the acceptor, increasing the final fluorescence intensity in solution.

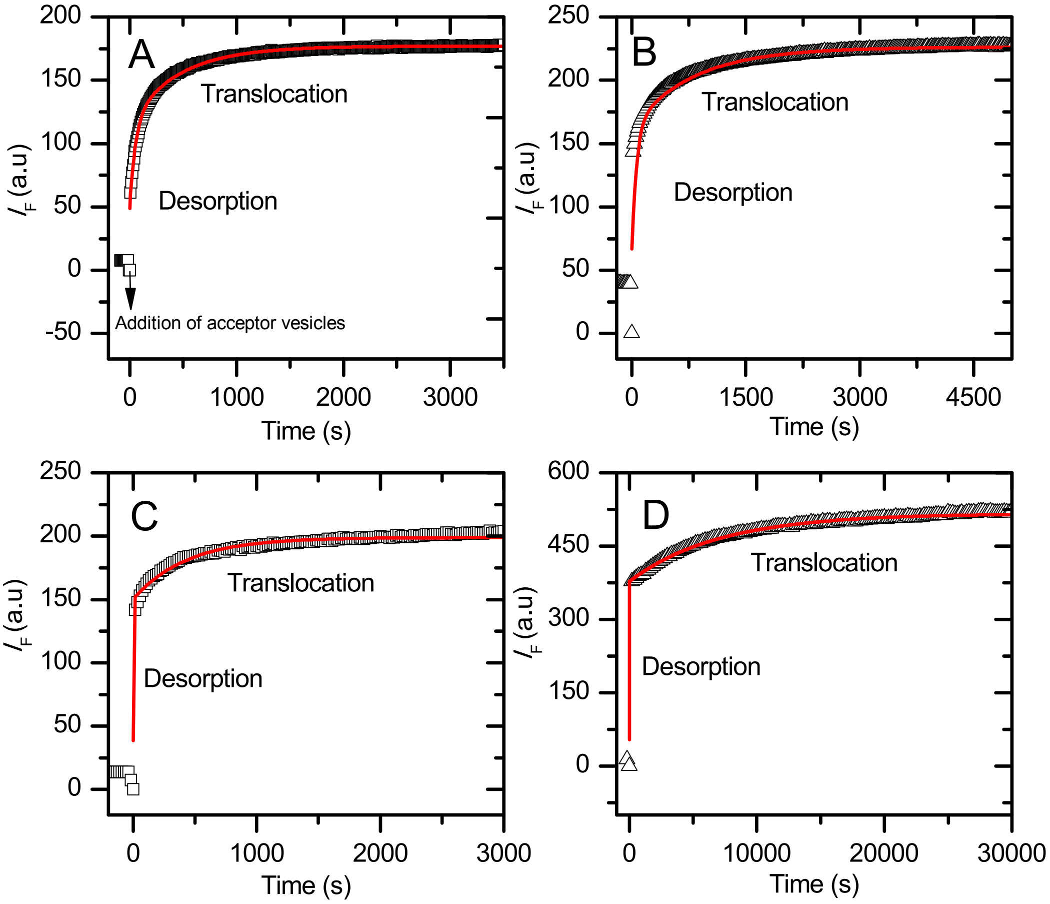

Figure VI.1. Typical curve at 25 ºC for the time dependence of the fluorescence intensity of RG-C_{14} (A and B) and CBF-C_{14} (C and D) upon transfer between 0.1mM (final concentration) donor vesicles and 1.2 mM (final) acceptor vesicles with the same lipid composition, POPC (□), POPC:CHOL(5:5) (Δ). At negative times the experimental points represent the fluorescence of each probe exclusively in the donor vesicles while at t= 0 s the acceptor LUVs were manually added. The red lines are the best fit of equations VI-1.

The system of differential equations given in VI-1, may be analytically solved if the two steps (desorption or translocation) occur at distinct times scales. The biphasic behaviour encountered indicates that the rate of translocation is much slower than the rate of insertion/desorption and, therefore, the analytical solution was encountered with the assumptions: ($k_f^D << k_-^D$; k_+^D [LV^D] and $k_f^A << k_-^A$; k_+^A [LV^A]. As referred above in the text it was assumed that the rate constant for translocation was equal in both directions (inner to outer and outer to inner; $k_f = k_{-f}$).This resulted in equations VI-2 for the rate constant of the fast step (β) and equilibrium distribution of probe in the acceptor LUVs ($ALV^A_{(t=\infty)}$).

$$\beta = \frac{k_{+}^{A}[LV^{A}] + k_{-}^{A}\left([LV^{D}]K_{L}^{D} + 1\right)}{[LV^{D}]K_{L}^{D} + \frac{k_{+}^{A}}{k_{-}^{D}}[LV^{A}] + 1}; \quad ALV_{(t=\infty)}^{A} = \frac{K_{L}^{A}[LV^{A}]}{K_{L}^{A}[LV^{A}] + [LV^{D}]_{T}K_{L}^{D} + 1} \qquad (VI\text{-}2)$$

According to equation VI-2, if the equilibrium binding constant for the acceptor is not known the accurate assessment of the rate constants for interaction with acceptor vesicles requires the determination of the experimental rate constant for the fast step (β) for different acceptor concentration. Moreover, the equilibrium binding constant (K_L^D) and desorption rate constant from the donor must be previously obtained.

When donor and acceptor vesicles with distinct lipid compositions are used, for $[LV^D] >> [LV^A]$ the exchange rate constant (β) is equal to desorption rate constant from the acceptor (k_-^A) while, for $[LV^A] >> [LV^D]$ β gives the desorption rate constant from the donor (k_-^D). Moreover, as the ratio between $[LV^A]/[LV^D]$ increases, β varies monotonically between the k_-^D and k_-^A with a characteristic dependence that reflects the relative partition of the amphiphile between the donor and acceptor vesicles. For vesicles with the same lipid composition there is no dependence of the transfer rate constant with the acceptor lipid concentration and the average value of beta gives the rate constant for desorption from the vesicles (Figure VI.2, Panel B). If the equilibrium binding constant is known the rate of insertion may be obtained from the desorption rate constant ($k_+ = K_L\, k_-$).

From Figure VI.1 it is clear a poorly defined desorption step and, experiments with shorter time length had to be performed independently for both probes, using the stopped-flow equipment. Moreover, for RG-C_{14} at lower temperatures, the two steps are mixed making the definition of both rate constants a difficult task. This was overcome through a global fit of the experimental results obtained for short and long times using the differential equations VI-1 integrated numerically (Figure VI.2, Panel A). In order to, increase the confidence and accuracy in RG-C_{14} desorption rate constant its dependence with the acceptor concentration was assessed (Figure VI.2, Panel B). Considering that there was no significant variation in k_-, its final value was an average for all acceptor concentrations.

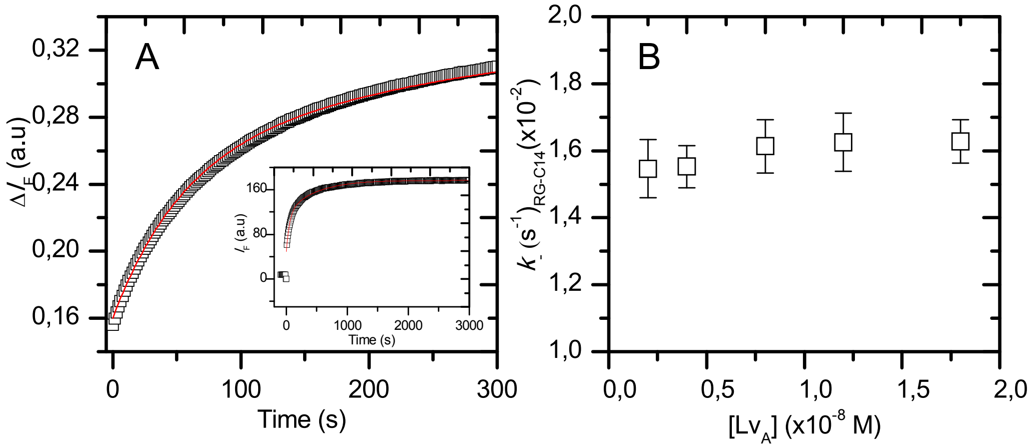

Figure VI.2. Panel A: Time dependence at 25 ºC of the RG-C_{14} fluorescence intensity variation upon its transfer between donor (0.1 mM) and acceptor (0.2 mM) POPC LUVs, using the stopped-flow equipment (short time experiment) and the steady-state fluorimeter results (long times, inset). The red line is the global fit of differential equations VI-1 to the experimental results with a k_- and k_f equal to 1.5×10^{-2} and 2.6×10^{-3} s^{-1}, respectively. Panel B: Dependence of desorption rate constant obtained with the acceptor concentration, leading to k_- equal to $(1.6 \pm 0.04)\times10^{-2}$ s^{-1}.

In opposition to RG-C_{14}, for CBF-C_{14} at pH 7.4 both processes are well separated in time (more than 1 order of magnitude) and the experimental data may be independently fitted (Figure VI.3; Panel A). In order to obtain the CBF-C_{14} β for distinct vesicles two distinct approaches were followed. In the first β for POPC was determined from experiments using vesicles with the same lipid composition. In this case, as aforementioned, β does not depend on the lipid concentration and, therefore, is equal to desorption rate constant (k_-) of CBF-C_{14} from POPC vesicles.

In the second approach, the experiments were performed from donor, POPC vesicles, to acceptor POPC:CHOL(5:5) or SPM:CHOL(6:4) vesicles and, a dependence of β with acceptor concentrations with a downward curvature was obtained (Figure VI.3, Panel B). Using distinct donor and acceptor vesicles the best fit to the experimental results using equation VI-2 required a previous knowledge of k_-^D and K_L^D for donor POPC at the temperature of interest, in order to determine both the insertion and desorption rate constants for the acceptor vesicles. Through the transfer between similar POPC vesicles (first methodology) the desorption of CBF-C_{14} from POPC was determined, moreover, a K_L^D of 2×10^{10} M^{-1} was previously known from independent experiments (see V.3 above) for POPC vesicles, at 25 ºC. Therefore, we were able to determine, from the best fit to the experimental results, the insertion and desorption of

CBF-C_{14} into/from acceptor vesicles using the transfer between POPC and different vesicles.

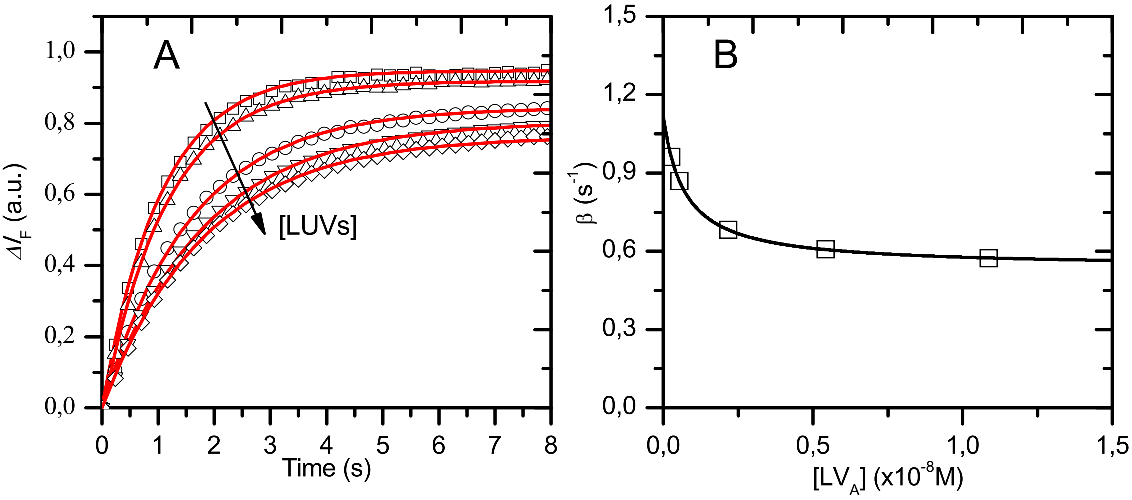

Figure VI.3. Panel A: Time dependence, at 25 ºC, of the CBF-C_{14} fluorescence intensity variation upon its transfer from donor POPC (0.1 mM) to acceptor POPC:CHOL(5:5) vesicles at 0.1, 0.2, 0.4, 2 and 4 mM. The arrow indicates the increase in acceptor concentrations. Panel B: Dependence of the exchange rate constant,*β*, with the POPC:CHOL(5:5) concentration. The best fit to the experimental data using equation VI-2 is also shown, with $k_-^A = 1.0\ s^{-1}$ and $k_-^D = 4.7\times10^{-1}\ s^{-1}$

From the insertion and desorption rate constants of CBF-C_{14}, determined for the acceptor vesicles, we may obtain the equilibrium binding constant ($K_L=k_+/k_-$). The K_L of CBF-C_{14} determined for POPC:CHOL(5:5) is $8.0\text{x}10^9\ M^{-1}$ and it is very similar to $7.5\text{x}10^9\ M^{-1}$ previously obtained from independent experiments using a distinct methodology (see V.3 above). The agreement between the equilibrium constants obtained using the different approaches for CBF-C_{14}, at 25 ºC, gives confidence on the methodologies followed in this work.

When using membranes with different lipid composition, and depending on the final experimental time, lipid transfer may occur between the donor and acceptor vesicles altering their composition. This is particularly relevant for membranes containing cholesterol because the exchange rate constant for this lipid is relatively fast occurring in the time scale of hundreds of minutes to hours depending on the vesicle concentration, temperature and lipid composition [224]. This process does not affect the experimental results obtained for insertion/desorption (occurring in less than 2 min) but may be relevant in the time scale necessary to define the translocation rate (hours).

Thus, the translocation was characterized from the exchange between vesicles with the same lipid composition. The kinetics for the association of CBF-C_{14} and RG-C_{14} with lipid bilayers of distinct lipid compositions is summarized in Table VI.1.

Table VI.1. Kinetic rate constants and equilibrium for the association of RG-C_{14} and CBF-C_{14} to lipid bilayer membranes at pH 7.4 and 25 ºC.

	RG-C_{14}(a)	CBF-C_{14}		
	k_- (s^{-1})	k_- (s-1)	k_+ ($M^{-1}s^{-1}$)(b)	K_L
POPC (l_d)	1.6±0.1 (×10^{-2})	4.7±0.8 (×10^{-1})	9.4±0.8 (×10^{9})	2.0 (×10^{10})
POPC:CHOL (5:5) (l_o)	7.0±2.0 (×10^{-2})	1.1±0.02	8.8±0.8 (×10^{9})	8.0 (×10^{9}) (c)
SpM:CHOL (6:4) (l_o)	1.5±0.4 (×10^{-1})	1.2±0.4	7.2±2.0 (×10^{9})	6.0 (×10^{9}) (c)

(a) Due to RG-C_{14} low water solubility we were not able to accurately measure K_L to POPC, therefore, the transfer was made between similar vesicles and only k_- may be obtained.

(b) The k_+ was obtained from k_- considering $K_L = 2.0\times10^{10} M^{-1}$, previously obtained for POPC, at 25 ºC (see section V.3).

(c) K_L obtained from k_- and k_+ using equation $K_L = \frac{k_+}{k_-}$

The desorption rate constant of CBF-C_{14}, at 25 ºC, from POPC, POPC:CHOL(5:5) and SpM:CHOL(6:4) is ≈ 25, ≈ 15 and 8 times higher, respectively, compared to that of RG-C_{14}. The, expectable, higher desorption rate constant of CBF-C_{14} was due to its negatively charged polar group, which confers a greater water solubility and, therefore, a presumable weaker interaction with the lipid bilayer (see V.2 for details). Moreover, it agrees with the fact that the estimated Kp of RG-C_{14} ($\approx 10^7$) to POPC is considerable higher than the one obtained for CBF-C_{14} ($7.5\text{x}10^5$), reflecting their different lipophilicity. Additionally the different values obtained for k_- of both probes has its origin in a different headgroup packing within the lipid bilayer interface, with the RG-C_{14} establishing stronger interactions with membranes compared to the CBF-C_{14}. This may be further enlightened from the thermodynamic decomposition of the energy evolved in the formation of the transition state in the desorption step.

Literature reports containing the equilibrium and kinetics of interaction of amphiphiles with lipid bilayers are scarce. Among them it is worth note the work of Nichols (1985)

[256] using NBD-PC and the work performed by this research group either using lipid derivatives (NBD-DMPE and NBD-LysoMPE) or fluorescent fatty amines (NBD-C_n) (Table VI.2) [134, 136]. By comparing the desorption rate constant obtained for CBF-C_{14} and RG-C_{14} with previous work from this research group, we observed that, in POPC, the results lie between those obtained for NBD-DMPE (4.7×10^{-6} s^{-1}) [136] and NBD-LysoMPE (15 s^{-1}) [134] being more similar to the NBD-C_{14} (1.2×10^{-2} s^{-1}) [141].

Table VI.2. Summary of the desorption and insertion rate constants, at 25 ºC, for different amphiphiles including this and other works from our research group.

	NBD-DMPE[(a)]		NBD-LysoMPE[(b)]		NBD-C_{14}[(c)]		**CBF-C_{14}**		**RG-C_{14}**
	k_- (s^{-1})	k_+ ($M^{-1}s^{-1}$)	k_- (s^{-1})	k_+ ($M^{-1}s^{-1}$)	k_- (s^{-1})	k_+ ($M^{-1}s^{-1}$)	k_- (s^{-1})	k_+ ($M^{-1}s^{-1}$)	k_- (s^{-1})
POPC (l_d)	4.7±1.8 $(\times10^{-6})$	6.2±0.5 $(\times10^{5})$	1.4±0.2 $(\times10^{1})$	2.6±0.3 $(\times10^{10})$	1.2±0.4 $(\times10^{-2})$	7.8±1.6 $(\times10^{9})$	4.7±0.8 $(\times10^{-1})$	2.0±0.6 $(\times10^{10})$	1.6±0.1 $(\times10^{-2})$
POPC:CHOL (5:5) (l_o)	1.2±0.2 $(\times10^{-5})$	1.1±0.1 $(\times10^{6})$	1.6±0.1 $(\times10^{1})$	1.3±0.1 $(\times10^{10})$	-	-	1.1±0.02	8.4±2.0 $(\times10^{9})$	7.0±2.0 $(\times10^{-2})$
SpM:CHOL (6:4) (l_o)	3.2±1.6 $(\times10^{-6})$	6.8±1.6 $(\times10^{4})$	2.9±0.1	6.9±0.1 $(\times10^{8})$	-	-	1.2±0.4	-	1.5±0.4 $(\times10^{-1})$

[(a)] [136]; [(b)] [134]; [(c)] [141].

Surprisingly, as the membrane ordering increases from pure POPC to POPC:CHOL(5:5) and SpM:CHOL(6:4) the desorption rate constant increases for both probes studied in this work. The observed variation is opposite to the one reported for the NBD-LysoMPE, and distinct from the non monotonic variation noticed for NBD-DMPE (Table VI.2). This is due to the distinct headgroup properties being the RG and CBF a more bulky polar group whose packing at the interface is more difficult.

According to the kinetic scheme (1) and rate constants shown above, the rate of the insertion step is described by the bimolecular insertion rate constant (k_+). Considering that vesicles are the reactant species this bimolecular insertion rate may be directly compared to the predicted diffusion rate constant ($k_{\mathrm{diff}}=4\pi r_{\mathrm{eff}} D_{\mathrm{eff}} N_A$). Where, the r_{eff} is the effective radius for the encounter between the amphiphile and the LUVs (given by the sum of both radii), D_{eff} is the effective translational diffusion coefficient and N_A is the Avogadro constant. The calculated diffusion controlled rate constant for the amphiphiles studied in this work and LUVs with a radius of 50 nm ($k_{\mathrm{diff}} \approx 2\times10^{11}$ M^{-1} s^{-1}, at 25 $^{\mathrm{o}}$C) is at least one order of magnitude larger than the rate constant for insertion obtained for CBF-C_{14} [257]. This is in agreement with the previous studies done by this group using other amphiphiles and indicates that insertion in lipid bilayers is not a diffusion controlled process (Table VI.2). The insertion rate constant of CBF-C_{14} is only slightly higher to the liquid disordered state, ($k_{+\ \mathrm{POPC}} > k_{+\ \mathrm{POPC:CHOL}}$), than to the liquid ordered state. Given that the membrane free volume decreases in the presence of cholesterol [258] the probability of finding a void with the correspondent size of the amphiphile is higher in those membranes compared to more ordered membranes. This leads to an increase in the insertion rate constant for POPC , in agreement with the previously reported values for NBD-LysoMPE [134]. Interestingly, the values found for insertion of the CBF-C_{14} are similar (by a factor of 2) to the values previously obtained for NBD-LysoMPE and NBD-C_{14}. However, a much larger difference exists in the insertion of NBD-DMPE, which has a two acyl chains. These results are particularly significant because they highlight the role of the hydrophobic portion of the amphiphile in the kinetics of the insertion process.

VI.3 Kinetics of Translocation of the RG-C_{14} and CBF-C_{14} in LUVs

The rate of translocation for the fluorescent amphiphiles was evaluated through the analysis of the slower step, resulting from their transfer between similar vesicles. In opposition to desorption, the translocation may take several hours and the transfer of cholesterol between vesicles would be likely to occur, modifying the properties of both donor and acceptor vesicles. Therefore, the use of similar donor and acceptor vesicles was a requirement in these experiments.

As aforementioned, the best fit of the experimental results was performed using the differential equations VI-1, either through a global analysis, obtaining both k_f and k_-, or, if the processes are well-separated in time, translocation was characterized maintaining desorption rate constant fixed in the value obtained from the analysis of the fast transfer experiments. In the second approach, a 15% variation of k_- was allowed to account for the uncertainty associated with this parameter.

Given the long times required to characterize the translocation step, one must evaluate whether some of the RhB-DPPE could be transferred from donor to acceptor vesicles and this was calculated from the rate constants available in the literature for NBD-DMPE [136] (Figure VI.4). We estimate that less than 5% of RhB-DPPE is transferred at all temperatures and acceptor concentrations for the different lipid compositions studied.

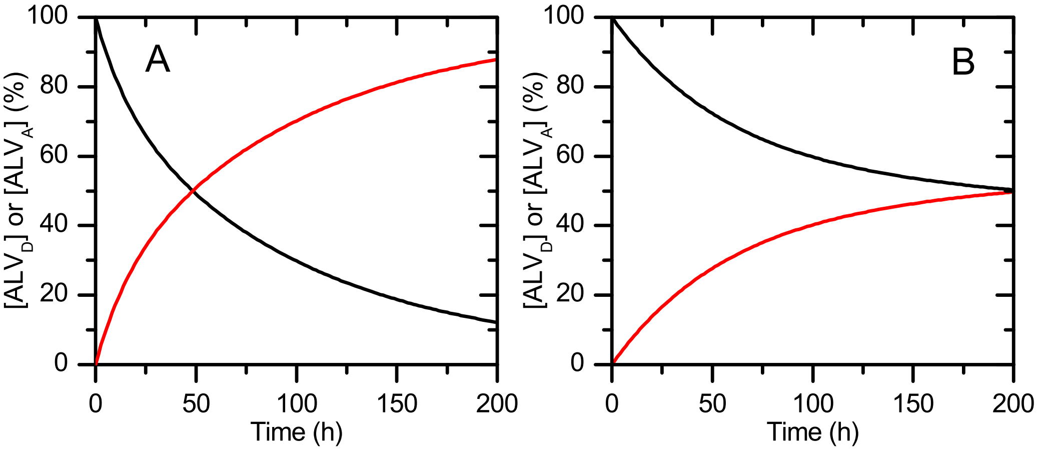

Figure VI.4. Simulation, at 25 ºC, of the percentage of quencher (RhB-DPPE) associated with donor (black line) and acceptor (red line) vesicles, for the worst case scenario considered in this work (higher concentration of acceptor vesicles), with the lipid composition POPC:CHOL(5:5) or SpM:CHOL(6:4), panel A or B respectively. The data was generated using the kinetic parameters of NBD-DMPE [136, 252].

The Figure VI.5 represents a typical experimental result obtained for RG-C_{14} and CBF-C_{14} in different membranes. As abovementioned (section VI.20 above) the biphasic behaviour is due to two distinct processes occurring during the total experimental time. A fast process, related to the interaction of the amphiphile with the outer leaflet of the acceptor vesicles and, a slower process due to its translocation. Considering that; i) the interaction of the amphiphile with acceptor vesicles is always through its outer leaflet (the one accessible to the aqueous media in contact with donor vesicles) and ii) the translocation of the amphiphile to the inner leaflet of the acceptor vesicles does not changes its quantum yield; one may ask why is there an increase in the fluorescence intensity when the amphiphile goes from the outer to the inner leaflet of acceptor vesicles? This is because translocation of the amphiphile to the inner leaflet of acceptor vesicles shifts the equilibrium between the amphiphile in the aqueous media and the outer leaflet of the monolayer, increasing the total amount of amphiphile in the acceptor vesicles.

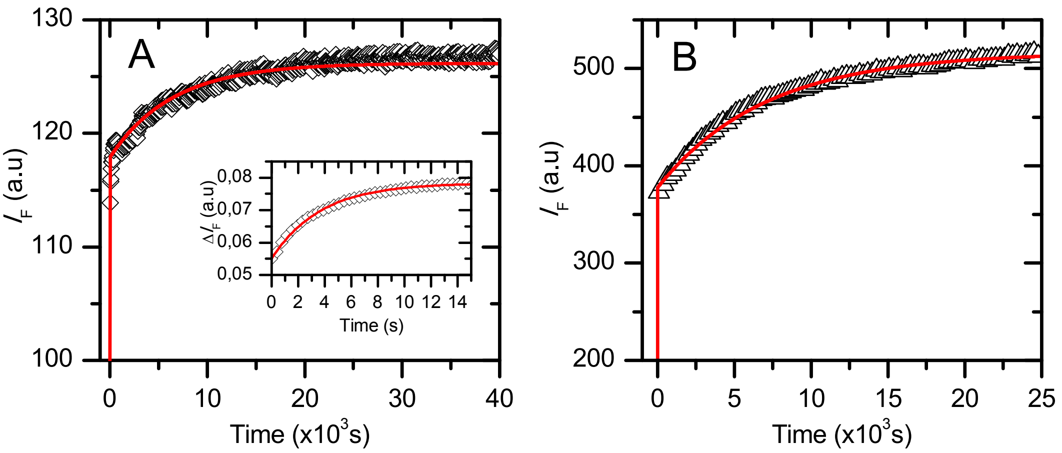

Figure VI.5. Time dependence ,at 25 ºC, of the fluorescence intensity of RG-C_{14} (A) and CBF-C_{14} (B) upon transfer between similar vesicles of SpM:CHOL(6:4) (A) and POPC:CHOL(5:5) (B), with a final lipid concentration of 0.1 mM for donor and 1.2 mM for the acceptor vesicles. The parameters for RG-C_{14} were obtained from the global best fit to the results obtained in two different times scales, the inset shows the best fit of the same parameters to the results obtained at small times, more sensitive to the desorption step. The red line is the best fit of the differential equations in VI-1 with k_{-}= 2.7×10^{-1} s^{-1} and k_f=1.6×10^{-4} s^{-1} for RG-C_{14} and k_f= 1.4×10^{-4} s^{-1} for CBF-C_{14} (B).

The transfer of the amphiphiles between vesicles requires a more complex analysis [259] than the transfer of the amphiphile from protein (monomerizing agent) or directly from water [135, 175]. Furthermore, some experiments using SpM:CHOL(6:4) carried a considerable amount of time to reach the plateau and, to discard any change in the membrane properties, *e.g* fusion between vesicles, the dependence of the RG-C_{14} translocation rate constant with the concentration of acceptor LUVs was studied (Figure VI.6). Within the range of the experimental error, it was observed that the rate of translocation was independent of the concentration of acceptor vesicles, giving confidence in the obtained results for k_f.

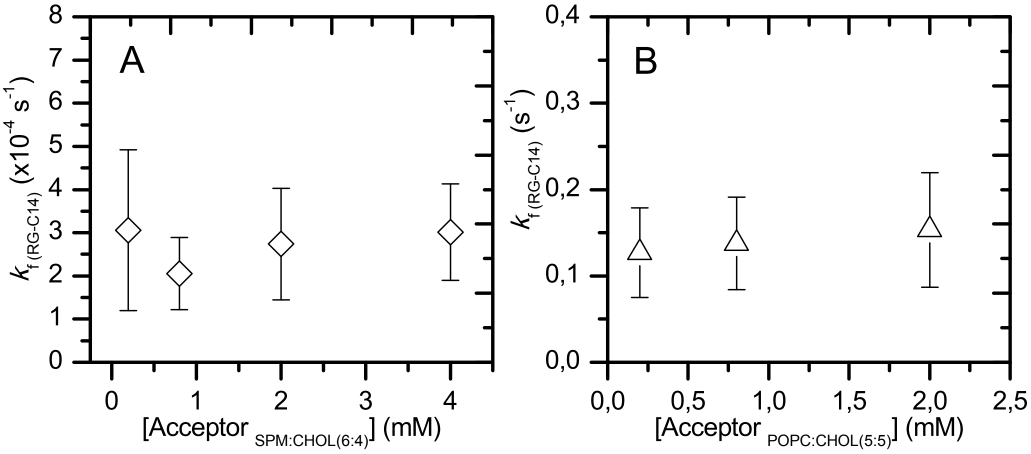

Figure VI.6. Dependence of RG-C_{14} translocation rate constant with the SpM:CHOL(6:4) (Panel A, 25 ºC) and POPC:CHOL(5:5) (Panel B, 55 ºC) acceptor concentration with an average $k_f \approx 2.7\pm0.4(\times10^{-4})$ $s^{-1}$and $1.4\pm0.1(\times10^{-1})$ s^{-1}, respectively.

The translocation rate constants of CBF-C_{14} and RG-C_{14} in distinct lipid compositions, at 25 ºC, are summarized below, in Table VI.3. The value of k_f for both probes decrease with the ordering of the membranes corroborating previous results obtained by our research group for similar membranes using other amphiphiles (see Table VI.4, below). The translocation rate of RG-C_{14} and CBF-C_{14} decreases with the membrane ordering, being smaller for SpM:CHOL(6:4) membranes, however, a less stark decrease is observed compared to NBD-DMPE and NBD-LysoMPE. These results confirm the fact that the SpM:CHOL(6:4) mixture is a more cohesive and ordered membrane and that the headgroup structural properties of the amphiphile have an important role its translocation.

Contrary to the experimental results obtained for the single chain amphiphile NBD-LysoMPE, both RG-C_{14} and CBF-C_{14} have a k_f larger (2-3 orders of magnitude) than the lipid derivative NBD-DMPE, for all membranes studied. Moreover, the values of k_f are approximately one and two orders of magnitude smaller, for RG-C_{14} and CBF-C_{14} respectively, than the fluorescent fatty amine NBD-C_{14}, in the liquid disordered POPC membrane. This is a consequence of the bulkiness of RG and CBF groups compared to NBD, moreover the presence of charges in those polar groups further contribute to a slower translocation.

The translocation of CBF-C_{14} is slower than RG-C_{14} according with the fact that the former has a negative charge while the latter is zwitterionic, at pH 7.4. Considering that upon translocation the amphiphile has to cross the hydrophobic core of the membranes, with a low dielectric constant, this is expected to be energetically more unfavourable for a negatively charged molecule (CBF) than for a zwitterionic one (RG).

In molecules, which contain ionizable groups (CBF-C_{14}) the observed translocation rate will, strongly, depend on the amphiphile ionization state once inserted in the bilayer. For instance, from Table VI.4 it is clear that for fatty acids the translocation rate is large in spite of the negative charge on their carboxylic headgroup ($pKa \approx 4.5$ in aqueous media). However, upon their partition to membranes a considerable shift in the carboxylic group p*K*a occurs, to higher values, and they are believed to translocate in its unionized form, which is considerably faster [260]. A shift of the pKa_2 and pKa_3 towards higher values was also observed for CBF-C_{14} in membranes.

Table VI.3. Values of the translocation rate constants in distinct lipid composition LUVs, at 25 ºC.

	Translocation rate (s^{-1})	
	RG-C_{14}	CBF-C_{14}
POPC (l_d)	$2.6\pm0.1(\times10^{-3})$	$2.1\pm0.2(\times10^{-3})$
POPC:CHOL(5:5) (l_o)	$9.5\pm2.0(\times10^{-4})$	$2.0\pm0.5(\times10^{-4})$
SpM:CHOL(6:4) (l_o)	$3.1\pm0.8(\times10^{-4})$	-

Given the lack of quantitative data reporting the translocation of amphiphiles in liposomes, the comparison of the experimental results is challenging. The few studies reported in literature for membranes in liquid disordered and gel phase have been collected in Table VI.4. Moreover, translocation of amphiphiles in lipid systems similar to those reported in this work, namely with POPC:CHOL(5:5) and SpM:CHOL(6:4), are even more scarce in literature and the only works found are from this research group using the NBD-DMPE, NBD-LysoMPE and NBD-C14 amphiphiles. Therefore, caution must be taken when comparing the obtained results with the ones reported by other authors, where the liposomes lipid composition and size are very distinct. Nevertheless, it is evident that for membranes in the liquid disordered phase, the phospholipids derivatives have a translocation characteristic time of several hours being significantly slower than the translocation for both RG-C_{14} and CBF-C_{14}.

Table VI.4. Literature reported data for the translocation of different amphiphiles in membranes

	Amphiphile	**System**	**Temp (ºC)**	**Membrane lipid**	**k_{f} (s^{-1})**	**Method**	**Ref.**
Lipid Derivatives	DMPC	LUV	30	DMPC	$\leq 2.1\times10^{-5}$	Transfer between vesicles	[261]
		SUV	30	DMPC	$\leq 2.1\times10^{-6}$	Transfer between vesicles	
	DPPC (a)	Non defined	30	Egg-PC	3.0×10^{-5}	Spin label paramagnetic	[262]
	NBD-DPPE	SUV	25	DPPC	$\leq 2.1\times10^{-5}$	Reduction by dithionite	[263]
			45	DPPC	$\approx 7.1\times10^{-4}$		
	NBD-DMPE	LUV	25	POPC	2.0×10^{-5}	Reduction by dithionite	[252]
				POPC:CHOL (5:5)	1.3×10^{-6}		
				SpM:CHOL (6:4)	4.6×10^{-8}		
	NBD-LysoMPE	LUV	25	POPC	8.4×10^{-6}	Reduction by dithionite	[252]
				POPC:CHOL (5:5)	2.8×10^{-7}		
				SpM:CHOL (6:4)	1.1×10^{-8}		
	[N-^{13}CH$_3$]DOPC		30	DOPC	$\geq 1.6\times10^{-5}$	Exchange protein	[264]
	C$_{12}$PN-PC	Non defined	37	POPC	5.6×10^{-7}	Transfer between vesicles (Pyrene-phospholipids)	[265]
	C$_{12}$PN-PA				5.5×10^{-6}		
	C$_{12}$PN-PE				1.9×10^{-5}		
	C$_{12}$PN-PG				2.8×10^{-6}		
Fatty Acids	Fatty acid (b)	LUV	37	EggPC	≥ 20	Pyranin	[260]
		SUV			≥ 69		
	9-(3-pyrenyl) nonanoic acid (PNA)	SUV	37	DMPC	≥ 17	Transfer between vesicles	[266]
			37	DPPC	≥ 17		
	Oleate (c)	LUV	25	EggPC	0.6	Transfer with BSA	[267]
Fatty Amine	NBD-C$_{14}$	LUV	25	POPC	4×10^{-1}	Reduction by dithionite	[141]

(a) Labeled in the polar region with paramagnetic nitroxide group.

(b) There was no apparent dependence of the k_f with acyl chain length for the fatty acids 14:0; 16:0; 18:0; 18:1, at pH 7.4.

(c) At pH 7.4

VI.4 Thermodynamics of the Interaction of RG-C_{14} and CBF-C_{14} with LUVs

In this section, we will address the thermodynamics of the interaction of RG-C_{14} and CBF-C_{14} with lipid bilayers, both in the liquid ordered (l_o) or in the liquid disordered state (l_d). The discussion and analysis of the experimental results will be supported on the Transition State Theory and models for the insertion/desorption and translocation processes, described in the literature.

VI.4.1 Transition State for Insertion/Desorption of RG-C_{14} and CBF-C_{14}

The results for CBF-C_{14} and RG-C_{14} insertion and desorption were analyzed based on the model developed by Aniansson *et al* 1976 [268], to describe the amphiphile monomer-micelle dissociation. This model has been widely used in the literature [219, 261], describing the energetics of the activated state in desorption of amphiphiles from lipid bilayers, and it can be pictorially described as:

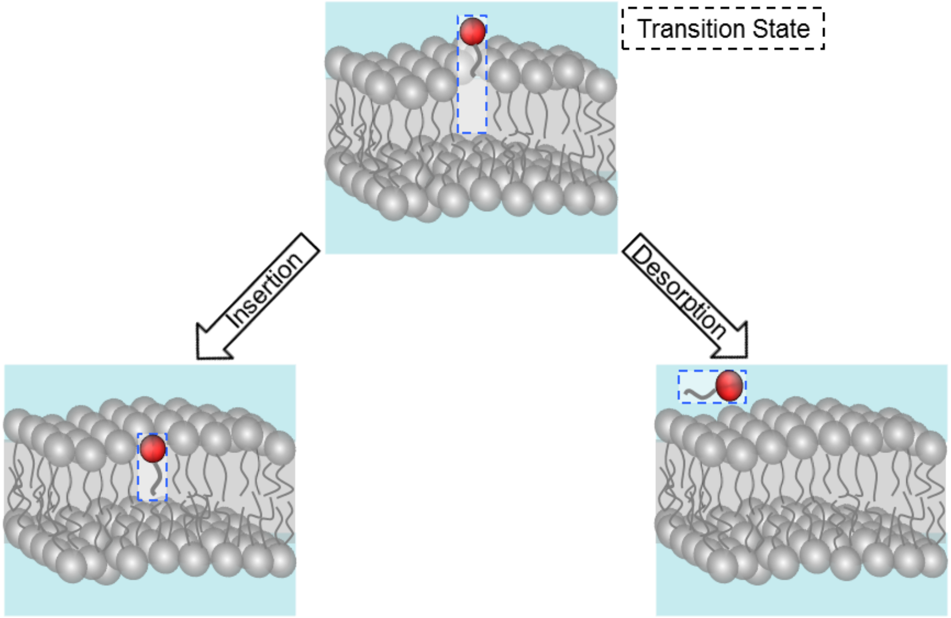

Figure VI.7. Schematic representation of the insertion into and desorption from lipid bilayers with the correspondent high energy transition state.

Briefly, when the insertion/desorption process is considered, the higher energy state is assumed to occur when the amphiphile moved, in the plane normal to the bilayer, and only the terminal carbon is preventing the membrane to collapse filling the cavity beneath the amphiphile. In this process, the amphiphile lost most of the interactions with the bilayer being, almost completely, in the aqueous phase. However, the lipids acyl chains had not yet relaxed and, in the transition state, two cavities are present which lead to an increase in enthalpy due to the loss of favourable water-water and lipid-amphiphile (or lipid-lipid) interactions. Being the amphiphile, in the transition state, extensively exposed to the water a reduction in the entropy of the system occurs. Nevertheless, there is an entropic compensation due to the increase in membrane entropy that results from a higher conformational freedom of the lipids next to the cavity, in the transition state.

Before development of the Transition State Theory an empirical Arrhenius equation was widely used, $k = Ae^{-\frac{E_a}{RT}}$, in the determination of energy for reactions. This law relates the activation energy (E_a) with the reaction rate constant k, being A the pre-exponential term, T the temperature in Kelvin and R the universal gas constant. Reformulating the Arrhenius equation, applying the natural logarithm to both sides, one obtains;

$$\ln k = \ln A - \frac{E_a}{RT} \tag{VI-3}$$

From an Arrhenius plot (ln *k* vs 1/T) a linear trend is predicted and the activation energy (E_a) may be obtained from the slope. However, using the Arrhenius equation we can only relate the rate constants with the activation energy. Therefore, to obtain the thermodynamic parameters for the transition state of the amphiphiles in the interaction with lipid bilayers the Transition State Theory (TST) must be used. This theory has three postulates:

1- From the reactants to the products, along a surface potential curve, the molecule has to overcome a region of high potential energy, which is the transition state. This must be the energy maximum in the reaction coordinate.

2- It is assumed that there is quasi-equilibrium between the molecules in the transition state and the reactants.

3- The rate of reaction (r) is given by the concentration of molecules in the transition state multiplied by the frequency, at which they pass towards the product state.

The TST, also called absolute-rate theory, was introduced in 1935 by Eyring and Polany [269-271] and provided the first theoretical attempt to determine the absolute reaction rates [272]. Using the TST postulates and assuming a frequency factor of $\nu = \frac{k_B}{h}T$, for the deactivation of the transition state, Eyring and Polanyi developed a thermodynamic formulation of the transition state theory (VI-4) which allowed to obtain the enthalpic ($\Delta^{\ddagger}H^0$) and entropic ($\Delta^{\ddagger}S^0$) contribution from the temperature dependence of the experimental rate constants.

$$k = \frac{k_B T}{h} e^{\frac{\Delta^{\ddagger} S^0}{R}} e^{-\frac{\Delta^{\ddagger} H^0}{RT}} \tag{VI-4}$$

This equation resembles the Arrhenius equation, except that $\Delta^{\ddagger}H^0$ appears instead of E_a being the pre exponential factor given by:

$$A = \frac{k_B T}{h} e^{\frac{\Delta^{\ddagger} S^0}{R}} \tag{VI-5}$$

Reformulating the equation (VI-4), applying the natural logarithm to both sides, one obtains;

$$\ln k = \ln\left(\frac{k_B T}{h}\right) + \frac{\Delta^{\ddagger} S^0}{R} - \frac{\Delta^{\ddagger} H^0}{RT} \tag{VI-6}$$

According to the linearized equation VI-6, from the experimental Arrhenius type plot, the $\Delta^{\ddagger}H^0$ and $\Delta^{\ddagger}S^0$ can be obtained with the least square analysis procedure. Moreover, the obtained $\Delta^{\ddagger}H^0$ and $\Delta^{\ddagger}S^0$can be easily converted into Gibbs free energy, $\Delta^{\ddagger}G^0$, using $\Delta^{\ddagger}G^0 = \Delta^{\ddagger}H^0 - T\Delta^{\ddagger}S^0$.

VI.4.2 Thermodynamics of CBF-C_{14} and RG-C_{14} Desorption from LUVs

From the temperature dependence of desorption rate constants, the thermodynamic parameters for desorption of RG-C_{14} and CBF-C_{14} from bilayers with distinct composition was recovered (Figure VI.8) (Table VI.5). However, given that K_L was not measured at different temperatures the thermodynamics for insertion of CBF-C_{14} and RG-C_{14} into LUVs can not be obtained from the experimental data (see equationVI-2).

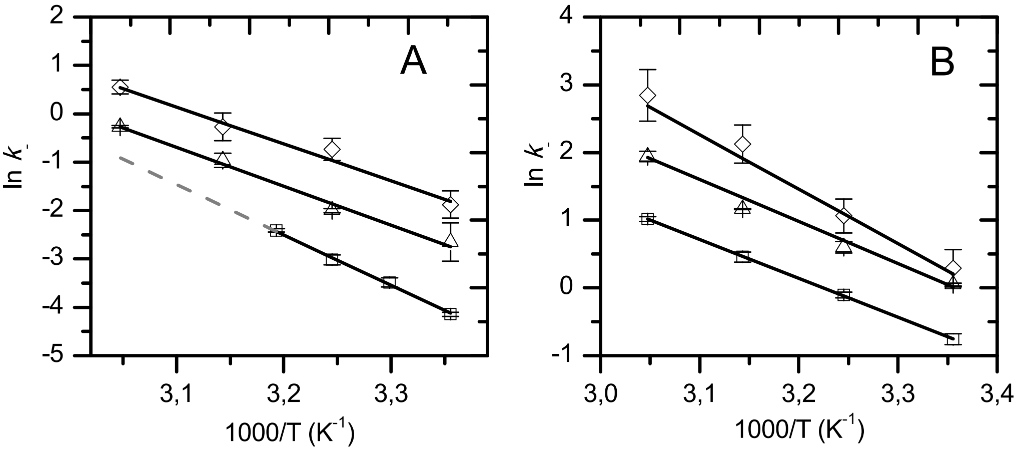

Figure VI.8. Arrhenius type plot for the desorption of RG-C_{14} (Panel A) and CBF-C_{14} (Panel B) from POPC (□), POPC:CHOL(5:5) (Δ) and SpM:CHOL(6:4) (◊), at pH 7.4. The average experimental value ± standard deviation of, at least, three independent experiments is shown. The line is the best fit of equation VI-6, the grey dashed line is the extrapolation of the desorption rate constant to temperatures not measured experimentally.

Table VI.5. Thermodynamic parameters, for desorption of RG-C_{14} and CBF-C_{14} from lipid bilayers.

T=25 ºC	RG-C_{14}			CBF-C_{14}		
	POPC l_d	POPC:CHOL (5:5) l_o	SpM:CHOL (6:4) l_o	POPC l_d	POPC:CHOL (5:5) l_o	SpM:CHOL (6:4) l_o
$\Delta^{\ddagger}G^0$ (kJmol^{-1})	83±0.1	80±1.0	78±0.5	75±2.0	73±0.5	72±1.5
$\Delta^{\ddagger}H^0$ (kJmol^{-1})	84±3.0	64±4.0	62±4.0	45±1.0	49±2.0	64±3.0
$T\Delta^{\ddagger}S^0$ (kJmol^{-1})	0.9±3.0	-16±4.0	-16±4.0	30±1.0	-24±2.0	-8±3.0

Considering the desorption step of amphiphiles from lipid bilayers the transition state is the one where the amphiphile is barely attached to the membrane interface and almost completely in the aqueous phase. This state requires the formation of two cavities, one in the monolayer from where the amphiphile is emerging and other in the interfacial water where it is inserting (see Figure VI.7, above). The formation of these two cavities requires a considerable amount of energy increasing the enthalpy of the system. However, the variation in the system's entropy results from two opposing effects: an increase due to the higher motion of membrane lipids in the surroundings of the cavity, and a decrease due to the ordering of water molecules around the non-polar surface of the amphiphile.

According to the results for desorption of both probes from the lipid bilayers, listed in Table VI.5, it is clear that the process is dominated by the enthalpic contribution, in agreement with previous reports (Lyso-MPE and NBD-DMPE) [134, 136, 141]. Interestingly, while for RG-C_{14} the $\Delta^{\ddagger}H^{0}$ increases with membrane ordering for CBF-C_{14} a reciprocal trend is observed, given their opposite dipole moment this could be due to their distinct interaction with membrane dipole potential. Assuming the same transition state for both amphiphiles, its formation is energetically more unfavourable for RG-C_{14} than for CBF-C_{14}, for all the membranes studied ($\Delta^{\ddagger}G^{0}_{RG\text{-}C14} > \Delta^{\ddagger}G^{0}_{CBF\text{-}C14}$). While for POPC and POPC:CHOL(5:5) this is due to a significantly higher enthalpic contribution for RG-C_{14} relative to CBF-C_{14}, for SpM:CHOL(6:4) the variation is essentially due to the entropic contribution. Considering that the acyl chain in both amphiphiles is the same (C=14), this enthalpy difference between both amphiphiles relies on a distinct interaction between the amphiphile headgroup and the bilayer interface, namely the interaction between the amphiphile dipole moment and the membrane dipole potential. Since that CBF-C_{14} has a negative charge, the positioning of this amphiphile, compared to that of RG-C_{14}, is shallower decreasing the interactions with membrane lipids. This is reasonable for membranes in l_o phase, where a more external positioning of CBF-C_{14} compared to RG-C_{14} was confirmed from fluorescence anisotropy measurements (V.6, above). In POPC, however, the localization of both probes was shown to be essentially the same and, nevertheless, CBF-C_{14} presents a considerable lower $\Delta^{\ddagger}H^{0}$. The exposed may be explained based on a stronger interaction of RG-C_{14} dipole moment with the dipole potential of POPC bilayers, due to their opposite orientation when the amphiphile is inserted. The entropy variation profile observed for both probes and for different membranes reveals a compensation effect. Systems with a lower enthalpy due to favorable interactions tend to have lower entropy as well.

VI.4.3 Thermodynamics of CBF-C_{14} and RG-C_{14} Translocation in LUVs

The transition state model for the translocation step is depicted in Figure VI.9. Briefly, upon translocation of a molecule from one monolayer to the other the high energy state is the one where the amphiphile lies in the midplane of the bilayer, oriented parallel to the membrane surface. Accordingly, the major contribution to the work involved in the translocation process is the one necessary to put the polar group in the non-polar membrane interior. However, a previous work done by this laboratory [141], studying a homologous series of fluorescence fatty amines, showed an effect of the acyl chain length on the translocation rate. Furthermore, results obtained in bilayers with a smaller thickness challenged this model and, for very polar solutes, a defect mediated translocation was considered [138]. The results for thermodynamic parameters for translocation are summarized in Table VI.6.

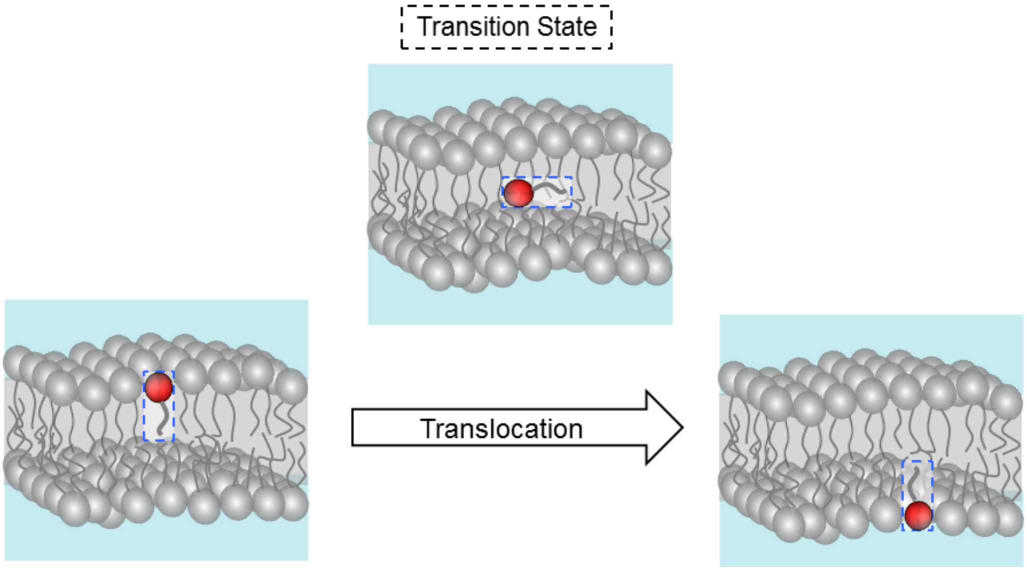

Figure VI.9. Schematic representation of the translocation of an amphiphile with the correspondent high energy transition state.

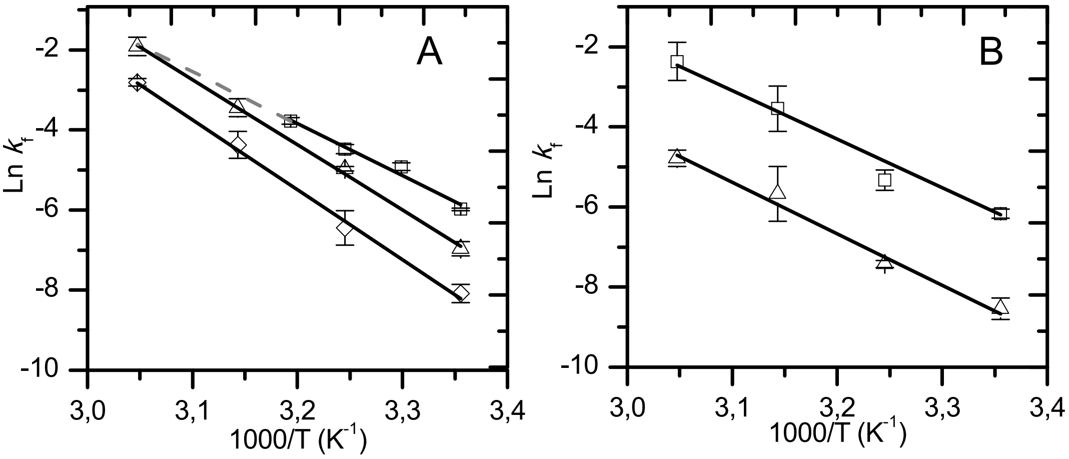

Figure VI.10. Arrhenius type plot for the translocation of RG-C_{14} (Panel A) and CBF-C_{14} (Panel B) in POPC (□), POPC:CHOL(5:5) (Δ) and SpM:CHOL(6:4) (◊) bilayers. The results show the average experimental value ± standard deviation of, at least, three independent experiments. The line is the best fit of equation VI-6 and the grey dashed line are the extrapolation of experimental results for POPC.

Table VI.6. Thermodynamic parameters for translocation of RG-C_{14} and CBF-C_{14} in lipid bilayers.

	RG-C_{14}			CBF-C_{14}	
T=25 ºC	POPC (l_d)	POPC:CHOL (5:5) (l_o)	SpM:CHOL (6:4) (l_o)	POPC (l_d)	POPC:CHOL (5:5) (l_o)
$\Delta^{\ddagger}G^0$ (kJmol^{-1})	88±0.1	90±0.5	93±0.6	88±0.3	94±0.7
$\Delta^{\ddagger}H^0$ (kJmol^{-1})	106±6.0	132±4.0	143±6.0	98±10	104±8.0
$T\Delta^{\ddagger}S^0$ (kJmol^{-1})	18±6.0	42±4.0	49±6.0	10±9.0	10±8.0

The results show an increase, for both amphiphiles, of the energy barrier ($\Delta^{\ddagger}G^0$) from POPC to SpM:CHOL(6:4) membranes. Given the currently accepted model for the transition state, the decrease in translocation rate for more ordered membranes can only be due to a variation in the Gibbs free energy of the transition state as a consequence of either a decrease in polarity at the bilayer midplane or a lower stabilization of the amphiphiles in the transition state. This is because the TST assumes a frequency for the deactivation of the transition state which does not depend on the physical state of the membrane. If we considered a smaller frequency factor for more ordered membranes, which is reasonable, the translocation rate constant could be smaller for ordered membranes, as observed, in spite of the same energy barrier ($\Delta^{\ddagger}G^0$). The frequency factors are however unknown and therefore, in this work we use the absolute rate theory with the same frequency factor for all membranes (k_BT/h) and the differences observed in the rate constants are tentatively interpreted in terms of the energetics of the transition state. This uncertainty affects the value obtained for the entropy variation upon formation of the transition state, but not the enthalpy variation.

The translocation of this amphiphiles is dominated by enthalpy has observed in other amphiphiles (Table VI.7). Moreover, the work required to place the NBD in the nonpolar bilayer center is higher than for both RG and CBF headgroups.

The enthalpy variation reports the interactions established by the amphiphile with neighboring lipids in its inserted state, moreover, it is further related with the work required to place a polar group in the bilayer midplane. If we consider that the work required to place the amphiphile headgroup in the membrane interior is not significantly different for membranes in either l_d or l_o phase, the results indicate that enthalpy of both probes in the inserted state is larger for more disordered membranes. Comparing both probes we observed an increase in $\Delta^{\ddagger}H^0$ for translocation of RG-C_{14} in bilayers in l_o phase relative to l_d, and a much smaller increase is observed for CBF-C_{14}. These results confirm that, in the liquid ordered membranes, the probes establish stronger interactions with neighboring lipids, which stabilize their inserted state, being this particularly evident for the RG-C_{14}. The increase in RG-C_{14} stabilization of the inserted sate compared to CBF-C_{14} in l_d and l_o, observed from the higher $\Delta^{\ddagger}H^0$, agrees with thermodynamic results for desorption and consolidate the argument that their distinct dipole moment orientation affects the kinetics of interaction with the membrane.

From the results we observed a significantly lower entropy variation, for l_o phase, upon formation of the transition state for CBF-C_{14} compared to RG-C_{14} which may be explained based on the formation of a membrane defect due to the presence of this amphiphile, larger for the case of CBF-C_{14}. This defect leads to an increase in the entropy of the amphiphile neighbouring lipids which in turn decreases the $\Delta^{\ddagger}S^0$ associated with the formation of the transition state. However, in the liquid disordered state the RG-C_{14} probe have a similar $\Delta^{\ddagger}S^0$ and $\Delta^{\ddagger}H^0$ to CBF-C_{14}, compatible with a deeper localization of CBF-C_{14}. This similar membrane location and an increase in the neutral fraction (higher p*K*a) of CBF-C_{14} in POPC contribute to similar thermodynamic parameters and rate constants between both probes in POPC.

Comparing the thermodynamic parameters obtained for RG-C_{14} with those reported for NBD-LysoMPE, we observe that in l_o phase the main difference is the entropic contribution, being higher for the former. Both probes have similar $\Delta^{\ddagger}H^0$ even though RG-C_{14} translocate faster than NBD-LysoMPE due its negative charge. For CBF-C_{14}, the NBD-LysoMPE establish more interactions with lipids being this enthalpy difference the main responsible for the translocation rate difference observed between these probes for all membranes.

Table VI.7. Thermodynamic parameters for translocation of NBD-DMPE and NBD-LysoMPE in lipid bilayers, recovered from literature.

	NBD-DMPE [(a)]			NBD-LysoMPE [(a)]		
T=25 ºC	POPC (l_d)	POPC:CHOL (5:5) (l_o)	SpM:CHOL (6:4) (l_o)	POPC (l_d)	POPC:CHOL (5:5) (l_o)	SpM:CHOL (6:4) (l_o)
$\Delta^{\ddagger}G^0$ ($kJmol^{-1}$)	98±1.0	104±4.0	112±2.0	99±0.3	109±1.0	116±1.0
$\Delta^{\ddagger}H^0$ ($kJmol^{-1}$)	119±5.0	143±2.0	153±8.0	131±2.0	133±5.0	141±12
$T\Delta^{\ddagger}S^0$ ($kJmol^{-1}$)	21±5.0	39±2.0	41±7.0	32±2.0	24±5.0	25±11

(a) [252]

VI.5 Effect of the pH in Kinetics and Thermodynamics of Interaction of CBF-C_{14} with LUVs

Carboxyfluorescein is a dye with three distinct ionization equilibria and its photophysical properties are sensitive to local pH. Considering that CBF-C_{14}, at pH 7.4, has a negative charge its effect in desorption and translocation rate constants may be significant. Therefore, this effect was evaluated through the k_- and k_f dependence with pH, in a range between 6 and 7.4. According to literature, in this pH range we are mostly changing the fraction of anionic and di-anionic CBF-C_{14}, considering that the reported pKa for this equilibrium in water is 6.4 and the other pKa values are 2.1 and 4.3, for the equilibrium between the cationic and neutral forms and between the neutral and anionic forms, respectively. However, from our previous results, in the range from pH= 3 to pH= 11, we found a pKa for CBF-C_{14} in membranes, which were significantly higher than the reported values in water. The distinct localization of the amphiphile in POPC and POPC:CHOL(5:5) leads to different ionization constants and, while in the former bilayer the $pKa_2 \approx 6.9 \pm 0.6$ and $pKa_3 \approx 8.9 \pm 0.5$, in the latter the recovered values were $pKa_2 \approx 5.2 \pm 0.4$ and $pKa_3 \approx 7.6 \pm 0.1$.

The expectations were that, upon the pH increase, the negatively charged fraction of CBF-C_{14} predominates, promoting opposite effects in the translocation and desorption rate constants. From the ionization constants of CBF-C_{14}, and by fitting the experimental results with the ionization equilibrium formalism, the rate constants for all the CBF-C_{14} species could be attained. Moreover, the temperature dependence at the different pH values was also recovered, and this enables a complete description of the thermodynamic parameters for the ionized and neutral species. In the next topic, we will address desorption and translocation rate constants as a function of the pH, for CBF-C_{14}, and characterize the thermodynamic parameters for the transition state. Finally, the extrapolation of the experimental results for the neutral and charged species of CBF-C_{14} will be further discussed.

VI.5.1 Effect of the pH in Desorption of CBF-C_{14} from LUVs

As aforementioned the desorption rate constant of CBF-C_{14}, from LUVs in l_d and l_o phase, was obtained for pH = 6; 6.5; 7 and 7.4 (Figure VI.11), being the results at pH 7.4 exposed and discussed in the previous sections. According to the time separation of desorption and translocation steps, which depended on the value of pH in opposite directions, the experimental results were fitted through a global analysis or each parameter was obtained from independent experiments. The Figure VI.11 shows the experimental results and their best fit at different pH. It is clear that as the pH decreases, the translocation and desorption steps became closer in time, with desorption CBF-C_{14} becoming slower while translocation is accelerated. This was predictable since that by lowering the pH we are promoting an increase in the fraction of monoanionic and neutral species in solution. Considering that both species are less water soluble than the dianionic, the final CBF-C_{14} desorption rate constant will decrease. Moreover, the translocation rate will increase due to the decrease in amphiphile polarity.

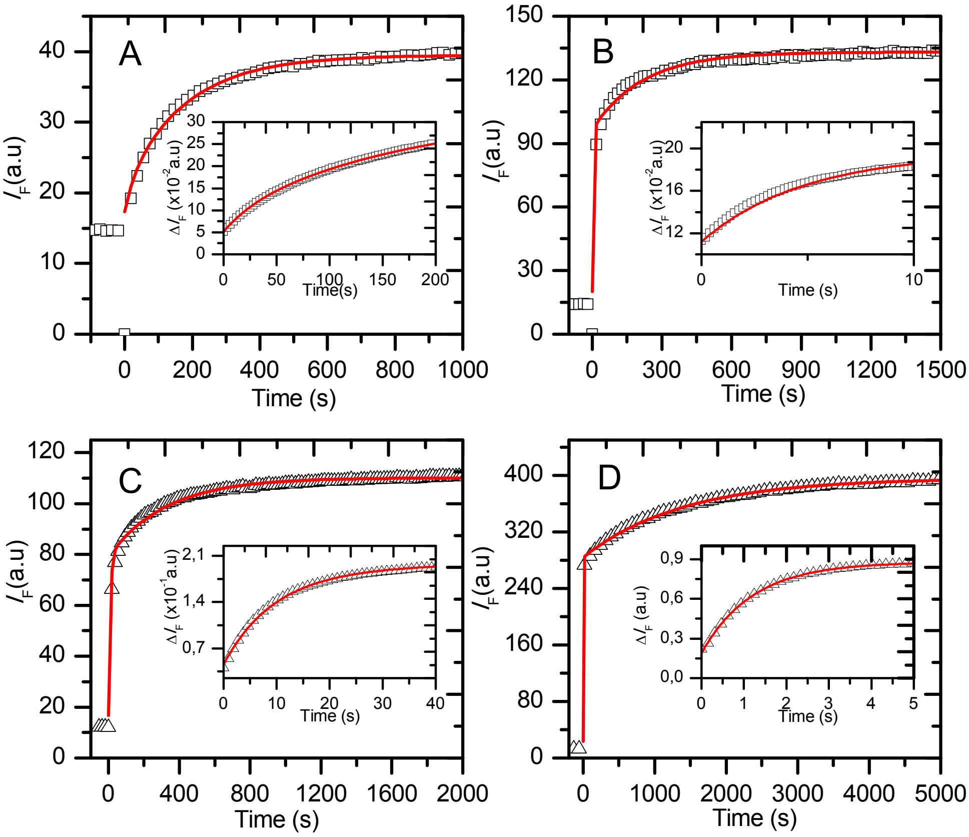

Figure VI.11. Typical curves, at 25 ºC for the time dependence of the fluorescence intensity of CBF-C_{14} upon transfer between 0.1 mM (final concentration) donor vesicles and 1.2 mM (final) acceptor vesicles with the same lipid composition, at pH= 6 (A and C) and pH= 7 (C, D), POPC (□), POPC:CHOL(5:5) (Δ). In inset there are the independent experimental curves for desorption step in a smaller timescale. The red line represents the best fit of equations VI-1.

Performing the experiments described above, Figure VI.11, between 25 ºC and 55 ºC, it is possible to obtain the temperature dependence of the desorption rate constant at different pH and lipid bilayers compositions (Figure VI.12). The kinetic data was used to generate the Arrhenius type plot for k_- of CBF-C_{14} allowing us to obtain the $\Delta^{\ddagger}H^0$, $\Delta^{\ddagger}S^0$ and $\Delta^{\ddagger}G^0$ at different pH and lipid bilayers, which are summarized in Table VI.8.

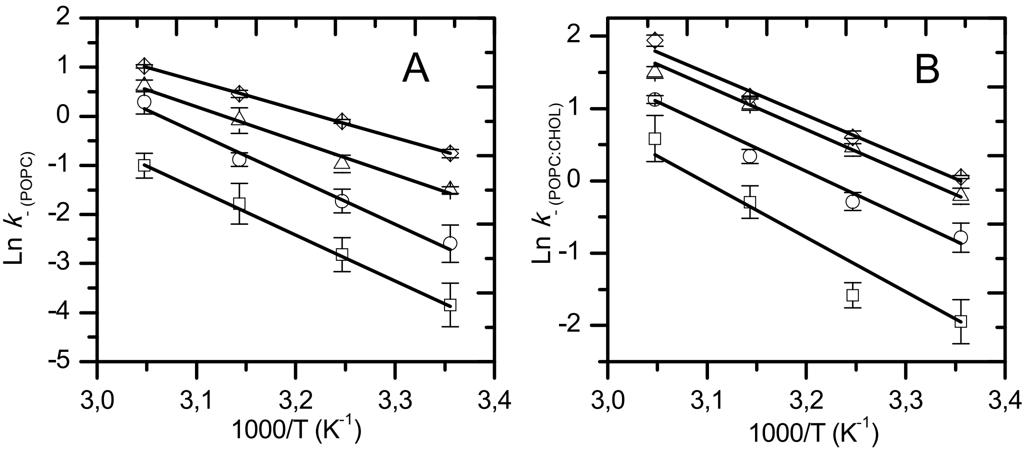

Figure VI.12. Arrhenius type plots for the desorption of CBF-C_{14} from POPC (Panel A) and POPC:CHOL(5:5) (Panel B) at pH= 6 (□); pH= 6.5 (○); pH= 7.0 (Δ) and pH= 7.4 (◊).The results show the average experimental value ± standard deviation of, at least, three independent experiments. The line is the best fit of equation VI-6.

Table VI.8. Thermodynamic parameters for the formation of the transition state and rate constant for desorption of CBF-C_{14} from lipid bilayers of POPC and POPC:Chol (5:5), at different values of pH.

T=25ºC	POPC (*l*$_d$)				POPC:CHOL(5:5) (*l*$_o$)			
pH≈	6.0	6.5	7.0	7.4	6.0	6.5	7.0	7.4
k_- (s^{-1})	2.1±0.9 (×10^{-2})	7.5±3.0 (×10^{-2})	2.2±0.2 (×10^{-1})	4.7±0.8 (×10^{-1})	1.4±0.6 (×10^{-1})	4.6±0.9 (×10^{-1})	8.1±0.9 (×10^{-1})	1.1±0.02
$\Delta^{\ddagger}G^0$ ($kJmol^{-1}$)	82±1.0	80±1.0	77±0.2	75±2.0	78±0.8	76±0.2	73±0.3	73±0.5
$\Delta^{\ddagger}H^0$ ($kJmol^{-1}$)	75±7.0	75±6.0	55±5.0	45±1.0	60±6.0	51±7.0	47±4.0	49±2.0
$T\Delta^{\ddagger}S^0$ ($kJmol^{-1}K$)	-7±7	-5±5	-22±5.0	-30±1.0	-18±6.0	-25±7.0	-26±4.0	-24±2.0
f CBF-C_{14}^{0} [(a)]	*0.89*	*0.72*	*0.45*	*0.24*	*0.15*	*0.05*	*0.01*	*0.004*
f CBF-C_{14}^{1-} [(a)]	*0.11*	*0.28*	*0.54*	*0.74*	*0.83*	*0.87*	*0.77*	*0.58*

[(a)] *f* CBF-C_{14}^{0} and *f* CBF-C_{14}^{1-} represent the molar fraction of the neutral and monoanionic species in solution, respectively, calculated from the values of p*K*a of CBF-C_{14} inserted in the bilayers obtained in this work (section V.5).

The results presented in Table VI.8 show some common trends for both membranes. There is an increase in k_- and consequently a decrease in the $\Delta^{\ddagger}G^0$ with the increase in the value of pH which is due, as referred earlier in the text, to an increase in the dianionic fraction of the CBF-C_{14}. The other observed trend is the decrease in the enthalpy variation for formation of the transition state with the increase in pH.

The positive enthalpy variation observed in the formation of the transition state in the desorption process is due to the formation of two cavities, one in the interfacial water and another in the monolayer from where the amphiphile is exiting. Considering that the $\Delta^{\ddagger}H^0$ for the formation of the water cavity is essentially the same for both membranes the observed differences are due to the interactions that the amphiphile establishes when inserted in the membrane such as, the interplay between the amphiphile dipole moment and membrane dipole potential. Accordingly, has the pH decreases the neutral form of CBF-C_{14} is more stabilized in the membrane leading to an increase in $\Delta^{\ddagger}H^0$ for both membranes studied.

A deeper localization of the headgroup for lower pH could be responsible for a bigger increase in the membrane entropy when going to the transition state, which may explain the increase in $T\Delta^{\ddagger}S^0$. Moreover, the higher pKa_2 and pKa_3 of CBF-C_{14} in POPC compared to POPC:CHOL(5:5) and its higher anisotropy (see V.6 above) corroborate the deeper positioning of the headgroup in the former membranes compared to the latter.

From the results it is clear that for POPC and POPC:CHOL(5:5) the differences are larger for $\Delta^{\ddagger}H^0$ than for $\Delta^{\ddagger}S^0$. This indicates that the interactions which are broken when going from POPC to POPC:CHOL(5:5) are not compensated by a corresponding increase in entropy, suggesting that a more ordered membrane is not able to take advantage of a nearby cavity to increase its conformational entropy.

Comparing the variations in the thermodynamic parameters with increase in the value of pH for both membranes, we observe that the decrease in $\Delta^{\ddagger}H^0$ (when going from pH=6 to 7.4) in POPC is significantly larger than in POPC:CHOL (5:5) and that the effect in $\Delta^{\ddagger}H^0$ is similar to that observed for $\Delta^{\ddagger}S^0$. This is probably related with the larger variation in the global charge of CBF-C_{14} in POPC than in POPC:CHOL (5:5) for this pH variation (-0.11 to -0.74 (-0.67)) in POPC versus -0.87 to -1.42 (-0.54) in POPC:CHOL (5:5)).

By knowing the values of k_- at different pH and the p*K*a of CBF-C_{14}, which was previously determined, we can calculate k_- for the different CBF-C_{14} species in solution. The global rate of translocation is given by:

$$k_- = k_-^0[CBF-C_{14}{}^0] + k_-^{1^-}[CBF-C_{14}{}^{1^-}] + k_-^{2^-}[CBF-C_{14}{}^{2^-}] \qquad (VI\text{-}7)$$

where k_-^0, $k_-^{1^-}$ and $k_-^{2^-}$ represent the desorption rate constant of the neutral monoanionic and dianionic species, respectively. The concentrations of each species ($[CBF-C_{14}{}^0],[CBF-C_{14}{}^{1^-}]$ and $[CBF-C_{14}{}^{2^-}]$) are calculated from the pH of the solution and the different ionization constants.

$$[CBF-C_{14}{}^0] = \frac{[CBF-C_{14}]_T}{1+\frac{K_{a2}K_{a1}}{(10^{-pH})^2}+\frac{K_{a1}}{10^{-pH}}};$$

$$[CBF-C_{14}{}^{1^-}] = \frac{K_{a1}\left[CBF-C_{14}{}^0\right]}{10^{-pH}}; \qquad (VI\text{-}8)$$

$$[CBF-C_{14}{}^{2^-}] = \frac{K_{a2}K_{a1}\left[CBF-C_{14}{}^0\right]}{\left(10^{-pH}\right)^2}$$

From the dependence of the observed desorption rate constant with pH, the rate constant of each CBF-C_{14} species may be calculated. The experimental results and the best fit are presented in Figure VI.13. Considering the limited pH range studied and given the complexity of the titration curve, with two ionization constants in the pH range considered, some concerns in recovering the kinetic constants are inevitable. First, the desorption at lower pH is very slow and given that there are no further data for pH lower than 6 the curve is not well defined in this region. Therefore, during the fit it was necessary to impose a constraint on the value of k_- for the neutral specie (≥ 0), otherwise the values would be meaningless. Moreover, given that the experimental points represent a very narrow region of the titration curve, the confidence in the desorption rate constant obtained for the species in solution was very small. For instance it is clear from Figure VI.13 (A) that the result for the dianionic species is obtained without the presence of any experimental results. Therefore, in order to obtain confident results for the different CBF-C_{14} species, a larger pH range must be covered including the plateau present at higher pH (≥8) and at low pH (≤6). Although it seems tempting to give the values for the desorption of the neutral mono and dianionic species of CBF-C_{14} from the best fit, the reasons aforementioned tell us that the more correct decision is to perform a more detailed study (higher pH range) before being compromised with any value.

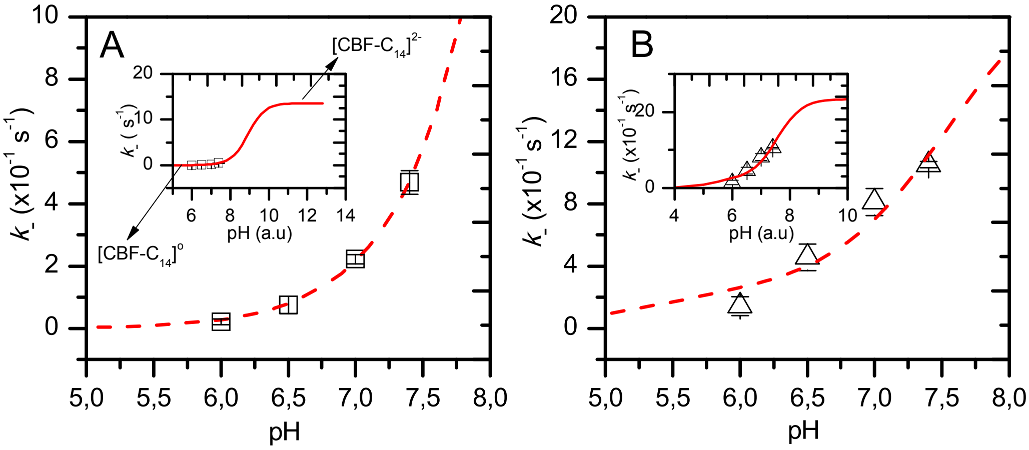

Figure VI.13. Desorption rate constants obtained, at 25 ºC, for CBF-C_{14} in POPC (□) and POPC:CHOL(5:5) (Δ) lipid bilayers at different pH buffer solutions. The line is the best fit of equations VI-7 and VI-8 to the experimental results, with pKa_2= 6.9, pKa_3= 8.9 and k_- for the neutral, monoanionic and dianionic equal to 0, 2.4×10^{-1} and 14 s^{-1}, for POPC. For POPC:CHOL(5:5) bilayers the best fit was performed with pKa_2= 5.3 and pKa_3= 7.6 with the k_- for the neutral monoanionic and dianionic forms equal to 0, 2.5×10^{-1} s^{-1} and 2.3 s^{-1}, respectively.

VI.5.2 Effect of the pH in Translocation of CBF-C_{14} in LUVs

Translocation is an essential step in the permeation of amphiphilic molecules and xenobiotics across cell membranes, moreover, the phospholipids in cells are subject to the transbilayer movement, which is crucial to maintain the cell membrane asymmetry (for details see II.2.3 above). The ionization state of an amphiphile strongly affects its translocation has shown recently, by our group, with the anti-psychotropic drug chlorpromazine [174]. Furthermore, fatty acids display a high dependence of the translocation rate constant with pH. This was elucidated based on an increase in the fraction of neutral form, due to the increase in pK_a upon the insertion in membranes [260].

From the experimental results shown above (see Figure VI.9) the translocation at different pH (6.0-7.4) was obtained. Moreover, performing the experiments at different temperatures, between 25 ºC and 55 ºC, the Arrhenius type plots and the thermodynamics for the translocation process at each pH were attained (Figure VI.14). In Table VI.9, there is a compilation of all the experimental results, at different pH, for CBF-C_{14}.

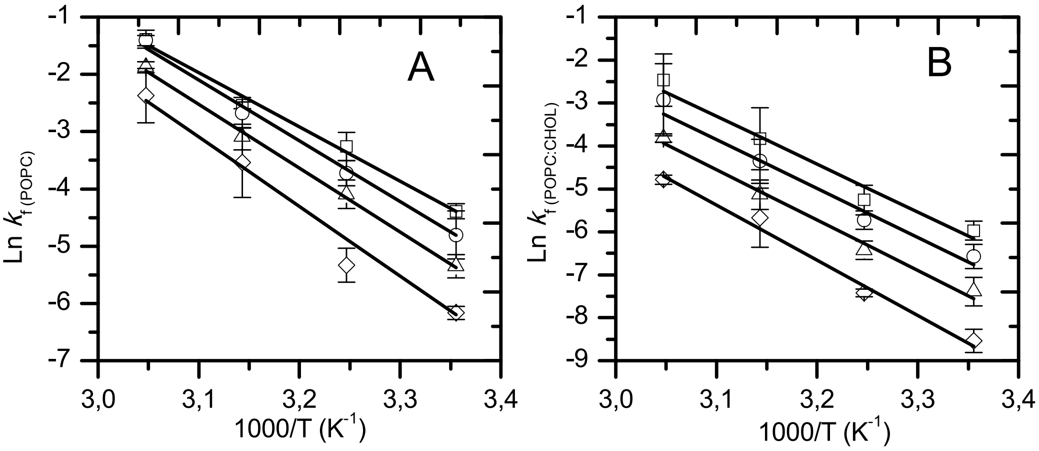

Figure VI.14. Arrhenius type plots for the translocation of CBF-C_{14} in bilayers of POPC (Panel A) and POPC:CHOL(5:5) (Panel B) at pH= 6 (□); pH= 6.5 (○); pH= 7.0 (Δ) and pH= 7.4 (◊).The results show the average experimental value ± standard deviation of, at least, three independent experiments. The line is the best fit of equation VI-6.

Table VI.9. Thermodynamic parameters, for the transition state, and rate constant for translocation of CBF-C_{14} in lipid bilayers at different pH.

T=25 ºC	POPC (l_d)				POPC:CHOL(5:5) (l_o)			
pH≈	6.0	6.5	7.0	7.4	6.0	6.5	7.0	7.4
k_f (s^{-1})	1.2±0.2 ($\times10^{-2}$)	8.2±3.0 ($\times10^{-3}$)	4.8±0.9 ($\times10^{-3}$)	2.1±0.2 ($\times10^{-3}$)	2.6±0.6 ($\times10^{-3}$)	1.4±0.4 ($\times10^{-3}$)	6.2±2.0 ($\times10^{-4}$)	2.0±0.5 ($\times10^{-4}$)
$\Delta^{‡}G^0$ ($kJmol^{-1}$)	84	85	86	88	88	90	92	94
$\Delta^{‡}H^0$ ($kJmol^{-1}$)	76±4.0	86±6.0	90±4.0	98±10	90±11	92±10	95±6.0	104±8.0
f CBF-$C_{14}^{0\,(a)}$	*0.89*	*0.72*	*0.45*	*0.24*	*0.15*	*0.05*	*0.01*	*0.004*
f CBF-$C_{14}^{1\,(b)}$	*0.11*	*0.28*	*0.54*	*0.74*	*0.83*	*0.87*	*0.77*	*0.58*

From the results summarized in Table VI.9 it is clear that, as expected, with the pH increase the rate of translocation decreases (approximately 1 order), in accordance to a more prominent fraction of negatively charged CBF-C_{14}. The increase in $\Delta^{‡}H^0$, with the pH, have two major contributions, one related with the interactions between the amphiphile and the membrane lipids, in the inserted state, and another owned to the desolvation of the amphiphile headgroup upon its translocation to the inner core of the bilayer. Considering that, as the pH increases, the headgroup of the CBF-C_{14} is more exposed to the aqueous phase we believe that the increase in enthalpy is due to the water displacement from the amphiphile headgroup. Moreover, upon this water displacement from the interfacial region an increase in entropy would be expectable with the pH, corroborating the obtained experimental results.

The different positioning of the headgroup in POPC and POPC:CHOL(5:5), once again, has a major effect in the translocation precisely due to its different solvation. In POPC CBF-C_{14} has a more internal localization in the membrane interface, compared to POPC:CHOL(5:5), corresponding to a lower solvation of the headgroup and, therefore, upon its transfer to the bilayer inner region a lower $\Delta^{‡}H^0$ and a higher $T^{‡}\Delta S^0$ are obtained. Furthermore, the enthalpy variation for the transition state, with the increase in pH, is higher for the POPC than for POPC:CHOL(5:5) due to a more extensive delocalization of the amphiphile headgroup and an higher global charge variation of

CBF-C_{14} in the former membrane than in the latter. Namely, in the POPC membranes, with the pH increase, there is a higher displacement of the headgroup towards the water phase than POPC:CHOL(5:5), which is already deeper inserted in the aqueous phase. A significant contribution to this deeper and shallower positioning of the amphiphile, both with the pH and the membrane composition, may be attributed to the amphiphile-membrane dipole interactions and this will be further discussed in the next topic.

Knowing the pH and the p*K*a of CBF-C_{14}, the translocation of the neutral, monoanionic and dianionic species may be obtained (Figure VI.15). Contrarily to what was observed in the desorption step, it is now the translocation of the dianionic species that is very slow. Therefore, the best fit was obtained assuming that the rate constant for translocation of $[\text{CBF-C}_{14}]^{2-}$ is equal to zero. Moreover, in POPC the k_f of the $[\text{CBF-C}_{14}]^{1-}$ had also to be equal to zero allowing only assessing, for this membrane, the k_f of the neutral species. Considering the lack of experimental data to correctly assess the translocation of the species we opted once again not to recover a value for the translocation rate constant.

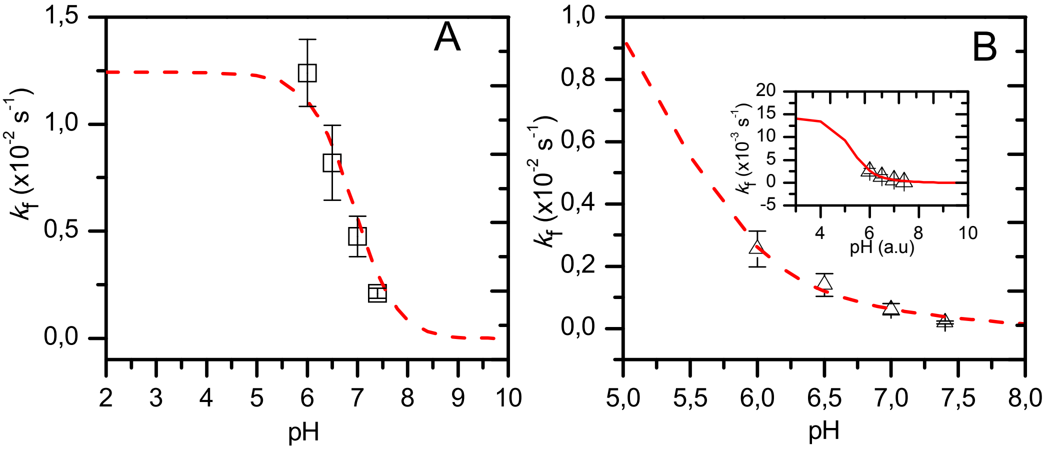

Figure VI.15. Translocation rate constants, at 25 ºC, obtained for CBF-C_{14} in POPC (□) and POPC:CHOL(5:5) (Δ) lipid bilayers at different values of pH. The line is the best fit of equations VI-7 and VI-8 to the experimental results, with p*K*a_2= 6.9, p*K*a_3= 8.9 and k_- for the neutral equal to 1.2×10^{-2} $s^{-1}$and 0 s^{-1} for the monoanionic and dianionic, in POPC. For POPC:CHOL(5:5) bilayers the best fit was performed with p*K*a_2= 5.3 and p*K*a_3= 7.6 with the k_- for the neutral, monoanionic and dianionic forms equal to 1.4×10^{-2} , 5.6×10^{-4} and 0 s^{-1}, respectively.

In the sections above the thermodynamics and kinetic parameters for the interaction of RG-C_{14} and CBF-C_{14} (at different ionization states) with bilayers, in the l_d and l_o phase, were discussed. However, the role of the membrane dipole potential and amphiphile dipole moment was, on purpose, vaguely addressed because it requires a deeper and more global analysis. Therefore in the next section the role of the electrostatic potential, in the above parameters, will be discussed.

VI.6 Role of Membrane Dipole Potential and Amphiphile dipole Moment in Kinetics and Thermodynamics of interaction with lipid bilayers, in l_d and l_o phase.

The dipole moment of the amphiphiles was determined through semi empirical calculations (V.7 above). When inserted in the membrane, the dipole moment orientation of the CBF-C_{14} has the same direction of the membrane dipole potential, while that of RG-C_{14} has an opposite orientation (Figure VI.16). This different orientation of the dipole moments of the amphiphiles may influence their interaction with lipid bilayers. Considering that the interaction between the amphiphile dipole moment and the membrane dipole potential is essentially of enthalpic origin in this topic we will, exclusively, refer to the enthalpy variations observed in the experimental results.

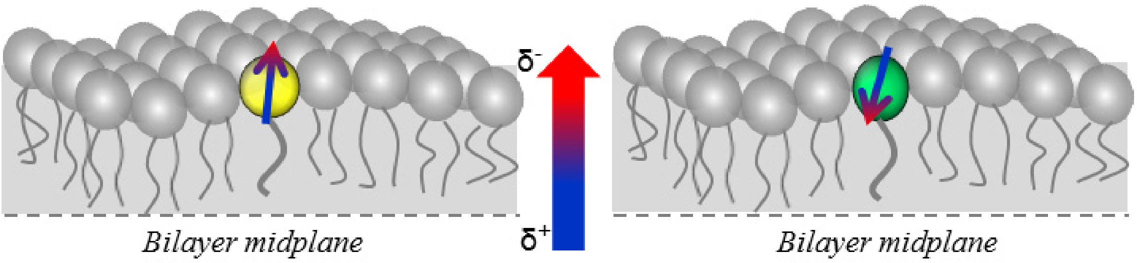

Figure VI.16. Schematic representation of CBF-C_{14} (yellow) and RG-C_{14} (green) and respective dipole moment orientation when inserted in a monolayer of lipids (grey). The large arrow represents the membrane dipole potential orientation with a gradient fill from blue (positive pole) to red (negative pole). Once inserted in the bilayer CBF-C_{14} and RG-C_{14} have distinct dipole orientations. The amphiphiles are exaggerated for a best understanding from the reader.

Let us consider first the desorption process at pH 7.4, where, the enthalpy and the entropy variation upon formation of the transition state was higher for the RG-C_{14} than for CBF-C_{14}, Table VI.5, while the rate constant was smaller Table VI.1. According to this, the opposite dipole orientation relative to the membrane dipole potential increases the stability of the inserted state of RG-C_{14} leading to an increase in enthalpy variation that dominates the energetic contribution. An interesting tendency was observed in the variation of $\Delta^{\ddagger}H^0$, for desorption, with the lipid composition of the bilayer. While for RG-C_{14} it decreases with membrane ordering (from POPC to SpM:CHOL (6:4)), for

CBF-C_{14} the opposite tendency is observed. This can be attributed to the difference in the interaction of the amphiphile dipole moment and membrane dipole potential, due to the headgroup localization in the membrane interface. Considering that it was observed, through fluorescence anisotropy and pK_a measurements, a more external positioning of the amphiphile headgroup with membrane ordering. The displacement of RG-$C_{14,}$ which inserted has a favourable interaction with membrane dipole potential, towards the water leads to a decrease in the strength of the interaction with the membrane dipole potential. Contrarily, a more external location of the polar headgroup of CBF-C_{14} leads to a more favourable (less unfavourable) electrostatic interaction. Consequently, while in RG-C_{14} the ordering of the membrane leads towards a decrease in the enthalpy variation for desorption, in CBF-C_{14} an increase is observed revealing a less unfavourable dipole interaction in the inserted state with the increase in membrane ordering Figure VI.17.

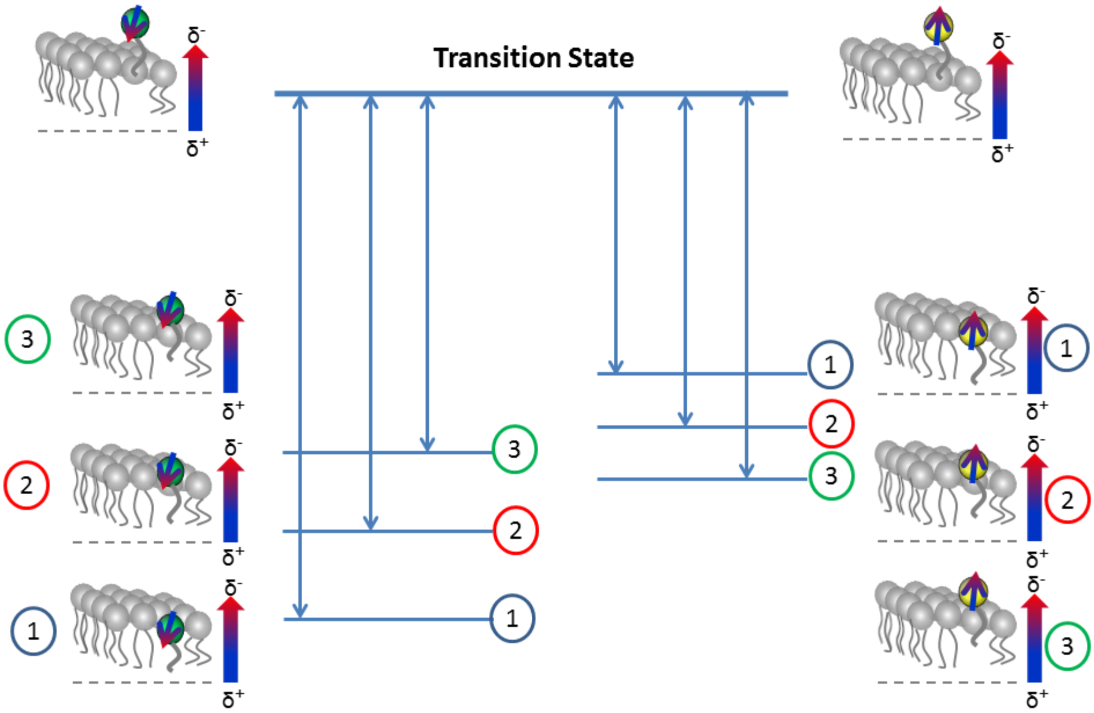

Figure VI.17. Schematic representation of the effect of RG-C_{14} (green amphiphile) and CBF-C_{14} (yellow amphiphile) interfacial headgroup localization in the enthalpy variation for the formation of the transition state in POPC (1), POPC:CHOL (5:5) (2) and SpM:CHOL (6:4) (3) membranes. The arrow in the amphiphile headgroup represents its dipole moment orientation and the thicker arrow represents the membrane dipole potential orientation, being the red and the blue ends the negative and the positive pole, respectively. For simplicity the energy was normalized for the transition state and the blue arrows represent the enthalpy variation from the inserted state to the transition sate.

The translocation results, at pH 7.4, showed that RG-C_{14} compared to CBF-C_{14}, has a higher enthalpy and entropy variation upon formation of the transition state. This highlights the increasing stability of the RG-C_{14}, when inserted in membrane, compared to CBF-C_{14} due to favourable dipole interaction. Moreover, the increase in membrane dipole potential, POPC:CHOL(5:5), rises the $\Delta^{\ddagger}H^0$, particularly for the RG-C_{14}, due to an increasing stability of its inserted state for those membranes. In POPC membranes, however, the $\Delta^{\ddagger}H^0$ is essentially the same for both amphiphiles because in this membranes the CBF-C_{14} has a higher neutral fraction (smaller dipole moment, $\mu \approx 9.4$ D).

At pH 7.4, CBF-C_{14} is negative while RG-C_{14} is a zwitterion. The translocation process requires placing the polar group in the inner core of the membrane and this is energetically more unfavourable (leading to higher activation energy and, consequently, a slower rate) for charged molecules. Therefore, ideally, the comparison should be made between the results of the neutral CBF-C_{14} and RG-C_{14}. However, the lack of experimental results describing the titration curve did not permit to characterize accurately k_- and k_f of the neutral CBF-C_{14}. From the pH dependence of the thermodynamic parameters associated with the desorption process, we observe that a decrease in pH leads to a higher $\Delta^{\ddagger}H^0$ due to an increase in the fraction of the neutral form (with smaller dipole moment) pointing to a less unfavourable interaction of CBF-C_{14} dipole moment with the membrane dipole potential. Moreover, this variation is less accentuated for POPC:CHOL(5:5) due to a much smaller neutral fraction in solution in the pH range studied when compared to POPC. In translocation, although the amphiphile dipole and membrane potential interactions have an important role certainly a major contribution comes from putting charges inside the membrane. Therefore, the decrease in neutral fraction as the pH increases leads to a higher enthalpy variation. This is particularly evident in POPC membranes where a higher charge variation occurs.

From the rationalization of the membrane potential with the orientation of the amphiphile dipole moment, it was shown that the opposite orientation of both leads to further stability of the amphiphile when inserted in the bilayer. This translates into larger activation energy in the processes of translocation and desorption resulting in smaller translocation and desorption rates, which may be extremely relevant when predicting the permeation of amphiphilic molecules across biological membranes.

Conclusions

In this work, we have characterized the kinetics and thermodynamics of interaction of two distinct amphiphiles with lipid bilayers having different physical properties. Moreover, the aqueous solubility, the relative equilibrium partition coefficient between the aqueous phase and the membranes and the probes localization in the lipid bilayers was also studied. The amphiphilic probes have a 14 carbons alkyl chain length attached to distinct fluorescent headgroup with different dipole moments. While the dipole moment of RG-C_{14} inserted in the membrane has an orientation opposite to the membrane dipole potential, in CBF-C_{14} the orientation of both dipoles is similar. This important characteristic of the amphiphiles headgroup allows establishing some conclusions, regarding the interplay between their dipole moment and the membrane dipole potential in the kinetics and thermodynamics of interaction with lipid bilayers. Our group has previously addressed this topic, speculating that the magnitude and the orientation of the dipole potential could affect the partitioning of amphiphiles to membranes with different dipole potentials, however no quantitative detail was given [224]. The complete kinetic and thermodynamic characterization performed in this work is a foremost step given that only a few authors have reported, with such detail, the interaction of amphiphiles with different lipid bilayers.

In order to reveal the effect of headgroup dipole moment and membrane dipole potential, in the interaction of RG-C_{14} and CBF-C_{14} with bilayers, it is crucial to assess their magnitude. For the amphiphiles, this was accomplished through semi empirical calculation and the dipole potential of membranes was obtained using monolayers formed at the air-water interface. The amphiphiles showed, as expected, an opposite orientation for their dipole moments, its magnitude being higher for CBF-C_{14} (23 D) than for RG-C_{14} (15 D). In monolayers, the experiments were performed with either pure or mixtures of lipids, to gain insight into the contribution from each lipid class and allow the estimation of the dipole potential of complex lipid mixtures present in biological membranes. The results showed a smaller dipole potential for SpM due to their hydroxyl group in the sphingosine alkyl chain. The dipole potential of monolayers showed an increase with the cholesterol content due to a higher packing of the lipids (smaller area per lipid), in accordance with other reported data [170]. In the quaternary mixture of POPC:CHOL:POPE:POPS(4:3:2:1), which mimmetize the inner leaflet of the plasma membrane, a smaller dipole potential than that of the ternary mixture

POPC:CHOL:POPE(5:3:2) was found, which was interpreted as an increase in the average area per lipid. This result highlights the effect of 10% of negatively charged lipid increasing the free volume, and disordering, of this quaternary mixture. Moreover, the dipole potential of membranes with the composition similar to the plasma membranes showed an orientation and magnitude that reinforces the transmembrane potential in those membranes.

The amphiphile CBF-C_{14} has a CAC of 2.5 nM, seen from fluorescence shifts to the predicted linear dependence with concentration. However, the aqueous solubility of RG-C_{14} (42 pM) was too small to be measured directly being estimated from the experimentally determined CAC for the homologous RG-C_{10} and the solubility dependence with the length of the alkyl group measured for the homologous series NBD-C_n [175]. The aqueous solubility of RG-C_{14} and CBF-C_{14} revealed that the latter is more soluble in the aqueous media than the former, as expected from its negative charge at pH=7.4. The partition between aqueous and lipid phases cannot be directly assessed for the case of RG-C_{14} whose solubility in the aqueous phase is below the sensitivity of the method used. Therefore, we have characterized the association of these amphiphiles with various bilayers from their transfer between liposomes. This allows recovering a relative partition coefficient (Kp_{rel}) between donor (POPC) vesicles and different acceptor vesicles. The value of Kp_{rel} obtained was smaller for CBF-C_{14} than for the homologous RG-C_{14} for all lipid compositions. Furthermore, for both fluorescent probes there is an increase in Kp_{rel} with the bilayer ordering. The rationalization in terms of membrane dipole potential was performed, for POPC:CHOL membranes, and a linear decrease of $\ln(Kp_{rel})$ and ΔG_{rel} with the dipole potential increase (which corresponds also to an increase in the membrane order) was observed for both probes. The aggregation of both probes in the distinct membranes was also studied. For RG-C_{14}, the time evolution was well described by a dimerization process, while for CBF-C_{14} there was no indications of aggregation in membranes. The aggregation of RG-C_{14} in more pronounced in liquid ordered membranes, (POPC:CHOL and SpM:CHOL), with equilibrium dimerization constants, K_d, of $7.0\pm1.5(\times10^2)$ and $9.0\pm2.5(\times10^2)$ M^{-1}, respectively. Moreover, for POPC:CHOL membranes an increase in the dipole potential leads to an increase in the RG-C_{14} K_d, indicating a stabilization of the amphiphile aggregated form. The localization of RG-C_{14} and CBF-C_{14} headgroup was assessed through fluorescence anisotropy and lifetimes measurements. As expected, the negatively charged CBF group was found to be located in a more external position, more exposed to the aqueous media, than the zwitterionic RG group for lipid bilayers containing cholesterol. However, and surprisingly, the location of the polar fluorescent groups of CBF-C_{14} and RG-C_{14} was very similar when the amphiphiles are inserted in POPC bilayers. This deeper localization for CBF-C_{14}, in POPC, is explained based on an increase in the neutral fraction of CBF-C_{14}, due to a shift of p*K*a for higher values.

In order to predict the passive permeation of a solute across biological membranes it is essential to know the kinetics of their interaction with lipid bilayers. Considering that most amphiphilic drugs have an asymmetric charge distribution (dipole moment) the interaction between amphiphiles with distinct dipole orientation and membranes with different dipole potential has a high relevance in pharmacokinetics and bioavailability. Therefore, in this work, we studied the kinetics of interaction between RG-C_{14} and CBF-C_{14} with lipid bilayers in the liquid disordered and liquid ordered phase. From the different steps that lead a molecule from one side of a bilayer to the other side, (insertion, translocation and desorption) the translocation and desorption were determined for different temperatures and the thermodynamics was obtained. Additionally, based on the estimated (RG-C_{14}) and experimentally (CBF-C_{14}) obtained binding constant to POPC and POPC:CHOL (5:5) at 25 ºC, it is predicted that the insertion rate process is not diffusion controlled ($k_{+} \ll k_{\mathrm{diff}}$) for both probes. The desorption of CBF-C_{14} from lipids bilayers was faster than for RG-C_{14}, moreover, it increases with the order of the membrane for both probes. These distinct rates reflect a more stabilized inserted state of the RG-C_{14} compared to the CBF-C_{14}, due to a stronger interaction between its dipole moment and membrane dipole potential. This is in clear contradiction with the information obtained from the effect of the membrane dipole potential on the relative partition coefficients for both probes. The elucidation of this aspect requires the quantitative characterization of the rate of insertion, but it may be anticipated that the increase in the membrane dipole potential decreases the rate of insertion for amphiphiles with the orientation of the dipole moment similar to RG-C_{14}. This dipole-dipole interaction established when the amphiphile is inserted in the bilayer is reflected in a larger $\Delta^{\ddagger}H^{0}$ for the desorption of RG-C_{14} as compared to that of CBF-C_{14}. In translocation, a smaller rate was obtained for CBF-C_{14} in accordance with its negative charge, although $\Delta^{\ddagger}H^{0}$ was higher for RG-C_{14} than for CBF-C_{14}. This, once again, reflects the different interactions between the dipole moment of the amphiphiles and the membrane dipole potential. Therefore, the antiparallel dipole moment orientation of RG-C_{14}, compared to CBF-C_{14}, favours its interaction with the membrane dipole potential when inserted in the bilayer increasing the value of $\Delta^{\ddagger}H^{0}$ for formation of the transition state in translocation. The results obtained for desorption of CBF-C_{14} at different pH were in agreement with the above interpretation. Accordingly, the increase in $\Delta^{\ddagger}H^{0}$ observed for desorption of CBF-C_{14} at lower pH reflects a more favourable (or less unfavourable) interaction with the membrane dipole potential stabilizing the inserted state.

This work showed that the polar region of an amphiphilic drug affects its interaction with lipid bilayers, both its partition and kinetics. Moreover, the comparison between probes with opposite dipole moments showed that the asymmetric charge distribution in the amphiphilic molecule has a fundamental role in the kinetics of its interaction with lipid bilayers. It was shown that a molecule with a dipole moment orientation antiparallel to the dipole potential of the membrane is more stabilized when inserted in the lipid bilayer and this results in slower rates of desorption and translocation. This is a significant achievement that represents a step forward in the establishment of rules to predict the permeability of drugs from their chemical structure.

Appendix

- **Chapter V. "Effect of Amphiphile Dipole Moment in Solubility and Partition to Lipid Bilayers in Liquid Ordered and Liquid Disordered Phases"**

V.3 Partition of RG-C14 and CBF-C14 between Donor POPC LUVs and Acceptor LUVs with Various Lipid Compositions

For amphiphiles which are soluble in the aqueous phase as monomers the complete kinetic scheme is given by:

$$A_w \underset{k_-}{\overset{k_+LV}{\rightleftharpoons}} ALV^{out} \underset{k_f}{\overset{k_{-f}}{\rightleftharpoons}} ALV^{in} \qquad (1)$$

The amphile as monomer collides with lipid vesicles as (LUV) and eventually inserts with a rate constant k_+ in the outer monolayer of the lipid bilayer (ALV^{out}). Then it may translocate to the inner leaflet with rate constant k_f or dissociate from the lipid bilayer with a rate constant k_-.

The kinetic scheme (1) is described by the following differential equations:

$$\begin{aligned}
\frac{d[ALV^{out}]}{dt} &= k_+[A_w][LV] + k_f[ALV^{in}] - [ALV^{out}]\left(k_- + k_{-f}\right) \\
\frac{d[ALV^{in}]}{dt} &= k_{-f}[ALV^{out}] - k_f[ALV^{in}] \\
\frac{d[A_w]}{dt} &= k_-[ALV^{out}] - k_+[A_w][LV] \\
\frac{d[ALV]}{dt} &= \frac{d[ALV^{out}]}{dt} + \frac{d[ALV^{in}]}{dt}
\end{aligned} \qquad (A\text{-}1)$$

With the following mass balance:

$$[A]_T = [A_w] + \left[ALV^{in}\right] + \left[ALV^{out}\right] \qquad (A\text{-}2)$$

To analytically solve the differential equations two approximations must be made.

- *Slow translocation rate approximation*

In some conditions the translocation rate constant is smaller when compared to the insertion and desorption characteristic time, in this case $\left[\mathrm{AL_V^{in}}\right]$=0, and we can describe the whole process by a differential equation of the form:

$$\frac{d[x]}{dt} = -\beta\left([x]+b\right) \tag{A-3}$$

Whose integration leads to an equation of the type:

$$[x]_{(t)} = [x]_{\infty} + \left([x]_0 - [x]_{(\infty)}\right)e^{\beta t} \tag{A-4}$$

From this approximation the exchange rate constant, β, and the concentration of amphiphile bound to lipid bilayers at equilibrium is given by:

$$\begin{gathered}\beta = k_+[LV]+k_- \\ [ALV]_{\infty} = \frac{K_L[LV][A]_T}{K_L[LV]+1}\end{gathered} \tag{A-5}$$

- *Fast Translocation step approximation.*

For a fast translocation step the concentration of amphiphile bound to lipid vesicles is given by:

$$\left[\mathrm{AL_V^{out}}\right] = \left[\mathrm{AL_V^{in}}\right]; \quad \left[\mathrm{AL_V}\right] = 2\left[\mathrm{AL_V^{out}}\right] \tag{A-6}$$

From the differential equations the exchange rate constant and the amphiphile bound to lipid bilayers at equilibrium is given by:

$$\beta = k_+[LV] + \frac{k_-}{2}$$

$$\left[ALV\right]_\infty = \frac{2K_L\left[LV\right]\left[A\right]_T}{2K_L\left[LV\right]+1} \qquad \textit{(A-7)}$$

Considering these two approximations both k_- and k_+ can be recovered from the linear dependence of the transfer rate (β) with the LUV concentration. In these solutions the $k_{-f} \approx k_f$.

V.4. Aggregation of RG-C14 and CBF-C14 in Lipid Bilayers

- In the case of Monomer dimer equilibrium we have the following kinetic scheme.

$$M + M \xleftrightarrow[k_1]{k_2} D \qquad \textit{(2)}$$

The rate equations that describe the scheme are:

$$\frac{d\left[D\right]}{dt} = \frac{d\Delta}{dt} = k_2\left[M\right]^2 - k_1\left[D\right] \qquad \textit{(A-8)}$$

$$\frac{d\left[A_2\right]}{dt} = -2k_2\left[M\right]^2 + k_1\left[D\right]. \qquad \textit{(A-9)}$$

Considering that:

$$\Delta = \Delta_D = \left[D\right]_t - \left[D\right]_\infty$$

$$\Delta_M = \left[M\right]_t - \left[M\right]_\infty \qquad \textit{(A-10)}$$

$$\Delta_D = \frac{1}{2}\Delta_M$$

where, the parameter Δ denotes the displacement from the equilibrium.

The substitution of equations *(A-9)* in the rate equation for dimer *(A-7)* gives:

$$\begin{aligned}\frac{d\Delta}{dt} &= k_2\left(\left[M\right]_\infty - 2\Delta\right)^2 - k_1\left(\left[D\right]_\infty - \Delta\right) \\ &= k_2\left[M\right]_\infty{}^2 - 4k_2\left[M\right]_\infty\Delta + 4\Delta^2 - k_1\left[D\right]_\infty + k_1\Delta\end{aligned} \qquad \textit{(A-11)}$$

Applying the equilibrium condition, $\frac{\left[D\right]}{\left[M\right]^2} = \frac{k_2}{k_1} \Leftrightarrow k_1\left[D\right] = k_2\left[M\right]^2$, to equation *(A-11)*:

$$\begin{aligned}\frac{d\Delta}{dt} &= -4k_2\left[M\right]_\infty\Delta + 4k_2\Delta^2 - k_1\Delta \\ &= \text{-}k_2\left[\left(4\left[M\right]_\infty + K_0\right)\Delta - 4\Delta^2\right],\end{aligned} \qquad \textit{(A-12)}$$

where

$$K_0 = \frac{k_1}{k_2}. \qquad \textit{(A-13)}$$

A rate equation of type

$$\frac{dc}{dt} = -\left(\lambda_1 c + \lambda_1 c^2\right), \qquad \textit{(A-14)}$$

has the following solution

$$c(t) = \frac{c(0)\exp(-\lambda_1 t)}{1 + (\lambda_2/\lambda_1)c(0)\left[1 - \exp(-\lambda_1 t)\right]} \qquad \textit{(A-15)}$$

therefore, the solution for equation *(A-11)* is given by:

$$\Delta_D(t) = \frac{\Delta(0)\exp\left(-kt\right)}{1 - \left(4k_2/k\right)\Delta(0)\left[1 - \exp(-kt)\right]} = -\frac{1}{2}\Delta_M(t) \qquad \textit{(A-16)}$$

where,

$$k = k_2(4\left[M\right]_\infty + K_0). \qquad \textit{(A-17)}$$

V.5. Spectral Properties of the RG-C14 and CBF-C14 in Liquid Ordered and Liquid Disordered Phases

The ionization equilibrium of CBF-C_{14} in solution is given by:

$$\begin{aligned} CBF-C_{14}^{0} &\xleftrightarrow{Ka_1} CBF-C_{14}^{1-}+H^{+} \\ CBF-C_{14}^{1-} &\xleftrightarrow{Ka_2} CBF-C_{14}^{2-}+H^{+} \end{aligned} \qquad (3)$$

where, $CBF-C_{14}^{0}$, $CBF-C_{14}^{1-}$, $CBF-C_{14}^{2-}$ represent the neutral, anionic and di-anionic species of the CBF-C_{14} in solution, respectively. The Ka_1 and Ka_2 are the equilibrium ionization constants given by:

$$\begin{aligned} Ka_1 &= \frac{\left[CBF-C_{14}^{1-}\right]\left[H^{+}\right]}{\left[CBF-C_{14}^{0}\right]} \\ Ka_2 &= \frac{\left[CBF-C_{14}^{2-}\right]\left[H^{+}\right]}{\left[CBF-C_{14}^{1-}\right]} \end{aligned} \qquad (A\text{-}18)$$

The mass Balance:

$$\left[CBF-C_{14}\right]_T = \left[CBF-C_{14}^{0}\right]+\left[CBF-C_{14}^{1-}\right]+\left[CBF-C_{14}^{2-}\right] \qquad (A\text{-}19)$$

Combining the equations A-1 and A-2 the concentration of each specie in solution may be obtained from the experimental pH.

$$\left[CBF-C_{14}^{1-}\right]=\frac{Ka_1\left[CBF-C_{14}^{0}\right]}{\left[H^+\right]}$$

$$\left[CBF-C_{14}^{2-}\right]=\frac{Ka_2Ka_1\left[CBF-C_{14}^{0}\right]}{\left[H^+\right]}$$

(A-20)

$$\left[CBF-C_{14}^{0}\right]=\frac{\left[CBF-C_{14}\right]_T}{1+\frac{Ka_1Ka_2}{\left[H^+\right]^2}+\frac{Ka_1}{\left[H^+\right]}}$$

The total absorption of the solution at a certain pH is given by the concentration of each species multiplied by the proportionality constant (φ_i).

$$I_{Abs}\;\alpha\;\left[CBF-C_{14}^{0}\right]\varphi_{CBF-C_{14}^{0}}+\left[CBF-C_{14}^{1-}\right]\varphi_{CBF-C_{14}^{1-}}+\left[CBF-C_{14}^{2-}\right]\varphi_{CBF-C_{14}^{2-}} \qquad (A\text{-}21)$$

- **ChapterVI “Effect of the Amphiphile Dipole Moment in the Kinetics of Interaction with Lipid Bilayers in Liquid Ordered and Liquid Disordered Phases”**

VI.2. Kinetics of RG-C14 and CBF-C14 Exchange between LUVs

The kinetic parameters of both probes used in this work were assessed *via* transfer between vesicles. The complete kinetic scheme and the set of differential equations for the transfer of the amphiphiles from a donor to acceptor vesicles are given below.

$$\begin{gathered} ALV_D^{in} \underset{k_{-f}^D}{\overset{k_f^D}{\rightleftharpoons}} ALV_D^{out} \underset{k_+^D}{\overset{k_-^D}{\rightleftharpoons}} A_w + LV_D \\ A_w + LV_A \underset{k_-^A}{\overset{k_+^A}{\rightleftharpoons}} ALV_A^{out} \underset{k_f^A}{\overset{k_{-f}^A}{\rightleftharpoons}} ALV_A^{in} \end{gathered} \tag{4}$$

where, A_w is the amphiphile (RG-C_{14} or CBF-C_{14}) as a monomer in the aqueous phase, ALV_D^{in} , ALV_D^{out} , ALV_A^{out} ALV_A^{in} represent the amphiphile associated with the inner (in) or the outer (out) leaflets in the donor (LV_D) and acceptor (LV_A) LUVs respectively. The k_f, k_- and k_+ represent the translocation, desorption and insertion rate constants respectively, in either donor (D) or Acceptor (A) vesicles.

The kinetic scheme (4) is described by the following ordinary differential equations

$$\frac{d\left[ALV_D^{out}\right]}{dt} = -\left[ALV_D^{out}\right]\left(k_-^D + k_{-f}^D\right) + k_+^D\left[LV_D\right]\left[A_w\right] + k_f^D\left[ALV_D^{in}\right]$$

$$\frac{d\left[ALV_A^{out}\right]}{dt} = -\left[ALV_A^{out}\right]\left(k_-^A + k_{-f}^A\right) + k_f^A\left[ALV_A^{in}\right] + k_+^A\left[A_w\right]\left[LV_A\right]$$

(A-22)

$$\frac{d\left[ALV_A^{in}\right]}{dt} = k_f^A\left[ALV_A^{out}\right] - k_{-f}^A\left[ALV_A^{in}\right]$$

$$\frac{d\left[ALV_D^{in}\right]}{dt} = k_{-f}^D\left[ALV_D^{out}\right] - k_f^D\left[ALV_D^{in}\right]$$

The mass balance:

$$\left[A\right]_T = \left[A\right]_w + \left[ALV_A^{out}\right] + \left[ALV_A^{in}\right] + \left[ALV_D^{out}\right] + \left[ALV_D^{in}\right] \qquad \textit{(A-23)}$$

To analytically solve the differential equations slow translocation in donor and acceptor vesicles was assumed and $k_{-f} = k_f$ in both acceptor (A) and donor (D) vesicles. The exchange rate constant (β) of the amphiphile bound to the acceptor vesicles (ALV^A), at equilibrium, is given by

$$\beta = \frac{k_+[LV^A] + k_-^A\left([LV^D]K_L^D + 1\right)}{[LVD]K_L^D + \frac{k_+^A}{k_-^D}[LV^A] + 1}; \quad ALV^A_{(t=\infty)} = \frac{K_L^A[LV^A]}{K_L^A[LV^A] + [LV^D]_T K_L^D + 1}$$

(A-24)

Where, K_L^A and K_L^D represent the equilibrium association constants of the amphiphiles to acceptor and donor vesicles, respectively.

From the equations is clear that for vesicles with the same lipid composition the desorption constant. Considering vesicles with distinct lipid composition if the [LV^D]>> [LV^A] the exchange rate is equal to desorption rate constant from the acceptor while, for [LV^A] >> [LV^D] the β gives desorption rate from donor

References

1. Xu, C. and L.M. Loew, *Activation of phospholipase C increases intramembrane electric fields in N1E-115 neuroblastoma cells.* Biophys J, 2003. **84**(6): p. 4144-56.

2. Alakoskela, J.M.I., T. Soderlund, J.M. Holopainen, and P.K.J. Kinnunen, *Dipole potential and head-group spacing are determinants for the membrane partitioning of pregnanolone.* Molecular Pharmacology, 2004. **66**(1): p. 161-168.

3. Estronca, L., M.J. Moreno, M.S.C. Abreu, E. Melo, and W.L.C. Vaz, *Solubility of amphiphiles in membranes: influence of phase properties and amphiphile head group.* Biochemical and Biophysical Research Communications, 2002. **296**(3): p. 596-603.

4. Deamer, D.W., *Membrane Permeability 100 years since Ernest Overton*. Vol. 48. 1999, current Topics in Membranes: Academic Press.

5. Bünning, E., *Ahead of His Time: Wilhelm Pfeffer, Early Advances in Plant Biology*, O.U.P. Canada, Editor. 1975.

6. Heimburg, T., *Thermal Biophysics of Membranes*, I.-V.V.G.C. KGaA, Editor. 2007: http://eu.wiley.com/WileyCDA/WileyTitle/productCd-3527404716.html. p. 378.

7. De Weer, P., *A Century of Thinking About Cell Membranes.* Annual Review of Physiology, 2000. **62**(1): p. 919-926.

8. Singer, S.J. and G.L. Nicolson, *The fluid mosaic model of the structure of cell membranes.* Science, 1972. **175**(4023): p. 720-31.

9. Vella, F., *Biochemistry (third edition): G Zubay. pp 1024. Brown, Dubuque, Iowa. 1993 ISBN 0-697-14267-5, 3 and 7.* Biochemical Education, 1993. **21**(2): p. 111-111.

10. Hianik, T., *Structure and physical properties of biomembranes and model membranes*, in *Acta Physica Slovaca. Reviews and Tutorials*. 2006. p. 687.

11. Eeman, M.D., M., *From biological membranes to biomimetic model membranes.* Biotechnol. Agron. Soc. Environ., 2010. **14**(4): p. 719-736.

12. Gennis, R., *Biomembranes*, ed. Springer-Verlag. 1989, New York.

13. Shevchenko, A. and K. Simons, *Lipidomics: coming to grips with lipid diversity.* Nature Reviews Molecular Cell Biology, 2010. **11**(8): p. 593-598.

14. Coskun, U. and K. Simons, *Cell membranes: the lipid perspective.* Structure, 2011. **19**(11): p. 1543-8.

15. van Meer, G., D.R. Voelker, and G.W. Feigenson, *Membrane lipids: where they are and how they behave.* Nat Rev Mol Cell Biol, 2008. **9**(2): p. 112-24.

16. Dowhan, W., *Molecular basis for membrane phospholipid diversity: why are there so many lipids?* Annu Rev Biochem, 1997. **66**: p. 199-232.

17. Spector, A.A. and M.A. Yorek, *Membrane lipid composition and cellular function.* J Lipid Res, 1985. **26**(9): p. 1015-35.

18. Boesze-Battaglia, K. and R. Schimmel, *Cell membrane lipid composition and distribution: implications for cell function and lessons learned from photoreceptors and platelets.* J Exp Biol, 1997. **200**(Pt 23): p. 2927-36.

19. Lee, A.G., *Annular events: lipid-protein interactions.* Trends in Biochemical Sciences, 1977. **2**(10): p. 231-233.

20. Lee, A.G., *Lipid-protein interactions in biological membranes: a structural perspective.* Biochim Biophys Acta, 2003. **1612**(1): p. 1-40.

21. van Meer, G., *Cellular lipidomics.* EMBO J, 2005. **24**(18): p. 3159-65.

22. Feigenson, G.W., *Phase behavior of lipid mixtures.* Nature Chemical Biology, 2006. **2**(11): p. 560-563.

23. Spector, A.A. and C.P. Burns, *Biological and Therapeutic Potential of Membrane Lipid Modification in Tumors.* Cancer Research, 1987. **47**(17): p. 4529-4537.

24. Pfleger, R.C., N.G. Anderson, and F. Snyder, *Lipid Class and Fatty Acid Composition of Rat Liver Plasma Membranes isolated by Zonal Centrifugation.* Biochemistry, 1968. **7**(8): p. 2826-2833.

25. Gorter, E. and F. Grendel, *On bimolecular layers of lipoids on the chromocytes of the blood.* Journal of Experimental Medicine, 1925. **41**(4): p. 439-443.

26. Tanford, C., *The Hydrophobic Effect. Formation of Micelles and Biological Membranes.* . Wiley-Interscience, New York,, 1973. **8**.

27. Israelachvili, J.N., D.J. Mitchell, and B.W. Ninham, *Theory of self-assembly of hydrocarbon amphiphiles into micelles and bilayers.* Journal of the Chemical Society, Faraday Transactions 2: Molecular and Chemical Physics, 1976. **72**: p. 1525-1568.

28. Wasungu, L. and D. Hoekstra, *Cationic lipids, lipoplexes and intracellular delivery of genes.* Journal of Controlled Release, 2006. **116**(2): p. 255-264.

29. Bangham, A.D. and R.W. Horne, *Negative staining of phospholipids and their structural modification by surface-active agents as observed in the electron microscope.* Journal of Molecular Biology, 1964. **8**(5): p. 660-IN10.

30. Kahya, N., D. Scherfeld, K. Bacia, and P. Schwille, *Lipid domain formation and dynamics in giant unilamellar vesicles explored by fluorescence correlation spectroscopy.* J Struct Biol, 2004. **147**(1): p. 77-89.

31. Holopainen, J.M., M.I. Angelova, and P.K. Kinnunen, *Vectorial budding of vesicles by asymmetrical enzymatic formation of ceramide in giant liposomes.* Biophys J, 2000. **78**(2): p. 830-8.

32. Rigaud, J.L., B. Pitard, and D. Levy, *Reconstitution of membrane proteins into liposomes: application to energy-transducing membrane proteins.* Biochimica et biophysica acta, 1995. **1231**(3): p. 223-246.

33. Brzustowicz, M.R. and A.T. Brunger, *X-ray scattering from unilamellar lipid vesicles.* Journal of Applied Crystallography, 2005. **38**(1): p. 126-131.

34. Harvey, T.M. and L.G. Jennifer, *Membrane curvature and mechanisms of dynamic cell membrane remodelling.* Nature, 2005. **438**(7068): p. 590-596.

35. Marsh, D., A. Watts, and P.F. Knowles, *Cooperativity of Phase-Transition in Single-Bilayer and Multi-Bilayer Lipid Vesicles.* Biochimica Et Biophysica Acta, 1977. **465**(3): p. 500-514.

36. Biltonen, R.L. and D. Lichtenberg, *The use of differential scanning calorimetry as a tool to characterize liposome preparations.* Chemistry and Physics of Lipids, 1993. **64**(1–3): p. 129-142.

37. Koynova, R. and M. Caffrey, *Phases and phase transitions of the phosphatidylcholines.* Biochimica Et Biophysica Acta-Reviews on Biomembranes, 1998. **1376**(1): p. 91-145.

38. Leventis, P.A. and S. Grinstein, *The distribution and function of phosphatidylserine in cellular membranes.* Annu Rev Biophys, 2010. **39**: p. 407-27.

39. Ziegler, A., *Thermodynamic studies and binding mechanisms of cell-penetrating peptides with lipids and glycosaminoglycans.* Adv Drug Deliv Rev. 2008 Mar 1;60(4-5):580-97. Epub 2007 Oct 22.

40. Opdenkamp, J.A.F., *Lipid Asymetry in Membranes.* Annual Review of Biochemistry, 1979. **48**: p. 47-71.

41. Devaux, P.F., *Protein Involvement in Translembrane Lipid Asymetry.* Annual Review of Biophysics and Biomolecular Structure, 1992. **21**: p. 417-439.

42. Gurtovenko, A.A., *Asymmetry of lipid bilayers induced by monovalent salt: Atomistic molecular-dynamics study.* Journal of Chemical Physics, 2005. **122**(24): p. 10.

43. Daleke, D.L., *Regulation of transbilayer plasma membrane phospholipid asymmetry.* J Lipid Res, 2003. **44**(2): p. 233-42.

44. Manno, S., Y. Takakuwa, and N. Mohandas, *Identification of a functional role for lipid asymmetry in biological membranes: Phosphatidylserine-skeletal protein interactions modulate membrane stability.* Proceedings of the National Academy of Sciences, 2002. **99**(4): p. 1943-1948.

45. Schlegel, R.A. and P. Williamson, *Phosphatidylserine, a death knell.* Cell Death Differ, 2001. **8**(6): p. 551-63.

46. Pomorski, T., S. Hrafnsdottir, P.F. Devaux, and G. van Meer, *Lipid distribution and transport across cellular membranes.* Semin Cell Dev Biol, 2001. **12**(2): p. 139-48.

47. Zwaal, R.F. and A.J. Schroit, *Pathophysiologic implications of membrane phospholipid asymmetry in blood cells.* Blood, 1997. **89**(4): p. 1121-32.

48. Bevers, E.M., P. Comfurius, D.W.C. Dekkers, and R.F.A. Zwaal, *Lipid translocation across the plasma membrane of mammalian cells.* Biochimica Et Biophysica Acta-Molecular and Cell Biology of Lipids, 1999. **1439**(3): p. 317-330.

49. Quinn, P.J., *Plasma membrane phospholipid asymmetry.* Subcell Biochem, 2002. **36**: p. 39-60.

50. O'Toole, P.J., C. Wolfe, S. Ladha, and R.J. Cherry, *Rapid diffusion of spectrin bound to a lipid surface.* Biochimica et Biophysica Acta (BBA) - Biomembranes, 1999. **1419**(1): p. 64-70.

51. Palfrey, H.C. and A. Waseem, *Protein Kinase-C in the Human-Erythrocyte - Translocation to the Plasma-Membrane and Phosphorylation of Bands 4.1 and 4.9 and other Membrane- Proteins* Journal of Biological Chemistry, 1985. **260**(29): p. 6021-6029.

52. Fadeel, B. and D. Xue, *The ins and outs of phospholipid asymmetry in the plasma membrane: roles in health and disease.* Critical Reviews in Biochemistry and Molecular Biology, 2009. **44**(5): p. 264-277.

53. Pennings, M., I. Meurs, D. Ye, R. Out, M. Hoekstra, T.J.C. Van Berkel, and M.V. Eck, *Regulation of cholesterol homeostasis in macrophages and consequences for atherosclerotic lesion development.* FEBS Letters, 2006. **580**(23): p. 5588-5596.

54. Luzzati, V. and F. Husson, *The Structure of the Liquid-Crystalline Phases of Lipid-Water Systems.* The Journal of Cell Biology, 1962. **12**(2): p. 207-219.

55. Tardieu, A., V. Luzzati, and F.C. Reman, *Structure and polymorphism of the hydrocarbon chains of lipids: A study of lecithin-water phases.* Journal of Molecular Biology, 1973. **75**(4): p. 711-733.

56. Sackmann, E. and H. Traeuble, *Crystalline-liquid phase transition of lipid model membranes. I. Use of spin labels and optical probes as indicators of the phase transition.* Journal of the American Chemical Society, 1972. **94**(13): p. 4482-4491.

57. Nagle, J.F., *Lipid bilayer phase transition: density measurements and theory.* Proc Natl Acad Sci U S A, 1973. **70**(12): p. 3443-4.

58. Lentz, B.R., Y. Barenholz, and T.E. Thompson, *Fluorescence depolarization studies of phase transitions and fluidity in phospholipid bilayers. 2. Two-component phosphatidylcholine liposomes.* Biochemistry, 1976. **15**(20): p. 4529-4537.

59. Westerman, P.W., M.J. Vaz, L.M. Strenk, and J.W. Doane, *Phase transitions in phosphatidylcholine multibilayers.* Proc Natl Acad Sci U S A, 1982. **79**(9): p. 2890-4.

60. Palffy-Muhoray, P., *The Diverse World of Liquid Crystals.* Physics Today, 2007. **60**(9): p. 54-60.

61. Alberts B, J.A., Lewis J, et al, *Molecular Biology of the Cell.* New York: Garland Science, 2002. **4th edition**.

62. Albon, N. and J.M. Sturtevant, *Nature of the gel to liquid crystal transition of synthetic phosphatidylcholines.* Proc Natl Acad Sci U S A, 1978. **75**(5): p. 2258-60.

63. Engelman, D.M., *X-ray diffraction studies of phase transitions in the membrane of Mycoplasma laidlawii.* Journal of Molecular Biology, 1970. **47**(1): p. 115-117.

64. Almeida, P.F.F., W.L.C. Vaz, and T.E. Thompson, *Lateral diffusion and percolation in two-phase, two-component lipid bilayers. Topology of the solid-phase domains in-plane and across the lipid bilayer.* Biochemistry, 1992. **31**(31): p. 7198-7210.

65. Chapman, D., R.M. Williams, and B.D. Ladbrooke, *Physical studies of phospholipids. VI. Thermotropic and lyotropic mesomorphism of some 1,2-diacyl-phosphatidylcholines (lecithins).* Chemistry and Physics of Lipids, 1967. **1**(5): p. 445-475.

66. Raghunathan, V.A. and J. Katsaras, *Structure of the $L_{C'}$ Phase in a Hydrated Lipid Multilamellar System.* Physical Review Letters, 1995. **74**(22): p. 4456-4459.

67. Janiak, M.J., D.M. Small, and G.G. Shipley, *Temperature and compositional dependence of the structure of hydrated dimyristoyl lecithin.* J Biol Chem, 1979. **254**(13): p. 6068-78.

68. Simons, K. and D. Toomre, *Lipid rafts and signal transduction.* Nat Rev Mol Cell Biol, 2000. **1**(1): p. 31-9.

69. Fantini, J. and F.J. Barrantes, *How cholesterol interacts with membrane proteins: an exploration of cholesterol-binding sites including CRAC, CARC, and tilted domains.* Front Physiol, 2013. **4**: p. 31.

70. Steck, T.L., J. Ye, and Y. Lange, *Probing red cell membrane cholesterol movement with cyclodextrin.* Biophys J, 2002. **83**(4): p. 2118-25.

71. Ipsen, J.H., G. Karlstrom, O.G. Mouritsen, H. Wennerstrom, and M.J. Zuckermann, *Phase equilibria in the phosphatidylcholine-cholesterol system.* Biochim Biophys Acta, 1987. **905**(1): p. 162-72.

72. Vist, M.R. and J.H. Davis, *Phase equilibria of cholesterol/dipalmitoylphosphatidylcholine mixtures: deuterium nuclear magnetic resonance and differential scanning calorimetry.* Biochemistry, 1990. **29**(2): p. 451-464.

73. Ulmius, J., H. Wennerstrom, G. Lindblom, and G. Arvidson, *Pronton NMR Bandshapes Studies of Lamellar Liquid-Crystals and Gel Phases Containing Lecithins and Cholesterol.* Biochimica Et Biophysica Acta, 1975. **389**(2): p. 197-202.

74. Mateo, C.R., A.U. Acuna, and J.C. Brochon, *Liquid-Crystalline Phases of Cholesterol Lipid Bilayers as revealed by the Fluorescence of Trans-Parinaric Acid.* Biophysical Journal, 1995. **68**(3): p. 978-987.

75. Dill, K.A.B.S., *Molecular driving forces : statistical thermodynamics in biology, chemistry, physics, and nanoscience*. 2nd Edition ed. 2005, London; New York: Garland Science.

76. Dill, K.A., T.M. Truskett, V. Vlachy, and B. Hribar-Lee, *Modeling water, the hydrophobic effect, and ion solvation.* Annu Rev Biophys Biomol Struct, 2005. **34**: p. 173-99.

77. Head-Gordon, T. and G. Hura, *Water structure from scattering experiments and simulation.* Chem Rev, 2002. **102**(8): p. 2651-70.

78. Rand, R.P., *Raising Water to New Heights.* Science, 1992. **256**(5057): p. 618-618.

79. Halina Abramczyk, B.B.-P., Jakub Surmacki, Joanna Jablonska-Gajewicz, Radzislaw Kordek, *Hydrogen bonds of interfacial water in human breast cancer tissue compared to lipid and DNA interfaces.* Journal of Biophysical Chemistry, 2011. **2**: p. 158-169.

80. Israelachvili, J. and H. Wennerstrom, *Role of hydration and water structure in biological and colloidal interactions.* Nature, 1996. **379**(6562): p. 219-225.

81. Verwey, E.J.W. and J.T.G. Overbeek, *Theory of the Stability of Lyophobic Colloids*. 1948, Elsevier: Theory of the stability of lyophobic colloids.

82. Leikin, S., V.A. Parsegian, D.C. Rau, and R.P. Rand, *Hydration Forces.* Annual Review of Physical Chemistry, 1993. **44**: p. 369-395.

83. Derjaguin, B.V. and N.V. Churaev, *Flow of nonfreezing water interlayers and frost heaving.* Cold Regions Science and Technology, 1986. **12**(1): p. 57-66.

84. Jedlovszky, P. and M. Mezei, *Orientational Order of the Water Molecules Across a Fully Hydrated DMPC Bilayer: A Monte Carlo Simulation Study.* The Journal of Physical Chemistry B, 2001. **105**(17): p. 3614-3623.

85. Jendrasiak, G.L., *The hydration of phospholipids and its biological significance.* The Journal of nutritional biochemistry, 1996. **7**(11): p. 599-609.

86. Bonn, M., H.J. Bakker, A. Ghosh, S. Yamamoto, M. Sovago, and R.K. Campen, *Structural Inhomogeneity of Interfacial Water at Lipid Monolayers Revealed by Surface-Specific Vibrational Pump−Probe Spectroscopy.* Journal of the American Chemical Society, 2010. **132**(42): p. 14971-14978.

87. Cheng, J.-X., S. Pautot, D.A. Weitz, and X.S. Xie, *Ordering of water molecules between phospholipid bilayers visualized by coherent anti-Stokes Raman scattering microscopy.* Proceedings of the National Academy of Sciences, 2003. **100**(17): p. 9826-9830.

88. Jendrasiak, G.L. and J.H. Hasty, *The hydration of phospholipids.* Biochimica et Biophysica Acta (BBA) - Lipids and Lipid Metabolism, 1974. **337**(1): p. 79-91.

89. Ho, C., S.J. Slater, and C.D. Stubbs, *Hydration and Order in Lipid Bilayers.* Biochemistry, 1995. **34**(18): p. 6188-6195.

90. Gawrisch, K., H.C. Gaede, M. Mihailescu, and S.H. White, *Hydration of POPC bilayers studied by H-1-PFG-MAS-NOESY and neutron diffraction.* European Biophysics Journal with Biophysics Letters, 2007. **36**(4-5): p. 281-291.

91. Jendrasiak, G.L. and J.C. Mendible, *Phospholipid Head-Group Orientation - Effect on Hydration and Electrical - Conductivity.* Biochimica Et Biophysica Acta, 1976. **424**(2): p. 149-158.

92. Arrais, D. and J. Martins, *Bilayer polarity and its thermal dependency in the l(o) and l(d) phases of binary phosphatidylcholine/cholesterol mixtures.* Biochim Biophys Acta, 2007. **1768**(11): p. 2914-22.

93. Leneveu, D.M.R., R P; Parsegian, V. A., *Measurement of forces between lecithin bilayers.* Nature, 1976. **259**(5544): p. 601-603.

94. Bonn, M., H. Bakker, Y. Tong, and E.G. Backus, *No Ice-Like Water at Aqueous Biological Interfaces.* Biointerphases, 2012. **7**(1-4): p. 1-5.

95. Schmidt, D., Q.-X. Jiang, and R. MacKinnon, *Phospholipids and the origin of cationic gating charges in voltage sensors.* Nature, 2006. **444**(7120): p. 775-779.

96. Honig, B.H., W.L. Hubbell, and R.F. Flewelling, *Electrostatic Interactions in Membranes and Proteins.* Annual Review of Biophysics and Biophysical Chemistry, 1986. **15**: p. 163-193.

97. Matos, C., B. de Castro, P. Gameiro, J.L. Lima, and S. Reis, *Zeta-potential measurements as a tool to quantify the effect of charged drugs on the surface potential of egg phosphatidylcholine liposomes.* Langmuir, 2004. **20**(2): p. 369-77.

98. Jones, M.N., *The surface properties of phospholipid liposome systems and their characterisation.* Adv Colloid Interface Sci, 1995. **54**: p. 93-128.

99. Brockman, H., *Dipole Potential of Lipid-Membranes.* Chemistry and Physics of Lipids, 1994. **73**(1-2): p. 57-79.

100. Gross, E., R.S. Bedlack, and L.M. Loew, *Dual-Wavelenth Ratiometric Fluorescence Measurement of the Membrane Dipole Potential.* Biophysical Journal, 1994. **67**(1): p. 208-216.

101. Liberman, Y.A. and V.P. Topaly, *Permeability of Bimolecular Phospholipid Membranes for Fat-Soluble Ions.* Biophysics-Ussr, 1969. **14**(3): p. 477-.

102. Clarke, R.J., *Effect of lipid structure on the dipole potential of phosphatidylcholine bilayers.* Biochimica et Biophysica Acta (BBA) - Biomembranes, 1997. **1327**(2): p. 269-278.

103. Wang, L., *Measurements and implications of the membrane dipole potential.* Annu Rev Biochem. 2012;81:615-35. Epub 2012 Mar 12.

104. Haydon, D.A. and S.B. Hladky, *Ion Transport Across Thin Lipid-Membranes - Critical discussion of Mechanisms in Selected Systems.* Quarterly Reviews of Biophysics, 1972. **5**(2): p. 187-&.

105. Langner, M. and K. Kubica, *The electrostatics of lipid surfaces.* Chemistry and Physics of Lipids, 1999. **101**(1): p. 3-35.

106. Büldt, G., H.U. Gally, J. Seelig, and G. Zaccai, *Neutron diffraction studies on phosphatidylcholine model membranes: I. Head group conformation.* Journal of Molecular Biology, 1979. **134**(4): p. 673-691.

107. Seelig, J., P.M. MacDonald, and P.G. Scherer, *Phospholipid head groups as sensors of electric charge in membranes.* Biochemistry, 1987. **26**(24): p. 7535-7541.

108. Starke-Peterkovic, T., N. Turner, M.F. Vitha, M.P. Waller, D.E. Hibbs, and R.J. Clarke, *Cholesterol Effect on the Dipole Potential of Lipid Membranes.* Biophysical Journal, 2006. **90**(11): p. 4060-4070.

109. Cseh, R. and R. Benz, *Interaction of Phloretin with Lipid Monolayers: Relationship between Structural Changes and Dipole Potential Change.* Biophysical Journal, 1999. **77**(3): p. 1477-1488.

110. Brown, M.F. and J. Seelig, *Ion-Induced Changes in Head Group Conformation of Lecithin Bilayers.* Nature, 1977. **269**(5630): p. 721-723.

111. Starke-Peterkovic, T. and R. Clarke, *Effect of headgroup on the dipole potential of phospholipid vesicles.* European Biophysics Journal, 2009. **39**(1): p. 103-110.

112. Pearson, R.H. and I. Pascher, *Molecular - Structure of Lecithin Dihydrate.* Nature, 1979. **281**(5731): p. 499-501.

113. Wong, P.T.T. and H.H. Mantsch, *High- Pressure Infrared Spectroscopy Evidence of Water Binding-Sites in 1,2 - Diacyl Phospholipids.* Chemistry and Physics of Lipids, 1988. **46**(3): p. 213-224.

114. Flewelling, R.F. and W.L. Hubbell, *The membrane dipole potential in a total membrane potential model. Applications to hydrophobic ion interactions with membranes.* Biophysical Journal, 1986. **49**(2): p. 541-552.

115. Gawrisch, K., D. Ruston, J. Zimmerberg, V.A. Parsegian, R.P. Rand, and N. Fuller, *Membrane Dipole Potentials, Hydration Forces, and the Ordering of Water at Membrane Surfaces.* Biophysical Journal, 1992. **61**(5): p. 1213-1223.

116. Hubner, W. and A. Blume, *Interactions at the lipid-water interface.* Chemistry and Physics of Lipids, 1998. **96**(1-2): p. 99-123.

117. Mingins, J., D. Stigter, and K.A. Dill, *Phospholipid Interactions in Model Membrane Systems.1. Experiments on Monolayers.* Biophysical Journal, 1992. **61**(6): p. 1603-1615.

118. Evans, S.D. and A. Ulman, *Surface potential studies of alkyl-thiol monolayers adsorbed on gold.* Chemical Physics Letters, 1990. **170**(5–6): p. 462-466.

119. Davies, J.T. and E. Rideal, *Interfacial Potentials.* Canadian Journal of Chemistry-Revue Canadienne De Chimie, 1955. **33**(5): p. 947-960.

120. Vogel, V. and D. Möbius, *Hydrated polar groups in lipid monolayers: Effective local dipole moments and dielectric properties.* Thin Solid Films, 1988. **159**(1-2): p. 73-81.

121. Peterson, U., D.A. Mannock, R. Lewis, P. Pohl, R.N. McElhaney, and E.E. Pohl, *Origin of membrane dipole potential: Contribution of the phospholipid fatty acid chains.* Chemistry and Physics of Lipids, 2002. **117**(1-2): p. 19-27.

122. Simon, S.A. and T.J. McIntosh, *Magnitude of the Solvation Pressure Depends on Dipole Potential.* Proceedings of the National Academy of Sciences of the United States of America, 1989. **86**(23): p. 9263-9267.

123. Jarvis, N.L. and M.A. Scheiman, *Surface potentials of aqueous electrolyte solutions.* The Journal of Physical Chemistry, 1968. **72**(1): p. 74-78.

124. Demchak, R.J. and T. Fort Jr, *Surface dipole moments of close-packed un-ionized monolayers at the air-water interface.* Journal of Colloid and Interface Science, 1974. **46**(2): p. 191-202.

125. Taylor, D.M., *Developments in the theoretical modelling and experimental measurement of the surface potential of condensed monolayers.* Advances in Colloid and Interface Science, 2000. **87**(2–3): p. 183-203.

126. Hol, W.G.J., *The role of the α-helix dipole in protein function and structure.* Progress in Biophysics and Molecular Biology, 1985. **45**(3): p. 149-195.

127. Adhya, L., T. Mapder, and S. Adhya, *Role of terminal dipole charges in aggregation of alpha-helix pair in the voltage gated K(+) channel.* Biochim Biophys Acta, 2013. **1828**(2): p. 845-50.

128. Rokitskaya, T.I., Y.N. Antonenko, and E.A. Kotova, *Effect of the dipole potential of a bilayer lipid membrane on gramicidin channel dissociation kinetics.* Biophys J, 1997. **73**(2): p. 850-4.

129. Providence, L.L., O.S. Andersen, D.V. Greathouse, R.E. Koeppe, 2nd, and R. Bittman, *Gramicidin channel function does not depend on phospholipid chirality.* Biochemistry, 1995. **34**(50): p. 16404-11.

130. Ostroumova, O.S., V.V. Malev, A.N. Bessonov, J.Y. Takemoto, and L.V. Schagina, *Altering the Activity of Syringomycin E via the Membrane Dipole Potential.* Langmuir, 2008. **24**(7): p. 2987-2991.

131. Ostroumova, O.S., Y.A. Kaulin, P.A. Gurnev, and L.V. Schagina, *Effect of Agents Modifying the Membrane Dipole Potential on Properties of Syringomycin E Channels.* Langmuir, 2007. **23**(13): p. 6889-6892.

132. Hertel, C., E. Terzi, N. Hauser, R. Jakob-Rotne, J. Seelig, and J.A. Kemp, *Inhibition of the electrostatic interaction between beta-amyloid peptide and membranes prevents beta-amyloid-induced toxicity.* Proc Natl Acad Sci U S A, 1997. **94**(17): p. 9412-6.

133. Yeagle, P.L., *The structure of biological membranes (2nd edn)* Vol. 23. 2005: CRC Press. 540.

134. Sampaio, J.L., M.J. Moreno, and W.L. Vaz, *Kinetics and thermodynamics of association of a fluorescent lysophospholipid derivative with lipid bilayers in liquid-ordered and liquid-disordered phases.* Biophys J, 2005. **88**(6): p. 4064-4071.

135. Abreu, M.S.C., L.M.B.B. Estronca, M.J. Moreno, and W.L.C. Vaz, *Binding of a Fluorescent Lipid Amphiphile to Albumin and its Transfer to Lipid Bilayer Membranes.* Biophysical Journal, 2003. **84**(1): p. 386-399.

136. Abreu, M.S., M.J. Moreno, and W.L. Vaz, *Kinetics and thermodynamics of association of a phospholipid derivative with lipid bilayers in liquid-disordered and liquid-ordered phases.* Biophys J. 2004 Jul;87(1):353-65.

137. Torchilin, V.P., *Recent advances with liposomes as pharmaceutical carriers.* Nature Reviews Drug Discovery, 2005. **4**(2): p. 145-160.

138. Paula, S., A.G. Volkov, A.N. Van Hoek, T.H. Haines, and D.W. Deamer, *Permeation of protons, potassium ions, and small polar molecules through phospholipid bilayers as a function of membrane thickness.* Biophys J, 1996. **70**(1): p. 339-48.

139. Mathai, J.C., S. Tristram-Nagle, J.F. Nagle, and M.L. Zeidel, *Structural determinants of water permeability through the lipid membrane.* J Gen Physiol, 2008. **131**(1): p. 69-76.

140. Bemporad, D., C. Luttmann, and J.W. Essex, *Computer simulation of small molecule permeation across a lipid bilayer: dependence on bilayer properties and solute volume, size, and cross-sectional area.* Biophys J, 2004. **87**(1): p. 1-13.

141. Cardoso, R.M.S., P.A.T. Martins, F. Gomes, S. Doktorovova, W.L.C. Vaz, and M.J. Moreno, *Chain-Length Dependence of Insertion, Desorption, and Translocation of a Homologous Series of 7-Nitrobenz-2-oxa-1,3-diazol-4-yl-Labeled Aliphatic Amines in Membranes.* Journal of Physical Chemistry B, 2011. **115**(33): p. 10098-10108.

142. Marrink, S.-J. and H.J.C. Berendsen, *Simulation of water transport through a lipid membrane.* The Journal of Physical Chemistry, 1994. **98**(15): p. 4155-4168.

143. Marrink, S.J. and H.J.C. Berendsen, *Permeation process of small molecules across lipid membranes studied by molecular dynamics simulations.* Journal of Physical Chemistry, 1996. **100**(41): p. 16729-16738.

144. Nagle, J.F., J.C. Mathai, M.L. Zeidel, and S. Tristram-Nagle, *Theory of passive permeability through lipid bilayers.* Journal of General Physiology, 2008. **131**(1): p. 77-85.

145. Xiang, T.X. and B.D. Anderson, *The relationship between permeant size and permeability in lipid bilayer membranes.* J Membr Biol, 1994. **140**(2): p. 111-22.

146. Lieb, W.R. and W.D. Stein, *Biological membranes behave as non-porous polymeric sheets with respect to the diffusion of non-electrolytes.* Nature, 1969. **224**(5216): p. 240-3.

147. Pardridge, W.M. and L.J. Mietus, *Transport of Steroid - Hormones through the Rat Blood-Brain-Barrier - Primary Role of Albumin - Bound Hormone.* Journal of Clinical Investigation, 1979. **64**(1): p. 145-154.

148. Young, R.C., R.C. Mitchell, T.H. Brown, C.R. Ganellin, R. Griffiths, M. Jones, K.K. Rana, D. Saunders, I.R. Smith, N.E. Sore, and T.J. Wilks, *Development of a new physicochemical model for brain penetration and its application to the design of centrally acting H2 receptor histamine antagonists.* J Med Chem, 1988. **31**(3): p. 656-71.

149. Abraham, M.H., *Hydrogen bond and other descriptors for thalidomide and its N-alkyl analogs; prediction of physicochemical and biological properties.* Eur J Pharm Sci, 2004. **21**(4): p. 465-9.

150. Abraham, M.H., A. Ibrahim, A.M. Zissimos, Y.H. Zhao, J. Comer, and D.P. Reynolds, *Application of hydrogen bonding calculations in property based drug design.* Drug Discov Today, 2002. **7**(20): p. 1056-63.

151. Walter, A. and J. Gutknecht, *Permeability of small nonelectrolytes through lipid bilayer membranes.* The Journal of Membrane Biology, 1986. **90**(3): p. 207-217.

152. Finkelstein, A., *Water and nonelectrolyte permeability of lipid bilayer membranes.* J Gen Physiol, 1976. **68**(2): p. 127-35.

153. Lipinski, C.A., F. Lombardo, B.W. Dominy, and P.J. Feeney, *Experimental and computational approaches to estimate solubility and permeability in drug*

discovery and development settings. Adv Drug Deliv Rev, 2001. **46**(1-3): p. 3-26.

154. Seixas de Melo, J. and P.F. Fernandes, *Spectroscopy and photophysics of 4- and 7-hydroxycoumarins and their thione analogs.* Journal of Molecular Structure, 2001. **565-566**(0): p. 69-78.

155. Hope, M.J., M.B. Bally, G. Webb, and P.R. Cullis, *Production of large unilamellar vesicles by a rapid extrusion procedure. Characterization of size distribution, trapped volume and ability to maintain a membrane potential.* Biochimica et Biophysica Acta (BBA) - Biomembranes, 1985. **812**(1): p. 55-65.

156. Bartlett, G.R., *Phosphorus Assay in Column Chromatography.* Journal of Biological Chemistry, 1959. **234**(3): p. 466-468.

157. Taylor, R.P., A.V. Broccoli, and C.M. Grisham, *Enzymatic and colorimetric determination of total serum cholesterol. An undergraduate biochemistry laboratory experiment.* Journal of Chemical Education, 1978. **55**(1): p. 63.

158. Luzardo, M.D., G. Peltzer, and E.A. Disalvo, *Surface potential of lipid interfaces formed by mixtures of phosphatidylcholine of different chain lengths.* Langmuir, 1998. **14**(20): p. 5858-5862.

159. MacDonald, R.C. and S.A. Simon, *Lipid monolayer states and their relationships to bilayers.* Proc Natl Acad Sci U S A. 1987 Jun;84(12):4089-93.

160. McLaughlin, S., B. Felix, and K. Arnort, *Electrostatic Potentials at Membrane-Solution Interfaces*, in *Current Topics in Membranes and Transport*. 1977, Academic Press. p. 71-144.

161. Zhan, H. and T. Lazaridis, *Influence of the membrane dipole potential on peptide binding to lipid bilayers.* Biophysical Chemistry, 2012. **161**(1): p. 1-7.

162. Cladera, J. and P. O'Shea, *Intramembrane molecular dipoles affect the membrane insertion and folding of a model amphiphilic peptide.* Biophysical Journal, 1998. **74**(5): p. 2434-2442.

163. Szabo, G., *Dual Mechanism for action of Cholesterol on Membrane-Permeability.* Nature, 1974. **252**(5478): p. 47-49.

164. Flewelling, R.F. and W.L. Hubbell, *Hydrophobic Ion Interactions with Membranes - Thermodynamic Analysis of Tetraphenylphosphonium Binding to Vesicles.* Biophysical Journal, 1986. **49**(2): p. 531-540.

165. Luchian, T. and L. Mereuta, *Phlorizin- and 6-ketocholestanol-mediated antagonistic modulation of alamethicin activity in phospholipid planar membranes.* Langmuir, 2006. **22**(20): p. 8452-8457.

166. Andersen, O.S., A. Finkelstein, I. Katz, and A. Cass, *Effect of Phloretin on Permeability of Thin Lipid-Membranes.* Journal of General Physiology, 1976. **67**(6): p. 749-771.

167. Simon, S.A., T.J. McIntosh, A.D. Magid, and D. Needham, *Modulation of the Interbilayers Hydration Pressure by the addition of Dipoles at the Hydrocarbon Water Interface.* Biophysical Journal, 1992. **61**(3): p. 786-799.

168. Franklin, J.C. and D.S. Cafiso, *Internal Electrostatic Potentials in Bilayers - Measuring and Controlling Dipole Potentials in Lipid Vesicles.* Biophysical Journal, 1993. **65**(1): p. 289-299.

169. McIntosh, T.J., A.D. Magid, and S.A. Simon, *Cholesterol modifies the short-range repulsive interactions between phosphatidylcholine membranes.* Biochemistry, 1989. **28**(1): p. 17-25.

170. Smaby, J.M., H.L. Brockman, and R.E. Brown, *Cholesterol's Interfacial Interactions with Sphingomyelins and Phosphatidylcholines:Hydrocarbon Chain Structure Determines the Magnitude of Condensation.* Biochemistry, 1997. **36**(8): p. 2338-2338.

171. Kiessling, V., C. Wan, and L.K. Tamm, *Domain coupling in asymmetric lipid bilayers.* Biochimica et Biophysica Acta (BBA) - Biomembranes, 2009. **1788**(1): p. 64-71.

172. Verkleij, A.J., R.F.A. Zwaal, B. Roelofsen, P. Comfurius, D. Kastelijn, and L.L.M. van Deenen, *The asymmetric distribution of phospholipids in the human red cell membrane. A combined study using phospholipases and freeze-etch electron microscopy.* Biochimica et Biophysica Acta (BBA) - Biomembranes, 1973. **323**(2): p. 178-193.

173. Lairion, F. and E.A. Disalvo, *Effect of Dipole Potential Variations on the Surface Charge Potential of Lipid Membranes.* Journal of Physical Chemistry B, 2009. **113**(6): p. 1607-1614.

174. Martins, P.c.T., A. Velazquez-Campoy, W.L.C. Vaz, R.M.S. Cardoso, J. ValÃ©rio, and M.J.o. Moreno, *Kinetics and Thermodynamics of Chlorpromazine Interaction with Lipid Bilayers: Effect of Charge and Cholesterol.* Journal of the American Chemical Society. **134**(9): p. 4184-4195.

175. Cardoso, R.M.S., H.A.L. Filipe, F. Gomes, N.D. Moreira, W.L.C. Vaz, and M.J. Moreno, *Chain Length Effect on the Binding of Amphiphiles to Serum Albumin and to POPC Bilayers.* The Journal of Physical Chemistry B. **114**(49): p. 16337-16346.

176. McIntosh, T.J., S.A. Simon, D. Needham, and C.H. Huang, *Interbilayer interactions between sphingomyelin and sphingomyelin/cholesterol bilayers.* Biochemistry, 1992. **31**(7): p. 2020-2024.

177. Lundkatz, S., H.M. Laboda, L.R. McLean, and M.C. Phillips, *Influence of Molecular Packing and Phospholipid Type on Rates of Cholesterol Exchange.* Biochemistry, 1988. **27**(9): p. 3416-3423.

178. McIntosh, T.J., S.A. Simon, D. Needham, and C.H. Huang, *Structure and cohesive properties of sphingomyelin/cholesterol bilayers.* Biochemistry, 1992. **31**(7): p. 2012-2020.

179. Niemela, P., M.T. Hyvonen, and I. Vattulainen, *Structure and dynamics of sphingomyelin bilayer: Insight gained through systematic comparison to phosphatidylcholine.* Biophysical Journal, 2004. **87**(5): p. 2976-2989.

180. Chiu, S.W., S. Vasudevan, E. Jakobsson, R.J. Mashl, and H.L. Scott, *Structure of Sphingomyelin Bilayers: A Simulation Study.* Biophysical Journal, 2003. **85**(6): p. 3624-3635.

181. Smaby, J.M., M.M. Momsen, H.L. Brockman, and R.E. Brown, *Phosphatidylcholine acyl unsaturation modulates the decrease in interfacial elasticity induced by cholesterol.* Biophysical Journal, 1997. **73**(3): p. 1492-1505.

182. Haldar, S., R.K. Kanaparthi, A. Samanta, and A. Chattopadhyay, *Differential Effect of Cholesterol and Its Biosynthetic Precursors on Membrane Dipole Potential.* Biophysical Journal. **102**(7): p. 1561-1569.

183. Marsh, D., *Lateral pressure in membranes.* Biochimica et Biophysica Acta (BBA) - Reviews on Biomembranes, 1996. **1286**(3): p. 183-223.

184. Lantzsch, G., H. Binder, and H. Heerklotz, *Surface Area per Molecule in Lipid/C12E. Membrane Seen by Fluorescence Resonance Energy Transfer* Journal of Fluorescence, 1994. **4**(4): p. 339-343.

185. Konig, B., U. Dietrich, and G. Klose, *Hydration and structural properties of mixed lipid/surfactant model membranes.* Langmuir, 1997. **13**(3): p. 525-532.

186. Mukhopadhyay, P., L. Monticelli, and D.P. Tieleman, *Molecular Dynamics Simulation of a Palmitoyl-Oleoyl Phosphatidylserine Bilayer with Na+ Counterions and NaCl.* Biophysical Journal, 2004. **86**(3): p. 1601-1609.

187. Rand, R.P. and V.A. Parsegian, *Hydration forces between phospholipid bilayers.* Biochimica et Biophysica Acta (BBA) - Reviews on Biomembranes, 1989. **988**(3): p. 351-376.

188. Smaby, J.M., H.L. Brockman, and R.E. Brown, *Cholesterol's Interfacial Interactions with Sphingomyelins and-Phosphatidylcholines: Hydrocarbon Chain Structure Determines the Magnitude of Condensation.* Biochemistry, 1994. **33**(31): p. 9135-9142.

189. Smaby, J.M. and H.L. Brockman, *Surface Dipole- Moments of Lipids at the Argon-Water Interface - Similarities among Glycerol-Ester based Lipids.* Biophysical Journal, 1990. **58**(1): p. 195-204.

190. Leekumjorn, S. and A.K. Sum, *Molecular characterization of gel and liquid-crystalline structures of fully hydrated POPC and POPE bilayers.* Journal of Physical Chemistry B, 2007. **111**(21): p. 6026-6033.

191. Taylor, D.M., O.N. De Oliveira Jr, and H. Morgan, *Models for interpreting surface potential measurements and their application to phospholipid monolayers.* Journal of Colloid and Interface Science, 1990. **139**(2): p. 508-518.

192. MacDonald, R.C., S.A. Simon, and E. Baer, *Ionic influences on the phase transition of dipalmitoylphosphatidylserine.* Biochemistry, 1976. **15**(4): p. 885-91.

193. Petrache, H.I., S. Tristram-Nagle, K. Gawrisch, D. Harries, V.A. Parsegian, and J.F. Nagle, *Structure and fluctuations of charged phosphatidylserine bilayers in the absence of salt.* Biophys J. 2004 Mar;86(3):1574-86.

194. Oliveira, O.N., D.M. Taylor, T.J. Lewis, S. Salvagno, and C.J.M. Stirling, *Estimation of group dipole moments from surface potential measurements on Langmuir monolayers.* Journal of the Chemical Society, Faraday Transactions 1: Physical Chemistry in Condensed Phases, 1989. **85**(4): p. 1009-1018.

195. Hauser, H., I. Pascher, R.H. Pearson, and S. Sundell, *Preferred conformation and molecular packing of phosphatidylethanolamine and phosphatidylcholine.* Biochim Biophys Acta, 1981. **650**(1): p. 21-51.

196. Jurkiewicz, P., L. Cwiklik, A.b.t. VojtÃ-Å¡kovÃ¡, P. Jungwirth, and M. Hof, *Structure, dynamics, and hydration of POPC/POPS bilayers suspended in NaCl, KCl, and CsCl solutions.* Biochimica et Biophysica Acta (BBA) - Biomembranes. **1818**(3): p. 609-616.

197. de Almeida, R.F.M., A. Fedorov, and M. Prieto, *Sphingomyelin/Phosphatidylcholine/Cholesterol Phase Diagram: Boundaries and Composition of Lipid Rafts.* Biophysical Journal, 2003. **85**(4): p. 2406-2416.

198. Ohvo-Rekila, H., B. Ramstedt, P. Leppimaki, and J.P. Slotte, *Cholesterol interactions with phospholipids in membranes.* Progress in Lipid Research, 2002. **41**(1): p. 66-97.

199. Sostarecz, A.G., C.M. McQuaw, A.G. Ewing, and N. Winograd, *Phosphatidylethanolamine-induced cholesterol domains chemically identified with mass spectrometric imaging.* Journal of the American Chemical Society, 2004. **126**(43): p. 13882-13883.

200. Latorre, R. and J.E. Hall, *Dipole Potential measurements in Asymetric Membranes.* Nature, 1976. **264**(5584): p. 361-363.

201. Gurtovenko, A.A. and I. Vattulainen, *Lipid transmembrane asymmetry and intrinsic membrane potential: Two sides of the same coin.* Journal of the American Chemical Society, 2007. **129**(17): p. 5358-5359.

202. Dunphy, J.T. and M.E. Linder, *Signalling functions of protein palmitoylation.* Biochimica et Biophysica Acta (BBA) - Molecular and Cell Biology of Lipids, 1998. **1436**(1–2): p. 245-261.

203. Linder, M.E. and R.J. Deschenes, *Palmitoylation: policing protein stability and traffic.* Nat Rev Mol Cell Biol, 2007. **8**(1): p. 74-84.

204. Brown, D.A., *Lipid Rafts, Detergent-Resistant Membranes, and Raft Targeting Signals.* Physiology, 2006. **21**(6): p. 430-439.

205. Melkonian, K.A., A.G. Ostermeyer, J.Z. Chen, M.G. Roth, and D.A. Brown, *Role of Lipid Modifications in Targeting Proteins to Detergent-resistant Membrane Rafts: Many Raft Proteins are Acylated, while few are Prenylated.* Journal of Biological Chemistry, 1999. **274**(6): p. 3910-3917.

206. Schroeder, R., E. London, and D. Brown, *Interactions between saturated acyl chains confer detergent resistance on lipids and glycosylphosphatidylinositol (GPI)-anchored proteins: GPI-anchored proteins in liposomes and cells show similar behavior.* Proceedings of the National Academy of Sciences, 1994. **91**(25): p. 12130-12134.

207. Levental, I., D. Lingwood, M. Grzybek, Ü. Coskun, and K. Simons, *Palmitoylation regulates raft affinity for the majority of integral raft proteins.* Proceedings of the National Academy of Sciences, 2010.

208. Baumgart, T., A.T. Hammond, P. Sengupta, S.T. Hess, D.A. Holowka, B.A. Baird, and W.W. Webb, *Large-scale fluid/fluid phase separation of proteins and*

lipids in giant plasma membrane vesicles. Proc Natl Acad Sci U S A, 2007. **104**(9): p. 3165-70.

209. Peitzsch, R.M. and S. McLaughlin, *Binding of acylated peptides and fatty acids to phospholipid vesicles: Pertinence to myristoylated proteins.* Biochemistry, 1993. **32**(39): p. 10436-10443.

210. Sengupta, P., A. Hammond, D. Holowka, and B. Baird, *Structural determinants for partitioning of lipids and proteins between coexisting fluid phases in giant plasma membrane vesicles.* Biochim Biophys Acta, 2008. **1**: p. 20-32.

211. Sigworth, F.J., *Voltage gating of ion channels.* Q Rev Biophys, 1994. **27**(1): p. 1-40.

212. Asawakarn, T., J. Cladera, and P. O'Shea, *Effects of the membrane dipole potential on the interaction of saquinavir with phospholipid membranes and plasma membrane receptors of Caco-2 cells.* Journal of Biological Chemistry, 2001. **276**(42): p. 38457-38463.

213. Voglino, L., T.J. McIntosh, and S.A. Simon, *Modulation of the binding of signal peptides to lipid bilayers by dipoles near the hydrocarbon-water interface.* Biochemistry, 1998. **37**(35): p. 12241-12252.

214. Saarma, M., *GDNF – a stranger in the TGF-β superfamily?* European Journal of Biochemistry, 2000. **267**(24): p. 6968-6971.

215. Stefanova, I., V. Horejsi, I. Ansotegui, W. Knapp, and H. Stockinger, *GPI-anchored cell-surface molecules complexed to protein tyrosine kinases.* Science, 1991. **254**(5034): p. 1016-1019.

216. Yue, T. and X. Zhang, *Signal transduction across cellular membranes can be mediated by coupling of the clustering of anchored proteins in both leaflets.* Physical Review E, 2012. **85**(1): p. 011917.

217. Li, S., X. Zhang, and W. Wang, *Cluster formation of anchored proteins induced by membrane-mediated interaction.* Biophys J, 2010. **98**(11): p. 2554-63.

218. Nichols, J.W. and R.E. Pagano, *Use of Resonance Energy-Transfer to Study the Kinetics of Amphiphile Transfer Between Vesicles.* Biochemistry, 1982. **21**(8): p. 1720-1726.

219. Nichols, J.W. and R.E. Pagano, *Kinetics of soluble lipid monomer diffusion between vesicles.* Biochemistry, 1981. **20**(10): p. 2783-2789.

220. Greenwood, A.I., S. Tristram-Nagle, and J.F. Nagle, *Partial molecular volumes of lipids and cholesterol.* Chem Phys Lipids, 2006. **143**(1-2): p. 1-10.

221. Krivanek, R., L. Okoro, and R. Winter, *Effect of cholesterol and ergosterol on the compressibility and volume fluctuations of phospholipid-sterol bilayers in the critical point region: a molecular acoustic and calorimetric study.* Biophys J, 2008. **94**(9): p. 3538-48.

222. Kucerka, N., M.P. Nieh, and J. Katsaras, *Fluid phase lipid areas and bilayer thicknesses of commonly used phosphatidylcholines as a function of temperature.* Biochim Biophys Acta, 2011. **1808**(11): p. 2761-71.

223. Saito, H. and W. Shinoda, *Cholesterol Effect on Water Permeability through DPPC and PSM Lipid Bilayers: A Molecular Dynamics Study.* Journal of Physical Chemistry B. **115**(51): p. 15241-15250.

224. Estronca, L.M.B.B., M.J. Moreno, and W.L.C. Vaz, *Kinetics and Thermodynamics of the Association of Dehydroergosterol with Lipid Bilayer Membranes.* Biophysical Journal, 2007. **93**(12): p. 4244-4253.

225. Selwyn, J.E. and Steinfel.Ji, *Aggregation Equilibria of Xanthene Dyes.* Journal of Physical Chemistry, 1972. **76**(5): p. 762-.

226. Chen, R.F. and J.R. Knutson, *Mechanism of Fluorescence Concentration Quenching of Carboxyfluorescein in Liposomes - Energy- Transfer to Nonfluorescent Dimers.* Analytical Biochemistry, 1988. **172**(1): p. 61-77.

227. Hamman, B.D., A.V. Oleinikov, G.G. Jokhadze, D.E. Bochkariov, R.R. Traut, and D.M. Jameson, *Tetramethylrhodamine Dimer Formation as a Spectroscopic Probe of the Conformation of Escherichia coli Ribosomal Protein L7/L12 Dimers.* Journal of Biological Chemistry, 1996. **271**(13): p. 7568-7573.

228. Tandford, C., *The Hydrophobic Effect: Formation of Micelles and Biological Membranes*. 2nd edition ed. 1991, New York: John Wiley and Sons, Inc.

229. De, S., S. Das, and A. Girigoswami, *Environmental effects on the aggregation of some xanthene dyes used in lasers.* Spectrochimica Acta Part A: Molecular and Biomolecular Spectroscopy, 2005. **61**(8): p. 1821-1833.

230. Biswas, S., S.C. Bhattacharya, P.K. Sen, and S.P. Moulik, *Absorption and emission spectroscopic studies of fluorescein dye in alkanol, micellar and microemulsion media.* Journal of Photochemistry and Photobiology A: Chemistry, 1999. **123**: p. 121-128.

231. Song, A., J. Zhang, M. Zhang, T. Shen, and J.a. Tang, *Spectral properties and structure of fluorescein and its alkyl derivatives in micelles.* Colloids and Surfaces A: Physicochemical and Engineering Aspects, 2000. **167**(3): p. 253-262.

232. Sjoback, R., J. Nygren, and M. Kubista, *Absorption and fluorescence properties of fluorescein.* Spectrochimica Acta Part A: Molecular and Biomolecular Spectroscopy, 1995. **51**(6): p. L7-L21.

233. Lyles, D.S., K.P. McKinnon, and J.W. Parce, *Labeling of the Cytoplasmatic Domain of the Influenza-Virus Hemagglutinin with Fluorescein Reveals Sites of Interaction with Membrane Lipid Bilayers.* Biochemistry, 1985. **24**(27): p. 8121-8128.

234. Kibblewhite, J., C.J. Drummond, F. Grieser, and P.J. Thistlethwaite, *Lipoidal eosin and fluorescein derivatives as probes of the electrostatic characteristics of self-assembled surfactant/water interfaces.* The Journal of Physical Chemistry, 1989. **93**(21): p. 7464-7473.

235. Tellinghuisen, J., P.M. Goodwin, W.P. Ambrose, J.C. Martin, and R.A. Keller, *Analysis of Fluorescence Lifetime Data for Single Rhodamine Molecules in Flowing Sample Streams.* Analytical Chemistry, 1994. **66**(1): p. 64-72.

236. Wilkerson, C.W., P.M. Goodwin, W.P. Ambrose, J.C. Martin, and R.A. Keller, *Detection and Lifetime Meaurement of Single Molecules in Flowing Samples*

Streams by Laser-Induced Fluorescence Applied Physics Letters, 1993. **62**(17): p. 2030-2032.

237. de Almeida, R.F.M., L.s.M.S. Loura, and M. Prieto, *Membrane lipid domains and rafts: current applications of fluorescence lifetime spectroscopy and imaging.* Chemistry and Physics of Lipids, 2009. **157**(2): p. 61-77.

238. Stillwell, W., L.J. Jenski, M. Zerouga, and A.C. Dumaual, *Detection of lipid domains in docosahexaenoic acid-rich bilayers by acyl chain-specific FRET probes.* Chemistry and Physics of Lipids, 2000. **104**(2): p. 113-132.

239. Leekumjorn, S. and A.K. Sum, *Molecular simulation study of structural and dynamic properties of mixed DPPC/DPPE bilayers.* Biophys J. 2006 Jun 1;90(11):3951-65. Epub 2006 Mar 13.

240. Kachel, K., E. Asuncion-Punzalan, and E. London, *The location of fluorescence probes with charged groups in model membranes.* Biochimica et Biophysica Acta (BBA) - Biomembranes, 1998. **1374**: p. 63-76.

241. Filipe, H.A.L., M.J. Moreno, and L.M.S. Loura, *Interaction of 7-Nitrobenz-2-oxa-1,3-diazol-4-yl-Labeled Fatty Amines with 1-Palmitoyl, 2-Oleoyl-sn-glycero-3-phosphocholine Bilayers: A Molecular Dynamics Study.* Journal of Physical Chemistry B, 2011. **115**(33): p. 10109-10119.

242. Marsh, D., *Polarity and permeation profiles in lipid membranes.* Proceedings of the National Academy of Sciences of the United States of America, 2001. **98**(14): p. 7777-7782.

243. Ramstedt, B. and J.P. Slotte, *Sphingolipids and the formation of sterol-enriched ordered membrane domains.* Biochimica et Biophysica Acta (BBA) - Biomembranes, 2006. **1758**(12): p. 1945-1956.

244. Dobson, P.D. and D.B. Kell, *Carrier-mediated cellular uptake of pharmaceutical drugs: an exception or the rule?* Nat Rev Drug Discov, 2008. **7**(3): p. 205-20.

245. Di, L., P. Artursson, A. Avdeef, G.F. Ecker, B. Faller, H. Fischer, J.B. Houston, M. Kansy, E.H. Kerns, S.D. Krämer, H. Lennernäs, and K. Sugano, *Evidence-based approach to assess passive diffusion and carrier-mediated drug transport.* Drug Discovery Today, 2012. **17**(15–16): p. 905-912.

246. Schlessinger, A., P. Matsson, J.E. Shima, U. Pieper, S.W. Yee, L. Kelly, L. Apeltsin, R.M. Stroud, T.E. Ferrin, K.M. Giacomini, and A. Sali, *Comparison of human solute carriers.* Protein Sci, 2010. **19**(3): p. 412-28.

247. Sugano, K., M. Kansy, P. Artursson, A. Avdeef, S. Bendels, L. Di, G.F. Ecker, B. Faller, H. Fischer, G. Gerebtzoff, H. Lennernaes, and F. Senner, *Coexistence of passive and carrier-mediated processes in drug transport.* Nat Rev Drug Discov, 2010. **9**(8): p. 597-614.

248. Mahar Doan, K.M., J.E. Humphreys, L.O. Webster, S.A. Wring, L.J. Shampine, C.J. Serabjit-Singh, K.K. Adkison, and J.W. Polli, *Passive permeability and P-glycoprotein-mediated efflux differentiate central nervous system (CNS) and non-CNS marketed drugs.* J Pharmacol Exp Ther, 2002. **303**(3): p. 1029-37.

249. Eytan, G.D., R. Regev, G. Oren, and Y.G. Assaraf, *The Role of Passive Transbilayer Drug Movement in Multidrug Resistance and Its Modulation.* Journal of Biological Chemistry, 1996. **271**(22): p. 12897-12902.

250. Seelig, A., *The Role of Size and Charge for Blood–Brain Barrier Permeation of Drugs and Fatty Acids.* Journal of Molecular Neuroscience, 2007. **33**(1): p. 32-41.

251. Zhao, Y.H. and M.H. Abraham, *Octanol/water partition of ionic species, including 544 cations.* J Org Chem, 2005. **70**(7): p. 2633-40.

252. Moreno, M.J., L.M. Estronca, and W.L. Vaz, *Translocation of phospholipids and dithionite permeability in liquid-ordered and liquid-disordered membranes.* Biophys J, 2006. **91**(3): p. 873-81.

253. Pokorny, A., P.F.F. Almeida, E.C.C. Melo, and W.L.C. Vaz, *Kinetics of amphiphile association with two-phase lipid bilayer vesicles.* Biophysical Journal, 2000. **78**(1): p. 267-280.

254. Pokorny, A., P.F.F. Almeida, and W.L.C. Vaz, *Association of a fluorescent amphiphile with lipid bilayer vesicles in regions of solid-liquid-disordered phase coexistence.* Biophysical Journal, 2001. **80**(3): p. 1384-1394.

255. Coreta-Gomes, F.M., W.L.C. Vaz, E. Wasielewski, C. Geraldes, and M.J. Moreno, *Quantification of cholesterol solubilized in bile salt micellar aqueous solutions using C-13 nuclear magnetic resonance.* Analytical Biochemistry, 2012. **427**(1): p. 41-48.

256. Nichols, J.W., *Thermodynamics and kinetics of phospholipid monomer-vesicle interaction.* Biochemistry, 1985. **24**(23): p. 6390-8.

257. Estronca, L.M., M.J. Moreno, J.A. Laranjinha, L.M. Almeida, and W.L. Vaz, *Kinetics and thermodynamics of lipid amphiphile exchange between lipoproteins and albumin in serum.* Biophys J, 2005. **88**(1): p. 557-65.

258. Falck, E., M. Patra, M. Karttunen, M.T. Hyvönen, and I. Vattulainen, *Impact of cholesterol on voids in phospholipid membranes.* The Journal of Chemical Physics, 2004. **121**(24): p. 12676-12689.

259. Almeida, P.F.F., *Lipid Transfer Between Vesicles: Effect of High Vesicle Concentration.* Biophysical Journal, 1999. **76**(4): p. 1922-1928.

260. Hamilton, J.A., *Fatty acid transport: difficult or easy?* Journal of Lipid Research, 1998. **39**(3): p. 467-481.

261. Wimley, W.C. and T.E. Thompson, *Exchange and flip-flop of dimyristoyl phosphatidylcholine in liquid-crystalline, gel and two-component, two-phase large unilamellar vesicles.* Biochemistry, 1990. **29**(5): p. 1296-1303.

262. McConnell, H.M. and R.D. Kornberg, *Inside-outside transitions of phospholipids in vesicle membranes.* Biochemistry, 1971. **10**(7): p. 1111-1120.

263. Moss, R.A. and S. Bhattacharya, *Transverse Membrane Asymmetry in Model Phospholipid Bilayers: NBD-Phosphatidylethanolamine and the Separation of Flip from Flop.* Journal of the American Chemical Society, 1995. **117**(33): p. 8688-8689.

264. De Kruijff, B. and K.W.A. Wirtz, *Induction of a relatively fast transbilayer movement of phosphatidylcholine in vesicles. A 13C NMR study.* Biochimica et Biophysica Acta (BBA) - Biomembranes, 1977. **468**(2): p. 318-326.

265. Homan, R. and H.J. Pownall, *Transbilayer diffusion of phospholipids: dependence on headgroup structure and acyl chain length.* Biochimica et Biophysica Acta (BBA) - Biomembranes, 1988. **938**(2): p. 155-166.

266. Doody, M.C., H.J. Pownall, Y.J. Kao, and L.C. Smith, *Mechanism and kinetics of transfer of a fluorescent fatty acid between single-walled phosphatidylcholine vesicles.* Biochemistry, 1980. **19**(1): p. 108-116.

267. Carley, A.N. and A.M. Kleinfeld, *Flip-flop is the rate-limiting step for transport of free fatty acids across lipid vesicle membranes.* Biochemistry, 2009. **48**(43): p. 10437-45.

268. Aniansson, E.A.G., S.N. Wall, M. Almgren, H. Hoffmann, I. Kielmann, W. Ulbricht, R. Zana, J. Lang, and C. Tondre, *Theory of the kinetics of micellar equilibria and quantitative interpretation of chemical relaxation studies of micellar solutions of ionic surfactants.* The Journal of Physical Chemistry, 1976. **80**(9): p. 905-922.

269. Evans, M.G. and M. Polanyi, *Some applications of the transition state method to the calculation of reaction velocities, especially in solution.* Transactions of the Faraday Society, 1935. **31**(0): p. 875-894.

270. Wynne-Jones, W.F.K. and H. Eyring, *The Absolute Rate of Reactions in Condensed Phases.* The Journal of Chemical Physics, 1935. **3**(8): p. 492-502.

271. Eyring, H., *The Activated Complex in Chemical Reactions.* The Journal of Chemical Physics, 1935. **3**(2): p. 107-115.

272. Steinfeld, J.I., Joseph S. Francisco, and William L. Hase, *Chemical Kinetics and Dynamics*. 2nd Edition ed. 1999, New Jersey: Prentice Hall.